Measuring the gravitational field of light, effects of cosmological expansion in frequency measurements of light, and propagation of optical solitons in background spacetimes

Dissertation

der Mathematisch-Naturwissenschaftlichen Fakultät
der Eberhard Karls Universität Tübingen
zur Erlangung des Grades eines
Doktors der Naturwissenschaften
(Dr. rer. nat.)

vorgelegt von
Felix Spengler
aus Reutlingen

Tübingen
2023

Gedruckt mit Genehmigung der Mathematisch-Naturwissenschaftlichen Fakultät der Eberhard Karls Universität Tübingen.

Tag der mündlichen Qualifikation:	19.04.2023
Dekan:	Prof. Dr. Thilo Stehle
1. Berichterstatter:	Prof. Dr. Daniel Braun
2. Berichterstatter:	Prof. Dr. Kostas Kokkotas

Abstract

This thesis focuses on different aspects of the interface between light and gravity. The contents can be divided into three thematic areas, corresponding with the connected publications and manuscripts. In the first chapter, measuring the gravitational near-field of a laser beam is discussed. The second and third chapters deal with the effects of gravity on the propagation of laser light. In particular, we focus first on the effects of cosmological expansion on local experiments and then on the effect of gravity on a soliton in a nonlinear medium.

In the first chapter, we calculate the gravitational field of laser pulses traveling back and forth in a cavity. We investigate their potential as sources of gravitational perturbations together with ultra-relativistic particle beams and modulated CW-cavities. These sources are then combined with three optomechanical detectors, and we calculate the expected responses of the detectors resulting from the source signals and the noise of the systems. We optimize over the parameters of one of the more promising detectors, a pendulum, for a one-week experiment. This allows us to show that measuring the gravitational signal of the planned high luminosity LHC is not too far-fetched. Thus, while we find that current detectors are unable to detect these gravitational signals, we also show that optimized and specialized detectors combined with future upgrades could open a pathway to the measurability of these signals. This would, in turn, be a stepping stone for accessing gravitational effects of non-classical states.

In the second chapter, we consider laser signals traveling in an expanding spacetime, such as Schwarzschild-de Sitter or McVittie spacetimes. We investigate the effects of the cosmological expansion on both the frequency measurements in a resonator and the frequency shift in double Doppler tracking are calculated for multiple observer fields. We then also estimate the potential bounds on the cosmological constant and the Hubble parameter that would result from these types of experiments, using state of the art optical clocks, are estimated. We find that frequency corrections linear in the Hubble constant are an artifact of unphysical observer choices but that, nevertheless, advancements in optical clocks may allow in the future useful bounds to the cosmological constant or the Hubble parameter.

Lastly, we consider the effect of a background spacetime on light traveling in nonlinear Kerr-media. We show that the medium and spacetime can be treated as a combined effective medium and use this in a simplified scenario to obtain a partial differential equation for the propagation of a soliton in a fiber. The propagation of solitons in these media is then simulated and the effects of the background spacetime studied. We also include the effect of mechanical deformations, i.e., photoelasticity, induced by the gravitational forces, which turns out to be the dominant effect.

Zusammenfassung

Der Schwerpunkt dieser Arbeit liegt auf verschiedenen Aspekten im Zusammenspiel von Licht und Schwerkraft. Der Inhalt dieser Arbeit kann in drei Themenbereiche unterteilt werden, die mit den zugehörigen Publikationen und Manuskripten korrespondieren. Die Messung des gravitativen Nahfeldes eines Laserstrahls wird im ersten Abschnitt behandelt. Der zweite und dritte Abschnitt befasst sich mit den Auswirkungen der Schwerkraft auf die Ausbreitung des Laserlichts. Dabei konzentrieren wir uns zunächst auf die Auswirkungen der kosmologischen Expansion auf lokale Experimente und dann auf die Wirkung der Gravitation auf ein Soliton in einem nichtlinearen Medium.

Im ersten Abschnitt berechnen wir das Gravitationsfeld von Laserpulsen, die sich in einem Hohlraum hin und her bewegen. Wir schätzen ihre Möglichkeiten als Quellen von Gravitationsstörungen zusammen mit ultra-relativistischen Teilchenstrahlen und modulierten CW-Resonatoren ab. Diese Quellen werden dann mit drei optomechanischen Detektoren kombiniert und wir berechnen die erwarteten Detektoramplituden, die sich aus den Quellensignalen und dem Rauschen der Systeme ergeben. Wir optimieren einen der vielversprechendsten Detektoren, ein Pendel, für ein einwöchiges Experiment und kommen in den Bereich der Messbarkeit des Gravitationssignals des geplanten LHC mit hoher Luminosität. Während wir feststellen, dass die derzeitigen Detektoren nicht in der Lage sind, diese Signale zu detektieren, können optimierte und spezialisierte Detektoren in Kombination mit zukünftigen Upgrades den Weg zur Messbarkeit dieser Art von Effekten eröffnen und somit ein möglicher Schritt zum Zugang zu Gravitationseffekten von nicht-klassischen Zuständen sein.

Im zweiten Abschnitt betrachten wir Lasersignale, die in einer expandierenden Raumzeit wie Schwarzschild-de Sitter oder McVittie propagieren. Die Auswirkungen der kosmologischen Expansion sowohl auf die Frequenzmessungen in einem Resonator als auch auf die Frequenzverschiebung bei der doppelten Dopplerverfolgung werden für mehrere Beobachterfelder berechnet. Außerdem werden die möglichen Grenzen für die kosmologische Konstante und den Hubble-Parameter abgeschätzt, die sich aus diesen Arten von Experimenten unter Verwendung modernster optischer Uhren ergeben würden. Wir stellen fest, dass Frequenzkorrekturen, die linear zur Hubble-Konstante sind, ein Artefakt der Wahl unphysikalischer Beobachter sind, dass aber dennoch Fortschritte bei optischen Uhren bald nützliche Grenzen für die kosmologische Konstante oder den Hubble-Parameter ermöglichen könnten.

Schließlich betrachten wir die Auswirkungen einer Hintergrundraumzeit auf Licht, das sich in nichtlinearen Kerr-Medien bewegt. Wir zeigen, dass das Medium und die Raumzeit als ein kombiniertes effektives Medium behandelt werden können und verwenden dies in einem vereinfachten Szenario, um eine partielle Differentialgleichung für die Ausbreitung eines Solitons in einer Faser für die Maxwell-Gleichungen zu erhalten. Die Ausbreitung von Solitonen in diesen Medien wird dann simuliert und die Auswirkungen der Hintergrundraumzeit untersucht. Insbesondere in Kombination mit der Photoelastizität eines deformierbaren Mediums können stark verstärkte Gravitationseffekte auftreten.

Acknowledgements

Over the course of the three and a half years I spent in Tübingen working on my PhD, many people supported me, motivated me, kept me good company and inspired me. In this acknowledgement, I would like to explicitly thank some of them.

Firstly, of course, my supervisor Daniel Braun. He always has time and an open ear for questions and physics problems, and seemingly limitless patience. I admire his endless curiosity and his will to understand the physical processes in the background of every result, and that he inspires the people around him to do the same.

Next, I would like to thank my co-supervisor Alessio Belenchia. He has worked as a Postdoc on most of my projects, shared an office with me, and has become a good friend. He has been a great help and his collaboration has given me a lot of new energy and motivation. Even though he always puts his own performance in the shade to highlight others, without his broad expertise and motivated input this work would not be what it is today.

Then, of course, I would like to thank Dennis Rätzel, he has accompanied and collaborated on all the projects of my PhD thesis. His great gift to explain gravitational physics has always been a great asset, and he has decisively advanced our projects with his constant will to better understand and better explain the processes.

Furthermore, I would like to thank many others from the D-Bau and the group: Mrs. Lorösch who takes care of everything and everyone. Emre, Nadia, Jirawat, Mathias, Kilian, Mahdi, Davide, Giovanni, and many others who kept me company and with whom I could talk about physics and other things.

I also received great support outside the university. First and foremost, of course, my fiancée Caro, who cared for me with endless love and support. Without her, I would not be the person I am today. There is no one I would rather have spent this time with, especially the time of the pandemic. Then, of course, my parents, who made this path possible for me in the first place and have always supported me in all my endeavors and always encouraged me to do my best.

Felix Spengler

Contents

1. Introduction

The theory of general relativity describes gravitational effects from milligram masses to universe scale structures and from motionless to ultrarelativistic systems. Light has, historically, been a central tool in exploring general relativity and testing its predictions. The theoretical descriptions of light and gravity interface at many levels, from the deflection of light in gravitational fields in the form of gravitational lensing, lense thirring, or frame dragging to the rarely considered gravitational field of light itself [1, 2, 3, 4].

In this thesis, we look at light both as a tool for exploring the geometry of spacetimes and as a source of the gravitational field. On the one hand, we study the gravitational field of light itself and analyze whether the gravitational signals can be shifted into the range of the measurable by using a cavity or ring resonator to create a periodic signal. On the other hand, the propagation of light in curved spacetimes is the subject of the other works contained in this thesis. We look at both the influence of an expanding universe on local experiments involving frequency measurements, and the effects of gravity on optical pulses propagating in a non-linear medium stationary in Schwarzschild spacetime.

In chapter 2 we extend on studies on the gravitational field of light [1, 2, 5] to calculate the periodic field generated by a light pulse in a cavity and that of a bunched particle beam. In the ultrarelativistic limit, the restmass of particles becomes negligible with respect to their total energy. Therefore in lowest order the gravitational field of the two beams can be calculated in the same manner starting from the principle of mass-energy equivalence. We work within the theory of linearized gravity, which is the weak field limit of general relativity, and calculate both the small perturbation of the metric caused by a Petawatt power laser pulses traveling back and forth in a high finesse cavity and that of the LHC. To study wether the gravitational signal of these sources is measurable, we combine the sources with several optomechanical sensors suitable for narrow bandwidth, small amplitude signals. First we look at the signal to noise ratio of a generic resonant mass detector and extend that calculation to a highly refined version of a resonant mass detector, using superfluid Helium, of which a prototype exists [6]. Then, we consider a high Q-factor pendulum [7] and propose an optimized version thereof, which, by going to a different regime of parameters and utilizing an altered detector geometry, shows a possible pathway to promising future experiments.

The focus is then changed in chapter 3 to the propagation of light in a curved spacetime and the effects of the expansion of the universe on local frequency measurements. Current observations [8] confirm that our universe is in a state of accelerated expansion at large scales. Both the ΛCDM cosmological model and the more simplified Friedmann-Lemaître-Robertson-Walker (FLRW) spacetime metric capture this effect. However, in local gravitating systems the effects of expansion have been the subject of a lively debate [9]. Handling solutions of general relativity that account both for a local gravitating effects and the expansion happening at large scale is difficult without resorting to strong simplification and heavy idealization. The simplified model we resort to in chapter 3 is the use of the McVittie metric, describing a spherical symmetric massive object embedded in an expanding FLRW spacetime. We will focus on the effect of the cosmological expansion on the frequency of propagating light. In particular, the frequency shift of a

resonator moving along different trajectories as well as a light signal exchanged between an observer, again moving along different trajectories, and a spacecraft.

The last topic, discussed in chapter 4, deals with the combined effects of a nonlinear medium and a curved background spacetime on the propagation of light. In recent years, the propagation of light in inhomogeneous optical media has increasingly been used as an analogue model of gravity, studying otherwise inaccessible quantum effects at horizons. This is inspired by the fact that light rays in a nondispersive medium propagate along geodesics of an effective optical metric [10]. Even at the level of the Maxwell equations, an effective medium can be constructed, with its properties only determined by the curved spacetime, for which the vacuum, curved spacetime Maxwell equations are equivalent to the ones in the effective medium, but in flat spacetime. We extend on this equivalency and show that the Maxwell equations for light in a medium and an additional background spacetime are equivalent to equations in flat spacetime with an effective spacetime medium constructed from both the metric and the background spacetime. In the limit of geometric optics, this can be reduced to a new refractive index obtained by multiplication of the mediums refractive index with the refractive index of the effective medium corresponding to the spacetime. We use this formalism, with some simplifications, to simulate the one dimensional propagation of a light pulse in a nonlinear fiber, which itself is placed in the gravitational field of the earth. As an additional complexity, we consider the fiber to be itself subject to gravity, deforming it and, through the effect of photoelasticity, altering its optical properties.

2. Perspectives of measuring the gravitational effects of laser and particle beams

Ever since the theoretically long predicted gravitational waves were first experimentally documented, all types of sources of gravitational signals have been the subject of increased scientific interest. High-energy, relativistic sources, which usually will be of low rest mass, pose an interesting frontier in this regard. They not only could offer a different class of tests of general relativity, constraints on extensions of general relativity, especially for quantum gravity effects [11, 12, 13, 14, 15]. For signals of cosmic sources the experimental setups are limited to just detection, hence proposals for man-made relativistic sources were already discussed early on [16, 17, 18].

Gravitational effects of light were studied early on in the twentieth century [1, 2, 5] with its many interesting properties. Both beams of light and pulses will attract test particles with a force proportional to distance^{-1}, similar to an infinitely extended massive cylinder, while the attraction of a more compact mass will scale with distance^{-2}. Higher order effects include frame dragging, polarization rotation, and other gravitomagnetic effects [19, 20, 21, 22, 3, 23, 4]. For a beam or pulse of relativistically moving massive particles, the gravitational influence is in lowest order equivalent to that of their photon equivalent [5, 24, 25, 26, 3, 23].

In this chapter we sketch the description of the attractive effects of state-of-the-art

high-energy relativistic sources and their interaction with resonant mass/pendulum type detectors and give results on the measurability of these effects.

2.1. Sources

Modern femtosecond laser pulses can reach up to a Petawatt in pulse power. We consider a series of high energy laser pulses oscillating to and fro in a cavity as a source of the gravitational field. In [A] the effective Newtonian potential close to the cavity axis resulting from this source is calculated within the theory of linearized gravity to be given as

$$\Phi(t) = \frac{4GP(t)}{c^3} \ln \rho, \tag{1}$$

where G is the gravitational constant, c is the speed of light in vacuum, ρ the distance from the beamline, and $P(t)$ the power passing through the cross-section of the cavity at the observers position. We assume a high average power pulsed laser [27] coupled into a large, high-finesse cavity using switchable mirrors and estimate that an average power of 20 GW could be achieved.

To achieve even higher average powers, we propose the use of a CW-laser, such as the one from [28], coupled into a high-finesse cavity resulting in an average power of up to 100 GW, and to then periodically modulate the energy periodically. While the standing wave will not be relativistic in its nature, it will still produce the same effective Newtonian potential given in eq. (1).

From a gravitational point of view, ultra relativistic particle beams are, given the negligible contribution of the rest mass, very similar to a laser beam [25, 24, 26]. Thanks to the high average power of 3.8 TW, the LHC is an obvious choice as the last source we'll consider. While there is already an internal frequency in the megahertz range to its signal due to the bunching of electrons in the ring, a periodic modulation of the beam's focal point position could be used to create a gravitational signal of lower frequency.

2.2. Sensors

We consider two types of detectors, first resonant mass detectors, where we look at an aluminum rod similar to a Weber bar [29] and a cylinder filled with superfluid helium-4 coupled parametrically to a superconducting microwave cavity [6]. Secondly, we consider mechanical harmonic oscillators. Motivated by the high gravitational sensitivities recently reported for a monolithic pendulum in [7, 30] and for a torsion balance in [31], we calculate the response of the first to our sources and use this as a base of a more optimal detector close to the parameter regime of the second.

Limiting ourselves to the one dimensional case, we can describe the deformable cylinder with a wave equation for the displacement field $u(x,t)$ given by [29]

$$\partial_t^2 u(x,t) - c_\mathrm{s}^2 \partial_x^2 u(x,t) = -\partial_x \Phi(x,t), \tag{2}$$

where x is the direction orthogonal to the sources axis of symmetry, and c_s is the speed of sound in aluminum. For the rod depicted in figure 2, the maximum amplitude on

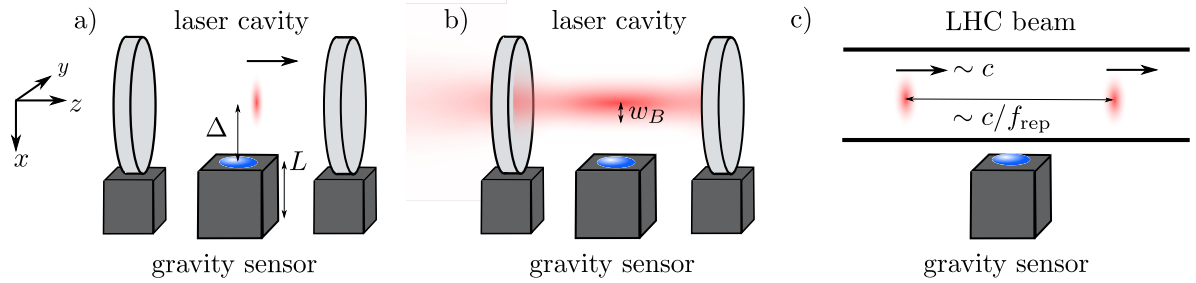

Figure 1: a) Laser pulse oscillating to and fro in a cavity. b) CW-laser focused to a narrow waist inside a cavity. Its intensity is modulated to create a periodic gravitational field. c) Ultrarelativistic particle bunches in an accelerator ring such as the LHC create a gravitational field very similar to that of laser pulses. In the vicinity of the waist of the laser beam or close to the beamline, a detector picks up resonant mechanical deformations due to the oscillating gravitational forces.

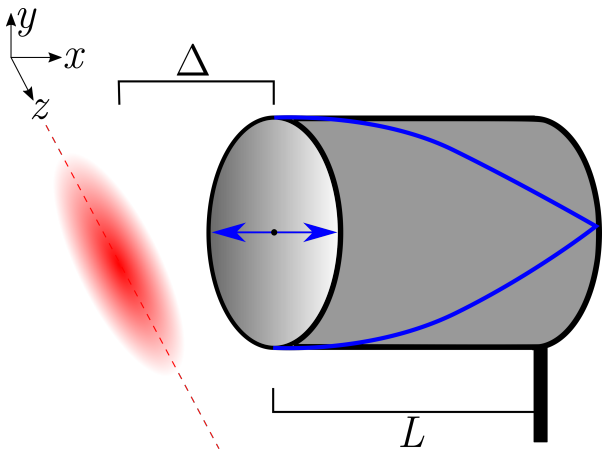

Figure 2: Schematic drawing of the deformable rod envisioned as a detector.

resonance with the ground mode is

$$A^{\mathrm{rod}}(\omega_0) = \frac{16GP_{\mathrm{cav}}^{\mathrm{avg}}Q}{\omega_0^3 c^3 \tau_p} \sin\left(\frac{\omega_0 \tau_{\mathrm{p}}}{2}\right) \int_{\Delta}^{L+\Delta} \mathrm{d}x \, \frac{2}{L} \cos\left(\frac{\pi}{2L}(x-\Delta)\right) \frac{1}{x} \tag{3}$$

where ω_0 is the frequency of the ground mode, $P_{\mathrm{cav}}^{\mathrm{avg}}$ is the power in the source cavity averaged over one oscillation period, Q is the material quality factor of the rod, and τ_{p} is the length of the rectangular pulse of the sources gravitational signal. As a gauge for the measurability of the signal, we consider the amplitude resulting from thermal noise $A_{\mathrm{th}} = \sqrt{\frac{\frac{4k_{\mathrm{B}}TQ}{\omega_0^3 M_{\mathrm{eff}}}}{\tau_{\mathrm{int}}}}$, where k_{B} is the Boltzmann constant, T is the temperature of the rod, M_{eff} is the effective mass of the ground mode of the rod, and τ_{int} is the integration time, as well as quantum noise given by the standard quantum limit (SQL) $A_{\mathrm{SQL}} = \sqrt{\frac{\frac{4\hbar Q}{M_{\mathrm{eff}}\omega_0^2}}{\tau_{\mathrm{int}}}}$, with the reduced Planck constant $\hbar$. Results for both the expected signal amplitude and dominant noise are given in table 1 for all different types of sources.

In [6] Singh et al. study the acoustic motion of superfluid helium-4 coupled parametrically to a superconducting microwave cavity as a detection scheme for continuous-wave gravitational signals. Instead of gravitational waves, we want to employ this prototype detector for the near-field sources we consider here. With the one-dimensional formalism we use to describe the deformable rod, we can also describe the ground mode of the helium in the cylindrical container, however, with two fixed ends instead of one. The maximum amplitude for resonant diving of the ground mode is given by

$$A^{\mathrm{He}}(\omega_0) = \frac{16GP_{\mathrm{cav}}^{\mathrm{avg}}Q_{\mathrm{He}}}{\omega_0^3 c^3 \tau_p} \sin\left(\frac{\omega_0 \tau_{\mathrm{p}}}{2}\right) \int_{\Delta}^{L+\Delta} \mathrm{d}x \, \frac{2}{L} \sin\left(\frac{\pi}{L}(x-\Delta)\right) \frac{1}{x}, \tag{4}$$

with a values for the prototype of $Q_{\mathrm{He}} = 6 \cdot 10^{10}$, $L = 4\,\mathrm{cm}$, $\omega_0 = 2\pi \cdot 2.8$ kHz, $M_{\mathrm{eff}} = 3\,\mathrm{g}$. The main sources of noise considered are once again thermal and quantum noise, for the prototype a temperature of $T = 5\,\mathrm{mK}$ is given. Values for both the expected amplitude and noise are given in table 1.

Next, we want to consider the sensitivity of a pendulum to the gravitational signal of the source. In [7] the properties of a monolithic pendulum were presented. From an already high quality factor $Q_{\mathrm{pend}} = 10^5$ at $\omega = 2\pi \cdot 4.4\,\mathrm{Hz}$, an optical spring is used to increase the stiffness of the system, upshifting its resonance frequency, while also increasing the new effective quality factor quadratically with the frequency. However, the optical spring also pumps energy into the system, which has to be removed using additional feedback cooling, strongly decreasing the quality factor to Q_{fb}, while leaving the resonance frequency untouched. At a frequency of $\omega_0 = 2\pi \cdot 280\,\mathrm{Hz}$, a sensitivity of $3 \cdot 10^{-14}\,\mathrm{m}/\sqrt{\mathrm{Hz}}$ was demonstrated with a quality factor of $Q_{\mathrm{fb}} = 250$, where the limiting factor was given by thermal noise. The displacement amplitude resulting from driving on resonance can be calculated just using the acceleration of the center of mass to be

$$A_{\mathrm{pend}}(\omega_0) = \frac{16GP_{\mathrm{cav}}^{\mathrm{avg}} \sin\left(\frac{\omega_0 \tau_{\mathrm{p}}}{2}\right) Q_{\mathrm{fb}}}{c^3 \omega_0^3 \tau_{\mathrm{p}}} \frac{1}{x_{\mathrm{com}}}, \tag{5}$$

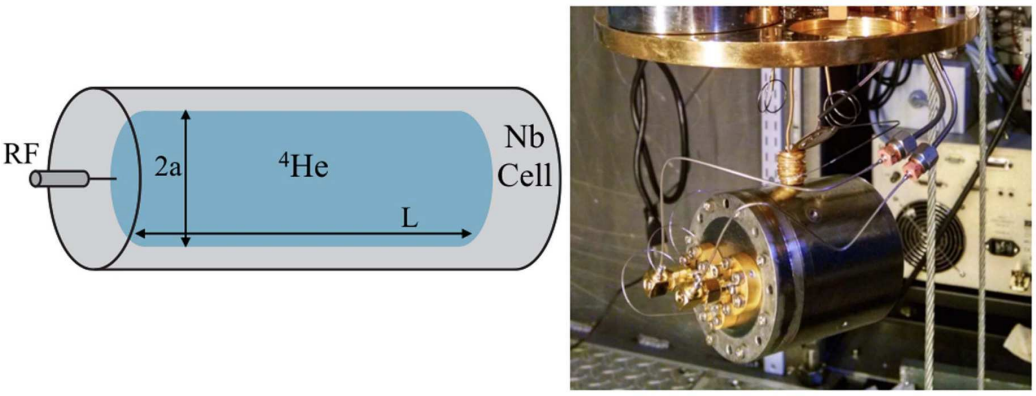

Figure 3: From "Detecting continuous gravitational waves with superfluid 4He" by S. Singh et al. in the *New Journal of Physics,* vol. 19 p. 073023 in July 2017 [6]. Schematic drawing of the superfluid helium-4 detector.

where $x_{\rm com}$ is the distance between the axis of symmetry of the source and the center of mass of the pendulum. The expected amplitude as well as the sensitivity are given in table 1.

Lastly, we want to demonstrate that a detector with an optimized geometry can be envisioned, close to able to bridge the large gap left between the signal and sensitivity of the detectors discussed prior for a realistic total experiment time of 1 week. Given the elongated geometry of our sources, a pendulum with a long cylindrical body would be beneficial. Intuitively, and also manifestly in the equations derived below, it is evident that the mass m should be as large as possible. At the same time, m cannot be made arbitrarily large, as otherwise the distance from the beam axis would have to be increased as well, which would lead to a decay of the signal $\propto 1/x_{\rm com}$. We therefore assume for the LHC as source a cylindrical detector mass that allows one to maintain $\rho = 200\,\mu$m. If we allow that cylinder to become as long as $L_{\rm cyl} = 0.5\,$m and determine the maximum mass as $m = 0.9\pi\varrho_{\rm Si}(\rho - \rho_{\rm min})^2\, L_{\rm cyl}$ (where 0.9 is a "fudge factor" that avoids that the detector mass touches the shielding), we find $m = 33\,$mg for $\rho_{\rm min} = 100\,\mu$m.
The total equilibrium noise reads

$$\bar{S}_{\rm xx,eq}(T,\omega,\Omega,Q,m) = \hbar\coth\left(\frac{\hbar\omega}{2k_BT}\right)\mathrm{Im}\chi_{\rm xx}(\omega,\Omega,Q,m) \quad (6)$$

$$\mathrm{Im}\chi_{\rm xx}(\omega,\Omega,Q,m) = \frac{Q\omega\Omega}{m(\omega^2\Omega^2 + Q^2(\omega^2-\Omega^2)^2)}\,, \quad (7)$$

with the quality factor $Q \equiv \Omega/(\gamma_0+\gamma)$. A transducer and amplifier add a back-action noise $\bar{S}_{\rm xx,add}$ that can be referred back to the input [32]. It is lower bounded by $\bar{S}_{\rm xx,addMin} = \hbar|\mathrm{Im}\chi_{\rm xx}|$. With this lowest possible value and the replacements $\Omega \to \omega_0$, $Q \to Q_{\rm fb}$, $T \to T_{\rm fb}$, one obtains for the total noise power to lowest order in γ/γ_0, that $\bar{S}_{\rm xx,tot}(T_{\rm fb},\omega,\omega_0,Q_{\rm fb},m) = \bar{S}_{\rm xx,eq} + \bar{S}_{\rm xx,addMin}$.

The maximum amplitude $A_{\rm pend}(\omega_0)$ of the harmonic oscillator is reached only asymptotically as a function of time, namely as $x_{\rm grav}(t) = x_{\rm grav}(1-\exp(-\omega_0 t/(2Q_{\rm fb})))$. We

	rod		liquid helium	pendulum
ω_0	$2\pi \cdot 10^3$ Hz	$2\pi \cdot 10^9$ Hz	$2\pi \cdot 2.8 \cdot 10^3$ Hz	$2\pi \cdot 280$ Hz
sensitivity	$1 \cdot 10^{-17} \frac{\mathrm{m}}{\sqrt{\mathrm{Hz}}}$	$4 \cdot 10^{-17} \frac{\mathrm{m}}{\sqrt{\mathrm{Hz}}}$	$1 \cdot 10^{-12} \frac{\mathrm{m}}{\sqrt{\mathrm{Hz}}}$	$2 \cdot 10^{-14} \frac{\mathrm{m}}{\sqrt{\mathrm{Hz}}}$
limiting factor	thermal noise	SQL	thermal noise	thermal noise
expected amplitude				
laser pulses	$2 \cdot 10^{-25}$ m	$2 \cdot 10^{-34}$ m	$1 \cdot 10^{-20}$ m	$3 \cdot 10^{-26}$ m
CW-cavity	$4 \cdot 10^{-25}$ m	$4 \cdot 10^{-34}$ m	$2 \cdot 10^{-20}$ m	$5 \cdot 10^{-26}$ m
LHC beam	$8 \cdot 10^{-24}$ m	$9 \cdot 10^{-32}$ m	$4 \cdot 10^{-19}$ m	$1 \cdot 10^{-24}$ m

Table 1: Comparison of the estimated sensitivity of the listed detectors with the expected amplitude of the sources considered on resonance and after the full build-up-time of the detector's oscillation. For the cases in which the main limiting factor is thermal noise, a temperature of 5 mK was assumed. Other parameters, see text.

assume that the total time $\tau_{\mathrm{tot}} = 1$ week for the experiment is split as $\tau_{\mathrm{tot}} = \tau_{\mathrm{r}} + \tau_{\mathrm{m}}$ into a time τ_{r} needed for the amplitude of the harmonic oscillator to rise to a certain level, and a measurement time τ_{m} used for reducing the noise. The total signal-to-noise ratio on resonance is then given by

$$S/N = x_{\mathrm{grav}} \left(1 - e^{-(\tau_{\mathrm{tot}} - \tau_{\mathrm{m}}) \frac{\omega_0}{2Q_{\mathrm{fb}}}}\right) \sqrt{\frac{\tau_{\mathrm{m}}}{\bar{S}_{\mathrm{xx,tot}}}} \simeq 0.01 \, \frac{(1 - e^{(\tau_{\mathrm{m}} - \tau_{\mathrm{tot}}) \frac{\omega_0}{2Q_{\mathrm{fb}}}}) \sqrt{Q_{\mathrm{fb}} m \, \tau_{\mathrm{m}}}}{\omega_0 \sqrt{1 + \coth \frac{4 \cdot 10^{-12} \omega_0}{T_{\mathrm{fb}}}}} \,, \qquad (8)$$

with all quantities are in SI units.

We insert the $m = 33\,\mathrm{mg}$ in eq.(8), and optimize S/N with respect to the parameters $\tau_{\mathrm{m}}, \omega_0, Q_{fb}$ and T_{fb}. With τ_{tot} kept equal to 1 week, in the range $1/\mathrm{s} \leq \omega_0 \leq 10^4/\mathrm{s}$, $1 \leq Q_{\mathrm{fb}} \leq 10^8$, $1\,\mathrm{nK} \leq T_{\mathrm{fb}}$ a maximum value $S/N \simeq 0.6$ is found for $\tau_{\mathrm{m}} = 3 \cdot 10^5\,\mathrm{s}$, $\omega_0 = 2\pi \cdot 0.16$ Hz, $Q_{\mathrm{fb}} = 1.2 \cdot 10^5$, and minimal T_{fb}. The optimal value for ω_0 is at the lower end of the parameter range, but reasonably close to the one for the existing torsion balance in [31] ($\omega_0 = 2\pi \times 3.59\,\mathrm{mHz}$), where, however, the mechanical quality factor was $Q = 4.9$ and a mass of 92.1 mg was used. It remains to be seen if the parameters that result from the optimization can be reached. Problematic appears mostly whether the temperature of the cooled mode of about 1 nK can be reached, especially at low frequencies.

The planned upgrade of the LHC to the high-luminosity LHC [33] should increase S/N by a factor 10. Another factor 2.9 is expected to be gained by switching to tungsten (with mass density $\varrho_{\mathrm{W}} = 19,250\,\mathrm{kg/m^3}$) as detector-mass material, all other optimized parameters remaining equal. Both factors combined would lead to a $S/N \simeq 16$.

3. Effects of cosmological expansion in frequency measurements of light

The ΛCDM standard cosmological model, in accordance with current observations [8], describes an accelerated expansion of the universe at large scales. This description is effective above the supercluster scales, where the evolution is dominated by the so-called Hubble flow. However, whether the cosmic expansion of spacetime can affect local gravitating systems has been the subject of a lively debate dating back to Einstein and Straus [9, 34]. Since then, a growing body of literature has tackled the issue of the existence of local effects of the cosmological expansion [35].

In this chapter, motivated by the rapid development of optical clocks and frequency standards [36] which are now reaching an uncertainty below the current value of the Hubble parameter $H_0 \approx 2.2 \cdot 10^{-18}\,1/\mathrm{s}$ when averaging over a minute, we investigate the effect of the global cosmological expansion on the frequency of propagating light signals, focusing on the frequency shift of a resonator moving along different trajectories and on the exchange of light signals between different observers.

3.1. Metrics, observer fields, and the proper detector frame

First derived in the early '30s [37], the McVittie metric is a spherically symmetric solution to Einstein's equations and describes a non-charged, non-rotating compact object in an expanding cosmological FLRW spacetime. As such, the McVittie metric reduces, by construction, to the exterior Schwarzschild solution at small radii and to FLRW asymptotically. We restrict ourselves to the case in which the FLRW asymptotic metric describes a spatially flat spacetime, in accordance with current cosmological observations.

In the following, we use mainly two coordinate representations for the McVittie metric, always assuming to be at distances from the central object much larger than its Schwarzschild radius. We also set $c = G = 1$ unless otherwise stated. In isotropic spherical coordinates, the McVittie metric reads

$$ds^2 = -\frac{\left(1-\frac{m(t)}{2r}\right)^2}{\left(1+\frac{m(t)}{2r}\right)^2}dt^2 + \left(1+\frac{m(t)}{2r}\right)^4 a(t)^2(dr^2 + r^2 d\theta^2 + r^2\sin^2\theta d\phi^2) \tag{9}$$

where we are using the $(-,+,+,+)$ signature. Here, $a(t)$ indicates the scale factor of the asymptotic FLRW metric. As discussed in [35], the matter content of the McVittie spacetime is assumed to consist of a perfect fluid moving along the integral curves of the (normalized) vector field ∂_t, and from the Einstein's equations one obtains $m(t) = m_0/a(t)$ with $m_0 = r_S/2$ the mass of the central object and r_S its Schwarzschild radius.

A second set of coordinates that will turn out to be useful are the areal radius coordinates. The areal radius is defined as

$$R(t,r) = \left(1+\frac{m(t)}{2r}\right)^2 a(t) r. \tag{10}$$

We can then adopt the change of coordinates $t \to t$, $r \to R$ and write the metric in areal radius coordinates as

$$ds^2 = -(1 - 2\mu(R) - h(R,t)^2)dt^2 - \frac{2h(R,t)dt\,dR}{\sqrt{1-2\mu(R)}} + \frac{dR^2}{1-2\mu(R)} + R^2 d\theta^2 + R^2 \sin^2\theta d\phi^2, \tag{11}$$

where $\mu(R) = m_0/R$, $h(R,t) = H(t)R$, and $H(t) = a'(t)/a(t)$ is the Hubble parameter as usual, with the prime indicating a derivative with respect to the coordinate time.

It should be noted that, considering the current estimates for the value of the Hubble parameter at the current time $H_0 \sim 70$ km/s/Mpc $\sim 2 \times 10^{-18}\,\mathrm{s}^{-1}$ in the ΛCDM paradigm, H_0' is of the same order of magnitude as H_0^2, hence, we will consider terms in H' as quadratic corrections in the Hubble parameter.

From the form of the metric in eq. (11) it is also immediate to see that, imposing the Hubble parameter to be equal to Hubble's constant $H(t) = H_0$, or choosing $a(t) = e^{H_0 t}$, we recover the line element of Schwarzschild-de Sitter spacetime with cosmological constant $\Lambda = 3H_0^2$ in areal radius coordinates.

The Schwarzschild-de Sitter (SdS) case will be of relevance in the following. The SdS metric has been used in the existing literature to investigate the effect of the cosmological constant on the local dynamics in a variety of situations [38, 39, 40, 41]. While the SdS metric encodes only the effect of the cosmological constant, it allows for analytical solutions where only numerics can be used with the general McVittie line element. We will thus resort to the SdS line element for some of the results involving geodesics in the following.

Before moving on, let us notice that SdS spacetime is static, and can be written in the time-independent, diagonal form[1] [42]

$$ds^2 = -\alpha(R)dt^2 + \alpha(R)^{-1}dR^2 + R^2(d\theta^2 + \sin^2\theta d\phi^2), \tag{12}$$

where $\alpha(R) = 1 - r_S/R - H_0^2 R^2$. We will refer to this in the following as using "manifestly static" coordinates.

To discuss results of measurements, we have to specify which timelike trajectories, i.e., observer fields, we are going to consider in the following.

In order to determine the frequency shift of the resonator, we will employ the metric and the Riemann tensor expressed in the proper detector frame [43]. The proper detector frame is defined, up to spatial rotations and with respect to a time-like trajectory γ, as the Fermi-Walker transported orthonormal tetrad $\{\mathbf{e}_\alpha\}$, $\alpha \in \{0,1,2,3\}$ with $\mathbf{e}_0 = \dot{\gamma}$ the normalized four-velocity along the trajectory (i.e., the specific observer field), that is

$$\begin{cases} \mathbf{e}_0 = \dot{\gamma} \\ 0 = \frac{D_F \mathbf{e}_a}{\mathrm{ds}} \equiv \frac{D\mathbf{e}_a}{\mathrm{ds}} - \left(\mathbf{e}_a, \frac{D\mathbf{e}_0}{\mathrm{ds}}\right)\mathbf{e}_0 + (\mathbf{e}_a, \mathbf{e}_0)\frac{D\mathbf{e}_0}{\mathrm{ds}}, \ \forall a \in \{1,2,3\} \end{cases} \tag{13}$$

[1] This form of the metric can be obtained from eq. (11), with the condition $H(t) = H_0$ constant, by performing the change of coordinates $t \to t + u(R)$ with $u'(R) = H_0 R / \left(\sqrt{1-2\mu(R)}\alpha(R)\right)$ as described e.g. in [42].

where $DX/ds = \mathbf{e}_0^\mu \nabla_\mu X$ is the covariant derivative of the Levi-Civita connection along the direction of $\mathbf{e}_0$ and $D\mathbf{e}_0/ds = \boldsymbol{a}$ its 4-acceleration. Due to the Fermi-Walker transport, the proper detector frame is said to be *non-rotating* and can be physically realized by an observer carrying along a clock defining time and a system of three gyroscopes with spin vectors orthogonal to each other defining the spatial reference frame [44]. Note that Fermi-Walker transport along a geodesic corresponds to parallel transport.

We are now in the position to discuss several observer fields which will be used in the following.

Cosmological observer

The first observer field that we consider is obtained by normalizing the ∂_t vector field in isotropic spherical coordinates (9). It is then given by

$$\mathbf{u} = \|\partial_t\|^{-1}\partial_t. \tag{14}$$

As we commented above, the perfect fluid matter content of McVittie spacetime moves along the integral lines of such an observer field. While in FLRW such a field is geodesic, this is not the case in McVittie (or SdS) spacetime. The cosmological observer corresponds to an observer at a constant coordinate radius r and, in the asymptotic region approximating FLRW, defines the so-called Hubble flow.

Kodama observer

The Kodama vector field ($\mathbf{v}_\mathrm{K}$) is the unique spherically symmetric vector field orthogonal to the gradient of the areal radius, corresponding to an observer at a constant areal radius.

As discussed in detail in [35, 45], the Kodama observer field is the natural substitute for a timelike Killing field in a time dependent spherically symmetric spacetime, coinciding with it in the static limit, i.e., where in our case McVittie reduces to the SdS spacetime. The Kodama observer field assumes the simple form

$$\mathbf{u}_\mathrm{K} = \frac{1}{\sqrt{1-2\mu(R)-h(R,t)^2}}\{1,0,0,0\} \tag{15}$$

in areal radius coordinates, and is, in general, not geodesic similar to the cosmological observer field in McVittie spacetime.

Geodesic observers

The previous two observer fields require a proper acceleration for a spacecraft to keep moving along their integral curves, in contrast to geodesic ones, which describe the realistic case of inertial observers in free-fall. We limit ourselves to the SdS limit of McVittie spacetime and work in manifestly static coordinates (12), where analytical expressions for timelike geodesics exist [46]. The symmetries of SdS spacetime allow us

to define the two conserved quantities energy E and angular momentum L that uniquely characterize the 4-velocity of the timelike trajectory as

$$\dot{\gamma} = \left\{ \frac{E}{\alpha(R)}, \sqrt{E^2 - \alpha(R)\left(1 + \frac{L^2}{R^2}\right)}, 0, \frac{L}{R^2} \right\} \tag{16}$$

where we are working in static coordinates, and consider motion in the equatorial plane ($\theta = \pi/2$). We limit ourselves to the two extreme cases of circular ($\dot{\gamma}_R = 0$) and radial ($L = 0$) geodesics.

3.2. Observer dependent frequency of a deformable resonator

In [47] a resonator, consisting of two mirrors connected by an elastic rod which itself is fixed to a support, affected by a curved background metric is studied. Based on this, we analyze here the effects of cosmological expansion on the frequency of a resonator on different trajectories.

Attached by a support to an observer, characterized by a timelike trajectory and its local proper detector frame, the resonator is subject to gravitational effects (cf. Fig. 4). We assume that the resonator is aligned along the, arbitrarily chosen, $\mathbf{e}_J$-direction, with $J \in \{1, 2, 3\}$ in the proper detector frame, and that the rod's elasticity is characterized by the material's speed of sound c_s.

The slowly varying acceleration and tidal forces induce internal stress within the rod, which accumulates along it, leading to a compression or elongation. The proper acceleration of the mirrors can be ignored if the mirrors are considered lightweight compared to the rod. Following the detailed derivation in [47], the change in length translates to a shift in the resonance frequency which, for a slowly moving observer, is given in eq.(29) of [47] as approximately

$$\frac{\Delta\omega}{\omega} \approx \frac{\mathbf{a}^J}{2c^2}\left(\frac{c^2}{c_s^2}\beta - \sigma\right) L_p + \frac{R_{0J0J}}{24}\left(2\frac{c^2}{c_s^2}(3\beta^2 + 1) - 3\sigma^2 - 6\sigma\beta + 1\right) L_p^2, \tag{17}$$

where ω is the resonance frequency of the oscillator in the absence of curvature and acceleration, $\mathbf{a}^J \equiv \boldsymbol{e}^J_\mu \boldsymbol{a}^\mu$ and $R_{0J0J} = \boldsymbol{e}^\alpha_0 \boldsymbol{e}^\beta_J \boldsymbol{e}^\gamma_0 \boldsymbol{e}^\delta_J R_{\alpha\beta\gamma\delta}$ are the proper acceleration and the Riemann curvature tensor components in the detector frame, $\beta\, L_p/2$ is the distance of the rod's support from the center of mass and $\sigma\, L_p/2$ is the distance of the point of measurement from the center-of-mass (cf. Fig. 4). By the choice of alignment, the acceleration and curvature parallel to the axis of the resonator are the only components to contribute in leading order to the frequency shift of the resonator.

The spatial component of the 4-acceleration, and the $0J0J$-components of the Riemann tensor, in the proper detector frame of the cosmological observer depend on the scale factor and therefore, after expanding $a(t) \approx a(t_0)(1 + H_0\Delta t)$, contain corrections at first order in the Hubble parameter H_0. Meanwhile, the same quantities in the proper detector frame of the Kodama observer and geodesic observer (albeit that the acceleration vanishes for the geodesic one) contain no corrections at linear order in H,

and H_0 respectively, only corrections $\mathcal{O}(H^2, H')$, and $\mathcal{O}(H_0^2)$ respectively. These contributions of the expansion to the frequency shift of the resonator are far too small to measure. For the most realistic case of a geodesic observer in SdS, assuming the value of $H_0 \sim 2.2 \times 10^{-18}\,\mathrm{s}^{-1}$, and a speed of sound $c_s = 5000\,\mathrm{m/s}$ (comparable to that of aluminium) the relative frequency shift of a resonator of length 10 m is only $\sim 10^{-42}$.

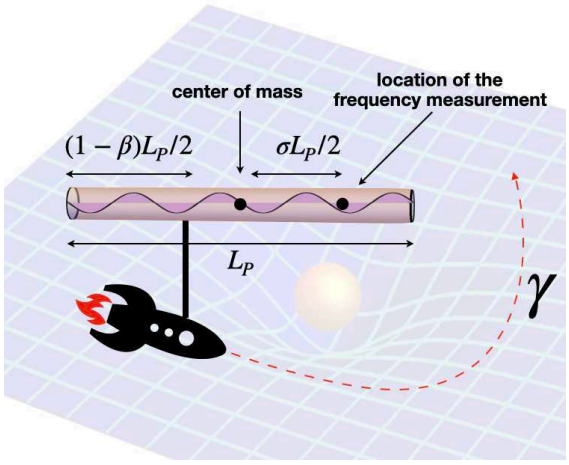

Figure 4: Pictorial representation of the resonator rod carried along a trajectory γ by an observer (the spacecraft) in a curved background. The observer trajectory γ is the one followed by the support point at which the resonator is fixed to the observer. The proper length of the resonator is denoted by L_p, the support point is at a distance $\beta L_p/2$ from the center of mass and the frequency measurement is performed in an arbitrary point of the resonator at a distance $\sigma L_p/2$ from the center of mass.

3.3. Redshift and satellite tracking

Having considered the impact of the global cosmological expansion on a local experiment, we conclude with a brief overview of the effect of the same expansion on the frequency redshift of signals exchanged between observers and the related concept of double Doppler tracking (DDT) depicted in figure 5. These kinematic effects have been treated in detail in the existing literature [40, 41, 48, 35]. Here, we focus on clarifying some of the results in the literature by following the derivation in [35].

In the case of FLRW spacetime, the redshift formula for exchanges of light signals between two observers following the Hubble flow is easily obtained. Consider two cosmological observers at r_0 and r_1 in isotopic spherical coordinates[2], then the ratio between the frequency emitted by the first observer and the one received by the second observer is given by $\omega_1/\omega_0 = a(t_0)/a(t_1) \sim 1 - H_0(t_1 - t_0)$, where we have assumed the leading order of the Hubble parameter to be $H_0 = \text{const.}$, and where the frequency measured

[2]In these coordinates the FLRW line element has the usual form $ds^2 = -dt^2 + a^2(t)(dr^2 + r^2 \sin\theta^2 d\phi^2 + d\theta^2)$.

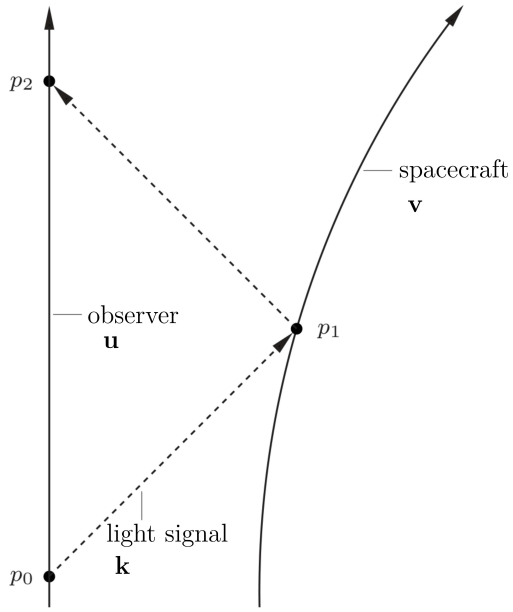

Figure 5: Adapted from "Influence of global cosmological expansion on local dynamics and kinematics" by M. Carrera and D. Giulini in Reviews of Modern Physics vol. 82 pp. 169 208, in January 2010 [35]. Illustration of the process of double Doppler tracking.

by an observer $\mathbf{u}$ is given by the scalar product between the observer field and the null tangent to the light signal $\mathbf{k}$, i.e. $\omega = |g(\mathbf{u}, \mathbf{k})|$. We notice that the redshift encodes a correction linear in the Hubble constant. As shown in [35], this persists also in the case in which a spherical inhomogeneity is included.

In order to address the effects of the background spacetime within DDT, we need to consider the ratio between the frequency emitted by an observer and the frequency received back by the same observer after the light signal has been reflected by an arbitrarily moving "spacecraft" (see fig. 5). In FLRW, considering the cosmological observer field and a spacecraft reflecting the light signal upon reception, this ratio can be broken into three terms $\omega_2(t_2)/\omega_0(t_0) = (\omega_2/\omega_1')(\omega_1'/\omega_1)(\omega_1/\omega_0)$. Here, the observer receiving (at $t = t_2$) and sending (at $t = t_0$) the signal is at a fixed value of the coordinate radius r. Also notice that, for the cosmological observer in FLRW, proper time coincides with the coordinate time t. The ratio ω_1'/ω_1 represents the ratio between the frequency immediately after and before the reflection *as measured by the cosmological observer at the point of reflection*. This ratio accounts for the relativistic Doppler shift due to the motion of the spacecraft relative to the observer field. The other two ratios are easily obtained from the previous expression of the single-way redshift. Altogether, one arrives at eq. (140) of [35]

$$\frac{\omega_2(t_2)}{\omega_0(t_0)} = \frac{a_0}{a_2}\left(2\frac{1-\beta^{\hat{\boldsymbol{k}}}_{\mathbf{u}}(\mathbf{v})}{1-\beta_{\mathbf{u}}(\mathbf{v})^2} - 1\right). \tag{18}$$

Here, we have considered a spacecraft with four velocity $\mathbf{v}$ whose relative velocity with respect to the observer field $\mathbf{u}$ at the reflection point is $\boldsymbol{\beta}_{\mathbf{u}}(\mathbf{v}) = (\mathbf{v}-|g(\mathbf{v},\mathbf{u})|\mathbf{u})/|g(\mathbf{v},\mathbf{u})|$ [35]. Furthermore, we have considered a null signal propagating radially between the emitter and the reflection point with tangent $\mathbf{k}$ whose normalized projection in the rest frame of the observer is $\hat{\boldsymbol{k}}$. Finally, with $\beta^{\hat{\boldsymbol{k}}}_{\mathbf{u}}$ we indicate the projection of the relative velocity along the unit vector $\hat{\boldsymbol{k}}$ in the rest frame of $\mathbf{u}$. Eq. (18) relates the frequency shift to the spacecraft spatial velocity and can be approximated to linear order in β and $H_0\Delta t_{20}$ with $\Delta t_{20} = t_2 - t_0$ giving $\omega_2(t_2)/\omega_0(t_0) \approx 1 - 2\beta^{\hat{\boldsymbol{k}}}_{\mathbf{u}}(\mathbf{v}) - H_0\Delta t_{20}$ showing once more a linear correction in H_0. It is clear from our previous discussion that the linear term in H_0 originates from the analogous term in the one-way redshift.

We now want to show that such linear corrections in H_0 are a peculiarity of the cosmological observer already in FLRW. This result then extends to the case of McVittie spacetime. A first hint of this fact is given by considering the simple case of de Sitter spacetime, and the Kodama observer field which, in the region of interest, is a timelike Killing vector field. The one way redshift is thus given by [49]

$$\frac{\omega_1}{\omega_0} = \frac{\sqrt{\alpha(R_0)}}{\sqrt{\alpha(R_1)}} = 1 + (R_1^2 - R_0^2)\frac{H_0^2}{2} + \mathcal{O}\left(H_0^4 R_1^4, H_0^4 R_2^4\right). \tag{19}$$

Note that the same expression holds in the case of SdS spacetime, where only the functional form of $\alpha(R)$ changes.

The previous expression shows that no contribution linear in H_0 appears while the leading corrections are proportional to H_0^2. The DDT ratio can be obtained in complete analogy to the previous case of the cosmological observer as

$$\frac{\omega_2}{\omega_0} = \left\{ 2\frac{1 - \beta^{\hat{\boldsymbol{k}}}_{\mathbf{u}_\mathrm{K}}(\mathbf{v})}{1 - \beta_{\mathbf{u}_\mathrm{K}}(\mathbf{v})^2} - 1 \right\}, \tag{20}$$

where we have used the fact that $\|\mathbf{u}_\mathrm{K}\|_{t=t_0}/\|\mathbf{u}_\mathrm{K}\|_{t=t_2} = 1$. This same argument extends straightforwardly to the case of SdS spacetime. Moreover, since SdS spacetime is a special case of the McVittie one, with $H' = 0$ (cf. eq. (22)), the argument should apply for the general case showing that the DDT ratio contains corrections at most quadratic in the Hubble parameter, which strongly limits the possibility to observe such effects. With little effort, the argument can be extended also to the rate of change of the DDT frequency, as is done in [B].

3.4. Differential acceleration & Expansion's effects estimate

An intuitive understanding of the differences between the observers considered can be gained through their proper acceleration in a weak field limit and the comparison to the Newtonian limit. The cosmological observer freely follows the Hubble flow, but accelerates against the gravitational pull of the central object. The spatial component of the 4-acceleration in the proper detector frame of the Kodama observer consists of the Newtonian gravitational acceleration due to a central mass m_0 at distance R, as well as

an inward acceleration that depends on the cosmological expansion. These terms result from the property of the Kodama observer to be located at a constant areal radius, which implies that it is accelerating against the gravitational effect of the cosmological expansion such that it will never join the Hubble flow.

To lowest non-trivial order, the radial proper acceleration of the Kodama observer in the corresponding proper detector frame becomes

$$\mathbf{a}_{\mathrm{K},R} = \frac{m_0}{R^2} - R(H^2(t) + H'(t))\,. \tag{21}$$

If the Kodama observer is realized and test matter is released by it, $\mathbf{a}_{\mathrm{K},R}$ is their differential acceleration. There exists an extended literature about the gravitational acceleration being proportional to H^2 due to the cosmological expansion and its local measurability [50, 51, 52, 53, 39, 54, 55, 56, 35].

By expanding all expressions to second order in HR, we can approximately diagonalize the McVittie metric in (11) by a redefinition of the time variable to obtain the line element

$$ds^2 \approx -\left(1 - \frac{2m_0}{R} - (H(t)^2 + H'(t))R^2\right)dt^2 + \left(1 + \frac{2m_0}{R} + H(t)^2R^2\right)dR^2 + R^2d\theta^2 + R^2\sin^2\theta d\phi^2 \tag{22}$$

in the weak field limit where $m_0/R \ll 1$, where we have also neglected terms proportional to $m_0H(t)^2R$ and $m_0H'(t)R$. Identifying the zero-component of the perturbation of the metric, with respect to the flat Minkowski metric, with a Newtonian potential, i.e. $g_{00} = -1 - 2\Phi = -1 + 2m_0G/(c^2R) + R^2(H^2 + H')/c^2$, leads to a gravitational redshift/time dilation proportional to $\Phi_{R=R_1} - \Phi_{R=R_0}$ for two observers located at R_1 and R_0.

The current value of the Hubble constant is $H_0 \sim 2.2 \times 10^{-18}\,\mathrm{s}^{-1}$ and that of the cosmological constant is $\Lambda = 3H_0^2\Omega_\Lambda/c^2 \sim 10^{-52}\ \mathrm{m}^{-2}$. Considering the ΛCDM model and neglecting the small contribution of radiation at present day, we obtain $H^2 + H' = (\Lambda c^2 - H_0^2)/2$, where we have taken into account that $\Omega_\Lambda + \Omega_m = 1$ in the ΛCDM model. If we consider the Sun as a central object, a relative clock accuracy of 10^{-19}, a spacecraft at a distance from the Sun comparable to the one of the Voyager 1, i.e., $R_1 \sim 23\times10^{12}$ m, a satellite at an earth like distance from the sun as the other observer, i.e., $R_2 \ll R_1$, and assuming precise knowledge of H_0^2, m_0 and R_2 from other measurements, we can push the bound to $|\Lambda| \lesssim 10^{-45}\,\mathrm{m}^{-2}$ or alternatively to $H_0^2 \lesssim 3 \times 10^{-29}\,\mathrm{s}^{-2}$, "only" seven orders of magnitude away from the currently accepted values. Considering a scaling of the clock uncertainty with the inverse of the square root of the averaging time [36] and the fact that currently an averaging time of the order of 10^2 s is needed to reach an uncertainty of the order of 10^{-19}, we see that to fill the six orders of magnitude gap would require around 10^6 years of integration time. It is thus clear that further advances in clock accuracy are needed to be able to assess cosmological quantities in this kind of local experiments.

4. Optical solitons in curved spacetimes

The properties of light propagating in optical media is a subject as old as optics itself. In recent years, the possibility to engineer novel metamaterials has opened the door to the so-called transformation optics [57], a field promising to enhance existing devices and create novel ones. At the basis of this revolution is the fact that, in the geometric optics limit – and neglecting dispersion –, light rays propagate in media following the geodesics of an effective Lorentzian metric, the so-called optical metric [10]. This has also led to the investigation of light in optical media as an analogue gravity model, i.e., a model in which field perturbations propagate *as if* in a curved spacetime background, particularly useful in the investigation of kinematic effects of quantum field theory in curved spacetime, like the Hawking radiation and cosmological particle production [58, 59, 60]. When also the effect of dispersion is considered, the metric description can be cast aside for a more powerful Hamiltonian formalism, giving rise to the so-called ray-optical structures [61, 62].

This analogy between optical media and curved spacetimes can be pushed even further by showing that Maxwell equations in vacuum, curved spacetime are equivalent to flat-spacetime Maxwell equations in the presence of a bi-anisotropic moving medium whose dielectric permittivity and magnetic permeability are determined entirely by the spacetime metric [63]. Spacetime itself can then be described as an optical medium at the level of full electromagnetism. It is then natural to wonder what would happen if light were to propagate in an optical medium placed in a curved spacetime. Far from being a far-fetched situation, this is exactly the case for light propagating in media on Earth due to the non-vanishing, albeit weak, gravitational field of our planet. In this work, we are interested in exactly this situation. In particular, while at the geometric optics level the formalism of ray-optical structures can be used, we aim here at a description, analogous to the one in [63], at the level of full Maxwell equations. Indeed, such a description allows for the modelling of the propagation of intense pulses in situations of physical interest, like soliton propagation in optical fibers, taking into account the effect of a weak gravitational field.

We show that light propagation in a medium in curved spacetime is equivalent to propagation in an effective medium in flat spacetime. We then use this formalism to investigate the propagation of intense light pulses in non-linear media, giving rise to optical solitons. Solitons, and more in general propagating pulses, in optical fibers are at the basis of several communication protocols. Given that fibers on Earth are *de facto* in a curved spacetime due to our planet's gravitational field, it is relevant to analyze how gravity influences light-pulses propagation. Our result allows us to set up a framework for the analysis of the effect of acceleration and curvature on the propagation of pulses in optical fibers in curved spacetimes. We numerically investigate some of these effects for the simple case of 1D propagation in the weak-field limit.

4.1. An effective "spacetime medium"

While light in media can propagate as in a curved spacetime, curved spacetime can also be seen as an effective medium with non-trivial permeability and permittivity [63, 64]. It is not difficult to generalize the derivations in [63, 64] to the case in which light propagates in an optical medium placed in curved spacetime. Also in this case it can be shown that Maxwell's equations are equivalent to Maxwell's equations in flat spacetime for an effective medium whose properties encode both the ones of the physical medium and of curved spacetime.

Indeed, consider a dielectric and permeable medium in curved spacetime characterized by a Lorentzian metric $g_{\mu\nu}$ with mostly plus signature. We follow here the notation of [62], also reported in the Supplemental Material of our manuscript [C]. Maxwell's equations in the absence of free charges and currents are given by

$$\nabla_k F^{*ik} = 0 \tag{23}$$

$$\nabla_k G^{ik} = 0, \tag{24}$$

where F^* is the Hodge dual of the electromagnetic tensor F, and G and F are related by the constitutive equations of the material. Choosing an observer field u^i, the electric and magnetic field strengths can be defined with respect to it as

$$B_a = -\frac{1}{2}\eta_{abcd}u^b F^{cd};\ E_i = F_{ij}u^j \tag{25}$$

$$H_a = -\frac{1}{2}\eta_{abcd}u^b G^{cd};\ D_i = G_{ij}u^j \tag{26}$$

$$F_{ab} = -\eta^{cd}_{ab}u_d B_c + 2u_{[a}E_{b]} \tag{27}$$

$$G_{ab} = -\eta^{cd}_{ab}u_d H_c + 2u_{[a}D_{b]}, \tag{28}$$

in the reference frame of the observer in which the medium is assumed to be at rest. Here $\eta_{ijkl} = \sqrt{-g}\delta_{ijkl}$ is the Levi-Civita tensor and $T_{[abc\ldots]}$ denotes the antisymmetrization of the tensor with respect to the indices in square brackets.

As discussed in [C], choosing $u^i = \delta^i_0/\sqrt{-g_{00}}$, the projection of Maxwell's equations in 3-dimensional form leads to

$$\delta^{\alpha\beta\gamma}\partial_\beta \mathcal{H}_\gamma - \partial_0 \mathcal{D}^\alpha = 0;\ \partial_l \mathcal{D}^l = 0 \tag{29}$$

$$\delta^{\alpha\beta\gamma}\partial_\beta \mathcal{E}_\gamma + \partial_0 \mathcal{B}^\alpha = 0;\ \partial_l \mathcal{B}^l = 0, \tag{30}$$

where $\mathcal{E}_\alpha = \sqrt{-g_{00}}E_\alpha$, $\mathcal{H}_\alpha = \sqrt{-g_{00}}H_\alpha$, and

$$\mathcal{D}^\alpha = -\sqrt{-g}\frac{g^{\alpha\beta}}{g_{00}}\mathfrak{D}_\beta - \delta^{\alpha\beta\gamma}\frac{g_{0\gamma}}{g_{00}}\mathcal{H}_\beta \tag{31}$$

$$\mathcal{B}^\alpha = -\sqrt{-g}\frac{g^{\alpha\beta}}{g_{00}}\mathfrak{B}_\beta + \delta^{\alpha\beta\gamma}\frac{g_{0\gamma}}{g_{00}}\mathcal{E}_\beta, \tag{32}$$

with $\mathfrak{B}_\alpha = \sqrt{-g_{00}}B_\alpha$, and $\mathfrak{D}_\alpha = \sqrt{-g_{00}}D_\alpha$. These expressions are equivalent to Maxwell's equations in flat spacetime in the presence of an optical medium. In particular, for a non-dispersive medium characterized by constitutive relations $D_a = \varepsilon^b_a E_b$,

and $B_a = \mu_a^b H_b$, the effective medium will be characterized by a dielectric and magnetic permeability given by the product of the material ones and the ones characterizing the curved spacetime [63, 64]. Indeed, expressing $\mathcal{D}^\alpha = \tilde{\varepsilon}^{\alpha\beta}\mathcal{E}_\beta + \tilde{\gamma}^\beta_\alpha \mathcal{H}_\beta$ and correspondingly $\mathcal{B}^\alpha = \tilde{\mu}^{\alpha\beta}\mathcal{H}_\beta - \tilde{\gamma}^\beta_\alpha \mathcal{E}_\beta$, where $\tilde{\gamma}^\beta_\alpha$ encode magnetoelectric effects, we see that

$$\tilde{\mu}^{\alpha\beta} = -\sqrt{-g}\frac{g^{\alpha\gamma}}{g_{00}}\mu_\gamma^{\ \beta} \tag{33}$$

$$\tilde{\varepsilon}^{\alpha\beta} = -\sqrt{-g}\frac{g^{\alpha\gamma}}{g_{00}}\varepsilon_\gamma^{\ \beta}, \tag{34}$$

and $\tilde{\gamma}^{\alpha\beta} = -\delta^{\alpha\beta\gamma} g_{0\gamma}/{g_{00}}^3$. As a direct consequence, whenever the refractive index of the *effective medium* can be defined, it will also be the product of the material refractive index times the vacuum spacetime effective one. The same result can be easily obtained at the level of geometric optics.

Finally, we make two observations relevant for the study of the propagation of light pulses. Firstly, a non-magnetic material in curved spacetime corresponds to a magnetic effective medium in Minkowski due to the "magnetic permeability" of the background spacetime. Secondly, when considering a non-linear material, we see that the non-linearity will also be affected by the curvature of spacetime as well as the linear polarizability.

4.2. Pulse propagation: Non-linear Schrödinger equation

We next consider the propagation of light pulses in a Kerr non-linear, non-magnetic material in curved spacetime. In particular, we focus on the case in which the material is in a stationary orbit of Schwarzschild spacetime and use isotropic coordinates. This situation well-captures the cases of interest for optical communication and laboratory experiments like, e.g., optical fibers hanging still above Earth's surface.

In flat spacetime, the non-linear Schrödinger equation (NLSE) is often used when considering the propagation of light pulses whose amplitude is well-described by a scalar envelope slowly varying with respect to the light period and wavelength [65, 66]. In the case of a medium stationary in Schwarzschild' spacetime, by employing the correspondence with an *effective medium* in flat spacetime as described in the previous section, the usual derivation of the NLSE can be carried out. However, the effective medium will be inhomogeneous due to the curved spacetime contribution to the polarizability and permeability of the material medium. This gives rise to extra terms in the NLSE which are of purely gravitational origin. Furthermore, another source of inhomogeneity in the medium can be included when considering the effect of tidal forces on the material that, through photoelasticity, render the refractive index position-dependent.

Neglecting for the moment photoelasticity, i.e., considering a rigid dielectric, we can write Maxwell's equation in flat spacetime for the effective medium in the familiar notation, using the fields and field strengths that we indicate with plain capital letters from

[3]Note that, in the case the material itself possesses magnetoelectric terms in the constitutive equations, i.e., $D_a = \varepsilon_a^b E_b + \gamma_a^b H_b$, and $B_a = \mu_a^b H_b - \gamma_a^b E_b$ then $\tilde{\gamma}^{\alpha\beta} = -\delta^{\alpha\beta\gamma}\frac{g_{0\gamma}}{g_{00}} - \sqrt{-g}\frac{g^{\alpha\delta}}{g_{00}}\gamma_\delta^\beta$

now on,

$$\nabla \cdot B = 0,\ \nabla \cdot D = 0 \tag{35}$$

$$\nabla \times E = -\partial_t B,\ \nabla \times H = \partial_t D, \tag{36}$$

where $D = \tilde{\varepsilon} E$ and $H = B/\tilde{\mu}$. Here $\tilde{\mu} = \tilde{\mu}(r)$ and $\tilde{\varepsilon} = \tilde{\varepsilon}(E, r, \omega)$ in frequency space, allowing us to account for the effect of material dispersion, are the permeability and permittivity of the effective medium. Expressing the Schwarzschild' spacetime metric in isotropic coordinates as $ds^2 = -\left(B(t,r)/A(t,r)\right)^2 dt^2 + A^4(t,r)\delta_{\alpha\beta}dx^\alpha dx^\beta$, with $A(r) = 1 + r_S/4r$ and $B(r) = 1 - r_S/4r$, with r_S the Schwarzschild radius, we have

$$\tilde{\varepsilon}(E, r, \omega) = \varepsilon_0 \varepsilon_{sp} \varepsilon = \varepsilon_0 \frac{A(r)^3}{B(r)} \left(1 + \chi^{(1)}(\omega) + 3\chi^{(3)} \frac{|E|^2}{\Omega}\right), \tag{37}$$

$$\tilde{\mu} = \tilde{\mu}(r) = \mu_0 \mu_{sp} = \mu_0 A(r)^3 B(r)^{-1}, \tag{38}$$

with $\Omega = A(r)^{-4}$ the conformal factor relating the spacial part of the metric with the flat, Euclidean one[4]. The explicit radial dependence in the linear part of these effective quantities comes from the curved spacetime optical properties encoded in the diagonal terms $\sqrt{-g}g^{\alpha\alpha}/g_{00}$ (cf. eq.(33)) that we define as $\varepsilon_{sp} = \mu_{sp} = A(r)^3 B(r)^{-1}$. The field dependency of $\tilde{\varepsilon}$ takes into account the non-linearity of the physical medium. Note also that dispersion implies that the dielectric permeability is a function of the physical frequency ω defined with respect to our stationary observer u^μ.

From eq. (35), and writing $D = \tilde{\varepsilon}_\ell E + P_{\mathrm{NL}}$, where $\tilde{\varepsilon}_\ell = \varepsilon_0 \varepsilon_{sp}(1 + \chi^{(1)}(\omega))$ is the linear part of the dielectric permeability in eq. (37) and P_{NL} is the non-linear polarization, we can then obtain the wave equation, in frequency space,

$$\nabla^2 E - \nabla(\nabla \cdot E) + \tilde{\mu}\tilde{\varepsilon}_\ell \nu^2 E = -\tilde{\mu}\nu^2 P_{\mathrm{NL}} - (\nabla \log(\mu_{sp})) \times (\nabla \times E)\,. \tag{39}$$

Here we indicate with ν the conjugate variable to the coordinate time t in the flat spacetime of the effective medium. Note that the homogeneous Maxwell equations imply that

$$\nabla \cdot E = -(\nabla \log \tilde{\varepsilon}_\ell) \cdot E - \frac{1}{\tilde{\varepsilon}_\ell} \nabla \cdot P_{\mathrm{NL}}, \tag{40}$$

and thus

$$\begin{aligned} -\nabla(\nabla \cdot E) = {} & (E \cdot \nabla)\nabla \log \tilde{\varepsilon}_\ell + ((\nabla \log \tilde{\varepsilon}_\ell) \cdot \nabla) E \\ & + (\nabla \log \tilde{\varepsilon}_\ell) \times (\nabla \times E) + \nabla \left(\frac{1}{\tilde{\varepsilon}_\ell}(\nabla \cdot P_{\mathrm{NL}})\right). \end{aligned} \tag{41}$$

Eq. (40) makes evident that $\nabla \cdot E$ is of the same order as the non-linearities and inhomogeneities in the electric permittivity, which is also why it is usually safely neglected in derivations of the NLSE.

[4]This conformal factor arises due to the fact that $E^a E_a$ in curved spacetime corresponds to $|E|^2/\Omega$ with $|E|^2 = E^a E^b \delta_{ab}$ the flat spacetime norm squared of the electric strength field.

The wave equation in eq. (39) is equivalent to Maxwell equations and, as such, presents the same level of complexity if analytical or numerical solutions are attempted. The NLSE is a scalar propagation equation for the electric field's slowly varying amplitude that allows one to numerically simulate the pulse propagation. We thus want to write the electric field as the product of a slowly varying amplitude times a phase propagating along the propagation direction, that we will identify with the z direction in the following. In this context, notice that the dispersion relation of the physical medium, in its rest frame, is given simply by $n(\omega) = c\kappa/\omega$, with κ the modulus of the spatial projection of the wave 4-vector. For the effective medium, this relation reads $\tilde{n} = c\tilde{\kappa}/\nu$, where $\tilde{n} = \sqrt{\varepsilon_{sp}\mu_{sp}}n$ is the product of the material refractive index and the "spacetime refractive index" $n_{sp} = \sqrt{\varepsilon_{sp}\mu_{sp}}$. Moreover, since ν is the frequency defined with respect to Minkowski coordinate time, i.e., the conjugate Fourier variable to t, it is related to the physical frequency, i.e., the one measured by a physical observer in curved spacetime, by the gravitational redshift $\nu = \omega\sqrt{-g_{00}}$. From the equivalence of the dispersion relations, we see that $\tilde{\kappa}(r) = \kappa n_{sp}(r)\sqrt{-g_{00}(r)}$. We will thus write $E(\mathbf{r}, t) \propto \mathcal{E}(\mathbf{r})e^{i(\tilde{\kappa}_0 z - \nu_0 t)} + cc.$, with $\tilde{\kappa}_0 = \tilde{\kappa}(r, \nu_0)$ evaluated at a central frequency ν_0.

In order to proceed with the derivation of the NLSE, and to further simplify our equations, we consider two separate situations of physical interest: (i) pulse propagation at approximately constant radius; (ii) pulse propagating radially.

4.2.1. Horizontal motion at (almost) constant radius

We assume the propagation direction of the light pulse to be the z axis taken to be perpendicular to the radial direction for horizontal motion (as is portrayed in case (i) of figure 6), and consider linearly polarized light propagating in a medium stationary on Earth for concreteness. Then, for propagation distances much smaller than Earth's radius ($r_\oplus$), i.e., $z \ll r_\oplus$, the horizontal motion can be considered as happening at a constant radius. With these approximations, the spacetime permeability and permittivity are constant functions of $r_\oplus$, $\mu_{sp} = \varepsilon_{sp} = A(r_\oplus)^3 B(r_\oplus)^{-1}$ and also the physical frequency is not changing with z. Thus, we see that in eq. (39) the last term on the right-hand side vanishes. We follow the derivation in [59] where the pulse propagation in a single-mode optical fiber was considered. Indeed, for $\mu_{sp}\,\varepsilon_{sp}$ constant, eq. (39) is formally equivalent to eq. (S1) of [59] in frequency space. We thus end up with an effective one dimensional problem for the slowly varying envelope, and the derivation of the NLSE is the textbook one [66]. In particular, recall that the slowly varying envelope approximation(s) (SVEA) consists in neglecting terms $\partial_z^2\mathcal{E} \ll \tilde{\kappa}_0\partial_z\mathcal{E}$ and $(\tilde{\kappa}_1/\tilde{\kappa}_0)\partial_t \ll 1$ on the basis that the envelope will contain many wavelengths and optical cycles. If we apply now the SVEA we end up with, in the time domain,

$$i(\partial_z + \tilde{\kappa}_1\partial_t)\mathcal{E} - \frac{\tilde{\kappa}_2}{2}\partial_t^2\mathcal{E} = -n_2\nu_0 n_{sp}(r_\oplus)\varepsilon_0\frac{|\mathcal{E}|^2}{\Omega}\mathcal{E}, \tag{42}$$

where $\tilde{\kappa}_i(\nu_0)$ are the coefficients of the power series expansion $\tilde{\kappa}(\nu) = \sum_n \tilde{\kappa}_n(\nu_0)/n!\,(\nu - \nu_0)^n$ in $\nu - \nu_0$ and we are considering Kerr non-linear media for which the nonlinear index is $n_2 = 3\chi^{(3)}/(2n(\omega_0)c\varepsilon_0)$.

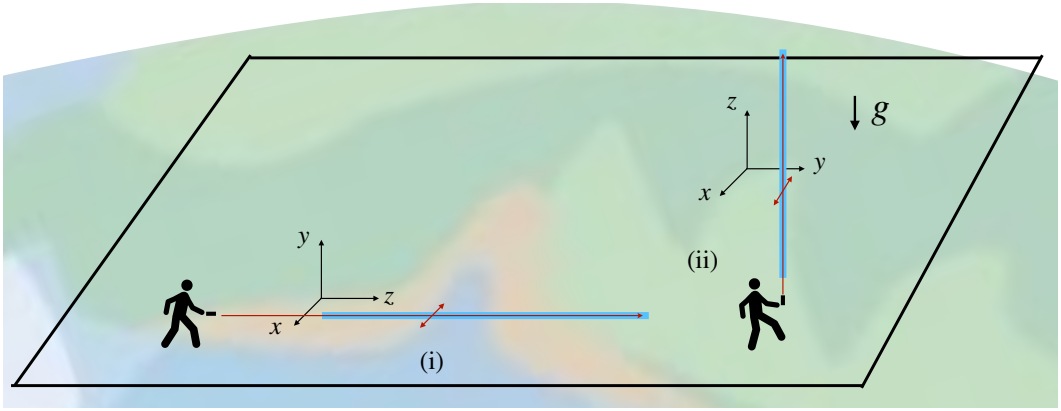

Figure 6: Geometry of the problem. The two cases considered are labelled by (i) and (ii). In (i), the light pulse propagates in a horizontal fiber positioned at $r_\oplus = r \sim$ constant. In (ii), the light pulse propagates in a vertically positioned fiber.

Considering an anomalous dispersive material, i.e., $\kappa_2(\nu_0) < 0$, an analytical solution of the NLSE can be found (see, e.g., [59]) and reads

$$\mathcal{E}(t,z) = \sqrt{\frac{\Omega|\tilde{\kappa}_2|}{\nu_0 n_2 n_{sp} \varepsilon_0 T_0^2}} \cosh\left(\frac{t-\tilde{\kappa}_1 z}{T_0}\right)^{-1} \exp\left(\frac{iz|\tilde{\kappa}_2|}{2T_0^2}\right), \tag{43}$$

where T_0 is the pulse length, and $1/\tilde{\kappa}_1$ is its speed of propagation. This reduces to the result from Philbin et al.[59] – eq.(S74) of the supplementary material in [59] – in the limit of $r_S \to 0$. From this expression, combined with the fact that $\tilde{\kappa}_1(\nu_0) = n_{sp}\kappa_1(\omega_0)$, we can conclude that the velocity of the horizontally propagating soliton in curved spacetime with respect to an observer comoving with the segment of the dielectric material[5] is given simply by $\kappa_1(\omega_0)^{-1}$.

4.2.2. Radial motion

Let us now consider the case in which the light pulse propagates radially along the z direction, as is portrayed in case (ii) of figure 6. Care is in order here, since now all the quantities appearing in the wave equation will change along the propagation direction, including the physical frequency that will be subject to gravitational redshift. Motivated by the symmetry of the problem, and in order to obtain a scalar, one-dimensional equation whose solution can be simulated, we assume that all the quantities entering the wave equation depend solely on z. This is tantamount to identifying the radial direction with the z-axis and work close to $x = y = 0$ so that $r = r_\oplus + z$, which is a reasonable assumption since we are considering the vertical propagation of a well localized pulse. With this approximation, the wave equations (39) reduce to a system of three decoupled

[5]Indeed note that proper length and proper time for an observer comoving with the segment of the dielectric material and in connection with coordinate quantities are given by $\ell = A^2\, z$ and $\tau = t\, B/A$ so that $v \equiv \ell/\tau = A^3 B^{-1} z/t = n_{sp}\tilde{v}$.

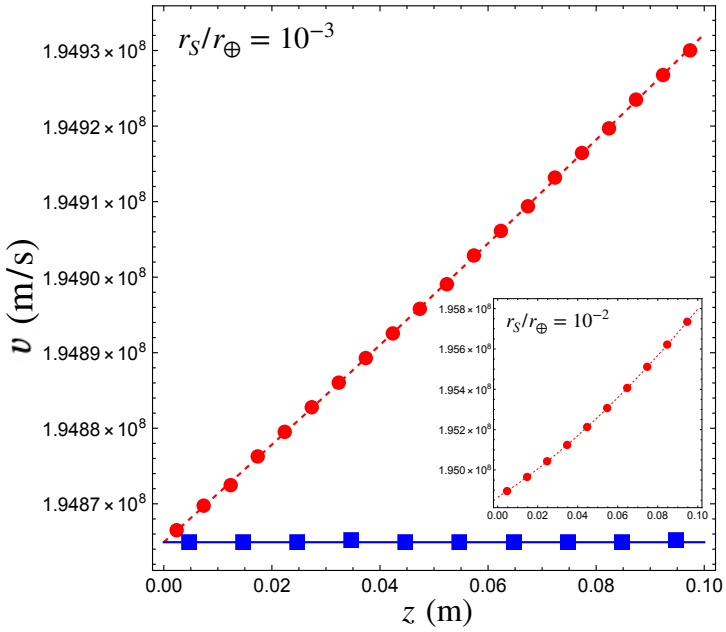

Figure 7: Velocity of the soliton along the fiber, with respect to an observer comoving with the segment of the dielectric material where the (peak of the) soliton is located, for $L = 0.1\,\mathrm{m}$, $r_s = 10^{-3} r_\oplus$, and including photoelasticity. The red, dashed and blue, solid curves represent the analytical expression in eq. (47) including or in the absence, respectively, of photoelasticity. The red points and blue squares are obtained by numerical simulations and agrees perfectly with the analytical formula of eq. (47). The inset shows the case with photoelasticity in which $r_s = 10^{-2} r_\oplus$. This shows a deviation from a purely linear relation between the velocity and the propagation distance.

equations [67]

$$\partial_z^2 E_{x(y)} + \tilde{\mu}\tilde{\varepsilon}_\ell \nu^2 E_{x(y)} = -\,\tilde{\mu}\nu^2 P_{\mathrm{NL},x(y)} + \left(\partial_z(\ln\tilde{\mu})\right)\partial_z E_{x(y)} \tag{44}$$

$$\partial_z^2 E_z + \tilde{\mu}\tilde{\varepsilon}_\ell \nu^2 E_z = -\,\tilde{\mu}\nu^2 P_{\mathrm{NL},z} - \partial_z\left(\frac{1}{\tilde{\varepsilon}_\ell}\partial_z P_{\mathrm{NL},z}\right) - 2(\partial_z \ln\tilde{\varepsilon}_\ell)\partial_z E_z - E_z\partial_z^2 \ln\tilde{\varepsilon}_\ell \tag{45}$$

It is immediate to realize that $E_z = 0$ is a solution of the corresponding equation so that we can consider the propagation of linearly polarized light (in a direction orthogonal to z) and we end up with a single equation of the form of eq. (44).

Proceeding as before with substituting the ansatz $E(z,t) \propto \mathcal{E}(z,t)e^{i(\tilde{\kappa}_0(z)z - \nu_0 t)} + cc.$, expanding $\tilde{\kappa}(z,\nu)$ around ν_0, and using the SVEA approximation(s) we obtain the NLSE given by

$$i(\partial_z + \tilde{\kappa}_1\partial_t)\mathcal{E} - \frac{\tilde{\kappa}_2}{2}\partial_t^2\mathcal{E} + 2i\frac{\partial_z\tilde{\kappa}_0}{2\tilde{\kappa}_0}\mathcal{E} + 2iz\frac{\partial_z\tilde{\kappa}_0}{2\tilde{\kappa}_0}\partial_z\mathcal{E} + iz\frac{\partial_z^2\tilde{\kappa}_0}{2\tilde{\kappa}_0}\mathcal{E} - z\partial_z\tilde{\kappa}_0\mathcal{E} - z^2\frac{(\partial_z\tilde{\kappa}_0)^2}{2\tilde{\kappa}_0}\mathcal{E}$$
$$= -n_2\nu_0 n_{sp}(r)\varepsilon_0|\mathcal{E}|^2\mathcal{E}/\Omega + \frac{\partial_z \ln n_{sp}}{2\tilde{\kappa}_0}\left(i\tilde{\kappa}_0\mathcal{E} + \partial_z\mathcal{E} + iz(\partial_z\tilde{\kappa}_0)\mathcal{E}\right). \tag{46}$$

Eq. (46) contains several additional terms with respect to the equation for the horizontal propagation due to the fact that now the wavevector $\tilde{\kappa}_0$ depends explicitly on the coordinate along the propagation direction and so does the refractive index, i.e., we are propagating in a gradient-index medium (GRIN)[6]. All geometrical quantities appearing in the equation are evaluated at $r_\oplus + z$. Finally, consistently with the horizontal propagation case, upon setting $\tilde{\kappa}_0$ constant, we return to eq. (42).

4.3. Including photoelasticity

Up until now, we have considered rigid dielectrics, i.e., dielectric media in which the speed of sound is infinite. For realistic materials, this is of course never the case and the dielectric gets deformed by the action of forces, including the tidal ones in our set-up. Let us consider an optical fiber as a paradigmatic example. In this case, the deformation due to the action of gravity will be relevant only for the case of vertical propagation.

Deformations of a dielectric lead to a change in the relative permeability of the material, and thus of the refractive index, a phenomenon known as photoelasticity [71]. The contributions to this effect coming from the curvature of spacetime and the inertial acceleration of the fiber can be separately accounted for following the discussion in [47]. Consider a fiber of length L hanging from at support located at $r_\oplus + L$. As far as the strain is within the elastic limit of the material, we can relate it with the stresses through a linear relation, i.e., Hooke's law. Thus, we write the strain tensor as $\mathcal{S}_{kl} = \frac{1}{Y}\sigma_{kl}$, where Y is the Young's modulus of the material and $\sigma_{kl} = \frac{F_k}{A_l}$ is the stress tensor given by the ratio between the force F_k in direction $\hat{e}_k$ and the cross-sectional area A_l normal to $\hat{e}_l$ upon which the force acts. The photoelastic (or acousto-optic) effect consists in the change of the relative electric permeability by $\Delta(\boldsymbol{\varepsilon}_r)^{-1}_{kl} = \mathcal{P}_{kl\,mn}\mathcal{S}_{mn}$, where $\mathcal{P}$ is the photoelastic tensor. In the following, we limit ourselves to the case of isotropic materials and a diagonal stress tensor (see [C] for the details of the computation). It should be noted that photoelasticity is far from negligible in the case under investigation and becomes the dominant effect in the vertical propagation scenario, overwhelming the effect related to the optical properties of the background spacetime.

While photoelasticity introduces a further radial dependence in the optical properties of the effective medium, this does not affect the form of eq. (46), which remains valid. The only difference is in the expressions for the quantities $\tilde{\kappa}_i$ and their derivatives, due to the fact that now the refractive index of the medium is given by $n(\omega) = \sqrt{1 + \chi_1(\omega) + \Delta\varepsilon_r(\omega)}$.

[6] See also [68, 69, 70] for early studies of soliton propagation in inhomogeneous media.

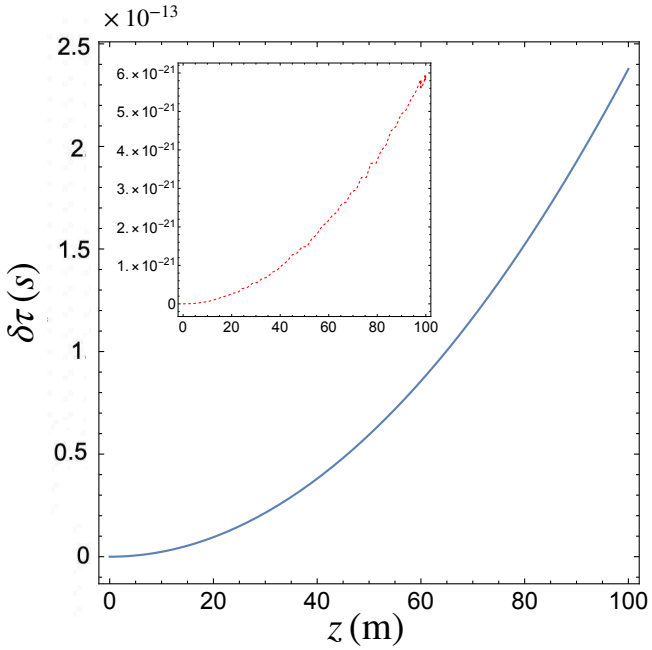

Figure 8: Time of arrival of the soliton for the case of propagation in the gravitational field of Earth for which we assume $r_S = 9 \times 10^{-3}\,\mathrm{m}$. The main figure shows the difference in time of arrival, with respect to an observer comoving with the segment of the dielectric material where the soliton is located, between vertically and horizontally propagating solitons over the propagation coordinate length z. The inset shows the same in the case photoelasticity is neglected.

4.4. Numerical results

While the wave equation in eq. (39) gives us the full Maxwell equations, including possibly interesting effects related to the vectorial nature of the electric field, and thus to the interplay between gravity and the light polarization, its numerical investigation is beyond the scope of the current work, and it is left for future investigations. Here, we focus on the propagation of light pulses as described by the simplified eq.(46), motivated by light propagation in optical fibers [59]. Note that in the case of eq. (42) an analytical solution was presented in eq. (43).

Equation (46) for the vertical propagation is solved numerically – being a non-linear PDE with coordinate dependent coefficients – using the split-step Fourier (SSF) method [65] and taking into account also the effect of the fiber deformation. For this purpose, we utilize the same fiber parameters as in [59] and initialize the temporal profile at $z = 0$ as the one of the input pulse in the same reference.

The intuition based on the SSF method– where the propagation equation (46) is rewritten in the form $\partial_z \mathcal{E} = \left(\hat{D} + \hat{N}\right)\mathcal{E}$ with the diffusive dynamics enclosed in the operator $\hat{D} = \hat{D}(z, \partial_t)$ – allows us to formulate the educated guess that the propagation

speed of the soliton, in the effective flat spacetime, is given by

$$\tilde{v} = \frac{1 + z\,\tilde{\kappa}_0'(z)/\tilde{\kappa}_0(z)}{\tilde{\kappa}_1(z)}. \tag{47}$$

Indeed, this appears as (the real part of) the inverse of the coefficient of the time derivative in $\hat{D}(z, \partial_t)$. Then, in order to translate this result into the speed measured by an observer comoving with the segment of the dielectric material where the soliton peak is located, we need to just multiply eq. (47) by the spacetime refractive index. That this intuition is indeed correct is verified by the numerical simulations reported in Fig. 7.

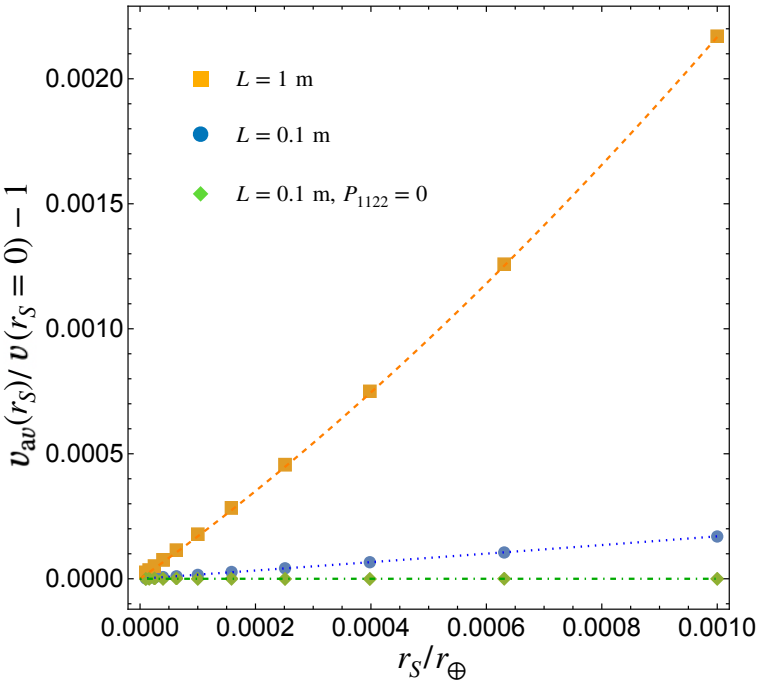

Figure 9: Change in average velocity (v_{av}) of the soliton in the fiber – with respect to the observer comoving with the dielectric – compared to the case with $r_S = 0$. Orange, square points correspond to the case of a $L = 1\,\mathrm{m}$ propagation with photoelasticity. Blue, round points correspond to the case of a $L = 0.1\,\mathrm{m}$ propagation with photoelasticity. Green, diamonds correspond to the case of a $L = 0.1\,\mathrm{m}$ propagation without photoelasticity. The lines correspond to the analytical result that fits perfectly the different sets of data.

We see that the z-dependence of the propagation velocity is strongly enhanced by the effects of mechanical deformation of the fiber with respect to the case in which photoelasticity is ignored. The z-dependence of the vertical propagation velocity without photoelasticity is weak, and the velocity is close to the one of the horizontal case. To quantify the latter statement, in Fig. 8 we show the difference in the (proper) time of arrival of the soliton for the case of propagation in the gravitational field of Earth, corresponding to a Schwarzschild radius that we take as $r_S = 9 \times 10^{-3}$ m. The main

figure shows

$$\delta\tau = |z(\sqrt{-g_{00}(r_\oplus + z)}\tilde{v}_\uparrow^{-1}) - \sqrt{-g_{00}(r_\oplus)}\tilde{v}_\rightarrow^{-1})|, \tag{48}$$

with $\tilde{v}_\uparrow$ and $\tilde{v}_\rightarrow$ the propagation velocities, in the effective flat spacetime, for vertical and horizontal propagation. The inset shows instead the case in which for the vertical propagation the photoelasticity is neglected, showing a much weaker dependence.

Finally, in Fig. 9 we show the deviation of the average velocity along the vertical direction $v_{av}(r_S)$ with respect to the constant velocity at $r_S = 0$ as a function of the dimensionless ratio $r_S/r_\oplus$. The average velocity is obtained numerically from the simulations as the ratio of the total length L and the propagation time of the soliton and transformed into the frame of the observer comoving with the fiber at its upper end-point – i.e., multiplied by $n_{sp}(r_\oplus + L)$. Analytically, we use $v_{av} = (\int_0^L v\,\mathrm{d}z)/L$ with $v = n_{sp}\tilde{v}$ and $\tilde{v}$ given in eq. (47). Fig. 9 shows once again the agreement between the simulated data and our analytical ansatz and it also shows that the photoelasticity is the main effect that allows one to have a sizable difference between the flat and curved spacetime propagation.

Another quantity characterizing the propagating pulse is its temporal width. In the horizontal propagation case, the duration of the pulse is constant. The same is not, in general, true when considering the vertical propagation. In the Supplemental Material of [C], we report the evolution of the temporal width along the fiber. In particular, our simulations show a focusing of the pulse which is however sizable only in the presence of photoelasticity.

5. Conclusion and Outlook

In this thesis, we have investigated the deep interplay between light and gravity by looking at the former as both a rarely appreciated source and a tool for the investigation of gravity. Due to the mass-energy equivalence, light is bound to possess a gravitational field. In chapter 2, we studied the measurability of the gravitational field sourced by laser and particle beams. For different potential sources – going from high power lasers to ultrarelativistic particles – we theoretically investigated the fundamental limitations of measuring their gravitational near-field with resonant mass detectors. A simplified theoretical version of a Weber-bar, i.e., a deformable aluminium rod, turned out to be the least suitable detector for the man-made periodic signals we envisioned. Meanwhile, both the prototype of a liquid helium container acting as a Weber-bar [6] and the high Q-factor pendulum [7] are only a few orders of magnitude away from being able to measure the gravitational signal of the highest average power source, a hypothetical frequency-modulated adaptation of the LHC particle beam, within the somewhat reasonable time span of one week (considering a detector already at full resonant amplitude). Indeed, by optimizing a high-Q mechanical oscillator, compatible with the discussed pendulum [7], with respect to the signal-to-noise ratio, we showed that an S/N ratio close to one is possible to achieve within only one week of total experiment time. Moreover, planned future upgrades to the LHC and further degrees of freedom in the optimization have the potential to increase S/N ratio by more than one order of magnitude. The realization

that gravitational effects of ultrarelativistic particle beams could become measurable at some point in the future opens a possible new experimental window to quantum gravitational effects. Non-classical states can be envisioned both for laser and particle beam sources, for which theoretical predictions are not yet existent. In this regard, our results offer a starting point for these future explorations. They also furnish the basis for further investigations aiming at a more detailed design of suitable detectors as well as the analysis of potential sources of noise, e.g., seismic noise, and even considering off-resonant detection regimes [31].

While measuring the gravitational field of light and ultrarelativistic sources was the focus of the first part of the thesis. In the projects summarized in Chapter 3 and 4, we focus instead on novel ways to use light as a tool to probe the structure of spacetime. In the project summarized in chapter 3, we dealt with the effects of the cosmological expansion on frequency measurements of laser signals in local experiments. We showed that, within the models of McVittie and Schwarzschild - de Sitter spacetimes, both the frequency of a deformable cavity and double Doppler tracking experiments are influenced by the expansion. However, the influence of the cosmological expansion is only quadratic in the Hubble parameter. We have shown that this conclusion is valid for physically justified observers, like freely falling or nearly stationary ones. Linear effects are also found, in line with the existing literature, but they apply to the cosmological observer already following the Hubble flow. Despite the high degree of idealization in the modeling of the local gravitational environment we had to resort to, our considerations show that the expansion of the universe can affect local experiments. The detection of such an influence is shown to be to an extent still beyond today's experimental capabilities. Nevertheless, our results for the effects of the cosmological expansion in double Doppler tracking experiments show that they may provide a possible future independent test of cosmological expansion, thanks to the rapidly improving precision of frequency measurements. In this context, it would be interesting to further investigate the best configuration of physical observers and experiments able to elicit the strongest signal of cosmic expansion on local scales

In the last project, a summary of which can be found in chapter 4, we have considered the propagation of light pulses in non-linear, non-magnetic media stationary in curved spacetime. Taking some intuition from the seminal work of Plebanski [63], we showed that light propagation in such media and spacetimes can be equivalently described as the propagation in an effective medium in flat spacetime whose electric and magnetic properties acquire a multiplicative factor encoding the spacetime structure. By virtue of approximations, we can derive a scalar NLSE describing the propagation of a light pulse. It is important to notice that, when solving the NLSE employing the SSF method, we are implicitly considering a unidirectional equation and ignoring any possible back-propagating field in the boundary conditions imposed, for all times, at $z = 0$. This means that backscattered light from the pulse is assumed negligible relative to the pulse itself, a condition common to all unidirectional envelope propagation equations [72]. While this is not a problem for the horizontal propagation, in which case only the weak non-linearity could give rise to back-reflection, in the case of the vertical propagation light is effectively propagating in a gradient-index medium with

the refracting index slowly varying in the propagation direction. This by itself can give rise to back-propagating fields , and effectively limits the validity of our treatment to regimes in which the photoelasticity allows to employ a unidirectional equation. Luckily, the regime of validity of the equation – which depends on the parameter chosen for the physical medium – can be readily estimated by following the discussion in [73] as we detail in the supplementary material of [C]. Given these caveats, the NLSE that we have derived shows that an optical pulse propagating radially in a Kerr non-liner medium stationary in Schwarzschild spacetime experiences a change in its propagation velocity captured by eq. (47). This effect is mostly due to photoelasticity which overwhelms the purely spatiotemporal effects encoded in the multiplicative, effective, refractive index n_{sp}. The difference in propagation velocity between the vertically and horizontally propagating pulses results, in turn, in a difference of the time of arrival of two pulses of the order of hundreds of femtoseconds in Earth's gravitational field, a fact that puts this difference in the reach of current technologies (see [74, 75, 76] and references therein).

Bibliography

References

[1] R. C. Tolman, P. Ehrenfest, and B. Podolsky, "On the gravitational field produced by light," *Phys. Rev.*, vol. 37, pp. 602–615, Mar 1931.

[2] W. B. Bonnor, "The gravitational field of light," *Communications in Mathematical Physics*, vol. 13, no. 3, pp. 163–174, 1969.

[3] F. Schneiter, D. Rätzel, and D. Braun, "The gravitational field of a laser beam beyond the short wavelength approximation," *Classical and Quantum Gravity*, vol. 35, no. 19, p. 195007, 2018.

[4] F. Schneiter, D. Rätzel, and D. Braun, "Rotation of polarization in the gravitational field of a laser beam–Faraday effect and optical activity," *Classical and Quantum Gravity*, vol. 36, p. 205007, Sept. 2019.

[5] P. C. Aichelburg and R. U. Sexl, "On the gravitational field of a massless particle," *General Relativity and Gravitation*, vol. 2, no. 4, pp. 303–312, 1971.

[6] S. Singh, L. A. D. Lorenzo, I. Pikovski, and K. C. Schwab, "Detecting continuous gravitational waves with superfluid 4He," *New Journal of Physics*, vol. 19, p. 073023, July 2017.

[7] N. Matsumoto, S. B. Cataño-Lopez, M. Sugawara, S. Suzuki, N. Abe, K. Komori, Y. Michimura, Y. Aso, and K. Edamatsu, "Demonstration of displacement sensing of a mg-scale pendulum for mm- and mg-scale gravity measurements," *Physical review letters*, vol. 122, no. 7, p. 071101, 2019.

[8] N. Aghanim, Y. Akrami, M. Ashdown, J. Aumont, C. Baccigalupi, M. Ballardini, A. Banday, R. Barreiro, N. Bartolo, S. Basak, *et al.*, "Planck 2018 results-vi. cosmological parameters," *Astronomy & Astrophysics*, vol. 641, p. A6, 2020.

[9] A. Einstein and E. G. Straus, "The influence of the expansion of space on the gravitation fields surrounding the individual stars," *Rev. Mod. Phys.*, vol. 17, pp. 120–124, Apr 1945.

[10] W. Gordon, "Zur lichtfortpflanzung nach der relativitätstheorie," *Annalen der Physik*, vol. 377, no. 22, pp. 421–456, 1923.

[11] E. Berti, K. Yagi, and N. Yunes, "Extreme gravity tests with gravitational waves from compact binary coalescences:(I) inspiral–merger," *General Relativity and Gravitation*, vol. 50, no. 4, pp. 1–45, 2018.

[12] J. B. Jiménez, L. Heisenberg, G. J. Olmo, and D. Rubiera-Garcia, "Born–Infeld inspired modifications of gravity," *Physics Reports*, vol. 727, pp. 1–129, 2018.

[13] D. Langlois, R. Saito, D. Yamauchi, and K. Noui, "Scalar-tensor theories and modified gravity in the wake of GW170817," *Phys. Rev. D*, vol. 97, p. 061501, Mar 2018.

[14] C. Barceló, R. Carballo-Rubio, and L. J. Garay, "Gravitational wave echoes from macroscopic quantum gravity effects," *Journal of High Energy Physics*, vol. 2017, no. 5, p. 54, 2017.

[15] A. Maselli, P. Pani, V. Cardoso, T. Abdelsalhin, L. Gualtieri, and V. Ferrari, "Probing Planckian Corrections at the Horizon Scale with LISA Binaries," *Phys. Rev. Lett.*, vol. 120, p. 081101, Feb 2018.

[16] L. Grishchuk and M. Sazhin, "Emission of gravitational waves by an electromagnetic cavity," *JETP*, vol. 38, p. 215, 1974.

[17] L. Grishchuk and M. Sazhin, "Excitation and detection of standing gravitational waves," *JETP*, vol. 41, p. 787, 1975.

[18] L. P. Grishchuk, "Gravitational waves in the cosmos and the laboratory," *Soviet Physics Uspekhi*, vol. 20, p. 319, Apr. 1977.

[19] D. E. Cox, J. G. O'brien, R. L. Mallett, and C. Roychoudhuri, "Gravitational Faraday effect produced by a ring laser," *Foundations of Physics*, vol. 37, no. 4-5, pp. 723–733, 2007.

[20] M. O. Scully, "General-relativistic treatment of the gravitational coupling between laser beams," *Physical Review D*, vol. 19, no. 12, p. 3582, 1979.

[21] P. Ji, S.-T. Zhu, and W.-D. Shen, "Gravitational perturbation induced by an intense laser pulse," *International journal of theoretical physics*, vol. 37, no. 6, pp. 1779–1791, 1998.

[22] P. Ji and Y. Bai, "Gravitational effects induced by high-power lasers," *The European Physical Journal C-Particles and Fields*, vol. 46, no. 3, pp. 817–823, 2006.

[23] F. Schneiter, D. Rätzel, and D. Braun, "Corrigendum: The gravitational field of a laser beam beyond the short wavelength approximation (2018 Class. Quantum Grav. 35 195007)," *Classical and Quantum Gravity*, vol. 36, p. 119501, May 2019.

[24] H. Balasin and H. Nachbagauer, "Boosting the Kerr geometry in an arbitrary direction," *Classical and Quantum Gravity*, vol. 13, no. 4, p. 731, 1996.

[25] C. Lousto and N. Sánchez, "The curved shock wave space-time of ultrarelativistic charged particles and their scattering," *International Journal of Modern Physics A*, vol. 5, no. 05, pp. 915–938, 1990.

[26] C. Barrabes and P. Hogan, "Lightlike boost of the Kerr gravitational field," *Physical Review D*, vol. 67, no. 8, p. 084028, 2003.

[27] E. Sistrunk, D. Alessi, A. Bayramian, K. Chesnut, A. Erlandson, T. Galvin, D. Gibson, H. Nguyen, B. Reagan, K. Schaffers, *et al.*, "Laser technology development for high peak power lasers achieving kilowatt average power and beyond," in *Short-pulse High-energy Lasers and Ultrafast Optical Technologies*, vol. 11034, p. 1103407, International Society for Optics and Photonics, 2019.

[28] "IPG Laser GmbH." `https://www.ipgphotonics.com/de/products/lasers/high-power-cw-fiber-lasers`, 2022.

[29] M. Maggiore, *Gravitational waves: Volume 1: Theory and experiments*. Oxford university press, 2008.

[30] S. B. Cataño Lopez, J. G. Santiago-Condori, K. Edamatsu, and N. Matsumoto, "High-Q milligram-scale monolithic pendulum for quantum-limited gravity measurements," *Phys. Rev. Lett.*, vol. 124, p. 221102, Jun 2020.

[31] T. Westphal, H. Hepach, J. Pfaff, and M. Aspelmeyer, "Measurement of Gravitational Coupling between Millimeter-Sized Masses," *arXiv:2009.09546 [gr-qc]*, Sept. 2020.

[32] A. A. Clerk, M. H. Devoret, S. M. Girvin, F. Marquardt, and R. J. Schoelkopf, "Introduction to quantum noise, measurement, and amplification," *Reviews of Modern Physics*, vol. 82, no. 2, p. 1155, 2010.

[33] M. W. Krasny, A. Petrenko, and W. Placzek, "High-luminosity Large Hadron Collider with laser-cooled isoscalar ion beams," *Progress in Particle and Nuclear Physics*, vol. 114, p. 103792, Sept. 2020.

[34] A. Einstein and E. G. Straus, "Corrections and additional remarks to our paper: The influence of the expansion of space on the gravitation fields surrounding the individual stars," *Rev. Mod. Phys.*, vol. 18, pp. 148–149, Jan 1946.

[35] M. Carrera and D. Giulini, "Influence of global cosmological expansion on local dynamics and kinematics," *Rev. Mod. Phys.*, vol. 82, pp. 169–208, Jan 2010.

[36] A. D. Ludlow, M. M. Boyd, J. Ye, E. Peik, and P. O. Schmidt, "Optical atomic clocks," *Rev. Mod. Phys.*, vol. 87, pp. 637–701, Jun 2015.

[37] G. C. McVittie, "The mass-particle in an expanding universe," *Monthly Notices of the Royal Astronomical Society*, vol. 93, pp. 325–339, 1933.

[38] J. Islam, "The cosmological constant and classical tests of general relativity," *Physics Letters A*, vol. 97, no. 6, pp. 239–241, 1983.

[39] M. Axenides, E. Floratos, and L. Perivolaropoulos, "Some dynamical effects of the cosmological constant," *Modern Physics Letters A*, vol. 15, no. 25, pp. 1541–1550, 2000.

[40] V. Kagramanova, J. Kunz, and C. Lämmerzahl, "Solar system effects in Schwarzschild–de Sitter space–time," *Physics Letters B*, vol. 634, no. 5-6, pp. 465–470, 2006.

[41] C. Lammerzahl, O. Preuss, and H. Dittus, "Is the physics within the solar system really understood?," in *Lasers, Clocks and Drag-Free Control*, pp. 75–101, Springer, 2008.

[42] B. C. Nolan, "Particle and photon orbits in McVittie spacetimes," *Classical and Quantum Gravity*, vol. 31, no. 23, p. 235008, 2014.

[43] W.-T. Ni and M. Zimmermann, "Inertial and gravitational effects in the proper reference frame of an accelerated, rotating observer," *Phys. Rev. D*, vol. 17, pp. 1473–1476, Mar 1978.

[44] C. W. Misner, K. Thorne, J. Wheeler, and S. Chandrasekhar, "Gravitation," *Physics Today*, vol. 27, no. 8, p. 47, 1974.

[45] M. Carrera, *Geometrical methods for kinematics and dynamics in relativistic theories of gravity with applications to cosmology and space physics*. PhD thesis, Universität Freiburg, 2010.

[46] E. Hackmann and C. Lämmerzahl, "Geodesic equation in Schwarzschild-(anti-)de Sitter space-times: Analytical solutions and applications," *Phys. Rev. D*, vol. 78, p. 024035, Jul 2008.

[47] D. Rätzel, F. Schneiter, D. Braun, T. Bravo, R. Howl, M. P. E. Lock, and Ivette Fuentes, "Frequency spectrum of an optical resonator in a curved spacetime," *New Journal of Physics*, vol. 20, no. 5, p. 053046, 2018.

[48] M. Carrera and D. Giulini, "On Doppler tracking in cosmological spacetimes," *Classical and Quantum Gravity*, vol. 23, no. 24, p. 7483, 2006.

[49] R. M. Wald, *General relativity*. University of Chicago press, 2010.

[50] R. Nandra, A. N. Lasenby, and M. P. Hobson, "The effect of an expanding universe on massive objects," *Monthly Notices of the Royal Astronomical Society*, vol. 422, no. 4, pp. 2945–2959, 2012.

[51] F. I. Cooperstock, V. Faraoni, and D. N. Vollick, "The influence of the cosmological expansion on local systems," *The Astrophysical Journal*, vol. 503, no. 1, p. 61, 1998.

[52] G. S. Adkins, J. McDonnell, and R. N. Fell, "Cosmological perturbations on local systems," *Physical Review D*, vol. 75, no. 6, p. 064011, 2007.

[53] R. H. Price and J. D. Romano, "In an expanding universe, what doesn't expand?," *American Journal of Physics*, vol. 80, no. 5, pp. 376–381, 2012.

[54] D. Giulini, "Does cosmological expansion affect local physics?," *Studies in History and Philosophy of Science Part B: Studies in History and Philosophy of Modern Physics*, vol. 46, pp. 24–37, 2014.

[55] K. Agatsuma, "The expansion of the universe in binary star systems," *Physics of the Dark Universe*, vol. 30, p. 100732, 2020.

[56] R. Nandra, A. N. Lasenby, and M. P. Hobson, "The effect of a massive object on an expanding universe," *Monthly Notices of the Royal Astronomical Society*, vol. 422, pp. 2931–2944, 05 2012.

[57] U. Leonhardt and T. G. Philbin, "Transformation optics and the geometry of light," in *Progress in optics*, vol. 53, pp. 69–152, Elsevier, 2009.

[58] C. Barceló, S. Liberati, and M. Visser, "Analogue gravity," *Living reviews in relativity*, vol. 14, no. 1, pp. 1–159, 2011.

[59] T. G. Philbin, C. Kuklewicz, S. Robertson, S. Hill, F. Konig, and U. Leonhardt, "Fiber-optical analog of the event horizon," *Science*, vol. 319, no. 5868, pp. 1367–1370, 2008.

[60] E. Rubino, F. Belgiorno, S. Cacciatori, M. Clerici, V. Gorini, G. Ortenzi, L. Rizzi, V. Sala, M. Kolesik, and D. Faccio, "Experimental evidence of analogue hawking radiation from ultrashort laser pulse filaments," *New Journal of Physics*, vol. 13, no. 8, p. 085005, 2011.

[61] J. Bicak and P. Hadrava, "General-relativistic radiative transfer theory in refractive and dispersive media.," *AAP*, vol. 44, pp. 389–399, Nov. 1975.

[62] V. Perlick, *Ray optics, Fermat's principle, and applications to general relativity*, vol. 61. Springer Science & Business Media, 2000.

[63] J. Plebanski, "Electromagnetic waves in gravitational fields," *Physical Review*, vol. 118, no. 5, p. 1396, 1960.

[64] F. de Felice, "On the gravitational field acting as an optical medium," *General Relativity and Gravitation*, vol. 2, no. 4, pp. 347–357, 1971.

[65] G. P. Agrawal, "Nonlinear fiber optics," in *Nonlinear Science at the Dawn of the 21st Century*, pp. 195–211, Springer, 2000.

[66] R. W. Boyd, *Nonlinear optics*. Academic press, 2020.

[67] S. Habib Mazharimousavi, A. Roozbeh, and M. Halilsoy, "Electromagnetic wave propagation through inhomogeneous material layers," *Journal of Electromagnetic Waves and Applications*, vol. 27, no. 16, pp. 2065–2074, 2013.

[68] H.-H. Chen and C.-S. Liu, "Solitons in nonuniform media," *Phys. Rev. Lett.*, vol. 37, pp. 693–697, Sep 1976.

[69] H. Chen and C.-S. Liu, "Nonlinear wave and soliton propagation in media with arbitrary inhomogeneities," *The Physics of Fluids*, vol. 21, no. 3, pp. 377–380, 1978.

[70] J. Herrera, "Envelope solitons in inhomogeneous media," *Journal of Physics A: Mathematical and General*, vol. 17, no. 1, p. 95, 1984.

[71] C.-L. Chen, *Foundations for guided-wave optics*. John Wiley & Sons, 2006.

[72] M. Kolesik, J. V. Moloney, and M. Mlejnek, "Unidirectional optical pulse propagation equation," *Phys. Rev. Lett.*, vol. 89, p. 283902, Dec 2002.

[73] P. Kinsler, "Optical pulse propagation with minimal approximations," *Phys. Rev. A*, vol. 81, p. 013819, Jan 2010.

[74] J. Lee, Y.-J. Kim, K. Lee, S. Lee, and S.-W. Kim, "Time-of-flight measurement with femtosecond light pulses," *Nature photonics*, vol. 4, no. 10, pp. 716–720, 2010.

[75] T. Fortier and E. Baumann, "20 years of developments in optical frequency comb technology and applications," *Communications Physics*, vol. 2, no. 1, pp. 1–16, 2019.

[76] E. D. Caldwell, L. C. Sinclair, N. R. Newbury, and J.-D. Deschenes, "The time-programmable frequency comb and its use in quantum-limited ranging," *Nature*, vol. 610, no. 7933, pp. 667–673, 2022.

Paper [A].
Perspectives of measuring gravitational effects of laser light and particle beams

Felix Spengler, Dennis Rätzel, and Daniel Braun
New Journal of Physics **24** 053021 (2022)
DOI: 10.1088/1367-2630/ac5372
URL: iopscience.iop.org/article/10.1088/1367-2630/ac5372

New Journal of Physics
The open access journal at the forefront of physics

Deutsche Physikalische Gesellschaft DPG IOP Institute of Physics

Perspectives of measuring gravitational effects of laser light and particle beams

New Journal of Physics
The open access journal at the forefront of physics

Deutsche Physikalische Gesellschaft DPG
IOP Institute of Physics

Published in partnership with: Deutsche Physikalische Gesellschaft and the Institute of Physics

OPEN ACCESS

RECEIVED
8 July 2021

REVISED
11 December 2021

ACCEPTED FOR PUBLICATION
9 February 2022

PUBLISHED
10 May 2022

PAPER

Perspectives of measuring gravitational effects of laser light and particle beams

Felix Spengler[1,*], **Dennis Rätzel**[2,3,*] and **Daniel Braun**[1,*]

[1] Eberhard-Karls-Universität Tübingen, Institut für Theoretische Physik, 72076 Tübingen, Germany
[2] Humboldt Universität zu Berlin, Institut für Physik, Newtonstraße 15, 12489 Berlin, Germany
[3] ZARM, Universität Bremen, Am Fallturm 2, 28359 Bremen, Germany
[*] Authors to whom any correspondence should be addressed.

E-mail: Felix-Maximilian.Spengler@Uni-Tuebingen.de, Dennis.Raetzel@ZARM.Uni-Bremen.de and Daniel.Braun@Uni-Tuebingen.de

Keywords: laboratory studies of gravity, optomechanics, gravitational nearfield, resonant mass detector, linearized gravity, LHC, laser pulse

Abstract

We study possibilities of creation and detection of oscillating gravitational fields from lab-scale high energy, relativistic sources. The sources considered are high energy laser beams in an optical cavity and the ultra-relativistic proton bunches circulating in the beam of the large hadron collider (LHC) at CERN. These sources allow for signal frequencies much higher and far narrower in bandwidth than what most celestial sources produce. In addition, by modulating the beams, one can adjust the source frequency over a very broad range, from Hz to GHz. The gravitational field of these sources and responses of a variety of detectors are analyzed. We optimize a mechanical oscillator such as a pendulum or torsion balance as detector and find parameter regimes such that—combined with the planned high-luminosity upgrade of the LHC as a source—a signal-to-noise ratio substantially larger than 1 should be achievable at least in principle, neglecting all sources of technical noise. This opens new perspectives of studying general relativistic effects and possibly quantum-gravitational effects with ultra-relativistic, well-controlled terrestrial sources.

1. Introduction

With the successful measurement of gravitational waves through LIGO, the measurement of gravitational signals from relativistic sources has gained a lot of interest as it is believed to lead to new insights about gravity, in particular, constraints on modifications of general relativity (GR) and potential effects of quantum gravity [1–5]. However, such experiments are limited to detection since the experimenter has no access to the cosmic sources of the signal.

Starting already in the 1970s, proposals were formulated for constructing terrestrial relativistic sources and detectors of their gravitational signals. E.g. in [6–8] a cylindrical microwave resonator was proposed as source of a standing gravitational wave and a second concentric cylinder as detector based on photon creation in one of its modes. But it was clear that with the existing technology at the time it was not realistic to create a sufficiently strong source whose radiation could be detected. In recent years there has been renewed interest in the creation and detection of gravitational waves in the lab [9–17].

The gravitational field of electromagnetic radiation has been studied early on [18–20]. It gives rise to a range of interesting effects, from an attraction that decays with the inverse of the distance instead of the inverse square [18–21] to frame dragging [22, 23] and other gravitomagnetic effects [24–30]. Their detection has been found to be extremely challenging, see e.g. [21, 23, 25–31]. The phenomenology of the gravitational field of relativistically moving matter is similar to that of light. It can be calculated by Lorentz boosting spacetimes of sources at rest. The result approaches the gravitational field of massless particles in the ultra-relativistic limit [20, 28, 29, 32–34].

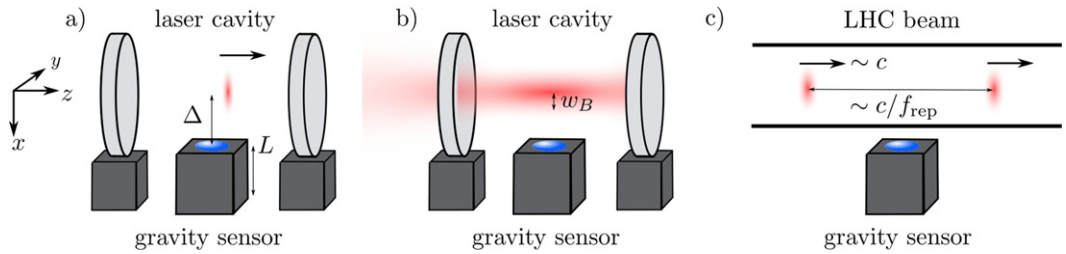

Figure 1. (a) Laser pulse oscillating to and fro in a cavity. (b) cw laser focused to a narrow waist inside a cavity. Its intensity is modulated to create a gravitational field oscillating at kHz frequency. (c) Ultrarelativistic particle bunches in an accelerator ring such as the LHC create a very similar gravitational field. In the vicinity of the waist of the laser beam or close to the beamline, a detector picks up resonant mechanical deformations due to the oscillating gravitational forces.

As technology has substantially progressed since some of the cited works have been published, both on the side of sources in the form of high-power lasers [35–37] and particle accelerators [38, 39], and in the metrology of extremely weak forces [40–45], it is worthwhile to reassess the possibility to detect the gravitational effects of light and of ultra-relativistic particle beams. Indeed, progress in this direction would enable the test of GR in a new, ultra-relativistic regime (in the sense of special relativity), with an energy–momentum tensor as the source term in Einstein's equations very different from the one that can be achieved with non-relativistic masses and purely Newtonian gravity, namely with a large off-diagonal component in Cartesian coordinates.

In this article we focus on the acceleration of non-relativistic sensor systems due to the gravitational field of light beams and ultra-relativistic particle beams such as the ones produced at the large hadron collider (LHC). We add several new aspects that improve the outlook for experimental observation. Most importantly, we consider trapping of laser light in a cavity, through which the circulating power can be drastically enhanced. Secondly, we consider modulation of the gravitational sources with an adjustable frequency in order to match them to the optimal sensitivity of existing detectors. Several approaches are investigated to that end. The simplest one consists in having laser pulses oscillate to and fro in a cavity, such that the length of the cavity determines the oscillation frequency of the gravitational signal. We also examine the possibility of slowly (kHz frequency) modulating the power with which the cavity is pumped using a continuous wave (cw) or pulsed laser. With the pump power, the power circulating in the cavity is modulated, and thus, also the strength of the gravitational field. Thirdly, we extend the analysis to ultra-relativistic particle beams such as available at the LHC. And finally, we examine several possible sensors for their suitability for measuring the created gravitational fields.

Our work is also motivated by current developments toward measuring gravitational effects of sources in a quantum mechanical superposition as a possible experimental road to understanding quantum gravitational effects [40, 42, 46, 47]. Creating quantum superpositions of sufficiently large masses is challenging, and it is therefore worthwhile to think about other sources that can be superposed quantum mechanically. We discuss perspectives in this direction for the gravitational sources studied in this paper in section 4.

2. Potential sources and their gravitational field

2.1. Laser pulses oscillating in a cavity

To create a strong, high frequency gravitational field, a source of high power and intensity is required. Modern femtosecond laser pulses can reach up to a Petawatt in pulse power. One such laser pulse oscillating in a cavity, as illustrated in figure 1, is a source of short bursts of high energy oscillating to and fro at high frequency. The perturbation to the metric and the resulting Riemann curvature tensor can be calculated within the theory of linearized gravity, as is done in appendix A and [28, 29].

For a continuous-wave (cw)-laser with power P and circular polarization, the curvature component relevant to a non-relativistic sensor based on a mechanical resonator with axis perpendicular to the beam line of the laser is, for an observer in the x–z-plane (i.e. $y = 0$) and in the approximation of a vanishing opening angle, given by

$$R_{0x0x} \simeq -4GP/(c^5\rho^2) \tag{1}$$

with G the gravitational constant, c the speed of light in vacuum, $\rho^2 = x^2 + y^2 = x^2$, and $x_0 = ct$.

Laser *pulses* were considered earlier in [18, 21] in the approximation of an infinitely thin light pencil of length L. A further exploration in appendix A for the simplified case of box shaped pulses oscillating to and

fro corroborates the result that close to the beam ($\rho \ll |z|, |z-D|$, where $z=0$ and $z=D$ are the positions of the two mirrors) equation (1) gives the correct result, limited, however, to a finite duration of the order of the length of the pulse (see figure 8 in [21]) but on the other hand with the cw-power P replaced by the power of the effective pulse in the cavity $P_{\mathrm{p}}^{\mathrm{cav}}$ (see equation (A23)). The curvature results in a tidal force between two infinitesimally separated points next to the beamline. However, there is no gravitational wave generated as this type of source is not quadrupolar in nature. Rather one can detect the gravitational near-field. In leading order, the gravitational near field acting on non-relativistic test matter can be described by a Newtonian gravitational potential $\Phi = \frac{4GP}{c^3}\ln\rho$.

The average power at a given cross-section of the beam inside the cavity is $P_{\mathrm{cav}}^{\mathrm{avg}} = \frac{2\tau_{\mathrm{p}}}{\tau_{\mathrm{rt}}} P_{\mathrm{p}}^{\mathrm{cav}}$, where τ_{p} is the length of the effective pulse in the cavity, and $\tau_{\mathrm{rt}} = \frac{2L_{\mathrm{cav}}}{c}$ is the round trip time in the cavity. As the power enters linearly into the gravitational potential, acceleration, and curvature, the considered gravitational effects will be proportional to the average power in the cavity.

Short pulses a pump laser emitting very short pulses has a broad spectrum in the frequency domain. Coupling these pulses into a cavity of high finesse $F \approx \frac{\pi (R_1 R_2)^{\frac{1}{4}}}{1-\sqrt{R_1 R_2}}$ [48] leads to an electric field strength inside the cavity

$$\tilde{E}_{\mathrm{cav}}(\omega) = \tilde{G}_{\mathrm{cav}}(\omega)\tilde{E}_{\mathrm{p}}(\omega), \quad \text{where} \quad \tilde{G}_{\mathrm{cav}}(\omega) = \frac{\sqrt{T_1}}{1-\sqrt{R_1 R_2}\,\exp(-i\omega\tau_{\mathrm{rt}})} \tag{2}$$

is the field transfer function, with the intensity transmissivity T_1 of the mirror struck by the pump beam, and the intensity reflectivities of the two mirrors $R_{1/2}$, where $T_1 = 1 - R_1$. An explicit calculation for the case of rectangular pulses can be found in appendix B, which is based on [49]. If the pulses are very short $\tau_{\mathrm{p}} \ll \tau_{\mathrm{rt}}$ and far apart $1/f_{\mathrm{rep}} \gg \tau_{\mathrm{L}}$, where $\tau_{\mathrm{L}} \approx \frac{2F}{\pi}\tau_{\mathrm{rt}}$ is the $1/e$ energy decay time and f_{rep} is the repetition rate of the pump laser, the pulse enters the cavity at an intensity $T_1 I_{\mathrm{p}}$, where the circulating power is enhanced by a factor $\frac{2F}{\pi}$, independent of the cavity length. Without any further modification the factors T_1 and $\frac{2F}{\pi}$ at best cancel up to a factor of 4 (assuming $R_1, R_2 \simeq 1$), leaving little to be gained (see appendix B, equation (B8)). The ways one could imagine improving upon this all involve changes to the mirror that couples the pump laser pulses to the cavity:

- An input coupler is a mirror which is significantly less reflective than what could be achieved with the best available mirrors. It increases the power deposited into the cavity when combined with impedance- and phase-matching techniques, yet also reduces the cavity finesse [50]. For example, in [51] input couplers are employed to realize enhancement cavities with kilowatt-average-power femtosecond pulses, increasing the average power circulating in the cavity to 670 kW, 10^3 times the 420 W average power of the pump laser. Using larger laser spots on the mirrors of the cavity should allow for even stronger pump lasers to be used. With stronger pump lasers, such as the BAT laser in [52] with an average pump power of $P_{\mathrm{pump}} = 300$ kW, an average power within the cavity in the 100 MW range seems plausible.
- A switchable mirror would allow for the full pump beam power to enter the cavity, which means the average cavity power is expected to be the pump laser power enhanced by a factor $\frac{2F}{\pi}$. Depending on the cavity's length and the pump laser's repetition rate, the mirror has to be moved on a timescale of 10^{-9} to 10^{-3} s, the slower end of which seems realistic. A mirror mounted on some mechanics might reduce the precision of its positioning and hence the cavity's finesse. Nonetheless, with a high finesse cavity ($\frac{2F}{\pi} \sim 10^5$) and high-average-power pump lasers ($P_{\mathrm{pump}} \approx 300$ kW [52]) an average power >20 GW in the cavity would be achievable.

One limitation when scaling to higher powers is damage to the mirrors. In [53] the cw intensity threshold was determined to be at around 100 MW cm^{-2} before thermal damage sets in. For sub-picosecond pulses the intensity threshold can be exceeded by at least an order of magnitude, as it is done in [51], as long as the average intensity on the mirrors does not exceed the thermal threshold. For 20 GW (100 MW) cavity power this needs a spot diameter on the mirrors of at least 16 cm (1.1 cm). For the input coupler the limitations are even stricter than for the end mirror as the power passes through the input coupler and creates more heating than when reflected at the surface of the reflecting mirror [51]. Large spot sizes require long cavities, as otherwise the mode in the cavity has a large opening angle and prevents positioning the sensor very close to the beam. For the cited spot-sizes of order 1–10 cm, a cavity length $L_{\mathrm{cav}} \gtrsim 1$ m suffices. In this work, the increase in power is accounted for by increasing the pulse duration by defining an effective pulse length

$$T_{\mathrm{p}}^{\mathrm{cav}} = T_{\mathrm{p}}^{\mathrm{pump}} f_{\mathrm{rep}} \tau_{\mathrm{rt}} \frac{2F}{\pi} = T_{\mathrm{p}}^{\mathrm{pump}} f_{\mathrm{rep}} \tau_{\mathrm{L}}. \tag{3}$$

For the BAT laser from [52], the repetition rate is $f_{\mathrm{rep}} = 10$ kHz and the pulse duration of the pump laser is $T_{\mathrm{p}}^{\mathrm{pump}} = 100$ fs. We further assume $F = 10^5$ and the signal to be at resonance with the sensor frequency

Table 1. Comparison of relevant numbers of the LHC beam and the laser-based sources from sections and 2.2: $P_{\mathrm{p}}^{\mathrm{cav}}$ pulse power, $P_{\mathrm{cav}}^{\mathrm{avg}}$ power averaged over time, w_{B} waist of beam. ω_0 is the desired signal frequency, assumed in section 3 to be one of the resonance frequencies of the detector.

	$P_{\mathrm{p}}^{\mathrm{cav}}$ (W)	$T_{\mathrm{p}}^{\mathrm{cav}}$	$P_{\mathrm{cav}}^{\mathrm{avg}}$ (W)	w_{B}
Pulses in cavity	3×10^{14}	100 fs ·10 kHz $\frac{8\times10^5}{\omega_0}$ [a]	2×10^{10}	$<100\,\mu$m
cw laser+cavity	2×10^{11}	$\frac{\pi}{\omega_0}$	1×10^{11}	$<100\,\mu$m
LHC	10^{14}	10^{-9} s[b]	3.8×10^{12}	16 μm

[a] A switchable mirror is assumed for the pulses in the cavity. The pulses are assumed to be effectively stacked together to a larger circulating effective pulse, see equation (3).
[b] The effective pulse length $T_{\mathrm{p}}^{\mathrm{cav}}$ for the LHC corresponds to a single proton bunch, but a much slower modulation of the beam on resonance with ω_0 can be envisaged.

$\tau_{\mathrm{rt}} = 2\frac{2\pi}{\omega_0}$, see e.g. table 1. This is consistent with the image of creating a 'train' of pulses (one could also imagine pulse stacking, i.e. increasing the pulse power instead). Laser pulses with far higher pulse powers exist. The National Ignition Facility achieves 5×10^{12} W peak power [36] but is not as suitable for our purposes due to its low repetition rates. Peak powers of up to 10×10^{15} W at repetition rates of up to 10 Hz exist [37] and others with peak powers on the order of 100×10^{15} W are planned [54], but will need to achieve higher average intensities and repetition rates in order to lead to measurable gravitational effects.

2.2. Modulated cw-pumping

Instead of creating a periodic signal by having laser pulses oscillate in a cavity, one could also consider using a cw laser. To create a periodic signal, one can pump the cavity for part of the period and allow for the intensity inside the cavity to decay before switching the pump beam back on for the next period, thus creating a modulated signal with modulation period τ_{mod}. Depending on τ_{L}, the energy within the cavity as a function of time looks more like a periodic sequence of effective pulses that have the form of rectangles—in the case of $\tau_{\mathrm{L}} \ll \tau_{\mathrm{mod}}$—or like a series of shark fins for $\tau_{\mathrm{L}} \sim \tau_{\mathrm{mod}}$ (see appendix B). We call $P_{\mathrm{p}}^{\mathrm{cav}}$ the maximum power of the effective pulse in the cavity.

Using a cw pump laser, the coupling to the cavity is no longer detrimental as for $\Delta\omega_{\mathrm{FWHM}} \sim 1/\tau_{\mathrm{L}} > \Delta\omega_{\mathrm{pump}}$, where $\Delta\omega_{\mathrm{pump}}$ is the line width of the pump beam, the pump beam couples almost fully to the cavity. The Newtonian gravitational potential for a thin light pencil in the form of a standing wave in the cavity is (see [18] and appendix A) $\Phi = \frac{4GP(t)}{c^3}\ \ln\ \rho$, where ρ is the distance from the beam line and $P(t)$ is the power passing through the cross section with the detector, i.e. $P(t) = P_{\mathrm{cav}}(t)$ in this case. For the slowly moving detectors envisaged here (speeds $v \ll c$), all equations of motion are the same for the source consisting of the standing light wave or the propagating one.

For long modulation periods $\tau_{\mathrm{mod}} \gg \tau_{\mathrm{L}}$, the maximum power of the effective pulse in the cavity is $P_{\mathrm{p}}^{\mathrm{cav}} = \frac{2F}{\pi}P_{\mathrm{pump}}$, for approximately half the modulation period. Commercially available cw laser systems reach continuous powers of 500 kW in multi-mode operation and up to 100 kW in single-mode operation (see[1] and e.g. [55]). Combining this with a high finesse cavity $F \sim 10^6$ leads to an average circulating power in the cavity of

$$P_{\mathrm{cav}}^{\mathrm{avg}} = \frac{1}{2}\frac{2F}{\pi}P_{\mathrm{pump}} \sim 100\,\mathrm{GW}. \tag{4}$$

The average power in the cavity can at most be a fraction $< \left(1 - e^{-\tau_{\mathrm{mod}}/(2\tau_{\mathrm{L}})}\right)$ of the maximum power $\frac{2F}{\pi}P_{\mathrm{pump}}$. For slowly decaying cavities, where $\tau_{\mathrm{mod}} \gtrsim \tau_{\mathrm{L}}$, techniques such as Q-switching or switchable mirrors are necessary to adequately modulate the amplitude[2].

[1] A single-mode has the advantage that one can focus it down to a spot size comparable to the wave length, i.e. one could get, at least in principle, much closer to the beam (oder 1 μm instead of ca 100 μm. Thus, while loosing a factor 25 in power one gains a factor 100 in distance, i.e. there is an overall improvement by a factor 4 over the multi-mode case, if such small distances from the beam can indeed be realized.

[2] Shorter cavities lead to lower τ_{L} at the same finesse and without decreasing the average power. The same considerations for the spot size and length of cavity as mentioned for the laser pulses apply also in the cw case for positioning the detector sufficiently close to the beam waist and neglecting higher order effects in the opening angle [28]. For a 1 m-long high-finesse cavity ($F \sim 10^6$) the decay time τ_{L} is in the low millisecond range, which is too slow for some of the proposed detector setups. This could be circumvented by implementing techniques such as Q-switching, with which the decay of energy within the cavity can be accelerated, and the aforementioned switchable mirrors. Also, the energy buildup can be modulated to a certain degree by pumping. For short modulation periods, $\tau_{\mathrm{mod}} \approx \tau_{\mathrm{L}}$, the cavity is never fully pumped.

2.3. The LHC

Instead of laser light, one can also investigate ultra relativistic particle beams consisting of high-energy bunches, such as the one at LHC, as gravitational sources. A particle beam in the relativistic limit is, from a gravitational perspective, the same as a laser beam: for example, the rest mass of the protons $m \simeq 938\ \mathrm{MeV}/c^2$ makes a negligible contribution to their energy for achievable particle energies of about 6.5 TeV and both charge and spin are irrelevant [32–34]. To very good approximation, the energy-momentum relationship is then $E = cp$ where p is the momentum of the protons, just as for photons. In the ring of the LHC there are 2808 bunches of protons at maximum capacity, each bunch with a total energy of $\sim 10^5$ J. One bunch is approximately 30 cm long, contains 1.15×10^{11} protons, and can be squeezed down to a transverse diameter of $\sim 16\,\mu m$ (see [38]). To excite a resonator at its eigenfrequency $\nu_0 = \omega_0/(2\pi)$, the bunches have to pass by the detector with rate ν_0, or the beam must be modulated with frequency ν_0. The 2808 bunches spread over a ring of 26 659 m length moving at speed close to c entail a rate of 31.2 MHz. A single bunch going around the ring passes with a frequency of 11 kHz. To achieve lower frequencies one could, for example, periodically modulate the beam position. This would result in a scheme similar to that of the cw laser cavity, where the LHC beam is active for half the sensor's oscillation period $\tau_\mathrm{p} = \frac{1}{2}\frac{2\pi}{\omega_0}$ with an effective pulse power $P_\mathrm{p}^\mathrm{cav} = P^\mathrm{LHC} = 2P_\mathrm{cav}^\mathrm{avg}$, where P^LHC is the nominal average power of the LHC. The pulse power of the LHC beam is orders of magnitude smaller than that of extreme-power laser pulses, but the proton bunches are much longer ($\sim$1 ns) than the laser pulses. This results in a higher average power of $P_\mathrm{cav}^\mathrm{avg} \approx 3.8 \times 10^{12}$ W, which is orders of magnitude larger than the average power of laser pulses oscillating in a cavity and about 40 times the average power that can be contained in a cavity pumped by the cw laser considered above (see table 1). Therefore, from the perspective of the strength of the gravitational source, the LHC beam might be preferable. A potential drawback compared to the laser-based sources is the lack of flexibility in frequency. This can be compensated, however, by considering detectors with tunable resonance frequency. Besides protons, it is also possible to use heavy nuclei, or partially ionized heavy atoms. The latter have the advantage that the corresponding beams can be laser-cooled (see the discussion in section 4.2). Upgrades of the LHC to use heavy ions are currently considered [56], and also under development at Brookhaven National Lab [57].

3. Detectors

We consider three types of detectors, a mechanical rod, a detector based on superfluid helium-4 coupled parametrically to a superconducting microwave cavity, and a mechanical harmonic oscillator, motivated by the monolithic pendulum from [58, 59] and the torsion balance from [40], with which recently very high levels of sensitivity for gravitational fields have been reached. The superfluid helium detector and the monolithic pendulum are optomechanical detectors close to the quantum limit. Quantum optomechanical detectors and different configurations have been studied in great detail over recent years, both theoretically and experimentally [60–62]. They have been considered for high precision sensing [63] in particular, force sensing [64] and theoretical work has been performed to derive general limits for sensing of oscillating gravitational fields with such systems [65, 66]. We take the mentioned types of detectors as starting points for examining the question what parameter values would need to be achieved such that they become suitable for measuring the gravitational forces considered in this paper.

3.1. Mechanical response of a rod

A spatially dependent gravitational acceleration compresses a 1D deformable resonator according to its Young modulus Y. The wave equation for the displacement field $u(x, t)$, describing the relative position of an element of the rod from its equilibrium location x, is given in [67, p. 416] as

$$\varrho_m \partial_t^2 u(x,t) - Y \partial_x^2 u(x,t) = -\varrho_m \partial_x \Phi(x,t), \tag{5}$$

where the resonator is extended in the x direction, orthogonal to the beam, and ϱ_m is its mass density. The length contraction due to modification of space-time is negligible in comparison to the elastic effect considered here, as it comes with an additional factor c_s^2/c^2 [68], where $c_\mathrm{s} = \sqrt{Y/\varrho_m}$ is the speed of sound in the rod's material.

The displacement field can be expanded into the spatial eigenmodes

$$w_n(x) = \cos\left(\left(n + \frac{1}{2}\right)\frac{\pi}{L}(x - \Delta)\right)$$

of the free equation of motion complying with the boundary conditions, i.e. the tip of the resonator distant from the source was chosen to be fixed in place by the support (hence $w_n(L + \Delta)$ has to vanish and

$\partial_x w_n|_{x=\Delta}$ has to vanish at the other tip), where $n \in \mathbb{N}_0$, Δ is the distance of the tip of the rod from the source, and L is the length of the resonator (see figure 1). The spatial eigenmodes are orthonormal with respect to the inner product $\langle a|b\rangle = (2/L)\int_{\Delta}^{\Delta+L} a(x)b(x)\,\mathrm{d}x$. The total displacement field is then given by $u(x,t) = \sum_{n=0}^{\infty}\xi_n(t)w_n(x)$. The differential equation for the temporal amplitude $\xi_n(t)$ resulting from the projection of (5) onto the nth spatial eigenmode is then given by

$$\ddot{\xi}_n(t) + \frac{\omega_n}{Q}\dot{\xi}_n(t) + \omega_n^2\xi_n(t) = -\frac{2}{L}\int_{\Delta}^{L+\Delta}\mathrm{d}x\, w_n(x)\partial_x\Phi(x,t), \tag{6}$$

where $\omega_n = c_\mathrm{s}\left(n+\frac{1}{2}\right)\frac{\pi}{L}$ is the frequency of the mode and a linear dissipation term $\gamma_n\partial_t u(x,t)$ with rate $\gamma_n = \varrho_m\frac{\omega_n}{Q}$ was added to equation (5) in order to include dissipation from the elastic modes of the resonator.

In the case of resonant excitation, the amplitude of the steady state solution in the lowest eigenmode $\xi_0(t) = A(\omega_0)\sin(\omega_0 t)$, reached after a transient time $\frac{Q}{\omega_0}$ is then given by

$$A(\omega_0) = \frac{Q}{\omega_0^2}\int_0^{2\pi/\omega_0}\mathrm{d}t\,\frac{\omega_0}{\pi}\cos(\omega_0 t)\int_{\Delta}^{L+\Delta}\mathrm{d}x\,\frac{2}{L}\cos\left(\frac{\pi}{2L}(x-\Delta)\right)(-\partial_x\Phi(x,t)), \tag{7}$$

where the integration of t over one mechanical period gives the Fourier component of the driving force corresponding to this mechanical mode. At this point we assumed the pulse to be centered around $t = 0$ and to be repeating at intervals of $\frac{2\pi}{\omega_0}$.

With the periodic Newtonian potential from appendix A

$$\Phi(x,t) = \frac{4GP_\mathrm{p}^\mathrm{cav}}{c^3}\ln(x)\Pi_\Sigma(t) \tag{8}$$

$$\Rightarrow -\partial_x\Phi(x,t) = -\frac{4GP_\mathrm{p}^\mathrm{cav}}{c^3}\frac{1}{x}\Pi_\Sigma(t), \tag{9}$$

where $P_\mathrm{p}^\mathrm{cav}$ is the pulse power in the cavity and $\Pi_\Sigma(t) = \sum_n\left[\Theta\left(t-\frac{n2\pi}{\omega_0}-\frac{\tau_\mathrm{p}}{2}\right)-\Theta\left(t-\frac{n2\pi}{\omega_0}+\frac{\tau_\mathrm{p}}{2}\right)\right]$ is a sum of rectangular pulses of duration τ_p. The integral over the oscillation period in equation (7) returns

$$\int_0^{2\pi/\omega_0}\mathrm{d}t\,\cos(\omega_0 t)\,\Pi_\Sigma(t) = \frac{2}{\pi}\sin\frac{\omega_0\tau_\mathrm{p}}{2} \approx \begin{cases}\frac{\omega_0\tau_\mathrm{p}}{\pi} & \text{for } \tau_{\mathrm{p}\omega_0} \ll 2\\ \frac{2}{\pi} & \text{for } \tau_\mathrm{p} \approx \frac{\pi}{\omega_0}\end{cases}. \tag{10}$$

With this, a resonant maximum amplitude of

$$A(\omega_0) = \frac{4GP_\mathrm{p}^\mathrm{cav}Q}{\omega_0^2c^3}\frac{2}{\pi}\sin\left(\frac{\omega_0\tau_\mathrm{p}}{2}\right)\int_{\Delta}^{L+\Delta}\mathrm{d}x\,\frac{2}{L}\cos\left(\frac{\pi}{2L}(x-\Delta)\right)\frac{1}{x} \tag{11}$$

$$\approx \frac{32GP_\mathrm{cav}^\mathrm{avg}Q}{\pi\omega_0c^3}\begin{cases}\begin{cases}\frac{1}{\omega_0\Delta} & \text{for } \tau_\mathrm{p}\omega_0 \ll 2\\ \frac{2}{\pi\omega_0\Delta} & \text{for } \tau_\mathrm{p} = \frac{\pi}{\omega_0}\end{cases} & \text{and } L \ll \Delta\\ \begin{cases}\frac{1}{c_\mathrm{s}}\ln\frac{L}{\Delta} & \text{for } \tau_\mathrm{p}\omega_0 \ll 2\\ \frac{2}{\pi c_\mathrm{s}}\ln\frac{L}{\Delta} & \text{for } \tau_\mathrm{p} = \frac{\pi}{\omega_0}\end{cases} & \text{and } L \gg \Delta\end{cases}, \tag{12}$$

where $P_\mathrm{cav}^\mathrm{avg} \equiv \frac{\text{energy in the cavity}}{\text{oscillation period}} = \frac{P_\mathrm{p}^\mathrm{cav}\tau_\mathrm{p}}{\frac{2\pi}{\omega_0}}$ is the power in the cavity averaged over one mechanical period, is reached in the steady state of prolonged driving. The logarithmic divergence of equation (9) for $L \gg \Delta$ is an artifact of idealizations of our model and will not be relevant in practice[3].

[3] Even though it might seem favorable to increase L because of the logarithmic scaling in equation (11), the inhomogeneous driving force leads to excitations of multiple mechanical modes which, for a non perfectly rigid support, can couple. Also, the distance between the detector and the beam has to be much smaller than the length of the source cavity (or radius of the ringresonator) for the contributions of the recoil of the mirrors (or deflecting magnetic fields) to be negligible. These two effects might lead to the break-down of the logarithmic scaling before it makes a difference.

Assuming for orientation numerical values of aluminum, $c_s = c_s^{Al} = 6420$ m s^{-1}, $\omega_0 = 2\pi \times 10^9$ Hz, $\Delta = w_B$[4], and $Q = 10^6$ for the rod, the laser cavity introduced in section 2.1 ($P_{cav}^{avg} = 20$ GW, $w_B \approx 100$ μm) would result in an amplitude of $A \approx 10^{-34}$ m at the freely oscillating tip.

At resonance, the noise spectral density for a resonant-bar type detector is given by

$$S_A^{th} = \frac{4k_B TQ}{\omega_0^3 M_{eff}} \Rightarrow A_{th} = \sqrt{\frac{S_A^{th}}{\tau_{int}}} \tag{13}$$

according to [67, p. 440], where $M_{eff} = \int \varrho_m A_R (w_0(x))^2 dx$ is the effective mass of the mode with the rod cross-section A_R, and A_{th} is the amplitude resulting from the thermal noise after integration time τ_{int}. At $\omega_0 = 2\pi \cdot 1$ GHz the thermal sensitivity limit for temperatures below $T = 48$ mK is already below the standard quantum limit (SQL) on noise spectral density for a resonant mass detector [69],

$$S_A^{SQL} = \frac{4\hbar Q}{M_{eff}\omega_0^2}. \tag{14}$$

At frequencies below the megahertz range, the thermal noise is the limiting factor. For $Q = 10^6$, $M_{eff} = \frac{\pi}{8}\varrho_{Al} L^3$ (assuming a constant aspect ratio) with the mass density of aluminum $\varrho_{Al} = 2.7$ g cm^{-3} and a frequency of $\omega_0 = 2\pi \cdot 1$ GHz the sensitivity is $\sqrt{S_A^{SQL}} \approx 4 \times 10^{-17}$ m $/\sqrt{\text{Hz}}$ meaning that for 1 year of integration time at best an amplitude of 10^{-20} m can be detected.

For the LHC, where the rate of bunches passing by is $\nu = 31.2$ MHz, for the purposes of this estimation, we assume that the same amount of protons is split into 88 925 bunches instead of 2808 such that we reach the frequency $\omega_0 = 2\pi \cdot 1$ GHz while keeping the same average power. With pulses filling half a period, the peak power is $P_p^{cav} = 2P_{cav}^{avg}$. Using the same $c_s = 6420$ m s^{-1} and $Q = 10^6$ and the values of the LHC ($P_{cav}^{avg} = 3.8 \times 10^{12}$ W, $w_B = 16$ μm) one would expect the resonant amplitude to be $A \approx 9 \times 10^{-32}$ m, which is at least two orders of magnitude larger than that caused by the oscillating laser pulse from section. For higher quality factors $Q = 10^8$ amplitudes of $A \approx 9 \times 10^{-30}$ m might be possible. At far lower frequencies, where the limit $L \gg \Delta$ becomes relevant in equation (9), a lower speed of sound, for example $c_s = 100$ m s^{-1}, is also beneficial. However, one quickly ends up with a meter long rod, outside the 'close to the beam' limit, whilst still not within range of detection.

To probe the limit $L \gg \Delta$, we assume $\omega_0 = 2\pi \cdot 1$ kHz, $Q = 10^6$, $c_s = 6420$ m s^{-1} implying an extreme $L \approx 4$ km. Then, the expected amplitude from the laser pulses in section is $A \approx 2 \times 10^{-25}$ m, for the cavity pumped with a modulated cw laser $A \approx 4 \times 10^{-25}$ m, while we expect an amplitude of $A \approx 8 \times 10^{-24}$ m for the LHC beam (which would have to be modulated to reach such low frequencies). Assuming a temperature of $T = 5$ mK the sensitivity is $\sqrt{S_A^{th}} \approx 10^{-17}$ m $/\sqrt{\text{Hz}}$, leaving the amplitudes still unmeasurable even for unreasonably long integration and rise times and an unreasonable rod length.

3.2. Superfluid helium detector

In [70] Singh *et al* study the acoustic motion of superfluid helium-4 coupled parametrically to a superconducting microwave cavity as a detection scheme for continuous-wave gravitational signals. With few theoretical adaptations the system can be adapted to the near-field case considered here. The very high Q-factors and sensitive microwave transducer means this is essentially a better version of the deformable rod considered in section 3.1. For the ground mode, the system's description can be reduced to a one dimensional problem and treated as in section 3.1, but with two fixed ends instead of one. The spatial displacement amplitude is then given by $w_0 = \sin\left(\frac{\pi}{L}(x - \Delta)\right)$.

The position noise spectral density of the temporal displacement field ξ is given by equation (11), when comparing to the result of Singh *et al* [70] a factor of 2 has to be added to obtain the single sided density ($\omega_0 > 0$). With the susceptibility on resonance $\chi = \frac{Q_{He}}{iM_{eff}\omega_0^2}$, this results in a thermal force noise spectral density (on resonance) of

$$S_{FF}^{th} = |\chi|^{-2} S_{\xi\xi}^{th} = 4k_B T M_{eff} \frac{\omega_0}{Q_{He}}. \tag{15}$$

Which implies a lower bound to the detectable force over an integration time τ_{int}, with 2σ uncertainty, of

$$\bar{F}_{min} \approx 2\sqrt{\frac{S_{FF}^{th}}{\tau_{int}}} = \sqrt{\frac{16k_B T M_{eff}\omega_0}{\tau_{int} Q_{He}}}. \tag{16}$$

[4] As the rod was chosen to be fixed by the support at its tip at the far side of the beam, the lowest eigenmode has wavelength $\lambda = 2\pi c_S \omega_0 = 4L$. The minimum distance from the beam is $\Delta \approx w_B$, where for the purposes of this estimation, we saturate this lower bound on Δ.

The Fourier component of the force corresponding to the considered lowest-frequency mode is given by

$$\bar{F}_{\text{eff}} = |\chi|^{-1} A(\omega_0) = \frac{16 G M_{\text{eff}} P_{\text{p}}^{\text{cav}}}{\pi L c^3} \sin\left(\frac{\omega_0 \tau_{\text{p}}}{2}\right) \int_{\Delta}^{\Delta+L} \frac{\sin\left(\frac{\pi(x-\Delta)}{L}\right)}{x} \mathrm{d}x. \tag{17}$$

Note the similarity of the amplitude $A(\omega_0)$ to the case of the mechanical rod detector in equation (9)[5]. Here, both signal and noise are given as a force, for better comparability to [70].

To get a feeling for the orders of magnitude, we start off with the numbers from the actual experimental setup from Singh *et al* [70]. We set $\tau_{\text{int}} = 250$ d, $Q_{\text{He}} = 6 \times 10^{10}$, $L = 4$ cm, $r = 1.8$ cm(radius), $c_{\text{s}} = 220$ m s^{-1}, and $\varrho_{\text{He}} = 145$ kg m^{-3}. This implies $\omega_0 = 2\pi \cdot 2.8$ kHz, $M_{\text{eff}} = 3$ g, $T = 5$ mK. This results in a minimum detectable force $\bar{F}_{\text{min}} \approx 4 \times 10^{-21}$ N. Choosing the LHC as a source, we assume $\Delta = w_{\text{B}}$ and set the average power to $P_{\text{p}}^{\text{cav}} = P^{\text{LHC}} = 3.8 \times 10^{12}$ W, $\tau_{\text{p}} = \frac{1}{2}\frac{2\pi}{\omega_0}$, resulting in $\bar{F}_{\text{eff}} \approx 6.6 \times 10^{-24}$ N. Going further from the beamline (by less than L) to account for shielding and the Helium container only decreases the effective force slightly (for $\Delta = 16\ \mu$m $\rightarrow \Delta = 3$ cm, F_{eff} decreases by a factor of 4) as there is limited contribution from the liquid Helium at the ends of the container to the ground mode.

Hence, at full amplitude and one week of integration time, the 4 cm prototype detector is lacking about 3.5 of magnitude in sensitivity. Under otherwise identical assumptions, the proposed first generation (0.5 m) detector will be about 2.5 orders of magnitude from being sensitive enough to detect the gravitational signal from the LHC.

3.3. High-Q milligram-scale monolithic pendulum

In a recent publication, Matsumoto *et al* [58] described the manufacturing of a pendulum and presented its properties. They found it to have a very high quality factor for a small scale system and even higher when combined with an optical spring. Different from the extended oscillators considered in the earlier subsections, the pendulum does not rely on the projection of the gravitational acceleration on an elastic mode but rather on the gravitational force on the pendulum mass relative to the support. A mechanical oscillator has to be of small scale to be close enough to the source for the gravitational acceleration to be significant, while the gravitational effects on the pivot point need to remain negligible.

For the $l = 1$ cm, $m = 7$ mg pendulum a mechanical Q-factor of $Q_m = 10^5$ was measured in [58] at $\omega_m = 2\pi \times 4.4$ Hz. Introducing an optical spring to shift the frequency, the effective Q-factor is expected to scale as

$$Q_{\text{eff}} \approx Q_m \left(\frac{\omega_0}{\omega_m}\right)^2 \tag{18}$$

for the damping model considered relevant for the pendulum (the effective frequency of the coupled system was renamed from ω_0 (Q_0) in the original work [58] to ω_m (Q_m) for consistency). An additional feedback cooling is necessary to stabilize and cool the system to a temperature T_{fb}, compensating the effect of heating through the optical spring. This reduces the Q-factor to Q_{fb}, which has the benefit of allowing shorter driving times. At $\omega_0 = 2\pi \times 280$ Hz the authors of [58] demonstrated a sensitivity of $3 \times 10^{-14}\ \text{m}/\sqrt{\text{Hz}}$ with a Q-factor of $Q_{\text{fb}} = 250$, with thermal motion the main source of noise. According to equation (11) this corresponds to a temperature of a few Millikelvin.

In an update to this Cataño-Lopez *et al* [59] described an improved version of this pendulum, with a measured mechanical Q-factor of $Q_m = 2 \times 10^6$ at a frequency of $\omega_m = 2\pi \times 2.2$ Hz, which with the optical spring is tunable in the frequency range of $400\ \text{Hz} < \frac{\omega_0}{2\pi} < 1800$ Hz.

For a pulsed-beam source, the gravitational acceleration in radial direction for the duration of a pulse is given by

$$a_{\text{grav}}^{\text{p}} = -\frac{4 G P_{\text{p}}^{\text{cav}}}{c^3} \frac{1}{\rho}, \tag{19}$$

where G is the Newton gravitational constant, $P_{\text{p}}^{\text{cav}}$ is the pulse power, and ρ is the distance from the beam. For this setup ρ is limited by the radius of the pendulum mass (1.5 mm) and the beam width ($\ll .5$ mm), so $\rho = 2$ mm is a reasonable estimate which might be substantially increased, however, if a cryostat is needed.

[5] In contrast to the spatial integral in equation (11), the one in (17) converges to ≈ 1.85 for $L \gg \Delta$. This is because of the different in boundary conditions, in particular, the logarithmic dependence stems from the overlap of the modefunction with the steep end of the $1/x$ driving force, whereas the modes of the helium have to vanish at the end of the container. However, the missing logarithmic dependence is basically irrelevant on realistic length scales. Assuming once again a constant aspect ratio, i.e., $M_{\text{eff}} \sim L^3$, we find a scaling of $\bar{F}_{\text{min}} \sim L$ and $\bar{F}_{\text{eff}} \sim L^2$, implying that the force should be detectable if L is large enough. However, limitations apply as is discussed in section 3.1.

The displacement resulting from prolonged ($\tau \sim \frac{2\pi Q_{\rm fb}}{\omega_0}$) driving on resonance is given by

$$x_{\rm grav} = \frac{\bar{a}_{\rm grav}}{\omega_0^2} Q_{\rm fb} = \frac{8GP_{\rm p}^{\rm cav}\ \sin\left(\frac{\omega_0\tau_{\rm p}}{2}\right) Q_{\rm fb}}{\pi c^3 \omega_0^2} \frac{1}{\rho}, \tag{20}$$

where $\bar{a}_{\rm grav}$ is the Fourier component of $a_{\rm grav}(t)$ on resonance, and $\sin\left(\frac{\omega_0\tau_{\rm p}}{2}\right)$ results from the overlap of the rectangular pulses with the sinusoidal oscillation calculated in equation (8). We now consider how the pendulum would react to the different gravitational sources discussed above.

3.3.1. Cavity pumped with cw laser

For the pendulum from [58] at $\omega_0 = 2\pi \times 280$ Hz and the cw laser cavity from section 2.2 with a power in the cavity of $P_{\rm p}^{\rm cav}$= 200 GW for half the oscillation period the expected amplitude resulting from the gravitational signal is $x_{\rm grav} \approx 3.1 \times 10^{-26}$ m. With the on-resonance SQL and thermal sensitivities [69] $\sqrt{S_{\rm SQL}} = 2x_{\rm zpf}\sqrt{\frac{Q_{\rm fb}}{\omega_0}} = \sqrt{\frac{4\hbar Q_{\rm fb}}{m\omega_0^2}} \approx 7 \times 10^{-17}\ {\rm m}/\sqrt{\rm Hz}$ and $\sqrt{S_{\rm th}} = 2 \times 10^{-14}\ {\rm m}/\sqrt{\rm Hz}$ (starting from room temperature, with only feedback cooling) this signal amplitude is not measurable.

The SQL refers to amplitude-and-phase measurements of that position. In principle, due to the precisely known frequency, quantum non-demolition measurements allow continuous monitoring of the oscillation [71]. With a 'single-transducer, back-action evading measurement', one can estimate a quadrature of the oscillator with an uncertainty that scales $\propto (\beta\omega_0\tau_m)^{-1/2}$, where τ_m is the relevant measurement time or inverse filter width, and β a numerical factor that can reach a value of order one (see equations (3.21a) and (3.21b) in [71] and equations (32) and (33) in [72]). After upconverting the kHz signal to the GHz regime one can use modern microwave amplifiers with essentially no added noise [73–76]. Upconversion to the microwave frequency range was already discussed in the 1980s [72] and can be achieved by having the sensor modulate the resonance frequency of a microwave cavity. Additional sensitivity can be gained with a large number N of sensors arranged along the laser beam or particle beam. Classical averaging their signal leads to a noise reduction of $1/\sqrt{N}$ in the standard deviation. When several sensors all couple to the same microwave cavity, one might even hope to achieve 'coherent averaging', in which case the noise reduction scales as $1/N$ [77, 78].

With $N = 1$ and a signal of 280 Hz, the sensitivity of the pendulum resulting from the standard quantum noise limit $\sqrt{S_{\rm SQL}} \approx 7 \times 10^{-17}\ {\rm m}/\sqrt{\rm Hz}$ is 3 orders of magnitude lower than that given by the thermal noise. For 1 week of measurement, the thermal noise still exceeds the signal generated by the modulated cw laser (respectively train of laser pulses) by 8 (almost 9) orders of magnitude.

3.3.2. LHC beam

The minimum frequency of one bunch of ultra-relativistic protons going around the ring of the LHC is in the kHz range (see section 2 2). Lower frequencies could be achieved by modulating the beam position with low frequency. The LHC as a source is expected to create almost 20 times larger amplitude than the considered cw-pumped cavity, due to the higher pulse power $P_{\rm p}^{\rm cav} = P^{\rm LHC}$ where an 'on-off' modulation of the LHC beam, similar to the cw cavity pumping scheme was assumed. After one week of measurement time one would be about 7 orders of magnitude off from measuring the signal with a single detector, 5 orders of magnitude starting at a temperature of $T = 5$ mK. Substantially more development will be needed to bridge this gap. Ideas in this direction are developed in the next section.

3.4. Optimizing the S/N

In this section we ask, what parameter values would be needed to achieve a signal-to-noise ratio comparable to 1 for a torsion balance or pendulum. We model both simply as damped harmonic oscillators, but keep in mind that their mechanial parameters and temperature can be substantially modified by using an optical spring and/or feedback cooling, and then compare to the existing setups described in [40, 58, 59]. We therefore continue to use $T_{\rm fb}$ for the final temperature, $Q_{\rm fb}$ for the final quality factor, and ω_0 as final resonance frequency $\times 2\pi$, regardless of how they might be achieved.

3.4.1. Optimization of a mechanical oscillator as detector and comparison to [40]

According to equation (5.60) in [69] the total position-noise power at frequency ω of a harmonic oscillator with (undamped) resonance frequency Ω measured with a transducer and amplifier that add back-action noise (referred back to the input) can be written as

$$\bar{S}_{xx,\rm tot}(T,\omega,\Omega,Q,m) = \frac{\gamma_0}{\gamma_0+\gamma}\bar{S}_{xx,\rm eq}(T,\omega,\Omega,Q,m) + \bar{S}_{xx,\rm add}(T,\omega,\Omega,Q,m), \tag{21}$$

where γ_0 is the intrinsic oscillator damping without coupling to the transducer and $\gamma \equiv \gamma(\omega)$ the damping with the coupling. The equilibrium noise (comprising both quantum noise and thermal noise at

temperature T) reads

$$\bar{S}_{xx,\mathrm{eq}}(T,\omega,\Omega,Q,m) = \hbar\coth\left(\frac{\hbar\omega}{2k_\mathrm{B}T}\right)\mathrm{Im}\chi_{xx}(\omega,\Omega,Q,m) \tag{22}$$

$$\mathrm{Im}\chi_{xx}(\omega,\Omega,Q,m) = \frac{Q\omega\Omega}{m(\omega^2\Omega^2+Q^2(\omega^2-\Omega^2)^2)}, \tag{23}$$

with the quality factor $Q\equiv\Omega/(\gamma_0+\gamma)$. To calculate $\bar{S}_{xx,\mathrm{add}}$, one needs to know the force noise power of the detector and amplifier, but $\bar{S}_{xx,\mathrm{add}}$ is lower bounded by $\bar{S}_{xx,\mathrm{addMin}} = \hbar|\mathrm{Im}\chi_{xx}|$. With this lowest possible value and the replacements $\Omega\to\omega_0$, $Q\to Q_\mathrm{fb}$, $T\to T_\mathrm{fb}$, one obtains for the total noise power to lowest order in γ/γ_0 (which slightly overestimates the contribution from $\bar{S}_{xx,\mathrm{eq}}(T,\omega,\omega_0,Q,m)$)

$$\bar{S}_{xx,\mathrm{tot}} = \hbar\left(1+\coth\left(\frac{\hbar\omega}{2k_\mathrm{B}T_\mathrm{fb}}\right)\right)\mathrm{Im}\chi_{xx}(\omega,\omega_0,Q_\mathrm{fb},m). \tag{24}$$

The maximum amplitude x_grav of the harmonic oscillator is given by equation (18) with $\sin(\tau_\mathrm{p}\omega_0/2)=1$, but is reached only asymptotically as function of time, namely as $x_\mathrm{grav}(t) = x_\mathrm{grav}(1-\exp(-\omega_0 t/(2Q_\mathrm{fb})))$. We assume that the total time $\tau_\mathrm{tot} = 1$ week for the experiment is split as $\tau_\mathrm{tot} = \tau_\mathrm{r}+\tau_m$ into a time τ_r needed for the amplitude of the harmonic oscillator to rise to a certain level, and a measurement time τ_m used for reducing the noise. The total signal-to-noise ratio on resonance is then given by

$$\begin{aligned} S/N &= x_\mathrm{grav}\left(1-\exp(-\omega_0(\tau_\mathrm{tot}-\tau_m)/(2Q_\mathrm{fb}))\right)\frac{\sqrt{\tau_m}}{\sqrt{\bar{S}_{xx,\mathrm{tot}}}} \\ &\simeq 0.01\,\frac{(1-e^{(\tau_m-\tau_\mathrm{tot})\frac{\omega_0}{2Q_\mathrm{fb}}})\sqrt{Q_\mathrm{fb}m\tau_m}}{\omega_0\sqrt{1+\coth\frac{4\cdot10^{-12}\omega_0}{T_\mathrm{fb}}}}, \end{aligned} \tag{25}$$

where a distance $\rho = 200\ \mu$m of the center of the detector mass from the beam axis was assumed. All quantities are in SI units. From this equation it is evident that the mass m should be as large as possible. At the same time, m cannot be made arbitrarily large, as otherwise the distance from the beam axis would have to be increased as well, which would lead to a decay of the signal $\propto 1/\rho$ for $\rho\gg\rho_\mathrm{min}$, where ρ_min is the minimum distance from the beam axis (which might contain a shielding of the particle beam in the case of the LHC, and which we assume to be $\rho_\mathrm{min} = 100\ \mu$m for the LHC but might have to be substantially increased when using a cryostat). In principle, for a spherical detector mass, a scaling $\propto m^{1/6}$ would still result, but it turns out that unrealistically large masses (larger than 1 kg) would be needed before this scaling gives an advantage over an alternative design with a cylindrical detector mass that allows to maintain $\rho = 200\ \mu$m. If we allow that cylinder to become as long as $L_\mathrm{cyl} = 0.5$ m and determine the maximum mass as $m = 0.9\pi\varrho_\mathrm{Si}(\rho-\rho_\mathrm{min})^2 L_\mathrm{cyl}$ (where 0.9 is a 'fudge factor' that avoids that the detector mass touches the shielding), we find $m = 33$ mg.

With that value inserted in equation (23), one can optimize S/N with respect to the parameters $\tau_m, \omega_0, Q_\mathrm{fb}$ and T_fb. With τ_tot kept equal to 1 week, in the range 1 rad/s $\leqslant\omega_0\leqslant 10^4$ rad/s, $1\leqslant Q_\mathrm{fb}\leqslant 10^8$, 1 nK $\leqslant T_\mathrm{fb}$ a maximum value $S/N\simeq 0.6$ is found for $\tau_m = 3\times10^5$ s, $\omega_0 = 2\pi\times 0.16$ Hz, $Q_\mathrm{fb} = 1.2\times10^5$, and minimal T_fb. The optimal value for ω_0 is at the lower end of the parameter range, but reasonably close to the one for the existing torsion balance in [40] ($\omega_0 = 2\pi\times 3.59$ mHz), where, however, the mechanical quality factor was $Q = 4.9$ and a mass of 92.1 mg was used. It remains to be seen if the parameters that result from the optimization can be reached. Problematic appears mostly, whether the temperature of the cooled mode of about 1 nK can be reached, especially at low frequencies.

3.4.2. Assumption of Q-scaling and comparison to [58]

The structural damping model used in [58] implies a quadratic scaling of the Q-factor with the resonance frequency (see equation (16)). Including this scaling behavior and allowing the modification of the resonance frequency by means of an optical spring, leads to frequencies in the 100 Hz to 1 kHz range being preferred by the optimization. This ultra-high Q-factor is, however, not reachable in practice as the optical spring introduces heating, and so the mechanical oscillator has to be cooled to stabilize the system. In existing systems, feedback cooling [58, 79], or a second optical spring tuned to the infrared [80] have been employed as cooling mechanisms. We assume an effective final temperature reached by feedback cooling of

$$T_\mathrm{fb} = 4T_\mathrm{bath}\frac{Q_\mathrm{fb}}{Q_\mathrm{eff}} = 4T_\mathrm{bath}\frac{Q_\mathrm{fb}}{Q_m\frac{\omega_0^2}{\omega_m^2}}, \tag{26}$$

Table 2. Comparison of the estimated sensitivity of the listed detectors with the expected amplitude of the sources considered on resonance and after the full build-up-time of the detector's oscillation. For the cases in which the main limiting factor is thermal noise, a temperature of 5 mK was assumed. Other parameters see text

	Rod		Liquid helium		Pendulum
ω_0	$2\pi \times 10^3$ Hz	$2\pi \times 10^9$ Hz	$2\pi \times 2.8 \times 10^3$ Hz		$2\pi \times 280$ Hz
Sensitivity	$1 \times 10^{-17}\mathrm{m}/\sqrt{\mathrm{Hz}}$	$4 \times 10^{-17}\mathrm{m}/\sqrt{\mathrm{Hz}}$	$2 \times 10^{-17}\mathrm{N}/\sqrt{\mathrm{Hz}}$	$1 \times 10^{-12}\mathrm{m}/\sqrt{Hz}$	$3 \times 10^{-14}\mathrm{m}/\sqrt{\mathrm{Hz}}$
Limiting factor	Thermal noise	SQL	Thermal noise		Thermal noise
Expected amplitude					
Laser pulses	2×10^{-25} m	2×10^{-34} m	2×10^{-25} N	1×10^{-20} m	3×10^{-26} m
cw cavity	4×10^{-25} m	4×10^{-34} m	3×10^{-25} N	2×10^{-20} m	5×10^{-26} m
LHC beam[a]	8×10^{-24} m	9×10^{-32} m	7×10^{-24} N	4×10^{-19} m	1×10^{-24} m

[a]Assuming the LHC beam can be modulated to produce a signal with appropriate frequency while maintaining the same average power.

as is expected in [58]. An initial temperature, before feedback cooling, of $T_{\mathrm{bath}} = 5$ mK is assumed and the parameter ranges are limited to 1 rad/s $< \omega_m <$ 10 000 rad/s, 1 rad/s $< \omega_0 <$ 10 000 rad/s, $1 < Q_m < 10^7$, and $1 < Q_{\mathrm{fb}} < 10^{10}$. We find $S/N \approx 0.077$ for the optimal parameters of $\omega_m = 2\pi \times 0.16$ Hz, $\omega_0 = 2\pi \times 600$ Hz, $Q_m = 10^7$, and $Q_{\mathrm{fb}} = 1.6 \times 10^8$. Compared to the generic optimization as seen above this seems underwhelming but if the scaling of Q and temperature can be attained, the final temperature of $T_{\mathrm{fb}} \approx 23$ nK would be more feasible than before.

3.4.3. Further possible improvements

A signal-to-noise ratio of 0.6 is still not good enough, but the planned upgrade of the LHC to the high-luminosity LHC [56] should increase S/N by a factor 10. Another factor 2.9 is expected to be gained by switching to tungsten (with mass density $\varrho_{\mathrm{W}} = 19,250\ \mathrm{kg\ m^{-3}}$) as detector-mass material, all other optimized parameters remaining equal. Both factors combined lead to an $S/N \simeq 16$.

The maximum of S/N found in the optimization is rather flat, especially with respect to the feedback cooling quality factor, such that there is a wide range of values with similar signal-to-noise ratios that allow one to take into account other engineering constraints not considered here and without such extreme effective temperatures. Hence, with the high-luminosity LHC and an optimized detector there is realistic hope that GR could be tested for the first time in this ultra-relativistic regime with a controlled terrestrial source and adapted optimized detector. Also without the upgrade of the LHC, further improvements from using a multitude of detectors (and possibly coherent averaging by coupling them all to the same read-out cavity [77, 78]) or longer integration times can be envisaged that would bring S/N to order one.

4. Discussion

4.1. Perspectives for measuring the gravitation of light or particle beams

We have theoretically investigated the fundamental limitations to measure the oscillating gravitational fields of lab-scale ultrarelativistic sources for three concrete examples: for laser beams, we have considered femtosecond-pulse lasers fed into a high finesse cavity, where they oscillate to and fro, and similarly, cw lasers used to pump a cavity periodically. For particle beams, we considered the LHC with its beam of proton bunches flying along the accelerator ring. All sources considered lead to oscillating curvature of space-time and acceleration of test particles with precisely controlled frequency up to the GHz range. In addition, we have given details on how modulations of these signals with much lower frequency, down to the kHz regime, can be achieved for all three example sources. In the latter regime, the LHC is the most promising ultrarelativistic source of gravity with a gravitational field strength 20 times stronger than the laser sources considered here.

We investigated three near-field detectors: a deformable rod offers force accumulation along its length thanks to its Young modulus. However, the spatial decrease of the studied gravitational effects limits the effects of force accumulation, resulting in immeasurably small amplitudes of the order of 8×10^{-24} m even in the case of the LHC as a source. In the liquid helium chamber from Singh *et al* [70], very high quality factors and low noise allow for sound wave buildup within the chamber. With the present experimental parameters [70], the gravitational force for the LHC is 3.5 orders of magnitude below the detectability limit of this detector with an averaging time of one week.

A pendulum from [58, 59] or a recently demonstrated torsion balance [40] turned out to be the most promising detectors. In the present form of the monolithic pendulum [58], the fully built-up signal from the LHC is 5 orders of magnitude away from the sensitivity achievable within 1 week of averaging time (assuming a starting temperature of $T = 5$ mK and a final temperature of $T_{\mathrm{fb}} = 12$ nK after a shift of the

resonance frequency via an optical spring and feedback cooling) with the benefit of a relatively small signal rise time.

Optimization of the signal-to-noise ratio of a mechanical oscillator as detector over its frequency, measurement time, quality factor and temperature in the parameter range provided in section 3.4.1, leads to an expectation of an S/N of about 0.6 with the LHC as source within one week of signal rise time and averaging. By using a denser material such as tungsten for the detector mass and profiting from the planned high-luminosity upgrade of the LHC an S/N ratio $\simeq 16$ appears possible with one week of measurement time for a single detector.

Our considerations concerned fundamental limitations so far, so that an S/N ratio larger than 1 should be considered a necessary condition, but would still make for a very difficult experiment with additional noise and engineering issues to be overcome (see e.g. [42]).

Important additional noise sources that have not been considered in our work include, for example, seismic and thermal noise that may be reduced by moving to a higher frequency regime. Therefore, while very high source frequencies (GHz) turned out to be detrimental for the considered detectors, it may still be interesting to investigate an intermediate frequency range above the kHz regime. In their current design, the superfluid helium detector [70] and the pendulum detector [59] need a source oscillating with a frequency of the order of kHz and 400 Hz to kHz, respectively. The pendulum's operation at higher frequencies might be possible and relatively easy to achieve, given that the relevant noise terms in the kHz range stem from suspension eigenmodes, which are changeable by design. Also in [81] parametric cooling into the ground state for pendulum-style gravitational sensors was demonstrated, reducing problems from thermal noise and seismic noise in an even larger frequency range. However, reaching the required low-temperatures in the nK regime in combination with the high quality factors will remain a huge challenge, even if the Q-scaling (16) and feedback cooling assumed in [58] is achieved.

4.2. Perspectives for quantum gravity experiments

The realization that the gravitational effect of light or high-energy particle beams might become measurable in the near future opens new experimental routes to quantum gravity, in the sense that it might become possible to study gravity of light or matter in a non-trivial quantum superposition. Concerning light, non-classical states of light, in particular in the form of squeezed light, have been studied and experimentally realized for a long time, and are now used for enhanced gravitational-wave-sensing in LIGO [82]. While the current records of squeezing were obtained for smaller intensities than relevant for the gravitational sources we consider here [83], squeezing and entanglement shared by many modes was already achieved for photon numbers on the order 10^{16} by using a coherent state in one of the modes [84]. This is substantially smaller than the $\sim 10^{21}$ photons estimated in the cavity in the example of the cw laser leading to 100 GW circulating power considered above, but one might hope that technology progresses to achieve at least a small amount of squeezing also for the high-power sources relevant here.

As for the high-energy particle beams, transverse 'coherent oscillations' of two colliding accelerator beams (including the ones at LHC) have already been studied [85–89] but these are of classical nature. Non-trivial quantum states of the beam are those that cannot be described by a positive semidefinite Glauber-Sudarshan P-function, a concept from quantum optics that is well established for harmonic oscillators and is hence applicable to small-amplitude transverse motion of the particle beam in the focusing regions where there is a linear restoring force. A stronger requirement would be a non-positive-semidefinite Wigner function, which can be applied to any system with a phase space. In order to reach such quantum states, it will be necessary to cool the particle beams. Efforts to do so are on the way or proposed for other motivations: cooling enhances the phase space density and hence the intensity of the beam in its center. In addition, new phases of matter in the form of classical crystalline beams attracted both theoretical and experimental interest at least since the 1980s [90–95]. Recently it was proposed to extend this work to create an 'ultracold crystalline beam' and turning an ion beam into a quantum computer. For this, the beam should become an ion Coulomb crystal cooled to such low temperatures that the de Broglie wavelength becomes larger than the particles' thermal oscillation amplitudes [96]. Ideally, for our purposes, the center-of-mass motion of the beam should be cooled to the ground state of the (approximate) harmonic oscillator that restrains locally, at the detector position, the transverse motion, before interesting quantum superpositions can be achieved.

However, even superpositions in longitudinal direction would create an interesting experimental situation for which there is currently no theoretical prediction. Experimental progress in this direction would allow a different kind of search for quantum gravity effects compared to popular current attempts to detect deviations from canonical commutation relations between conjugate observables as predicted by various quantum-gravity candidates (see e.g. [97]). Different techniques for cooling particle beams are available (see e.g. [98, 99] for overviews): Stochastic cooling (measurement of deviation from the ideal

beam-line and fast electronic counter-measures further down the beamline) was used at CERN for producing high-intensity anti-proton beams from 1972 till 2017 and is still used there for anti-proton deceleration, as well as at Forschungszentrum Jülich (COSY experiment) and GSI Helmholtzzentrum für Schwerionenforschung GmbH (Heavy Ion storage ring ESR); electron cooling (absorption of entropy by a co-propagating electron beam of much lower energy and entropy), and a modern cousin of it, 'coherent electron cooling' [100], under development at Brookhaven National Lab for ion energies up to 40 GeV/u for Au^{+79} ions [57, 101]; and laser cooling, with which longitudinal temperatures on the order of mK have been reached for moderately relativistic ion beams [102, 103]. Laser cooling is most efficient for longitudinal cooling, but transverse cooling can be achieved to some extent through sympathetic cooling [104]. Laser cooling is now proposed for an ultrarelativistic heavy-ion upgrade of the LHC [56]. Despite all these techniques, ground states of the transverse center-of-mass motion have never been reached in any ultra-relativistic particle beam as far as we know, nor was it perceived as an important goal. We hope that the perspective of winning the race to the first quantum gravity experiment will change this. As Grishchuk put it [11]. 'The laboratory experiment is bound to be expensive, but one should remember that a part of the cost is likely to be reimbursed from the Nobel prize money!' The successful development of ion-trap quantum computers, where ground-state cooling of collective modes of ion crystals has become standard, might lend credibility to the feasibility of the endeavor.

Acknowledgments

We thank Daniel Estève for discussion, correspondence and references, and for proposing the idea to look at pulses in a cavity; Werner Vogelsang for a discussion on particle accelerator beams, Nobuyuki Matsumoto and Eddy Collin for correspondence. DR acknowledges funding by the Marie Skłodowska-Curie Action IF program—Project-Name 'Phononic Quantum Sensors for Gravity" (PhoQuS-G)—Grant Number 832250. We acknowledge support by Open Access Publishing Fund of University of Tübingen.

Appendix A. Gravitational field of a laser-pulse in a cavity

Following the calculation of the gravitational field of a box shaped laser pulse of length L emitted at $z = 0$ and absorbed at $z = D$ from [18, 21], we extend the calculation to an oscillation of a short pulse ($L < D$) between 0 and D. For a pulse propagating along the $\pm z$-direction the energy momentum tensor is given by $T_{00} = T_{zz} = \mp T_{0z} = \mp T_{z0} = u(z,t)\delta(x)\delta(y)A$, where $u(z,t)$ is the energy density of the electromagnetic field in 3D and A is the effective transverse area. This energy momentum tensor violates the continuity equation as the recoil of the mirrors is neglected. However, ultimately only positions very close to the beam will be considered where these contributions vanish [18]. The energy density is given by

$$u(z,t) = u_{\mathrm{p}}\Theta(z)\Theta(D-z)\sum_{n=0}^{\infty}\left(\chi_{+}^{n}(z,t)+\chi_{-}^{n}(z,t)\right), \tag{A1}$$

where

$$\chi_{+}^{n}(z,t) = \left(\Theta\left(ct-2nD-z\right)-\Theta\left(ct-2nD-z-L\right)\right) \tag{A2}$$

$$\chi_{-}^{n}(z,t) = \left(\Theta\left(ct-(2n+1)D+(z-D)\right)-\Theta\left(ct-(2n+1)D+(z-D)-L\right)\right) \tag{A3}$$

delimit the profile of the pulse injected at $t = 0$ and reflected $2n$ times ($2n+1$ times) traveling in positive (negative) z-direction, and $u_{\mathrm{p}} = \frac{E_{\mathrm{p}}}{LA}$ is the pulse energy density.

From the wave equation in the Lorenz gauge

$$\Box h_{\mu\nu} = -\frac{16\pi G}{c^4}T_{\mu\nu} \tag{A4}$$

the metric perturbation can be calculated using the Green's function

$$h_{\mu\nu}(\vec{r},t) = \frac{4G}{c^4}\int \mathrm{d}^3r'\,\frac{T_{\mu\nu}(\vec{r}',t-|\vec{r}-\vec{r}'|/c)}{|\vec{r}-\vec{r}'|}. \tag{A5}$$

Given the energy–momentum tensor, the metric perturbation can be decomposed into $h_{\mu\nu} = h^{+}_{\mu\nu} + h^{-}_{\mu\nu}$ and the only non-zero elements of $h^{\pm}_{\mu\nu}$ are $h^{\pm}_{00} = h^{\pm}_{zz} = \mp h^{\pm}_{z0} = \mp h^{\pm}_{0z} \equiv h^{\pm}$, with

$$h^{\pm}(x,y,z,t) = \frac{4Gu_{\mathrm{p}}A}{c^4}\int_0^D \mathrm{d}z'\,\frac{\sum_n \chi_{\pm}^{n}\left(z',t-\sqrt{\rho^2+(z-z')^2}/c\right)}{\sqrt{\rho^2+(z-z')^2}}, \tag{A6}$$

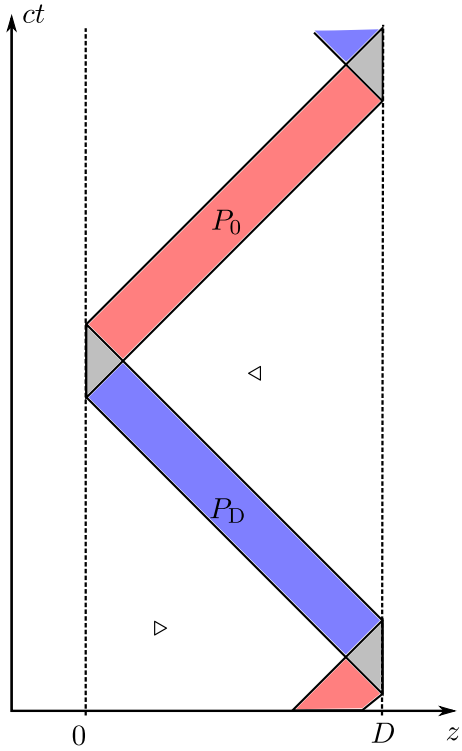

Figure 2. Spacetime is split into zones by the light cones of the reflection events of a pulse oscillating between two mirrors.

$\rho = \sqrt{x^2 + y^2}$, and $u_p A = \frac{P}{c}$.

The box function χ_+^n imposes the additional boundaries of $a_+^n < z' < b_+^n$, with

$$a_+^n = z + \frac{(ct - 2nD - L - z)^2 - \rho^2}{2(ct - 2nD - L - z)} \tag{A7}$$

$$b_+^n = z + \frac{(ct - 2nD - z)^2 - \rho^2}{2(ct - 2nD - z)}. \tag{A8}$$

Similarly, the box function χ_-^n adds the constraints of $a_-^n < z' < b_-^n$, with

$$b_-^n = z - \frac{(ct - (2n+1)D - L + (z - D))^2 - \rho^2}{2\,(ct - (2n+1)D - L + (z - D))} \tag{A9}$$

$$a_-^n = z - \frac{(ct - (2n+1)D + (z - D))^2 - \rho^2}{2\,(ct - (2n+1)D + (z - D))}. \tag{A10}$$

Following [21] the substitution $\zeta(z') = z' - z + \sqrt{\rho^2 + (z' - z)^2}$ is used to further simplify the integration. The constraints turn into

$$\zeta(0) = r - z \tag{A11}$$

$$\zeta(D) = r_D - (z - D) \tag{A12}$$

$$\zeta(a_+^n) = ct - 2nD - L - z \tag{A13}$$

$$\zeta(b_+^n) = ct - 2nD - z \tag{A14}$$

$$\zeta(b_-^n) = \frac{\rho^2}{ct - (2n+1)D - L + (z - D)} \tag{A15}$$

$$\zeta(a_-^n) = \frac{\rho^2}{ct - (2n+1)D + (z - D)}, \tag{A16}$$

where $r = \sqrt{\rho^2 + z^2}$, and $r_D = \sqrt{\rho^2 + (z - D)^2}$.

For an observer positioned at $z \in (L, D - L)$ there are 4 different space-time zones (see figure 2)

P_0^n: $2nD < ct - r < 2nD + L$ causally connected to the reflection at $z = 0, ct = 2nD$.

$\triangleright^n$: $2nD + r + L < ct < (2n+1)D + r_D$ not causally connected to any reflection events, but causally connected to the pulse traveling from $z = 0, ct = 2nD$ to $z = D, ct = (2n+1)D$.

P_D^n: $(2n+1)D < ct - r_D < (2n+1)D + L$ causally connected to the reflection at $z = D, ct = (2n+1)D$.

$\triangleleft^n$: $(2n+1)D + r_D + L < ct < (2n+2)D + r$ not causally connected to any reflection events, but causally connected to the pulse traveling from $z = D, ct = (2n+1)D$ to $z = 0, ct = (2n+2)D$.

The metric perturbation is then given by

$$h^+ = \frac{4GP}{c^5}\begin{cases} \ln\dfrac{\zeta(b_+^n)}{\zeta(0)} = \ln\dfrac{ct_{2n} - z}{r - z} & \text{for } (z,t) \in P_0^n, \\ \ln\dfrac{\zeta(b_+^n)}{\zeta(a_+^n)} = \ln\dfrac{ct_{2n} - z}{ct_{2n} - L - z} & \text{for } (z,t) \in \triangleright^n, \\ \ln\dfrac{\zeta(D)}{\zeta(a_+^n)} = \ln\dfrac{r_D - (z-D)}{ct_{2n+1} - L - (z-D)} & \text{for } (z,t) \in P_D^n, \\ 0 & \text{for } (z,t) \in \triangleleft^n, \end{cases} \tag{A17}$$

caused by the pulses starting from $z = 0$ and

$$h^- = \frac{4GP}{c^5}\begin{cases} \ln\dfrac{\zeta(b_-^{n-1})}{\zeta(0)} = \ln\dfrac{\rho^2}{(ct_{2n} - L + z)(r - z)} & \text{for } (z,t) \in P_0^n, \\ 0 & \text{for } (z,t) \in \triangleright^n, \\ \ln\dfrac{\zeta(D)}{\zeta(a_-^n)} = \ln\dfrac{(r_D - (z-D))(ct_{2n+1} + (z-D))}{\rho^2} & \text{for } (z,t) \in P_D^n, \\ \ln\dfrac{\zeta(b_-^n)}{\zeta(a_-^n)} = \ln\dfrac{ct_{2n+1} + (z-D)}{ct_{2n+1} - L + (z-D)} & \text{for } (z,t) \in \triangleleft^n, \end{cases} \tag{A18}$$

caused by the pulses returning from $z = D$, where $t_j := t - jD/c$.

Following [21], the only independent non-vanishing elements of the Riemann curvature tensor are given by

$$R_{0z0z} = -\frac{1}{2}\left(\frac{1}{c}\partial_t + \partial_z\right)^2 h^+ - \frac{1}{2}\left(\frac{1}{c}\partial_t - \partial_z\right)^2 h^- \tag{A19}$$

$$R_{0z0i} = -R_{0zzi} = -\frac{1}{2}\partial_i\left(\frac{1}{c}\partial_t + \partial_z\right) h^+ - \frac{1}{2}\partial_i\left(\frac{1}{c}\partial_t - \partial_z\right) h^- \tag{A20}$$

$$R_{0i0j} = R_{zizj} = -\frac{1}{2}\partial_i\partial_j(h^+ + h^-) \tag{A21}$$

$$R_{0izj} = \frac{1}{2}\partial_i\partial_j(h^+ - h^-), \tag{A22}$$

where $i, j \in \{x, y\}$.

Given the explicit form of h^+ and h^- from equations (A17) and (A18), the curvature is.

P_0^n: $R_{0z0z} = \frac{4GP}{c^5}\frac{z}{r^3}$, $R_{0z0i} = 0$, $R_{0i0j} = \frac{4GP}{c^5}\frac{z}{\rho^2 r}\left(\delta_{ij} - \frac{r_i r_j}{\rho^2 r^2}(2r^2 + \rho^2)\right)$, $R_{0izj} = -\frac{4GP}{c^5}\frac{1}{\rho^2}\left(\delta_{ij} - \frac{2r_i r_j}{\rho^2}\right)$

$\triangleright^n$: $R_{\mu\nu\rho\sigma} = 0 \forall \mu, \nu, \rho, \sigma$

P_D^n: $R_{0z0z} = \frac{4GP}{c^5}\frac{D-z}{r_D^3}$, $R_{0z0i} = 0$, $R_{0i0j} = \frac{4GP}{c^5}\frac{(D-z)}{r_D\rho^2}\left(\delta_{ij} - \frac{r_i r_j}{r_D^2\rho^2}(2r_D^2 + \rho^2)\right)$, $R_{0izj} = \frac{4GP}{c^5}\frac{1}{\rho^2}\left(\delta_{ij} - \frac{2r_i r_j}{\rho^2}\right)$

$\triangleleft^n$: $R_{\mu\nu\rho\sigma} = 0 \forall \mu, \nu, \rho, \sigma$.

In the limit $\rho \ll r, r_D$, the only independent components of the curvature in leading order are

$$R_{0i0j} = -R_{0izj} = \frac{4GP}{c^5}\frac{1}{\rho^2}\left(\delta_{ij} - 2\frac{r_i r_j}{\rho^2}\right) \equiv \mathcal{R} \qquad \forall (z,t) \in P_0^n \tag{A23}$$

$$R_{0i0j} = \mathcal{R} = R_{0izj} \qquad \forall (z,t) \in P_D^n, \tag{A24}$$

with $\rho \ll z, (z - D)$. A simplified metric perturbation resulting in the same curvature tensor as equation (A23) is given by

$$\tilde{h}^+ = \begin{cases} -\dfrac{8GP}{c^5}\ln\rho & \text{for } (z,t) \in P_0^n \\ 0 & \text{else} \end{cases}, \qquad \tilde{h}^- = \begin{cases} -\dfrac{8GP}{c^5}\ln\rho & \text{for } (z,t) \in P_D^n \\ 0 & \text{else} \end{cases}. \tag{A25}$$

The geodesic equation for a test particle at position x^μ is given in coordinate time $t = \frac{1}{c}x^0$ by

$$\frac{\mathrm{d}^2x^\mu}{\mathrm{d}t^2} = -\Gamma^\mu_{\alpha\beta}\frac{\mathrm{d}x^\alpha}{\mathrm{d}t}\frac{\mathrm{d}x^\beta}{\mathrm{d}t} + \Gamma^0_{\alpha\beta}\frac{\mathrm{d}x^\alpha}{\mathrm{d}t}\frac{\mathrm{d}x^\beta}{\mathrm{d}t}\frac{\mathrm{d}x^\mu}{\mathrm{d}t}. \tag{A26}$$

For a non-relativistic test particle this reduces to

$$\ddot{x}^a = -c^2\Gamma^a_{00} + \mathcal{O}\left(\frac{v^2}{c^2}\right), \tag{A27}$$

with the linearized Christoffel symbol

$$\Gamma^\rho_{\mu\nu} = \frac{1}{2}\eta^{\lambda\rho}(\partial_\mu h_{\nu\lambda} + \partial_\nu h_{\lambda\mu} - \partial_\lambda h_{\mu\nu}) \implies \Gamma^a_{00} = -\frac{1}{2}\partial_a\tilde{h}_{00}. \tag{A28}$$

The acceleration a non-relativistic sensor experiences is therefore equivalent to that from a Newtonian potential

$$\Phi = \frac{4GP}{c^3}\ln\rho \tag{A29}$$

for the duration of the pulse passing by (P_0, P_D) with the potential vanishing at all other times.

Appendix B. Intensity in a Fabry–Pérot resonator

The considerations here follow those from [49] closely but are modified to reflect the setups used in this work.

For a Fabry–Pérot resonator consisting of two mirrors with field reflection coefficients $\sqrt{R_1}$, $\sqrt{R_2}$ and field transmission coefficients $\sqrt{T_1}$, $\sqrt{T_2}$, the field in cavity (at the face of mirror 1) resulting from a pump beam striking mirror 1 can be written as

$$E_{\mathrm{cav}}(t) = \sqrt{R_1R_2}E_{\mathrm{cav}}(t-\tau_{\mathrm{rt}}) + \sqrt{T_1}E_{\mathrm{pump}}(t) \tag{B1}$$

in the time domain, where τ_{rt} is the time for one round trip in the cavity. In the frequency domain this can be written as

$$\tilde{E}_{\mathrm{cav}}(\omega) = \tilde{G}(\omega)\tilde{E}_{\mathrm{pump}}(\omega), \quad \text{with} \quad \tilde{G}(\omega) = \frac{\sqrt{T_1}}{1-\sqrt{R_1R_2}\mathrm{e}^{-\mathrm{i}\omega\tau_{\mathrm{rt}}}}. \tag{B2}$$

B.1. Single monochromatic rectangular pulse

For a monochromatic pump field of frequency ω_{E} and length τ_{p} entering the cavity at $t = 0$ the pump field is given by

$$E^{\mathrm{p}}_{\mathrm{pump}}(t) = E_0\mathrm{e}^{\mathrm{i}\omega_{\mathrm{E}}t}\Pi_{\tau_{\mathrm{p}}}(t), \quad \text{with} \quad \Pi_{\tau_{\mathrm{p}}}(t) = \Theta(t) - \Theta\left(t-\tau_{\mathrm{p}}\right) \tag{B3}$$

$$\implies \tilde{E}^{\mathrm{p}}_{\mathrm{pump}}(\omega) = E_0\tau_{\mathrm{p}}\mathrm{e}^{-\mathrm{i}\omega\tau_{\mathrm{p}}/2}\,\mathrm{sinc}((\omega-\omega_{\mathrm{E}})\tau_{\mathrm{p}}). \tag{B4}$$

The corresponding Fourier transformed field amplitude in the cavity is then given through equation (B2) by

$$\tilde{E}^{\mathrm{p}}_{\mathrm{cav}}(\omega) = E_0\frac{\sqrt{T_1}\mathrm{e}^{-\mathrm{i}\omega\tau_{\mathrm{p}}/2}}{1-\sqrt{R_1R_2}\mathrm{e}^{-\mathrm{i}\omega\tau_{\mathrm{rt}}}}\tau_{\mathrm{p}}\,\mathrm{sinc}((\omega-\omega_{\mathrm{E}})\tau_{\mathrm{p}}) \tag{B5}$$

$$\implies E^{\mathrm{p}}_{\mathrm{cav}}(t) = E_0\sqrt{T_1}\sum_{n=0}^{\infty}(R_1R_2)^{n/2}\mathrm{e}^{\mathrm{i}\omega_{\mathrm{E}}(t-n\tau_{\mathrm{rt}})}\Pi_{\tau_{\mathrm{p}}}(t-n\tau_{\mathrm{rt}}). \tag{B6}$$

For a very short pulse $\tau_{\mathrm{p}} \ll \tau_{\mathrm{rt}}$, none of the addends will overlap and the intensity in the cavity is

$$I^{\mathrm{p}}_{\mathrm{cav}}(t) = |E^{\mathrm{p}}_{\mathrm{cav}}(t)|^2 = E_0^2T_1\sum_{n=0}^{\infty}(R_1R_2)^n\Pi_{\tau_{\mathrm{p}}}(t-n\tau_{\mathrm{rt}}). \tag{B7}$$

The pulse enters the cavity with an intensity reduced by T_1 and is reduced by a further factor R_1R_2 for each subsequent round trip. The average power in the cavity relative to that of the pump laser is then given by

$$\frac{P_{\mathrm{cav}}}{P_0} = T_1\sum_{n=0}^{\infty}(R_1R_2)^n = \frac{T_1}{1-R_1R_2} = \frac{1-R_1}{1-R_1R_2} \lesssim 1. \tag{B8}$$

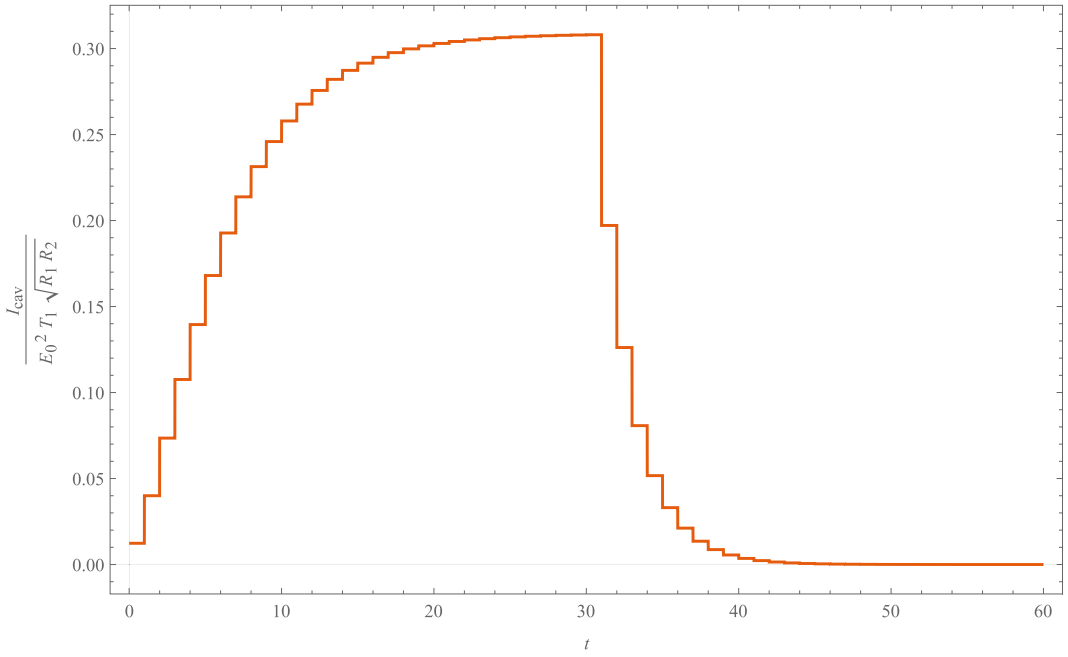

Figure 3. Intensity inside the cavity resulting from a long ($\tau_p \gg \tau_{rt}$) rectangular pulse of monochromatic or spectrally narrow light. The time is given in units of τ_{rt}.

For long pulses ($\tau_p \gg \tau_{rt}$) and a resonant cavity ($\omega_E \tau_{rt} = 2\pi m$) only addends from $n_{min} = \max\left(0, \left\lceil \frac{t-\tau_p}{\tau_{rt}} \right\rceil\right)$ to $n_{max} = \max\left(0, \left\lfloor \frac{t}{\tau_{rt}} \right\rfloor\right)$ contribute for any given time, returning

$$E^p_{cav}(t) = E_0 \sqrt{T_1} \left[\frac{1 - (R_1 R_2)^{\frac{n_{max}+1}{2}}}{1 + \sqrt{R_1 R_2}} - \frac{1 - (R_1 R_2)^{\frac{n_{min}+1}{2}}}{1 + \sqrt{R_1 R_2}} \right] \tag{B9}$$

$$= E_0 \sqrt{T_1} \sqrt{R_1 R_2} \frac{(R_1 R_2)^{n_{min}/2} - (R_1 R_2)^{n_{max}/2}}{1 + \sqrt{R_1 R_2}}. \tag{B10}$$

The intensity for this long-pulse resonant cavity case can be described as a 'jagged shark fin' and is plotted in figure 3.

B.2. Series of monochromatic rectangular pulses

A series of periodic pulses separated by time τ_{rt} can be written as a sum of pulses $E^{\Sigma}_{pump}(t) = \sum_k E^p_{pump}(t - k\tau_{rep})$. As all of the operations on the field are linear the pump field equation (B5) can be used to find

$$E^{\Sigma}_{cav}(t) = \sum_k E^p_{cav}(t - k\tau_{rep}). \tag{B11}$$

For repetition times much longer than the lifetime of a pulse in the cavity $\tau_{rep} \gg \tau_L \sim \frac{\tau_{rt}(R_1 R_2)^{1/4}}{1-\sqrt{R_1 R_2}}$, and the pulse length $\tau_{rep} \gg \tau_p$, the addends barely overlap such that there is no interference between consecutive pulses. In this case the intensity in the cavity is just that of the singular pulse repeating periodically.

ORCID iDs

Felix Spengler https://orcid.org/0000-0002-9295-8587
Dennis Rätzel https://orcid.org/0000-0003-3452-6222
Daniel Braun https://orcid.org/0000-0001-8598-2039

References

[1] Berti E, Yagi K and Yunes N 2018 *Gen. Relativ. Gravit.* **50** 1
[2] Beltrán Jiménez J, Heisenberg L, Olmo G J and Rubiera-Garcia D 2018 *Phys. Rep.* **727** 1
[3] Langlois D, Saito R, Yamauchi D and Noui K 2018 *Phys. Rev.* D **97** 061501
[4] Barceló C, Carballo-Rubio R and Garay L J 2017 *J. High Energy Phys.* JHEP05(2017)054

[5] Maselli A, Pani P, Cardoso V, Abdelsalhin T, Gualtieri L and Ferrari V 2018 *Phys. Rev. Lett.* **120** 081101
[6] Grishchuk L and Sazhin M 1974 *JETP* **38** 215
[7] Grishchuk L and Sazhin M 1975 *JETP* **41** 787
[8] Grishchuk L P 1977 *Sov. Phys. Usp.* **20** 319
[9] Portilla M and Lapiedra R 2001 *Phys. Rev.* D **63** 044014
[10] Ballantini R, Bernard P, Chiaveri E, Chincarini A, Gemme G, Losito R, Parodi R and Picasso E 2003 *Class. Quantum Grav.* **20** 3505
[11] Grishchuk L P 2003 Electromagnetic generators and detectors of gravitational waves (arXiv:gr-qc/0306013)
[12] Rudenko V N 2004 Very high frequency gravitational waves in laboratory and space *Gravitation and Kosmology* vol 10 pp 41–9
[13] Baker R M L and Baker B S 2012 *Syst. Cyber. Inf.* **10** 8
[14] Kolosnitsyn N I and Rudenko V N 2015 *Phys. Scr.* **90** 074059
[15] Füzfa A 2018 arXiv:1702.06052 [gr-qc]
[16] Chen P 2021 SRGW2021—ARIES WP6 workshop: storage rings and gravitational waves (https://indi.to/cqnYK)
[17] Jowett J 2021 SRGW2021—ARIES WP6 workshop: storage rings and gravitational waves (https://indi.to/Jr7kx)
[18] Tolman R C, Ehrenfest P and Podolsky B 1931 *Phys. Rev.* **37** 602
[19] Bonnor W B 1969 *Commun. Math. Phys.* **13** 163
[20] Aichelburg P C and Sexl R U 1971 *Gen. Relativ. Gravit.* **2** 303
[21] Rätzel D, Wilkens M and Menzel R 2016 *New J. Phys.* **18** 023009
[22] Mallett R L 2000 *Phys. Lett.* A **269** 214
[23] Strohaber J 2013 *Gen. Relativ. Gravit.* **45** 2457
[24] Cox D E, O'Brien J G, Mallett R L and Roychoudhuri C 2007 *Found. Phys.* **37** 723
[25] Scully M O 1979 *Phys. Rev.* D **19** 3582
[26] Ji P, Zhu S-T and Shen W-D 1998 *Int. J. Theor. Phys.* **37** 1779
[27] Ji P and Bai Y 2006 *Eur. Phys. J.* C **46** 817
[28] Schneiter F, Rätzel D and Braun D 2018 *Class. Quantum Grav.* **35** 195007
[29] Schneiter F, Rätzel D and Braun D 2019 *Class. Quantum Grav.* **36** 119501
[30] Schneiter F, Rätzel D and Braun D 2019 *Class. Quantum Grav.* **36** 205007
[31] Ji P, Bai Y and Wang L 2007 *Phys. Rev.* D **75** 024010
[32] Balasin H and Nachbagauer H 1996 *Class. Quantum Grav.* **13** 731
[33] Loustó C O and Sánchez N 1990 *Int. J. Mod. Phys.* A **05** 915
[34] Barrabes C and Hogan P 2003 *Phys. Rev.* D **67** 084028
[35] Nakamura K, Mao H-S, Gonsalves A J, Vincenti H, Mittelberger D E, Daniels J, Magana A, Toth C and Leemans W P 2017 *IEEE J. Quantum Electron.* **53** 1
[36] L. L. N. Laboratory 2016 National ignition facility user guide 2016 (https://nifuserguide.llnl.gov/)
[37] Aléonard M *et al* 2011 *WHITEBOOK ELI - Extreme Light Infrastructure; Science and Technology with Ultra-Intense Lasers* ed G Korn (Germany: THOSS Media GmbH)
[38] CERN 2022 *Facts and figures about LHC* https://home.cern/resources/faqs/facts-and-figures-about-lhc, https://lhc-machine-outreach.web.cern.ch/beam.htm
[39] GSI 2013 *Beam properties* https://www.gsi.de/en/work/accelerator_operations/accelerators/heavy_ion_synchrotron_sis18/beam_properties.htm
[40] Westphal T, Hepach H, Pfaff J and Aspelmeyer M 2020 arXiv:2009.09546 [gr-qc]
[41] Komori K, Enomoto Y, Ooi C P, Miyazaki Y, Matsumoto N, Sudhir V, Michimura Y and Ando M 2020 *Phys. Rev.* A **101** 011802
[42] Schmöle J, Dragosits M, Hepach H and Aspelmeyer M 2016 *Class. Quantum Grav.* **33** 125031
[43] Kapner D 2007 *Phys. Rev. Lett.* **98** 021101
[44] Hoyle C D, Kapner D J, Heckel B R, Adelberger E G, Gundlach J H, Schmidt U and Swanson H E 2004 *Phys. Rev.* D **70** 042004
[45] Schreppler S, Spethmann N, Brahms N, Botter T, Barrios M and Stamper-Kurn D M 2014 *Science* **344** 1486
[46] Pikovski I, Vanner M R, Aspelmeyer M, Kim M S and Brukner Č 2012 *Nat. Phys.* **8** 393–7
[47] Belenchia A, Wald R M, Giacomini F, Castro-Ruiz E, Brukner Č and Aspelmeyer M 2018 *Phys. Rev.* D **98** 126009
[48] Ismail N, Kores C C, Geskus D and Pollnau M 2016 *Opt. Express* **24** 16366
[49] Cesini G, Guattari G, Lucarini G and Palma C 1977 *Opt. Acta* **24** 1217
[50] Pupeza I 2012 *Power Scaling of Enhancement Cavities for Nonlinear Optics* (*Springer Theses*) (New York: Springer)
[51] Carstens H *et al* 2014 *Opt. Lett.* **39** 2595
[52] Sistrunk E *et al* 2019 Laser technology development for high peak power lasers achieving kilowatt average power and beyond *SPIE Optics + Optoelectronics* vol 11034 ed P Bakule and C L Haefner (Prague 1–4 April 2019) pp 1–8
[53] Schwartz O, Axelrod J J, Tuthill D R, Haslinger P, Ophus C, Glaeser R M and Müller H 2017 *Opt. Express* **25** 14453
[54] Cartlidge E 2018 The light fantastic *Science* **359** 382–5
[55] IPG Laser GmbH 2022 https://ipgphotonics.com/de/products/lasers/high-power-cw-fiber-lasers
[56] Krasny M W, Petrenko A and Płaczek W 2020 *Prog. Part. Nucl. Phys.* **114** 103792
[57] Litvinenko V N 2017 Brookhaven national lab update on status of experimental demonstration
[58] Matsumoto N, Cataño-Lopez S B, Sugawara M, Suzuki S, Abe N, Komori K, Michimura Y, Aso Y and Edamatsu K 2019 *Phys. Rev. Lett.* **122** 071101
[59] Cataño-Lopez S B, Santiago-Condori J G, Edamatsu K and Matsumoto N 2020 *Phys. Rev. Lett.* **124** 221102
[60] Marquardt F and Girvin S 2009 *Physics* **2** 40
[61] Metcalfe M 2014 *Appl. Phys. Rev.* **1** 031105
[62] Millen J, Monteiro T S, Pettit R and Vamivakas A N 2020 *Rep. Prog. Phys.* **83** 026401
[63] Arcizet O *et al* 2006 *Phys. Rev. Lett.* **97** 133601
[64] Ranjit G, Cunningham M, Casey K and Geraci A A 2016 *Phys. Rev.* A **93** 053801
[65] Schneiter F, Qvarfort S, Serafini A, Xuereb A, Braun D, Rätzel D and Bruschi D E 2020 *Phys. Rev.* A **101** 033834
[66] Qvarfort S, Plato A D K, Bruschi D E, Schneiter F, Braun D, Serafini A and Rätzel D 2020 Optimal estimation of time-dependent gravitational fields with quantum optomechanical systems (arXiv:2008.06507)
[67] Maggiore M 2008 *Gravitational Waves: Theory and Experiments* vol 1 (Oxford: Oxford University Press)
[68] Rätzel D, Schneiter F, Braun D, Bravo T, Howl R, Lock M P E and Fuentes I 2018 *New J. Phys.* **20** 053046
[69] Clerk A A, Devoret M H, Girvin S M, Marquardt F and Schoelkopf R J 2010 *Rev. Mod. Phys.* **82** 1155

[70] Singh S, Lorenzo L A D, Pikovski I and Schwab K C 2017 *New J. Phys.* **19** 073023
[71] Caves C M, Thorne K S, Drever R W P, Sandberg V D and Zimmermann M 1980 *Rev. Mod. Phys.* **52** 341
[72] Braginsky V B, Vorontsov Y I and Thorne K S 1980 *Science* **209** 547
[73] Ockeloen-Korppi C F, Damskägg E, Pirkkalainen J-M, Heikkilä T T, Massel F and Sillanpää M A 2016 *Phys. Rev.* X **6** 041024
[74] Ockeloen-Korppi C F, Damskägg E, Pirkkalainen J-M, Heikkilä T T, Massel F and Sillanpää M A 2017 *Phys. Rev. Lett.* **118** 103601
[75] Zhong L *et al* 2013 *New J. Phys.* **15** 125013
[76] T'oth L D, Bernier N R, Nunnenkamp A, Feofanov A K and Kippenberg T J 2017 *Nat. Phys.* **13** 787
[77] Fraïsse J M E and Braun D 2015 *Ann. Phys.* **527** 701–12
[78] Braun D and Popescu S 2014 *Quantum Measurements and Quantum Metrology* vol 2
[79] Buonanno A and Chen Y 2002 *Phys. Rev.* D **65** 042001
[80] Rehbein H, Müller-Ebhardt H, Somiya K, Danilishin S L, Schnabel R, Danzmann K and Chen Y 2008 *Phys. Rev.* D **78** 062003
[81] Hartwig D, Petermann J and Schnabel R 2020 arXiv:2012.12158
[82] Aasi J *et al* 2013 *Nat. Photon.* **7** 613
[83] Vahlbruch H, Mehmet M, Danzmann K and Schnabel R 2016 *Phys. Rev. Lett.* **117** 110801
[84] Keller G, D'Auria V, Treps N, Coudreau T, Laurat J and Fabre C 2008 *Opt. Express* **16** 9351
[85] Alexahin Y I 1996 *Part. Accel.* **54** 183
[86] Buffat X, Papotti G, Herr W, Calaga R, Pieloni T, Giachino R and White S 2014 Coherent beam–beam mode in the LHC *Contribution to the ICFA Mini-Workshop on Beam–Beam Effects in Hadron Colliders, CERN* (Geneva, Switzerland 18–22 March 2013) pp 227–30
[87] Alexahin Y, Grote H, Herr W and Zorzano M 2001 *CERN-LHC-Project-Report-469* 5
[88] Zorzano M P and Zimmermann F 1999 *LHC Project Report 314* 19
[89] Yokoya K and Koiso H 1990 *Part. Accel.* **27** 181
[90] Schiffer J P and Kienle P 1985 *Z. Phys.* A **321** 181
[91] Schätz T, Schramm U and Habs D 2001 *Nature* **412** 717
[92] Wei J and Sessler A M 2003 *18th Advanced ICFA Beam Dynamics Workshop on Quantum Aspects of Beam Physics* (New York: AIP) p 176
[93] Tanabe M, Ishikawa T, Nakao M, Souda H, Ikegami M, Shirai T, Tongu H and Noda A 2008 *Appl. Phys. Exp.* **1** 028001
[94] Schramm U, Schätz T and Habs D 2001 *Phys. Rev. Lett.* **87** 184801
[95] Schramm U, Schätz T, Bussmann M and Habs D 2003 *J. Phys. B: At. Mol. Opt. Phys.* **36** 561
[96] Brown K and Roser T 2020 *Phys. Rev. Accel. Beams* **23** 054701
[97] Vasileiou V, Granot J, Piran T and Amelino-Camelia G 2015 *Nat. Phys.* **11** 344
[98] Sessler A M 1996 The cooling of particle beams *AIP Conf. Proc.* vol 356 (Austin, Texas) pp 391–407
[99] Steck M 2015 Beam cooling Talk at CAS Warsaw (indico.cern.ch/event/361988/contributions/1775715/attachments/1157463/1697398/beamcooling-steck-cas2015.pdf)
[100] Litvinenko V N and Derbenev Y S 2009 *Phys. Rev. Lett.* **102** 114801
[101] Litvinenko V N, Wang G, Kayran D, Jing Y, Ma J and Pinayev I 2018 arXiv:1802.08677 [physics]
[102] Hangst J S, Kristensen M, Nielsen J S, Poulsen O, Schiffer J P and Shi P 1991 *Phys. Rev. Lett.* **67** 1238
[103] Schröder S *et al* 1990 *Phys. Rev. Lett.* **64** 2901
[104] Miesner H-J, Grimm R, Grieser M, Habs D, Schwalm D, Wanner B and Wolf A 1996 *Phys. Rev. Lett.* **77** 623

Paper [B].
Influence of cosmological Expansion in local Experiments

Felix Spengler, Alessio Belenchia, Dennis Rätzel, and Daniel Braun
Classical and Quantum Gravity **39** 055005 (2022)
DOI: 10.1088/1361-6382/ac4954
URL: iopscience.iop.org/article/10.1088/1361-6382/ac4954

Influence of cosmological expansion in local experiments

OPEN ACCESS
IOP Publishing
Classical and Quantum Gravity
Class. Quantum Grav. **39** (2022) 055005 (27pp)
https://doi.org/10.1088/1361-6382/ac4954

Influence of cosmological expansion in local experiments

Felix Spengler[1], Alessio Belenchia[1,2,*], Dennis Rätzel[3] and Daniel Braun[1]

[1] Institut für Theoretische Physik, Eberhard-Karls-Universität Tübingen, 72076 Tübingen, Germany
[2] Centre for Theoretical Atomic, Molecular, and Optical Physics, School of Mathematics and Physics, Queens University, Belfast BT7 1NN, United Kingdom
[3] Humboldt Universität zu Berlin, Institut für Physik, Newtonstraße 15, 12489 Berlin, Germany

E-mail: alessio.belenchia@uni-tuebingen.de

Received 17 September 2021, revised 21 December 2021
Accepted for publication 7 January 2022
Published 3 February 2022

Abstract

Whether the cosmological expansion can influence the local dynamics, below the galaxy clusters scale, has been the subject of intense investigations in the past three decades. In this work, we consider McVittie and Kottler spacetimes, embedding a spherical object in a FLRW spacetime. We calculate the influence of the cosmological expansion on the frequency shift of a resonator and estimate its effect on the exchange of light signals between local observers. In passing, we also clarify some of the statements made in the literature.

Keywords: cosmological expansion, redshift, spacetime physics, general relativity

(Some figures may appear in colour only in the online journal)

1. Introduction

The large scale structure of the Universe is described by way of the ΛCDM cosmological model which is in accordance with current observations showing an accelerated expansion of the Universe [1]. The accelerated expansion is well captured by the cosmological Friedmann–Lemaître–Robertson–Walker (FLRW) spacetime metric, once visible matter, dark matter and dark energy are accounted for in the energy density of the Universe. This description

*Author to whom any correspondence should be addressed.

is effective above the supercluster scales, where space can be considered homogeneous to a good approximation. At these scales, the evolution is dominated by the so-called Hubble flow, with structures receding from each other with relative velocities linearly proportional to their relative distance in first approximation.

However, whether the cosmic expansion of spacetime can affect local gravitating systems has been the subject of a lively debate dating back to Einstein and Straus in the 1940s [2, 3]. Since then, a growing body of literature has tackled the issue with sometimes conflicting predictions on the existence of local effects of the cosmological expansion [4–25] (see the review [25], and references therein, for a detailed account of the literature up to 2010).

The major problem in addressing unambiguously which structures in the Universe participate in the expansion and which do not resides in the difficulty of handling the solutions of general relativity (GR) outside extremely simplified and idealized scenarios. Ideally, one should be able to account for the local environment such as the one in the Solar System and, at the same time, consider the larger environment in which the former is embedded and which, in turn, will not be described by a cosmological solution to Einstein's equations in general [17]. Since such detailed description is not currently available, we are led to consider simplified scenarios with varying degrees of approximation. As highlighted in [25], while this is totally justified from a methodological point of view, it also demands for a conservative interpretation of the final results as indicating more likely an upper-bound on the effects of cosmic expansion on local systems than an accurate estimate.

With these clarifications at hand, in this work we consider the effect of the global cosmological expansion on local scales using the McVittie metric [26], describing a spherical symmetric object embedded in an expanding FLRW spacetime, and its limit case when spacetime is asymptotically de Sitter. We will focus on the effect of the cosmic expansion on the frequency of propagating light signals. In particular, we consider the effect of the expansion on the frequency shift of a resonator moving along different trajectories. We also briefly review the effect of the expansion on the exchange of light signals between different observers and clarify some statements present in the literature in this regard.

This investigation is motivated by the rapid development of optical clocks. The great advancements in the field of optical clocks [27–36] in the past 20 years—gaining about five orders of magnitude in accuracy—open potential new windows of exploration of fundamental physics allowing to measure time and frequency with unprecedented precision. Just this year, a measurement of the frequency ratio between three atomic clocks with a fractional frequency uncertainty below 8×10^{-18} was reported in [37] and fractional stability of optical clocks to one part in 10^{18} [35] or even in 10^{19} [38] over average times of hundreds of seconds have been reached. Moreover, new concepts like nuclear clocks are being explored which promise even better frequency standards. It should be noted that in SI units the current value of the Hubble parameter is around 10^{-18} s^{-1} such that relative frequency shifts over 1 s—e.g. in a space-bound cavity or Doppler measurements—linearly proportional to it (if any) would be comparable to the current optical clocks' uncertainty, when averaging for $\sim 10^2$ s. It is then intriguing to investigate if the effect on local systems of the cosmic expansion can be of this order of magnitude, and whether current or near future experiments employing quantum technological platforms could have any hope to detect such effects.

The work is organized as follows: in section 2, we discuss the model of spherical symmetric object embedded in an expanding FLRW spacetime that we use in the rest of the work, as well as the different observer fields we consider. Section 3 briefly reviews the derivation of the frequency shift in a resonator in curved spacetime [39]. Here we show how the cosmic expansion affects the resonator, depending on its trajectory. In section 4, we use the previous results to clarify some aspects of the imprint of the global cosmological expansion on the

kinematic effects related to the exchange of light signals between different observers. Section 5 presents estimates of the magnitude of the effects previously discussed. Finally, in section 6 we conclude with a discussion of our results and outlooks.

2. Expanding Universe with a spherical inhomogeneity

In the existing literature, several techniques and approaches have been used to study the impact of the cosmological evolution on local systems. Beyond using perturbation theory and improved Newtonian calculations, exact solutions to the Einstein's equations have been found that describe an inhomogeneity embedded in an expanding FLRW spacetime. As discussed in detail in [25], two alternatives have been investigated. The first amounts to matching two known solutions of Einstein's equations, one representing the cosmological FLRW spacetime and the other the geometry induced by the isolated inhomogeneity. This has been the basis for the Einstein–Straus vacuole solution [2, 3, 40]. The second requires finding exact solutions of Einstein's equations, with the only constraint of approximating each of the two known solutions of interest in some region.

In this work, we will follow the second strategy and consider it as a viable approach for describing a local system embedded in an expanding spacetime whose metric is the so called McVittie metric. Firstly derived in the early '30s [26], the McVittie metric is a spherically symmetric solution to Einstein's equations and describes a non-charged, non-rotating compact object in an expanding cosmological FLRW spacetime. As such, the McVittie metric reduces, by construction, to the exterior Schwarzschild solution at small radii and to FLRW asymptotically. We restrict ourselves to the case in which the FLRW asymptotic metric describes a spatially flat spacetime, in accordance with current cosmological observations. The analytical properties of the McVittie solution were carefully analyzed in [41–44] where also the properties of the timelike and lightlike geodesics of the metric are considered[4].

In the following, we use mainly two coordinate representations for the McVittie metric, always assuming to be at distances from the central object much larger than its Schwarzschild radius. We also set $c = G = 1$ unless otherwise stated. In isotropic spherical coordinates, the McVittie metric reads

$$\mathrm{d}s^2 = -\frac{\left(1-\frac{m(t)}{2r}\right)^2}{\left(1+\frac{m(t)}{2r}\right)^2}\mathrm{d}t^2 + \left(1+\frac{m(t)}{2r}\right)^4 a(t)^2(\mathrm{d}r^2 + r^2\mathrm{d}\theta^2 + r^2\sin^2\theta\mathrm{d}\phi^2), \tag{1}$$

where we are using the $(-+++)$ signature. Here, $a(t)$ indicates the scale factor of the asymptotic FLRW metric. As discussed in [25] and references therein, the matter content of the McVittie spacetime is assumed to consist of a perfect fluid moving along the integral curves of the (normalized) vector field ∂_t. Following [25], from the Einstein's equations we have $m(t) = m_0/a(t)$ with $m_0 = r_S/2$ the mass of the central object[5] and r_S its Schwarzschild radius.

A second set of coordinates that will turn out to be useful are the areal radius coordinates. The areal radius is defined as

$$R(t,r) = \left(1+\frac{m(t)}{2r}\right)^2 a(t) r. \tag{2}$$

[4] In [25, 41, 42, 45], the singularity properties of the McVittie spacetime are considered. In the following, we work always far away from the Schwarschild radius ($r \gg r_S$) and thus do not concern ourselves with such issues.

[5] In physical units, $m_0 = GM/c^2 = r_S/2$, where G is the gravitational constant, c is the speed of light, and M is the mass of the central object.

We can then adopt the change of coordinates $t \to t$, $r \to R$ and rewrite the metric, in the region $R > 2m_0$, in areal radius coordinates as

$$\begin{aligned} \mathrm{d}s^2 = &- \left(1 - 2\mu(R) - h(R,t)^2\right) \mathrm{d}t^2 - \frac{2h(R,t)}{\sqrt{1-2\mu(R)}} \mathrm{d}t\, \mathrm{d}R \\ &+ \frac{1}{1-2\mu(R)} \mathrm{d}R^2 + R^2 \mathrm{d}\theta^2 + R^2 \sin^2\theta \mathrm{d}\phi^2, \end{aligned} \tag{3}$$

where $\mu(R) = m_0/R$, $h(R,t) = H(t)R$, and $H(t) = a'(t)/a(t)$—where the prime indicates derivative with respect to the coordinate time—is the Hubble parameter as usual.

Before proceeding it should be noted that, considering the current estimates for the value of the Hubble parameter at the current time $H_0 \sim 70\ \mathrm{s}^{-1}\ \mathrm{km\ Mpc}^{-1} \sim 2 \times 10^{-18}\ \mathrm{s}^{-1}$ in the ΛCDM paradigm (cf appendix A), H_0' is of the same order of magnitude as H_0^2. Thus, in the following we will consider terms in H' as quadratic corrections in the Hubble parameter.

2.1. Limiting case: Kottler spacetime

From the form of the metric in equation (1), it is immediate to see that, for $m_0 \to 0$, we recover the FLRW metric in spherical isotropic coordinates while imposing $a(t) = 1$, we obtain the exterior Schwarzschild metric. Furthermore, from the form of the metric in equation (3) it is also immediate to see that, imposing the Hubble parameter to be constant $H(t) = H_0$—where H_0 is the so-called Hubble's constant—or equivalently, choosing $a(t) = \mathrm{e}^{H_0 t}$, we recover the line element of Schwarzschild–de Sitter (or Kottler [46]) spacetime with cosmological constant $\Lambda = 3H_0^2$ in areal radius coordinates.

The Schwarzschild–de Sitter (SdS) case will be of relevance in the following. The SdS metric has been used in the existing literature to investigate the effect of the cosmological constant on the local dynamics in a variety of situations [8, 16, 24, 47] and has also been generalized to include a rotating, axis-symmetric central object, which yields the Kerr–de Sitter metric [18, 48–50]. While the SdS metric encodes only the effect of the cosmological constant, it nonetheless allows for analytical solutions where only numerics can be used with the general McVittie line element. We will thus resort to the SdS line element for some of the results in the following.

Before moving on, let us notice that SdS spacetime is static, and indeed the metric can be rewritten in the time-independent, diagonal form[6] [44]

$$\mathrm{d}s^2 = -\alpha(R)\mathrm{d}t^2 + \alpha(R)^{-1}\mathrm{d}R^2 + R^2(\mathrm{d}\theta^2 + \sin^2\theta \mathrm{d}\phi^2), \tag{4}$$

where $\alpha(R) = 1 - r_\mathrm{S}/R - H_0^2 R^2$. We will refer to this in the following as using 'manifestly static' coordinates.

2.2. Observer fields and the proper detector frame

In the next section, we are going to consider the frequency shift induced by the cosmological expansion in a resonator attached to a support moving along a given trajectory in spacetime. It is thus useful to specify which timelike trajectories we are going to consider in the following.

Independently of the specific observer field, in order to determine the frequency shift of the resonator, we will employ the metric and the Riemann tensor expressed in the proper detector frame [51]. The proper detector frame is defined, up to spatial rotations and with respect

[6] This form of the metric can be obtained from equation (3), with the condition $H(t) = H_0$ constant, by performing the change of coordinates $t \to t + u(R)$ with $u'(R) = H_0 R/\left(\sqrt{1-2\mu(R)}\alpha(R)\right)$ as described e.g. in [44].

to a time-like trajectory γ, as the Fermi–Walker transported orthonormal tetrad $\{\mathbf{e}_\alpha\}$, $\alpha \in \{0,1,2,3\}$ with $\mathbf{e}_0 = \dot{\gamma}$ the normalized four-velocity along the trajectory, that is

$$\begin{cases} \mathbf{e}_0 = \dot{\gamma} \\ 0 = \dfrac{D_F \mathbf{e}_a}{\mathrm{d}s} \equiv \dfrac{D\mathbf{e}_a}{\mathrm{d}s} - \left(\mathbf{e}_a, \dfrac{D\mathbf{e}_0}{\mathrm{d}s}\right)\mathbf{e}_0 + (\mathbf{e}_a, \mathbf{e}_0)\dfrac{D\mathbf{e}_0}{\mathrm{d}s}, \quad \forall\ a \in \{1,2,3\}, \end{cases} \tag{5}$$

where $DX/\mathrm{d}s = \mathbf{e}_0^\mu \nabla_\mu X$ is the covariant derivative of the Levi-Civita connection along the direction of $\mathbf{e}_0$ and $D\mathbf{e}_0/\mathrm{d}s = \boldsymbol{a}$ its four-acceleration. Due to the Fermi–Walker transport, the proper detector frame is said to be *non-rotating* and can be physically realized by an observer carrying along a clock defining time and a system of three gyroscopes with spin vectors orthogonal to each other defining the spatial reference frame [52]. Note that Fermi–Walker transport along a geodesic corresponds to parallel transport.

We are now in the position to consider several different observer fields which will be used in the following.

2.2.1. Cosmological observer. The first observer field that we consider is obtained normalizing the ∂_t vector field in isotropic spherical coordinates (1). It is then given by

$$\mathbf{u} = \|\partial_t\|^{-1}\partial_t. \tag{6}$$

As we commented above, the perfect fluid matter content of McVittie spacetime moves along the integral lines of such an observer field. While in FLRW such a field is geodesic, this is not the case in McVittie (or SdS) spacetime. The cosmological observer corresponds to an observer at a constant coordinate radius r and, in the asymptotic region approximating FLRW, defines the so-called Hubble flow.

The four-acceleration $\boldsymbol{a} = \nabla_{\mathbf{u}}\mathbf{u}$ of this field is given by

$$\boldsymbol{a} = \left\{0, \frac{\frac{m(t)}{r^2 a^2(t)}}{\left(1-\frac{m(t)}{2r}\right)\left(1+\frac{m(t)}{2r}\right)^5}, 0, 0\right\}, \tag{7}$$

i.e., purely radial and outward pointing in these coordinates at the fixed value of r.

2.2.2. Kodama observer. The Kodama observer field is the normalized version of the Kodama vector field, which is a naturally distinguished field in spherically symmetric spacetimes. Indeed, the Kodama vector field ($\mathbf{v}_\mathrm{K}$) is the unique (up to a sign) spherically symmetric vector field orthogonal to the gradient of the areal radius. Thus, upon normalization, we obtain a naturally distinguished observer field $\mathbf{u}_\mathrm{K} = \|\mathbf{v}_\mathrm{K}\|^{-1}\mathbf{v}_\mathrm{K}$ corresponding to an observer at a constant areal radius.

As discussed in detail in [25, 53], to which we refer the interested reader for further details, the integral curves of the Kodama observer are worldlines which 'stay' at constant areal radius and are orthogonal to the orbits of the SO(3) isometry group. These are the key properties of the Kodama observer field, making it the natural substitute for a timelike Killing field in an arbitrary spherically symmetric spacetime. This holds true in McVittie spacetime where, in general, no timelike Killing vector field is present. Furthermore, the Kodama vector field coincides with the timelike Killing vector field in the limit in which McVittie reduces to the SdS spacetime.

Starting from equation (1), and using the fact that $m(t) = m_0/a(t)$, the Kodama vector field is given as

$$\mathbf{v}_{\mathrm{K}} = \partial_t - H(t)R\|\partial_r\|^{-1}\partial_r. \tag{8}$$

However, due to the properties of the Kodama vector field, it is convenient to work with it in areal radius coordinates equation (3) in which the Kodama vector field assume the simple form $\mathbf{v}_{\mathrm{K}} = \{1, 0, 0, 0\}$. The Kodama observer field is finally obtained as

$$\mathbf{u}_{\mathrm{K}} = \frac{1}{\sqrt{1 - 2\mu(R) - h(R,t)^2}}\{1, 0, 0, 0\}. \tag{9}$$

It should be noted that, the Kodama observer field is, in general, not geodesic similarly to the cosmological observer field in McVittie spacetime. The four-acceleration can be easily computed by fixing, without loss of generality, $\theta = \pi/2$ and is given by

$$\boldsymbol{a}_{\mathrm{K}} = \left\{ \frac{RH(t)\left(RH'(t) - \frac{(\mu(R)-h^2(R,t))(1-2\mu(R)-h^2(R,t))}{R\sqrt{1-2\mu(R)}}\right)}{(1 - 2\mu(R) - h^2(R,t))^2}, \frac{m_0}{R^2} \right.$$
$$\left. - \frac{R\sqrt{1 - 2\mu(R)}H'(t)}{1 - 2\mu(R) - h^2(R,t)} - RH(t)^2, 0, 0 \right\}, \tag{10}$$

for the observer at fixed areal radius R.

In FLRW, the Kodama observer would still be not geodesic, contrary to the cosmological one and, given the fact that the expression for the areal radius reduces to $R = a(t)r$, would correspond to an observer at a constant proper distance from the origin of the coordinate system. In the limit in which $a(t) = 1$, the Kodama observer is just the stationary one of Schwarzschild spacetime.

2.2.3. Geodesic observers. Among the better physically justified observers to consider there are undoubtedly geodesic observers, i.e., inertial observers in free-fall. Indeed, the previous two observer fields require a proper acceleration for a spacecraft to keep on moving along their integral curves, in contrast to geodesic ones.

Timelike geodesics in McVittie spacetime have been carefully analyzed in [44]. Unfortunately, for a general geodesic there are no analytical expressions and also finding the associated proper detector frame analytically is a tall order. Thus, in the following, when speaking of geodesic observers, we will consider the SdS limit of McVittie spacetime and work in manifestly static coordinates (4). In the case of SdS, analytical expressions for timelike geodesics have been derived [54] albeit involving hyper-elliptic integrals. Since we consider the SdS spacetime metric, our conclusions for what regards geodesic observers will be concerned with the local effects of a cosmological constant.

As discussed in [54], the symmetries of SdS spacetime allow to define the two conserved quantities energy E and angular momentum L that, together with the normalization condition for the four-velocity $\dot{\gamma}$ of a timelike ($\epsilon = 1$) or null ($\epsilon = 0$) geodesic trajectory, uniquely characterize the four-velocity of the trajectory as

$$\dot{\gamma} = \left\{ \frac{E}{\alpha(R)}, \sqrt{E^2 - \alpha(R)\left(\epsilon + \frac{L^2}{R^2}\right)}, 0, \frac{L}{R^2} \right\}, \tag{11}$$

where we are working in static coordinates, and we have restricted ourselves, without loss of generality, to motion in the equatorial plane ($\theta = \pi/2$).

In the following, we focus on circular and radial geodesics. The former give a crude approximation of the physical motion of planets in the Solar System, while the latter describe the motion of an infalling or outwards escaping spacecraft. Radial geodesics are easily determined by fixing $L = 0$ and are parameterized by the energy E. The corresponding Fermi transported tetrad that defines the proper detector frame is derived in appendix B. Circular orbits are instead obtained by demanding that $\dot{R} = 0$ and $\ddot{R} = 0$, where the dot stands for derivative with respect to the proper time along the geodesic, and we parameterize the trajectory as $\gamma(\tau) = (t(\tau), R(\tau), 0, \phi(\tau))$ with τ the proper time. Also for this case, the Fermi transported tetrad is derived in appendix B. Furthermore, the results for the circular geodesics can be easily generalized to include a central spinning object, i.e., working with the Kerr–de Sitter spacetime metric. We report this case in appendix B5 for the interested reader.

3. Frequency shift for a local resonator

In [39] a resonator, consisting of two mirrors connected by an elastic rod which itself is fixed to a support, affected by a curved background metric is studied. Based on this, we analyze here the effects of cosmological expansion on the frequency of a resonator on different trajectories.

Attached by a support to an observer, which is characterized by a timelike trajectory and its local proper detector frame, the resonator is subject to gravitational effects of the metric (cf figure 1). We indicate the spatial coordinates in the proper detector frame as $\{x, y, z\}$ along the directions defined by the spatial part of the Fermi–Walker transported tetrad $\{\boldsymbol{e}^{\mu}_{J}\}$ introduced in (5) and whose explicit expressions are given in appendix B for different observers[7]. We assume that the resonator is aligned along the, arbitrarily chosen, J-direction, with $J \in \{x, y, z\}$ in the proper detector frame and that the rod's elasticity is characterized by the material's speed of sound c_{s}.

The slowly varying acceleration and tidal forces induce internal stress within the rod, which accumulates along it leading to a compression or elongation. Other contributions to the change in length are the relativistic length contraction which is subleading by a factor c_{s}^2/c^2, the effects resulting from transverse proper acceleration, and change in trajectory of the light pulse which are second order effects in the perturbation of the proper detector frame metric. The proper acceleration of the mirrors can be ignored if the mirrors are considered lightweight compared to the rod. Additional effects of tidal acceleration in transverse directions are negligible for a slim rod. Following the detailed derivation in [39], the change in length translates to a shift in the resonance frequency which, in quadratic order of the metric perturbation and in the limit of a slowly moving observer, is given in equation (29) of [39] by

$$\frac{\Delta\omega}{\omega} \approx \frac{\mathbf{a}^J}{2c^2}\left(\frac{c^2}{c_{\mathrm{s}}^2}\beta - \sigma\right) L_{\mathrm{p}} + \frac{R_{0J0J}}{24}\left(2\frac{c^2}{c_{\mathrm{s}}^2}(3\beta^2+1) - 3\sigma^2 - 6\sigma\beta + 1\right) L_{\mathrm{p}}^2, \tag{12}$$

[7] Note that, as detailed in [39], the proper detector frame coordinates used for the derivation of the frequency shift are valid for distances from the point of expansion much smaller than $\min\left\{c^2/|\mathbf{a}^J|, 1/|R^M_{NPQ}|^{1/2}, |R^M_{NPQ}|/|\partial_K R^M_{NPQ}|\right\}$, where $\mathbf{a}^J = \boldsymbol{e}^J_{\mu}\boldsymbol{a}^{\mu}$ is the non-gravitational acceleration with respect to a local freely-falling frame while $R_{MNPQ} = \boldsymbol{e}^{\alpha}_{M}\boldsymbol{e}^{\beta}_{N}\boldsymbol{e}^{\gamma}_{P}\boldsymbol{e}^{\delta}_{Q}R_{\alpha\beta\gamma\delta}$ are the proper detector frame components of the Riemann tensor.

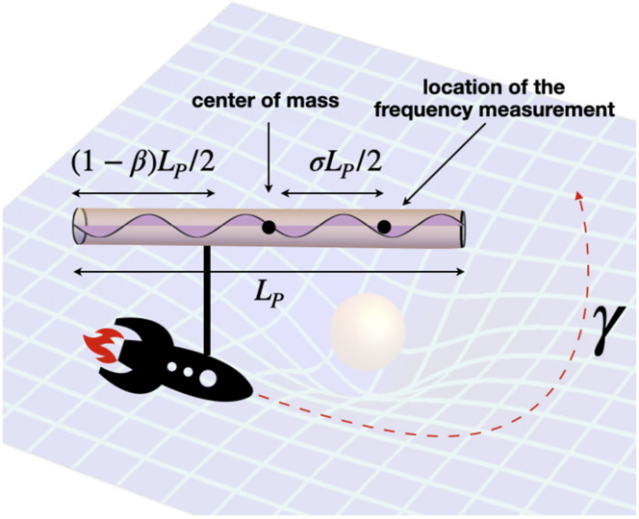

Figure 1. Pictorial representation of the resonator rod carried along a trajectory γ by an observer (the spacecraft) in a curved background. The observer trajectory γ is the one followed by the support point at which the resonator is fixed to the observer. The proper length of the resonator is denoted by L_p, the support point is at a distance $\beta L_\mathrm{p}/2$ from the center of mass and the frequency measurement is performed in an arbitrary point of the resonator at a distance $\sigma L_\mathrm{p}/2$ from the center of mass.

where ω is the resonance frequency of the oscillator in the absence of curvature and acceleration, $\mathbf{a}^J \equiv \boldsymbol{e}^J_\mu \boldsymbol{a}^\mu$ and $R_{0J0J} = \boldsymbol{e}^\alpha_0 \boldsymbol{e}^\beta_J \boldsymbol{e}^\gamma_0 \boldsymbol{e}^\delta_J R_{\alpha\beta\gamma\delta}$ are the proper acceleration and the Riemann curvature tensor components in the detector frame, $\beta L_\mathrm{p}/2$ is the distance of the rod's support from the center of mass and $\sigma L_\mathrm{p}/2$ is the distance of the point of measurement from the center-of-mass (cf figure 1). Note that we have re-inserted the speed of light for clarity of exposition. By design, i.e., by the choice of alignment, the acceleration and curvature parallel to the axis of the resonator are the only components to contribute in leading order to the frequency shift of the resonator. Analytic formulae for the relevant proper acceleration and curvature tensor elements and the impact of cosmological expansion on these are given for some relevant observer field in the following.

3.1. Cosmological observer

For the cosmological observer, the spatial component of the four-acceleration in the proper detector frame is given by

$$\mathbf{a} = \left(\frac{\frac{m(t)}{a(t)r^2}}{\left(1-\frac{m(t)}{2r}\right)\left(1+\frac{m(t)}{2r}\right)^3}, 0, 0 \right). \tag{13}$$

An expansion to second order in $ra'(t)/a(t)$ and first order in $r^2a''(t)/a(t)$ (here, derivatives are taken with respect to coordinate time) of the relevant terms of the Riemann curvature tensor in the proper detector frame results in

$$R_{0x0x} \approx -\frac{2m(t)}{r^3 a(t)^2}\frac{1}{\left(1+\frac{m(t)}{2r}\right)^6} + \frac{m(t)}{r}\frac{1}{1-\frac{m(t)}{2r}}\left(\frac{a'(t)}{a(t)}\right)^2 - \frac{\left(1+\frac{m(t)}{2r}\right)}{\left(1-\frac{m(t)}{2r}\right)}\frac{a''(t)}{a(t)}, \tag{14}$$

$$R_{0y0y} = R_{0z0z} \approx \frac{m(t)}{r^3 a(t)^2}\frac{1}{\left(1+\frac{m(t)}{2r}\right)^6} + \frac{m(t)}{r}\frac{1}{1-\frac{m(t)}{2r}}\left(\frac{a'(t)}{a(t)}\right)^2 - \frac{\left(1+\frac{m(t)}{2r}\right)}{\left(1-\frac{m(t)}{2r}\right)}\frac{a''(t)}{a(t)}, \tag{15}$$

where we see that in the radially aligned $\boldsymbol{e}_x^\mu$ direction the curvature is different from the two orthogonal directions. Apart from the $\left(a'(t)/a(t)\right)^2$ and $a''(t)/a(t)$ factors, the cosmological expansion only enters as $ra(t)$ in both the Riemann tensor and the acceleration in the Fermi–Walker transported detector frame. Expanding the scale factor $a(t) \approx a(t_0)(1 + H_0\Delta t)$ gives terms linear in H_0 in both the acceleration and the curvature, all suppressed by factors m_0/r. As we show in the following, this is not the case for the other observers that we consider, which do not follow the Hubble flow. Note that, in the limit $m(t)/r \to 0$, i.e., when the usual FLRW metric is recovered, we remain with corrections quadratic in H_0 in agreement with previous results in the literature [10].

3.2. Kodama observer

Similarly, starting from the McVittie metric in areal radius coordinates, we can calculate the quantities relevant to the frequency shift of a resonator on the trajectory of a Kodama observer. The spatial component of four-acceleration in the proper detector frame is given by

$$\mathbf{a}_\mathrm{K} = \left(\frac{\frac{m_0}{R^2} - RH^2(t)}{\sqrt{1 - R^2H(t)^2 - \frac{2m_0}{R}}} - \frac{\sqrt{1-\frac{2m_0}{R}}RH'(t)}{\left(1 - R^2H(t)^2 - \frac{2m_0}{R}\right)^{3/2}}, 0, 0\right). \tag{16}$$

The relevant components of the Riemann tensor in the detector frame, i.e., the ones entering (12), are given by

$$R_{0x0x} = -\frac{H'(t)}{\sqrt{1-\frac{2m_0}{R}}} - H(t)^2 - \frac{2m_0}{R^3}, \tag{17}$$

$$R_{0y0y} = R_{0z0z} = \frac{m_0}{R^3} - H^2(t) - \frac{\sqrt{1-\frac{2m_0}{R}}H'(t)}{1 - R^2H(t)^2 - \frac{2m_0}{R}}. \tag{18}$$

It should be noted that, both the proper acceleration and any component of the Riemann curvature tensor in the proper detector frame do not contain any linear term in the Hubble parameter H nor any instance of $a(t)$ from which a linear term in H_0 could arise when expanded for small time differences. The same is true for the Ricci and Einstein tensors and the scalar curvature and it is in stark contrast to the case of the cosmological observer. Finally, it is worth mentioning that, performing the same calculations starting from the McVittie metric in isotropic coordinates calls for some care. Indeed, one needs to impose the constancy of the areal radius, characteristic of the Kodama observer, in order to correctly account for correction to the resonator frequency and obtain results that agree with the one discussed here.

3.3. Geodesic observers

As discussed in the previous section, finding the proper detector frame for a general geodesic observer in McVittie spacetime is a tall order. We thus focus on geodesics in SdS spacetime working in static coordinates.

Let us first consider an observer freely-falling along an equatorial circular geodesic. The Riemann curvature tensor in the proper detector frame is given by

$$R_{0x0x} = \frac{-3\frac{r_S}{R^3}\alpha(R)\cos\left(\phi\sqrt{4-\frac{6r_S}{R}}\right) - H_0^2\left(4-9\frac{r_S}{R}\right) - \frac{r_S}{R^3}}{2\left(2-3\frac{r_S}{R}\right)}, \tag{19}$$

$$R_{0y0y} = \frac{1}{2-3\frac{r_S}{R}}\left(\frac{r_S}{R^3} - 2H_0^2\right) \tag{20}$$

$$R_{0z0z} = \frac{3\frac{r_S}{R^3}\alpha(R)\cos\left(\phi\sqrt{4-\frac{6r_S}{R}}\right) - H_0^2\left(4-9\frac{r_S}{R}\right) - \frac{r_S}{R^3}}{2\left(2-3\frac{r_S}{R}\right)}. \tag{21}$$

Note that, the trigonometric functions appearing in these expressions originate from requiring the detector frame to be non-rotating (see also appendix B).

In the case of a radial, equatorial geodesic in SdS, characterized by a vanishing angular momentum $L = 0$, we find for the components of interest of the proper detector frame Riemann tensor

$$R_{0x0x} = -\frac{r_S}{R^3} - H_0^2, \tag{22}$$

$$R_{0y0y} = R_{0z0z} = \frac{r_S}{2R^3} - H_0^2. \tag{23}$$

Note that, these expressions coincide, at a fixed value of the areal radius, with the ones of the Kodama observer (17) in the limit $H(t) \to H_0$.

The previous expressions show that, for both the circular and the radial geodesics, the leading order correction to the frequency shift of the resonator resulting from the cosmological expansion is proportional to H_0^2. Let us also notice that the same conclusion can be reached for the particular case of circular geodesics in Kerr–de Sitter spacetime [55–57], in which a central rotating body is considered (cf appendix B for additional details).

4. Redshift and satellite tracking

Having considered the impact of the global cosmological expansion on a local experiment, we conclude with a brief overview of the effect of the same expansion on the frequency redshift of signals exchanged between observers and the related concept of double Doppler tracking (DDT). These kinematic effects have been treated in detail in the existing literature [8, 9, 24, 25]. Here, we focus on clarifying some of the results in the literature by following the derivation in [25].

In the case of FLRW spacetime, the redshift formula for exchanges of light signals between two observers following the Hubble flow is easily obtained. Consider two cosmological observers at r_0 and r_1, respectively, in isotopic spherical coordinates[8], then the ratio between

[8] In these coordinates the FLRW line element has the usual form $\mathrm{d}s^2 = -\mathrm{d}t^2 + a^2(t)(\mathrm{d}r^2 + r^2\sin\theta^2\mathrm{d}\phi^2 + \mathrm{d}\theta^2)$.

the frequency emitted by the first observer and the one received by the second observer is given by $\omega_1/\omega_0 = a(t_0)/a(t_1) \sim 1 - H_0(t_1 - t_0)$, where we have assumed the leading order of the Hubble parameter to be $H_0 = \text{const.}$, and where the frequency measured by an observer $\mathbf{u}$ is given by the scalar product between the observer field and the null tangent to the light signal $\mathbf{k}$, i.e. $|g(\mathbf{u}, \mathbf{k})|$. We notice that the redshift encodes a correction linear in the Hubble constant. As shown in [25], this persists also in the case in which a spherical inhomogeneity is included.

The DDT, as the name suggests, is a technique used to track the position of spacecrafts. In order to address the DDT, we need to consider the ratio between the frequency emitted by an observer and the frequency received back by the same observer after the light signal has been reflected by an arbitrarily moving 'spacecraft'. In FLRW, considering the cosmological observer field and a spacecraft reflecting back the light signal upon reception, this ratio can be broken into three terms $\omega_2(t_2)/\omega_0(t_0) = (\omega_2/\omega_1')(\omega_1'/\omega_1)(\omega_1/\omega_0)$. Here, the observer receiving (at $t = t_2$) and sending (at $t = t_0$) the signal is at a fixed value of the coordinate radius r. Also notice that, for the cosmological observer in FLRW, proper time coincides with the coordinate time t. The ratio ω_1/ω_1' represents the ratio between the frequency at the reflection point *as measured by the cosmological observer at that point* and the frequency after reflection as measured by the same observer. This ratio accounts for the relativistic Doppler shift due to the motion of the spacecraft relative to the cosmological observer field at the reflection point. The other two ratios are easily obtained from the previous expression of the single-way redshift. All together, one arrives at equation (140) of [25]

$$\frac{\omega_2(t_2)}{\omega_0(t_0)} = \frac{a_0}{a_2}\left(2\frac{1-\beta^{\hat{\boldsymbol{k}}}_{\mathbf{u}}(\mathbf{v})}{1-\beta_{\mathbf{u}}(\mathbf{v})^2} - 1\right). \tag{24}$$

Here, we have considered a spacecraft with four velocity $\mathbf{v}$ whose relative velocity with respect to the observer field $\mathbf{u}$ at the reflection point is $\boldsymbol{\beta}_{\mathbf{u}}(\mathbf{v}) = (\mathbf{v} - |g(\mathbf{v},\mathbf{u})|\mathbf{u})/|g(\mathbf{v},\mathbf{u})|$ [25]. Furthermore, we have considered a null signal propagating radially between the emitter and the reflection point with tangent $\mathbf{k}$ whose normalized projection in the rest frame of the observer is $\hat{\boldsymbol{k}}$. Finally, with $\beta^{\hat{\boldsymbol{k}}}_{\mathbf{u}}$ we indicate the projection of the relative velocity along the unit vector $\hat{\boldsymbol{k}}$ in the rest frame of $\mathbf{u}$. Equation (24) relates the frequency shift to the spacecraft spatial velocity and can be approximated to linear order in β and $H_0\Delta t_{20}$ with $\Delta t_{20} = t_2 - t_0$ giving $\omega_2(t_2)/\omega_0(t_0) \approx 1 - 2\beta^{\hat{\boldsymbol{k}}}_{\mathbf{u}}(\mathbf{v})_{p_1} - H_0\Delta t_{20}$ showing once more a linear correction in H_0. It is clear from our previous discussion that the linear term in H_0 originates from the analogous term in the one-way redshift.

The last step in accounting for the DDT is to differentiate the previous expression with respect to the proper time of the observer at reception of the reflected signal. In [25], this calculation is detailed, and its result is

$$\frac{1}{\omega_0(t_0)}\frac{\mathrm{d}\omega_2(t_2)}{\mathrm{d}t_2} \approx -2\left\{\alpha^{\hat{\boldsymbol{k}}}_{\mathbf{u}}(1 - 3\beta^{\hat{\boldsymbol{k}}}_{\mathbf{u}} - 3H_0\Delta t_{20}/2) + H_0\beta^{\hat{\boldsymbol{k}}}_{\mathbf{u}}\right\}, \tag{25}$$

where now $\alpha^{\hat{\boldsymbol{k}}}_{\mathbf{u}}$ is the relative spatial acceleration of the spacecraft trajectory with respect to the observer field in the direction of the unit vector $\hat{\boldsymbol{k}}$. It should be emphasized here that, in the rate of the DDT ratio above, not all the corrections linear in H_0 can be traced back to the one-way redshift. Indeed, the derivative with respect to t_2 is also responsible for the introduction of such corrections as can be easily seen from equation (143) in [25].

We now want to show that such linear corrections in H_0 are a peculiarity of the cosmological observer already in FLRW. This result then extends trivially to the case of McVittie spacetime.

A first hint of this fact is given by considering the simple case of de Sitter spacetime[9], and the Kodama observer field which, in the region of interest, is a timelike Killing vector field. The one way redshift is thus given by [58]

$$\frac{\omega_1}{\omega_0} = \frac{\sqrt{\alpha(R_0)}}{\sqrt{\alpha(R_1)}} = 1 + (R_1^2 - R_0^2)\frac{H_0^2}{2} + \mathcal{O}\left(H_0^4 R^4\right), \tag{26}$$

with R the largest scale among R_0 and R_1 entering the problem and $\alpha(R) = 1 - H_0^2 R^2$. Note that the same expression holds in the case of SdS spacetime, where only the functional form of $\alpha(R)$ changes (see also section 5 for an alternative way to compute the one-way redshift for the Kodama observer). Moreover, we point out that the expression for the redshift as expressed in [8] contains an error—in that R_0 and R_1 are interchanged.

The previous expression shows that no contribution linear in H_0 appears while the leading corrections are proportional to H_0^2. It also tells us immediately that the only possible source of corrections linear in H_0 in the DDT rate could be the time derivative. However, no contributions of this nature arise from the time derivative. A simple way to see this is to work in static coordinates for de Sitter spacetime. In these coordinates the Kodama observer field is $\mathbf{u}_\mathrm{K} = \alpha^{-1/2}\partial_t$ and the proper time for such an observer coincides with the coordinate time to first order in $H_0 R$. We can thus ignore the difference between the proper and the coordinate time. The DDT ratio can be obtained in complete analogy to the previous case of the cosmological observer as

$$\frac{\omega_2}{\omega_0} = \left\{ 2\frac{1 - \beta^{\hat{k}}_{\mathbf{u}_\mathrm{K}}(\mathbf{v})}{1 - \beta_{\mathbf{u}_\mathrm{K}}(\mathbf{v})^2} - 1 \right\}, \tag{27}$$

where we have used the fact that $\|\mathbf{u}_\mathrm{K}\|_{t=t_0}/\|\mathbf{u}_\mathrm{K}\|_{t=t_2} = 1$. Next, by using the null condition for an inward directed (assuming $R_1 > R_2 = R_0$) radial lightlike geodesic

$$\int_{t_1(t_2)}^{t_2} \mathrm{d}t = -\int_{R_1(t_1(t_2))}^{R_2} \frac{\mathrm{d}R}{\alpha}, \tag{28}$$

we obtain

$$\frac{\mathrm{d}t_1}{\mathrm{d}t_2} = \left(1 + \beta^{\hat{k}}_{\mathbf{u}_\mathrm{K}}(\mathbf{v})\right)^{-1}, \tag{29}$$

where it can be shown that the relative spatial velocity of the spacecraft at the reflection point has the form $\beta^{\hat{k}}_{\mathbf{u}_\mathrm{K}}(\mathbf{v}) = \alpha(R_1)^{-1}\mathrm{d}R_1/\mathrm{d}t_1$ (cf appendix C). We then see that this derivative does not contain any correction proportional to H_0 so that the rate of the DDT will have leading corrections quadratic in the Hubble parameter. This same argument extends straightforwardly to the case of SdS spacetime (cf appendix C). Moreover, since SdS spacetime is a special case of the McVittie one, with $H' = 0$ (cf equation (31)), the argument should apply for the general case showing that the DDT ratio and rate contain corrections at most quadratic in the Hubble parameter, which strongly limits the possibility to observe such effects.

In order to strengthen our point, let us consider also a generic, freely falling observer field in SdS spacetime. In the equatorial plane, this observer field is parameterized as in equation (11) with $\epsilon = 1$. From the form of the metric in equation (4), and the parameterization of timelike and null geodesics in equation (11), it is easy to deduce that the leading order corrections of the redshift ratio have to be at least of second order in the Hubble constant so that also a generic

[9] See also appendix C for further details.

geodesic observer does not have access to corrections linear in H_0 in the frequency ratio of the DDT.

5. Differential acceleration & expansion's effects estimate

An intuitive understanding of the differences between the observers considered can be gained through their proper acceleration in a weak field limit and the comparison to the Newtonian limit. In equations (13) and (16) the proper acceleration is given for the cosmological observer and the Kodama observer, respectively, while it vanishes for the geodesic observer by definition. We immediately see that equation (13) contains only an acceleration due to the central object that is, to lowest order in $m_0/a(t)r$, the Newtonian gravitational acceleration due to a mass m_0 at a distance $a(t)r$. We can conclude that the cosmological observer freely follows the Hubble flow but accelerates against the gravitational pull of the central object, which agrees with its standard interpretation. In equation (16), we find a term of lowest order in m_0/R and HR that coincides with the Newtonian gravitational acceleration due to a central mass m_0 at distance R. The additional terms represent an inward acceleration that depends on the cosmological expansion. These terms result from the property of the Kodama observer to be located at constant areal radius, which implies that it is accelerating against the gravitational effect of the cosmological expansion such that it will never join the Hubble flow.

To lowest non-trivial order, the radial proper acceleration of the Kodama observer in the corresponding proper detector frame becomes

$$\mathbf{a}_{\mathrm{K,R}} = \frac{m_0}{R^2} - R(H^2(t) + H'(t)). \tag{30}$$

If the Kodama observer is realized and test matter is released by it, $\mathbf{a}_{\mathrm{K,R}}$ is their differential acceleration. We recognized that the small quantities $H^2(t), H'(t) \sim H_0^2$ are multiplied by the potentially large quantity R. This seems like a potential opportunity for a measurement of Hubble parameter H_0 and the cosmological constant Λ. However, in the described setup, the fundamental challenge would be to realize the Kodama observer without knowledge of the cosmological acceleration. The only obvious possibility seems to be a measurement of the distance to the central object, which seems very challenging, in particular, for very large R.

The acceleration in equation (30) is equivalent, up to a sign, to the gravitational acceleration appearing in the Newtonian limit of a gravitating spherically symmetric central object in an expanding spacetime (e.g. see equation (87) in [59] and equation (1) of [7]). The sign change is the result of $\mathbf{a}_{\mathrm{K,R}}$ being the non-gravitational acceleration necessary to compensate for the gravitational one. There exists an extended literature about the gravitational acceleration being proportional to H^2 due to the cosmological expansion and its local measurability [7, 13, 14, 16, 19, 22, 23, 25, 59] that we do not review here.

By expanding all expressions to second order in HR, we can approximately diagonalize the McVittie metric in (3) by a redefinition of the time variable to obtain the line element (see appendix D for details)

$$\begin{aligned} \mathrm{d}s^2 \approx &- \left(1 - \frac{2m_0}{R} - (H(t)^2 + H'(t))R^2\right) \mathrm{d}t^2 \\ &+ \left(1 + \frac{2m_0}{R} + H(t)^2R^2\right) \mathrm{d}R^2 + R^2\mathrm{d}\theta^2 + R^2 \sin^2\theta \mathrm{d}\phi^2 \end{aligned} \tag{31}$$

in the weak field limit where $m_0/R \ll 1$, where we have also neglected terms proportional to $m_0H(t)^2R$ and $m_0H'(t)R$. Identifying the zero-component of the perturbation of the metric,

with respect to the flat Minkowski metric, with a Newtonian potential, i.e. $g_{00} = -1–2\Phi = -1 + 2m_0G/(c^2R) + R^2(H^2 + H')/c^2$, leads to a gravitational redshift/time dilation proportional to $m_0(1/R_1 - 1/R_2) + (R_1^2 - R_2^2)(H^2 + H')/2$ for two observers located at R_1 and R_0.[10] Alternatively, this expression for the redshift can be directly deduced from the effective gravitational acceleration $-\mathbf{a}_{\mathrm{K,R}}$ by interpreting it in terms of an effective metric in the Newtonian limit.

The current value of the Hubble constant is $H_0 \sim 2.2 \times 10^{-18}\ \mathrm{s}^{-1}$ and that of the cosmological constant is $\Lambda = 3H_0^2\Omega_\Lambda/c^2 \sim 10^{-52}\ \mathrm{m}^{-2}$. Considering the ΛCDM model and neglecting the small contribution of radiation at present day, we obtain $H^2 + H' = (\Lambda c^2 - H_0^2)/2$, where we have taken into account that $\Omega_\Lambda + \Omega_m = 1$ in the ΛCDM model (see appendix A for further details). Following [8], and using equation (31), by assuming Earth as the central object, a satellite at an altitude of $R_1 = 15\,000\ \mathrm{km} \gg R_0$, and assuming a clock comparison accuracy of 10^{-15} and no deviation in the frequency redshift with respect to the prediction of Einstein's theory without cosmological expansion, we can estimate an upper bound to the cosmological constant of $|\Lambda| \lesssim 2 \times 10^{-29}\ \mathrm{m}^{-2}$ (compare with [8]) assuming precise knowledge of H_0^2, m_0 and R_2 from other measurements. This translates to an upper bound on H_0^2, based on the same parameters, of $H_0^2 \lesssim 10^{-12}\ \mathrm{s}^{-2}$ assuming Λ, m_0 and R_2 to be known precisely. If we consider instead the Sun as a central object, a relative clock accuracy of 10^{-19}, and a spacecraft at a distance from the Sun comparable to the one of the Voyager 1, i.e. $R_1 \sim 23 \times 10^{12}$ m, we can push the bounds to $|\Lambda| \lesssim 10^{-45}\ \mathrm{m}^{-2}$ and $H_0^2 \lesssim 3 \times 10^{-29}\ \mathrm{s}^{-2}$, 'only' seven orders of magnitude away from the currently accepted values. Considering a scaling of the clock uncertainty with the inverse of the square root of the averaging time [27] and the fact that currently an averaging time of the order of 10^2 s is needed to reach an uncertainty of the order of 10^{-19}, we see that to fill the six orders of magnitude gap would require around 10^6 years of integration time. It is thus clear that further advances in clock accuracy are needed to be able to assess cosmological quantities in this kind of local experiments.

In addition to redshift measurements, another option to estimate the non-Newtonian gravitational acceleration due to the cosmological expansion would be, for example, its accumulated effect on a spacecraft which could be measured, in principle, by Doppler tracking the time evolution of the spacecraft's velocity. However, the basic mechanism would be a frequency comparison which should result in similar fundamental limits as we have found for gravitational redshift measurements above. The situation becomes even worse if one tries to measure the Hubble or cosmological constant through the frequency shift of a resonator, as described in section 3. For a geodesic observer in SdS (see section 3.3), assuming the value of $H_0 \sim 2.2 \times 10^{-18}\ \mathrm{s}^{-1}$, and a speed of sound $c_\mathrm{s} = 5000\ \mathrm{m\ s}^{-1}$ (comparable to that of aluminium) the relative frequency shift of a resonator of length 10 m is only $\sim 10^{-42}$, which is many orders of magnitude away from measurability.

6. Discussion

In this work we have investigated the impact of the global cosmological evolution on a very local experiment, i.e., on the frequency shift in a resonator. In order to model something akin to a local inhomogeneous environment immersed in an expanding Universe, we have considered the McVittie metric. This metric describes a spherical object embedded in a FLRW cosmological spacetime and, together with its limiting case of Schwarzschild–de Sitter spacetime, has

[10] Here, we assume that the derivatives of the components of the metric with respect to t are much smaller than their derivatives with respect to R to recover the stationary weak field situation (see e.g. [60]).

been largely used in the literature exploring local effects of the cosmological expansion (cf [25] and references therein). A word of caution is in order here to correctly interpret the results obtained in this work, as well as in the existing literature. As already discussed in the introduction—and highlighted in, e.g., [17, 25]—to fully address the problem of the local effects of global expansion in GR it would be necessary to model the hierarchy of embedded systems, from the Solar system to the cosmological solution passing through galaxies and cluster scales, at the level of at least controlled approximations to exact GR's solutions. While this is currently a tall order, resorting to (crude) approximations like McVittie spacetime and the SdS spacetime can guide us in obtaining estimates of the effects of global expansion in local systems. The caveat is that such estimates, like the ones obtained in this work, have to be interpreted as upper bounds to the effects of interest since, in realistic systems, the effects of the cosmological expansion would be further obscured by the growing complexity of local structures.

With these considerations at hand, in this work we have considered the shift in the frequency of an optical resonator, moving on various trajectories in McVittie and SdS spacetimes, due to the cosmic expansion. We have shown that this frequency shift is proportional to H_0^2 in the case of freely-falling observers as well as the Kodama observer field. The former are physically interesting since they do not require the knowledge of the underlying spacetime to be realized. The latter, i.e. the Kodama observer field, an observer at a constant value of the areal radius, is instead geometrically singled-out in spherically symmetric spacetimes. Linear terms appear when considering observers following the Hubble flow—which however makes them unpractical for local experiments. This is in accordance with the results in the existing literature, where several other effects—from light bending to perihelion precession—have been investigated leading to corrections with the same proportionality to the square of the Hubble parameter. Despite the smallness of the current value of H_0 that casts these effects outside current technological possibilities, similarly to all other effects studied previously, they nonetheless show the imprint that the cosmic expansion can have on localized systems and their dynamics.

In the last part of our work, we have reviewed the effect of the cosmic expansion on the redshift ratio and DDT in order to clarify some claims present in the literature. In particular, we have shown that linear corrections H to the redshift and DDT emerge when considering the cosmological observer but are not otherwise present in general. We have argued that the general result consists of corrections that are at least quadratic in H, placing these effects on the same footing as the others effects discussed in the literature.

In conclusion, despite the high degree of idealization of the local gravitational environment entailed by the McVittie or SdS metric, the expansion of the Universe is able to affect local experiments albeit in a way that place its detection beyond current technological capabilities.

Acknowledgments

The authors wish to thank Domenico Giulini for inspiring conversations. A Belenchia and D Braun acknowledge support from the Deutsche Forschungsgemeinschaft (DFG, German Research Foundation) Project Number BR 5221/4-1. D Rätzel thanks the Humboldt Foundation and the Marie Sklodowska-Curie Action IF program ('Phononic Quantum Sensors for Gravity' Grant Number 832250—PhoQuS-G) for support.

Data availability statement

All data that support the findings of this study are included within the article (and any supplementary files).

Appendix A. ΛCDM

In the ΛCDM model, the scale factor of the FLRW spacetime is given by

$$a(t) = \left(\frac{1-\Omega_\Lambda}{\Omega_\Lambda}\right)^{1/3} \sinh^{2/3}\left(\frac{t}{t_\Lambda}\right), \tag{A1}$$

where $t_\Lambda = 2/\left(3H_0\sqrt{\Omega_\Lambda}\right)$ is the cosmological timescale, the contribution Ω_{rad} to the total matter content of the Universe was considered to be negligible, and we used the approximation $\Omega_m + \Omega_\Lambda = 1$. For the Hubble parameter we obtain

$$H(t) = \frac{\dot{a}(t)}{a(t)} = H_0\sqrt{\Omega_\Lambda}\,\coth\left(\frac{t}{t_\Lambda}\right), \tag{A2}$$

where $H_0 = H(t_0)$ is the current value of the Hubble parameter at the present age of the Universe t_0, such that $a(t_0) = 1$. The leading order of the non-Newtonian contribution to the curvature of McVittie spacetime from equation (17) is then given by

$$-(H^2(t_0) + H'(t_0)) = \frac{1}{2}(H_0^2 - \Lambda). \tag{A3}$$

Appendix B. Proper detector frames: Fermi–Walker transported tetrads for various observers

As discussed in the main text, the proper detector frame can be defined along any timelike worldline as an orthonormal tetrad whose timelike element coincides with the normalized tangent to the worldline and the remaining orthogonal spacelike elements are Fermi–Walker transported along the worldline. In other terms, given a worldline γ whose normalized tangent we call $\dot{\gamma}$, the proper detector frame is defined via

$$\begin{cases} \mathbf{e}_0 = \dot{\gamma} \\ 0 = \dfrac{D_F\mathbf{e}_a}{\mathrm{d}s} \equiv \dfrac{D\mathbf{e}_a}{\mathrm{d}s} - \left(\mathbf{e}_a, \dfrac{D\mathbf{e}_0}{\mathrm{d}s}\right)\mathbf{e}_0 + (\mathbf{e}_a, \mathbf{e}_0)\dfrac{D\mathbf{e}_0}{\mathrm{d}s}, \quad \forall\, a \in \{1,2,3\}. \end{cases} \tag{B1}$$

solving the system of coupled differential equations defined above for a general timelike curve in McVittie spacetime is a tall order. Other methods for determining the proper detector frame have also been developed [61, 62] which however do not alleviate the problem of finding analytical expressions for McVittie spacetime. Nonetheless, the cases considered in the main text are such that the Fermi–Walker (FW) transported tetrad can actually be constructed by solving the above system of differential equations. This holds for the cosmological and Kodama observer in a general McVittie spacetime, and for radial and circular geodesic observers in SdS spacetime.

In this appendix we report the explicit form of the tetrads for completeness.

B.1. Cosmological observer in McVittie spacetime

The FW transported tetrad for the cosmological observer in McVittie spacetime in isotopic coordinates and in matrix form where each line is one of the tetrad vectors $\mathbf{e}_J$ reads

$$\mathbf{e}^{\mu}_{J} = \begin{pmatrix} \frac{\left(1+\frac{m(t)}{2r}\right)}{\left(1-\frac{m(t)}{2r}\right)} & 0 & 0 & 0 \\ 0 & \frac{1}{a(t)\left(1+\frac{m(t)}{2r}\right)^2} & 0 & 0 \\ 0 & 0 & \frac{1}{ra(t)\left(1+\frac{m(t)}{2r}\right)^2} & 0 \\ 0 & 0 & 0 & \frac{1}{ra(t)\left(1+\frac{m(t)}{2r}\right)^2} \end{pmatrix}. \tag{B2}$$

This tetrad is trivially obtained. Indeed, the spatial unit vectors $\mathbf{e}_r, \mathbf{e}_\theta, \mathbf{e}_\phi$ are just the normalized versions of the vectors $\partial_r, \partial_\theta$ and ∂_ϕ respectively.

B.2. Kodama observer in McVittie spacetime

The FW transported tetrad for the Kodama observer in McVittie spacetime in areal radius coordinates and in matrix form where each line is one of the tetrad vectors reads

$$\mathbf{e}^{\mu}_{J} = \begin{pmatrix} \sqrt{\frac{1}{1-2\mu(R)-h^2(R,t)}} & 0 & 0 & 0 \\ -\frac{h(R,t)}{\sqrt{(1-2\mu(R))\left(1-2\mu(R)-h^2(R,t)\right)}} & \sqrt{1-2\mu(R)-h^2(R,t)} & 0 & 0 \\ 0 & 0 & \frac{1}{R} & 0 \\ 0 & 0 & 0 & \frac{1}{R\sin\theta} \end{pmatrix}. \tag{B3}$$

This tetrad is easily obtained: the spatial unit vectors $\mathbf{e}_\theta, \mathbf{e}_\phi$ are just the normalization of the vectors $(0,0,1,0)$ and $(0,0,0,1)$, respectively. For what concerns $\mathbf{e}_R$, it is easily found by just imposing $g(\mathbf{e}_0, \mathbf{e}_R) = 0$ and $g(\mathbf{e}_R, \mathbf{e}_R) = 1$ with an ansatz $\mathbf{e}_R = (v_0, v_R, 0, 0)$.

B.3. Radial geodesic observer in SdS spacetime

The FW transported tetrad for the radial geodesic observer in SdS spacetime in manifestly static coordinates and in matrix form where each line is one of the tetrad vectors is given by

$$\mathbf{e}^{\mu}_{J} = \begin{pmatrix} \frac{E}{\alpha(R)} & \sqrt{E^2-\alpha(R)} & 0 & 0 \\ \frac{\sqrt{E^2-\alpha(R)}}{\alpha(R)} & E & 0 & 0 \\ 0 & 0 & \frac{1}{R} & 0 \\ 0 & 0 & 0 & \frac{1}{R\sin\theta} \end{pmatrix}. \tag{B4}$$

This tetrad is easily obtained: the spatial unit vectors $\mathbf{e}_\theta, \mathbf{e}_\phi$ are just the normalization of the vectors $(0,0,1,0)$ and $(0,0,0,1)$ respectively. For what concerns $\mathbf{e}_R$, it is easily found by just imposing $g(\mathbf{e}_0, \mathbf{e}_R) = 0$ and $g(\mathbf{e}_R, \mathbf{e}_R) = 1$ with an ansatz $\mathbf{e}_R = (v_0, v_R, 0, 0)$.

B.4. Circular orbit geodesic observer in SdS spacetime

In the case of a circular geodesic orbits, deriving the FW transported tetrad turns out to be more demanding than in the previous cases. Following [63], imposing the condition $\dot{R} = 0$ in equation (11) allows to fix the value of the conserved energy E and subsequently imposing the four-acceleration to be vanishing fixes the conserved angular momentum as

$$E^2 = R\frac{\alpha(R)^2}{R - 3r_S/2} \tag{B5}$$

$$L^2 = R^2\frac{r_S - 2H_0^2R^3}{2R - 3r_S}. \tag{B6}$$

It should be noted that in SdS spacetime circular geodesics exist in the region $3r_S/2 < R < (r_S/2H_0)^{1/3}$.

At this point, we should notice that the vector $\tilde{\boldsymbol{e}}_\theta = \|g_{\theta\theta}\|^{-1}\partial_\theta$ is FW transported (i.e., parallel transported) along the circular geodesic. With this observation, we can complete the orthonormal tetrad adding the spatial vector $\tilde{\boldsymbol{e}}_r = \|g_{rr}\|^{-1}\partial_r$ and the spatial vector $\tilde{\boldsymbol{e}}_\phi$ that can be obtained by requiring it to be orthonormal with the previous three. The tetrad thus formed is not FW transported. However, we can now linearly superpose $\tilde{\boldsymbol{e}}_r$ and $\tilde{\boldsymbol{e}}_\phi$ like $a(\phi)\tilde{\boldsymbol{e}}_r + b(\phi)\tilde{\boldsymbol{e}}_\phi$ and impose this vector to be FW transported. This results in two linearly independent differential equations for the coefficients $a(\phi), b(\phi)$

$$\sqrt{2}\sqrt{R}a(\phi)\sqrt{2R - 3r_S} + 2Rb'(\phi) = 0$$

$$\frac{2a'(\phi)}{\sqrt{R}} - \frac{\sqrt{2}b(\phi)\sqrt{2R - 3r_S}}{R} = 0,$$

whose solution is readily obtained as

$$a(\phi) = c_1\,\cos\left(\frac{\phi\sqrt{2R - 3r_S}}{\sqrt{2}\sqrt{R}}\right) + \sqrt{1 - c_1^2}\,\sin\left(\frac{\phi\sqrt{2R - 3r_S}}{\sqrt{2}\sqrt{R}}\right),$$

$$b(\phi) = \sqrt{1 - c_1^2}\,\cos\left(\frac{\phi\sqrt{2R - 3r_S}}{\sqrt{2}\sqrt{R}}\right) - c_1\,\sin\left(\frac{\phi\sqrt{2R - 3r_S}}{\sqrt{2}\sqrt{R}}\right),$$

where also the normalization of the linear combination has been used and c_1 is an integration constant that we fix to one in one case and to zero in the other in order to obtain two new vectors $\mathbf{e}_r$ and $\mathbf{e}_\phi$ which complete the FW transported tetrad. Finally, the FW transported tetrad for the circular orbit geodesic observer in SdS spacetime in static coordinates and in matrix form where each line is one of the tetrad vectors, is given by

$$\mathbf{e}^{\mu}_{J} = \begin{pmatrix} \sqrt{\dfrac{2R}{2R-3r_{\rm S}}} & 0 & 0 & \sqrt{\dfrac{r_{\rm S}/R-2H_0^2R^2}{R(2R-3r_{\rm S})}} \\ -\sqrt{\dfrac{r_{\rm S}-2H_0^2R^3}{(2R-3r_{\rm S})\alpha(R)}}\sin\left(\phi\sqrt{1-\dfrac{3r_{\rm S}}{2R}}\right) & \sqrt{\alpha(R)}\cos\left(\phi\sqrt{1-\dfrac{3r_{\rm S}}{2R}}\right) & 0 & -\sqrt{\dfrac{2\alpha(R)}{R(2R-3r_{\rm S})}}\sin\left(\phi\sqrt{1-\dfrac{3r_{\rm S}}{2R}}\right) \\ 0 & 0 & \dfrac{1}{R} & 0 \\ \sqrt{\dfrac{r_{\rm S}-2H_0^2R^3}{(2R-3r_{\rm S})\alpha(R)}}\cos\left(\phi\sqrt{1-\dfrac{3r_{\rm S}}{2R}}\right) & \sqrt{\alpha(R)}\sin\left(\phi\sqrt{1-\dfrac{3r_{\rm S}}{2R}}\right) & 0 & \sqrt{\dfrac{2\alpha(R)}{R(2R-3r_{\rm S})}}\cos\left(\phi\sqrt{1-\dfrac{3r_{\rm S}}{2R}}\right) \end{pmatrix}. \tag{B7}$$

It is important to note that a circular trajectory in SdS spacetime is characterized by an angular velocity $\omega^2 = r_{\rm S}/(2R^3) - H_0^2$ [63]. This is exactly the quantity entering the trigonometric functions in the tetrad elements. Indeed $\dot{\phi} = L/R^2$ from the angular momentum conservation, which implies $\phi = \tau L/R^2$, where τ is the proper time of the observer. Then, from the expression for the angular momentum of the circular geodesics, we can easily check that the argument of the trigonometric functions appearing in the tetrad is $\omega\tau = \sqrt{r_{\rm S}/(2R^3) - H_0^2}\tau$.

B.5. Bonus: circular orbit geodesic observer in Kerr–deSitter spacetime

A straightforward generalization of the SdS spacetime, which account for axially symmetric rotating central objects, instead of a spherical symmetric one, is the so called Kerr–de Sitter (KdS) spacetime [55–57]. The properties of the geodesic of KdS spacetime have been extensively considered in the existing literature and also the effect of the cosmological constant on the local dynamics have been considered [18, 48–50].

Following [50], we can write the KdS metric in Boyer–Lindquist stationary coordinates as

$$\begin{aligned} {\rm d}s^2 = &-\frac{\Delta_r}{\chi^2\rho^2}({\rm d}t - a\sin^2\theta{\rm d}\phi)^2 + \frac{\rho^2}{\Delta_r}{\rm d}r^2 + \frac{\rho^2}{\Delta_\theta}{\rm d}\theta^2 \\ &+ \frac{\Delta_\theta\sin^2\theta}{\chi^2\rho^2}\left(a{\rm d}t - (r^2+a^2){\rm d}\phi\right)^2, \end{aligned} \tag{B8}$$

where

$$\Delta_r = (1-H^2r^2)(r^2+a^2) - r_{\rm S}r \tag{B9}$$

$$\Delta_\theta = 1 + a^2H^2\cos^2\theta \tag{B10}$$

$$\chi = 1 + a^2H^2 \tag{B11}$$

$$\rho^2 = r^2 + a^2\cos^2\theta \tag{B12}$$

and $a = J/M$ is the angular momentum per mass of the central spinning object. Also recall that $H^2 = \Lambda/3$, where Λ is the cosmological constant. Note that the KdS spacetime is stationary but *not* static, and it reduces to SdS spacetime in static coordinates for $a \to 0$.

As discussed in e.g. [49], the geodesics of the KdS metric are characterized by four constants of integration given by energy per unit mass (E), angular momentum per unit mass (L), normalization of the tangent (μ) and the modified Carter's constant (Q). Timelike equatorial geodesics are found by imposing $\theta = \pi/2$, $\mu = -1$, and $Q = 0$. Further imposing the equatorial orbit to be circular fixes also the last two constants of integration.

The FW tetrad for an equatorial circular orbit in KdS spacetime can be obtained by following the same steps as in the case of SdS spacetime. Due to the lengthy expressions for both the tetrad and the components of the Riemann tensor in the proper detector frame of a geodesic observer

following a circular trajectory, we do not report them here. We limit ourselves to note that it is easy to verify that the Riemann tensor in the proper detector frame does not contain any linear term in H and thus also the frequency shift for a resonator in KdS spacetime has no linear term in H.

Appendix C. Doppler tracking and redshift: further details

In the main text, we have considered the redshift and DDT in FLRW spacetime for the cosmological and the Kodama observer field. In this appendix, we offer some further detail on those expressions and their derivation.

In the following, given an observer field $\mathbf{u}$, the frequency of a light signal characterized by the vector $\mathbf{k}$ as measured by the observer is the scalar product between the observer field and $\mathbf{k}$, i.e. $\omega = g(\mathbf{u}, \mathbf{k})$, where g is the metric symmetric tensor.

C.1. Redshift ratio in FLRW

Let us consider the FLRW metric in isotropic, spherical coordinates

$$\mathrm{d}s^2 = -\mathrm{d}t^2 + a^2(t)\mathrm{d}r^2 + a^2(t)r^2(\sin\,\theta^2\mathrm{d}\phi^2 + \mathrm{d}\theta^2). \tag{C1}$$

In these coordinates, the cosmological observer is given by $\mathbf{u} = \partial_t$ and it is a geodesic observer whose proper time coincides with the coordinate time. The expression for the redshift ratio for a light signal exchanged between two observers following the integral lines of $\mathbf{u}$ can be obtained in several ways, from using the fact that the cosmological observer is a conformal Killing vector field to brute force computations. For example, consider the two observers to be at r_0 and r_1 respectively. A radial null signal exchanged between these two is characterized by a null vector $\mathbf{k} = (1/a(t), 1/a(t)^2, 0, 0)$ coming from the geodesic equation and the normalization of the null vector $g(\mathbf{k}, \mathbf{k}) = 0$. Thus, one immediately finds

$$\frac{\omega_1}{\omega_0} \equiv \frac{g(\mathbf{u}, \mathbf{k})_{p_1}}{g(\mathbf{u}, \mathbf{k})_{p_0}} = \frac{a(t_0)}{a(t_1)}, \tag{C2}$$

where $p_i = (r_i, t_i), i = 0, 1$ are the spacetime points (suppressing the angular coordinates) at which the observers are located when receiving the light signal.

In the case of the Kodama observer, in isotropic coordinates this observer is expressed as

$$\mathbf{u}_\mathrm{K} = \frac{(1, -Hr, 0, 0)}{\sqrt{1 - H^2R^2}}, \tag{C3}$$

where $R = a(t)r$ and $\alpha(R) = 1 - H^2R^2$ is the norm of the Kodama vector field[11]. The redshift formula thus reads

$$\begin{aligned}\frac{\omega_1}{\omega_0} &\equiv \frac{g(\mathbf{u}_\mathrm{K}, \mathbf{k})|_{p_1}}{g(\mathbf{u}_\mathrm{K}, \mathbf{k})|_{p_0}} = \frac{\sqrt{1 - H(t_0)^2R_0^2}}{\sqrt{1 - H(t_1)^2R_1^2}} \left(\frac{1 + H(t_1)R_1}{1 + H(t_0)R_0}\right) \frac{a_0}{a_1} \\ &\approx (1 + \mathcal{O}(H^2, H')) \left(1 + H(t_0)R_1 - H(t_0)R_0 + \mathcal{O}((HR)^2, H'R^2)\right) \\ &\quad \times (1 - H(t_0)\Delta t_{10} + \mathcal{O}((HR)^2, H'R^2)) \\ &\approx 1 + \mathcal{O}((HR)^2, H'R^2),\end{aligned} \tag{C4}$$

[11] This is equal to $\alpha(R) = 1 - r_\mathrm{S}/R - H_0^2R^2$ in the SdS case.

where in the second line we have expanded both the scale factor and the Hubble parameter and finally used the fact that[12] $\Delta t_{10} = R_1 - R_0 + \mathcal{O}(HR)$. This expression shows that, for the radially propagating light rays, the linear contributions in HR from the second and third term cancel. This result is in accordance with the simpler analytical derivation shown in the text, where we considered the special case of de Sitter. Indeed, for de Sitter, or SdS for that matter, the Kodama vector field is a timelike Killing vector field so that we can use the fact that the scalar product between a Killing field and $\mathbf{k}$ is constant along the null geodesic [58]. Thus, we have

$$\frac{\omega_1}{\omega_0} = \frac{g(\mathbf{u}_\mathrm{K}, \mathbf{k})|_{p_1}}{g(\mathbf{u}_\mathrm{K}, \mathbf{k})|_{p_0}} = \frac{\sqrt{\alpha(R_0)}}{\sqrt{\alpha(R_1)}}, \tag{C5}$$

where in the final result we are left with only the ratio of the norms of the Kodama vector field thanks to the conservation law discussed, and $\alpha(R) = 1 - r_\mathrm{S}/R - H_0^2 R^2$ with $r_\mathrm{S} = 0$ in the case of de Sitter spacetime.

C.2. Double Doppler tracking

Building on the results of the previous section, it is clear that when considering the Kodama observer in de Sitter (or SdS) spacetime, equation (27) of the main text can be obtained by combining the results coming from the relativistic Doppler effect (see reference [25]) with the fact that

$$\frac{\omega_2}{\omega_1'}\frac{\omega_1}{\omega_0} = \frac{\sqrt{\alpha(R_0)}}{\sqrt{\alpha(R_2)}} = 1, \tag{C6}$$

where we have used the fact that the Kodama observer is at a fixed value of the areal radius so that $R_0 = R_2$. If considering the general case of FLRW spacetime, equation (C4) shows us that there would be a correction which, however, is at least quadratic in H, so that we can safely neglect it.

This shows that no correction linear in H should be expected in the DDT redshift ratio for light signals exchanged between Kodama observers. In order to prove that this is also the case for the rate of change of the DDT ratio, we need to show that differentiating the redshift ratio with respect to the proper time of the observer at the reception point does not introduce any linear correction. Note that this is not *a priori* obvious since in the case of the cosmological observer, part of the linear corrections in H are introduced exactly by this derivative.

Let us consider the Kodama observer in de Sitter spacetime (the derivation can be extended straightforwardly to the case of SdS). The Kodama observer field is given, in static coordinates, by $\mathbf{u}_\mathrm{K} = \alpha^{-1/2}\partial_t$. Thus, the coordinate time and the proper time of the Kodama observer are the same at linear order in H_0 and we can focus on the derivative with respect to the coordinate time of the receiver in the DDT scheme.

Note that the expression we are interested in differentiating with respect to t_2, i.e. equation (27), contains only quantities that depend on t_1. Thus, we need to obtain $\mathrm{d}t_1/\mathrm{d}t_2$. Following [25], we can use the null condition for an inward directed (assuming $R_1 > R_2 = R_0$) radial, lightlike geodesic to get

$$\int_{t_1(t_2)}^{t_2} \mathrm{d}t = -\int_{R_1(t_1(t_2))}^{R_2} \frac{\mathrm{d}R}{\alpha(R)}, \tag{C7}$$

[12] For a radial null geodesic $0 = \mathrm{d}s^2 = -\mathrm{d}t^2 + a^2(t)\mathrm{d}r^2 = -[\mathrm{d}t + \mathrm{d}R/(1 - RH)][\mathrm{d}t - \mathrm{d}R/(1 + RH)]$. In lowest order (for constant $H(t)$) this implies $\Delta t_{10} = \log[(1 + HR_1)/(1 + HR_0)]/H \approx \Delta R_{10} + \mathcal{O}(HR)$.

and then take the derivative with respect to t_2, with the understanding that R_2 is constant for the Kodama observer. In this way we arrive at[13]

$$\frac{\mathrm{d}t_1}{\mathrm{d}t_2} = \left(1 + \frac{\mathrm{d}R_1/\mathrm{d}t_1}{1 - H^2 R_1^2}\right)^{-1}. \tag{C8}$$

At this point, note that the spatial, unit vector $\hat{\boldsymbol{k}}$—i.e., the normalized spatial projection of the lightlike vector $\boldsymbol{k} = \left(E/\alpha, E, 0, 0\right)$ in the rest frame of the Kodama observer—is $\hat{\boldsymbol{k}} = \sqrt{\alpha}\partial_R$ and this implies that the projection of the relative spatial velocity of the spacecraft at the reflection point with respect to the observer field $\boldsymbol{\beta}_{\mathbf{u}_\mathrm{K}}(\mathbf{v}) = (\mathbf{v} - |g(\mathbf{v}, \mathbf{u}_\mathrm{K})|\mathbf{u}_\mathrm{K})/|g(\mathbf{v}, \mathbf{u}_\mathrm{K})|$ along $\hat{\boldsymbol{k}}$ has the form

$$\beta^{\hat{\boldsymbol{k}}}_{\mathbf{u}_\mathrm{K}}(\mathbf{v}) \equiv -\frac{g(\hat{\boldsymbol{k}}, \mathbf{v})}{g(\mathbf{u}_\mathrm{K}, \mathbf{v})} = \frac{1}{\alpha(R_1)}\frac{\mathrm{d}R_1}{\mathrm{d}t_1}, \tag{C9}$$

where $\mathbf{v}$ is the spacecraft four-velocity. With this last expression we have

$$\frac{\mathrm{d}t_1}{\mathrm{d}t_2} = \left(1 + \beta^{\hat{\boldsymbol{k}}}_{\mathbf{u}_\mathrm{K}}(\mathbf{v})\right)^{-1}, \tag{C10}$$

from which we see that this derivative does not introduce any correction linear in H.

Finally, it should be noted that, in reference [25] in order to arrive at the expression reported in equation (25) the authors need to differentiate the relative velocity with respect to t_1. In the case of the Kodama observer, we can follow the same derivation as in [25, 53] with the only caveat that additional corrections will appear when computing the derivatives of $\beta^{\hat{\boldsymbol{k}}}_{\mathbf{u}_\mathrm{K}}$ and $\beta^2_{\mathbf{u}_\mathrm{K}} = \|\boldsymbol{\beta}_{\mathbf{u}_\mathrm{K}}\|^2$ with respect to t_1. In particular, we would have that $\mathrm{d}/\mathrm{d}t_1 = \left(\mathrm{d}t_1/\mathrm{d}\tau_1\right)^{-1}\mathrm{d}/\mathrm{d}\tau_1$, where τ_1 is the arc-length of the spacecraft trajectory. Contrary to the case of the cosmological observer, this is not identical to the covariant 'observer' derivative, $\nabla^{\mathbf{u}}_{\mathbf{v}}$ defined in equation (130) of reference [25] (see also [9, 53]), anymore. Indeed, acting on a scalar function f

$$\nabla^{\mathbf{u}_\mathrm{K}}_{\mathbf{v}} f = |g(\mathbf{u}_\mathrm{K}, \mathbf{v})|^{-1}\frac{\mathrm{d}f}{\mathrm{d}\tau_1} = \frac{1}{\alpha^{1/2}}\frac{\mathrm{d}f}{\mathrm{d}t_1}, \tag{C11}$$

from which,

$$\frac{\mathrm{d}}{\mathrm{d}t_1} f = \alpha^{1/2}\nabla^{\mathbf{u}_\mathrm{K}}_{\mathbf{v}} f. \tag{C12}$$

Thus, in computing $\mathrm{d}\beta^{\hat{\boldsymbol{k}}}_{\mathbf{u}_\mathrm{K}}(\mathbf{v})/\mathrm{d}t_1$ and $\mathrm{d}\beta^2_{\mathbf{u}_\mathrm{K}}(\mathbf{v})/\mathrm{d}t_1$, we get:

- $\mathrm{d}\beta^{\hat{\boldsymbol{k}}}_{\mathbf{u}_\mathrm{K}}(\mathbf{v})/\mathrm{d}t_1 = \alpha^{1/2}\nabla^{\mathbf{u}_\mathrm{K}}_{\mathbf{v}}\beta^{\hat{\boldsymbol{k}}}_{\mathbf{u}_\mathrm{K}}(\mathbf{v}) = \alpha^{1/2}\left(h_{\mathbf{u}_\mathrm{K}}(\boldsymbol{\alpha}_{\mathbf{u}_\mathrm{K}}(\gamma), \hat{\boldsymbol{k}}) + h_{\mathbf{u}_\mathrm{K}}(\boldsymbol{\beta}_{\mathbf{u}_\mathrm{K}}(\mathbf{v}), \nabla^{\mathbf{u}_\mathrm{K}}_{\mathbf{v}}\hat{\boldsymbol{k}})\right)$, where h is the spatial metric in the rest frame of the observer field, and we have introduced the relative spatial acceleration of the spacecraft trajectory with respect to the observer field $\boldsymbol{\alpha}_{\mathbf{u}_\mathrm{K}}(\gamma)$.
- $\mathrm{d}\beta^2_{\mathbf{u}_\mathrm{K}}(\mathbf{v})/\mathrm{d}t_1 = \alpha^{1/2}\nabla^{\mathbf{u}_\mathrm{K}}_{\mathbf{v}}\beta^2_{\mathbf{u}_\mathrm{K}}(\mathbf{v}) = 2\alpha^{1/2}h_{\mathbf{u}_\mathrm{K}}(\boldsymbol{\beta}_{\mathbf{u}_\mathrm{K}}(\mathbf{v}), \boldsymbol{\alpha}_{\mathbf{u}_\mathrm{K}}(\gamma))$,

where we have used the identities in equations (3.16) and (3.17) in [53] and, as in the main text, we indicate with $\boldsymbol{\alpha}_{\mathbf{u}_\mathrm{K}}(\gamma) = \nabla^{\mathbf{u}_\mathrm{K}}_{\mathbf{v}}\boldsymbol{\beta}_{\mathbf{u}_\mathrm{K}}(\mathbf{v})$ the relative spatial acceleration of the spacecraft trajectory γ with respect to the observer field. However, it is clear that the corrections appearing will be at least quadratic in H and cannot give rise to any linear correction in H in the

[13] In the case of SdS we would have $\alpha(R_1)$ in the denominator of the right-hand side of (C8).

DDT expression. Indeed, putting together the results listed above and taking the derivative of equation (27), i.e.,

$$\frac{\omega_2}{\omega_0} = \left\{ 2\frac{1-\beta^{\hat{\boldsymbol{k}}}_{\mathbf{u}_\mathrm{K}}(\mathbf{v})}{1-\beta_{\mathbf{u}_\mathrm{K}}(\mathbf{v})^2} - 1 \right\}, \tag{C13}$$

we arrive at

$$\begin{aligned}\frac{1}{\omega_0}\frac{\mathrm{d}\omega_2}{\mathrm{d}\tau_2} = \alpha(R)^{-1/2}(1+\beta^{\hat{\boldsymbol{k}}}_{\mathbf{u}_\mathrm{K}}(\mathbf{v}))^{-1}\Bigg[&-2\Big(h_{\mathbf{u}_\mathrm{K}}(\boldsymbol{\alpha}_{\mathbf{u}_\mathrm{K}}(\gamma),\hat{\boldsymbol{k}}) \\ &+ h_{\mathbf{u}_\mathrm{K}}(\boldsymbol{\beta}_{\mathbf{u}_\mathrm{K}}(\mathbf{v}),\nabla^{\mathbf{u}_\mathrm{K}}_{\mathbf{v}}\hat{\boldsymbol{k}})\Big)(1-\beta^2_{\mathbf{u}_\mathrm{K}}(\mathbf{v}))^{-1} \\ &+ 4h_{\mathbf{u}_\mathrm{K}}(\boldsymbol{\beta}_{\mathbf{u}_\mathrm{K}}(\mathbf{v}),\boldsymbol{\alpha}_{\mathbf{u}_\mathrm{K}}(\gamma))\frac{(1-\beta^{\hat{\boldsymbol{k}}}_{\mathbf{u}_\mathrm{K}}(\mathbf{v}))}{(1-\beta^2_{\mathbf{u}_\mathrm{K}}(\mathbf{v}))^2}\Bigg]\end{aligned} \tag{C14}$$

to be compared with equations (8.12) and (144) of [25, 53] respectively. In particular, an even clearer picture can be obtained following [25, 53] and considering a radially escaping spacecraft so that $\boldsymbol{\beta}_{\mathbf{u}_\mathrm{K}} = \beta^{\hat{\boldsymbol{k}}}_{\mathbf{u}_\mathrm{K}}\hat{\boldsymbol{k}}$, $\boldsymbol{\alpha}_{\mathbf{u}_\mathrm{K}} = \alpha^{\hat{\boldsymbol{k}}}_{\mathbf{u}_\mathrm{K}}\hat{\boldsymbol{k}}$ with $\alpha^{\hat{\boldsymbol{k}}}_{\mathbf{u}_\mathrm{K}} = h_{\mathbf{u}_\mathrm{K}}(\boldsymbol{\alpha}_{\mathbf{u}_\mathrm{K}},\hat{\boldsymbol{k}})$—where we now suppress the arguments of the $\alpha^{\hat{\boldsymbol{k}}}_{\mathbf{u}_\mathrm{K}}$ and the $\beta^{\hat{\boldsymbol{k}}}_{\mathbf{u}_\mathrm{K}}$ for ease of notation. In this case we obtain

$$\begin{aligned}\frac{1}{\omega_0}\frac{\mathrm{d}\omega_2}{\mathrm{d}\tau_2} &= -2\alpha(R)^{-1/2}\alpha^{\hat{\boldsymbol{k}}}_{\mathbf{u}_\mathrm{K}}(1+\beta^{\hat{\boldsymbol{k}}}_{\mathbf{u}_\mathrm{K}})^{-3} \\ &= 2\left(1+\frac{H_0^2R^2}{2}\right)\alpha^{\hat{\boldsymbol{k}}}_{\mathbf{u}_\mathrm{K}}(1+\beta^{\hat{\boldsymbol{k}}}_{\mathbf{u}_\mathrm{K}})^{-3} + \mathcal{O}(H_0^4R^4),\end{aligned} \tag{C15}$$

which shows that only corrections quadratic, or higher, in H_0R appear in the DDT rate.

Appendix D. Weak field regime of McVittie spacetime

In the following, we will diagonalize the McVittie metric in areal radius coordinates in equation (3) to second order in HR. First, we find that the inverse of the McVittie metric is

$$g^{\mu\nu} = \begin{pmatrix} \dfrac{1}{1-\frac{2m_0}{R}} & -\dfrac{H(t)R}{\sqrt{1-\frac{2m_0}{R}}} & 0 & 0 \\ -\dfrac{H(t)R}{\sqrt{1-\frac{2m_0}{R}}} & 1-\dfrac{2m_0}{R}-H(t)^2R^2 & 0 & 0 \\ 0 & 0 & \dfrac{1}{R^2} & 0 \\ 0 & 0 & 0 & \dfrac{1}{R^2\sin^2\theta} \end{pmatrix}. \tag{D1}$$

We define the time coordinate

$$\tau = t - \int \mathrm{d}R\,\frac{g^{01}}{g^{11}} \approx t - \Sigma(R)H(t)R^2/2 \tag{D2}$$

which we approximated to second order in HR and defined

$$\Sigma(R) = 16\frac{m_0^2}{R^2}\left(1-\frac{2m_0}{R}\right)^{-1/2}{}_2F_1\left(-\frac{1}{2},3,\frac{1}{2},1-\frac{2m_0}{R}\right), \tag{D3}$$

where ${}_2F_1$ is the hypergeometric function, and find that the inverse McVittie metric becomes

$$g^{\mu\nu} \approx \begin{pmatrix} -\dfrac{1-\Sigma(R)H'(t)R^2}{1-\frac{2m_0}{R}} - \dfrac{H(t)^2R^2}{\left(1-\frac{2m_0}{R}\right)^2} & 0 & 0 & 0 \\ 0 & 1-\dfrac{2m_0}{R}-H(t)^2R^2 & 0 & 0 \\ 0 & 0 & \dfrac{1}{R^2} & 0 \\ 0 & 0 & 0 & \dfrac{1}{R^2\sin^2\theta} \end{pmatrix} \tag{D4}$$

also in second order in HR. The corresponding approximate expression for the McVittie metric is

$$g_{\mu\nu} \approx \begin{pmatrix} -\left(1-\dfrac{2m_0}{R}\right)(1+\Sigma(R)H'(t)R^2)+H(t)^2R^2 & 0 & 0 & 0 \\ 0 & \dfrac{1}{1-\frac{2m_0}{R}}+\dfrac{H(t)^2R^2}{\left(1-\frac{2m_0}{R}\right)^2} & 0 & 0 \\ 0 & 0 & R^2 & 0 \\ 0 & 0 & 0 & R^2\sin^2\theta \end{pmatrix}. \tag{D5}$$

In the weak-field regime, where $m_0/R \ll 1$, we can consider this as a linear perturbed Minkowski metric and identify a Newtonian potential via the relation $g_{00} = -1\text{–}2\Phi$. We find

$$g \approx \mathrm{diag}\left(-1+\frac{2m_0}{R}+(H(t)^2+H'(t))R^2, 1 + \frac{2m_0}{R}+H(t)^2R^2, \frac{1}{R^2}, \frac{1}{R^2\sin^2\theta}\right). \tag{D6}$$

where we neglected terms proportional to $m_0H(t)^2$ and $m_0H'(r)$. The Newtonian potential becomes

$$\Phi = -\frac{m_0}{R} - \frac{1}{2}(H(t)^2+H'(t))R^2. \tag{D7}$$

Note the similarity of (D6) to the SdS metric in manifestly static coordinates in (4). In contrast to the latter case, in the case of the perturbatively diagonalized McVittie metric, there is also a time-dependent spatial component.

ORCID iDs

Felix Spengler https://orcid.org/0000-0002-9295-8587
Alessio Belenchia https://orcid.org/0000-0002-0347-6763
Dennis Rätzel https://orcid.org/0000-0003-3452-6222
Daniel Braun https://orcid.org/0000-0001-8598-2039

References

[1] Planck Collaboration *et al* 2020 Planck 2018 results: VI. Cosmological parameters *Astronomy & Astrophysics* **641** A6
[2] Einstein A and Straus E G 1945 The influence of the expansion of space on the gravitation fields surrounding the individual stars *Rev. Mod. Phys.* **17** 120–4
[3] Einstein A and Straus E G 1946 Corrections and additional remarks to our paper: the influence of the expansion of space on the gravitation fields surrounding the individual stars *Rev. Mod. Phys.* **18** 148–9
[4] Dicke R H and Peebles P J E 1964 Evolution of the solar system and the expansion of the universe *Phys. Rev. Lett.* **12** 435–7
[5] Bonnor W B 2000 A generalization of the Einstein–Straus vacuole *Class. Quantum Grav.* **17** 2739
[6] Mashhoon B, Mobed N and Singh D 2007 Tidal dynamics in cosmological spacetimes *Class. Quantum Grav.* **24** 5031
[7] Nandra R, Lasenby A N and Hobson M P 2012 The effect of an expanding universe on massive objects *Mon. Not. R. Astron. Soc.* **422** 2945–59
[8] Kagramanova V, Kunz J and Lämmerzahl C 2006 Solar system effects in Schwarzschild–de Sitter space-time *Phys. Lett.* B **634** 465–70
[9] Carrera M and Giulini D 2006 On Doppler tracking in cosmological spacetimes *Class. Quantum Grav.* **23** 7483
[10] Kopeikin S M 2015 Optical cavity resonator in an expanding universe *Gen. Relativ. Gravit.* **47** 5
[11] Arakida H 2009 Time delay in Robertson–McVittie spacetime and its application to increase of astronomical unit *New Astron.* **14** 264–8
[12] Arakida H 2011 Application of time transfer function to McVittie spacetime: gravitational time delay and secular increase in astronomical unit *Gen. Relativ. Gravit.* **43** 2127–39
[13] Agatsuma K 2020 The expansion of the universe in binary star systems *Phys. Dark Universe* **30** 100732
[14] Giulini D 2014 Does cosmological expansion affect local physics? *Stud. Hist. Phil. Sci.* B **46** 24–37
[15] Aghili M E, Bolen B and Bombelli L 2017 Effect of accelerated global expansion on the bending of light *Gen. Relativ. Gravit.* **49** 1–14
[16] Axenides M, Floratos E G and Perivolaropoulos L 2000 Some dynamical effects of the cosmological constant *Mod. Phys. Lett.* A **15** 1541–50
[17] Bolen B, Bombelli L and Puzio R 2001 Expansion-induced contribution to the precession of binary orbits *Class. Quantum Grav.* **18** 1173
[18] Kerr A W, Hauck J C and Mashhoon B 2003 Standard clocks, orbital precession and the cosmological constant *Class. Quantum Grav.* **20** 2727
[19] Price R H and Romano J D 2012 In an expanding universe, what does not expand? *Am. J. Phys.* **80** 376–81
[20] Iorio L 2006 Can solar system observations tell us something about the cosmological constant? *Int. J. Mod. Phys.* D **15** 473–5
[21] Jetzer P and Sereno M 2006 Two-body problem with the cosmological constant and observational constraints *Phys. Rev.* D **73** 044015
[22] Adkins G S, McDonnell J and Fell R N 2007 Cosmological perturbations on local systems *Phys. Rev.* D **75** 064011
[23] Cooperstock F I, Faraoni V and Vollick D N 1998 The influence of the cosmological expansion on local systems *Astrophys. J.* **503** 61
[24] Lammerzahl C, Preuss O and Dittus H 2008 Is the physics within the solar system really understood? *Lasers, Clocks and Drag-free Control* (Berlin: Springer) pp 75–101
[25] Carrera M and Giulini D 2010 Influence of global cosmological expansion on local dynamics and kinematics *Rev. Mod. Phys.* **82** 169–208
[26] McVittie G C 1933 The mass-particle in an expanding universe *Mon. Not. R. Astron. Soc.* **93** 325–39
[27] Ludlow A D, Boyd M M, Ye J, Peik E and Schmidt P O 2015 Optical atomic clocks *Rev. Mod. Phys.* **87** 637–701
[28] Hinkley N, Sherman J A, Phillips N B, Schioppo M, Lemke N D, Beloy K, Pizzocaro M, Oates C W and Ludlow A D 2013 An atomic clock with 10^{-18} instability *Science* **341** 1215–8
[29] Nemitz N, Ohkubo T, Takamoto M, Ushijima I, Das M, Ohmae N and Katori H 2016 Frequency ratio of Yb and Sr clocks with 5×10^{-17} uncertainty at 150 s averaging time *Nat. Photon.* **10** 258–61

[30] Chou C-W, Hume D B, Koelemeij J C J, Wineland D J and Rosenband T 2010 Frequency comparison of two high-accuracy Al^+ optical clocks *Phys. Rev. Lett.* **104** 070802
[31] Takamoto M, Hong F-L, Higashi R and Katori H 2005 An optical lattice clock *Nature* **435** 321–4
[32] Ichiro U, Masao T, Manoj D, Takuya O and Hidetoshi K 2015 Cryogenic optical lattice clocks *Nat. Photon.* **9** 185–9
[33] Nicholson T L *et al* 2015 Systematic evaluation of an atomic clock at 2×10^{-18} total uncertainty *Nat. Commun.* **6** 1–8
[34] McGrew W F *et al* 2018 Atomic clock performance enabling geodesy below the centimetre level *Nature* **564** 87–90
[35] Bothwell T, Kedar D, Oelker E, Robinson J M, Bromley S L, Tew W L, Ye J and Kennedy C J 2019 JILA SrI optical lattice clock with uncertainty of 2.0×10^{-18} *Metrologia* **56** 065004
[36] Brewer S M, Chen J-S, Hankin A M, Clements E R, Chou C W, Wineland D J, Hume D B and Leibrandt D R 2019 $^{27}Al^+$ quantum-logic clock with a systematic uncertainty below 10^{-18} *Phys. Rev. Lett.* **123** 033201
[37] Boulder Atomic Clock Optical Network BACON Collaboration 2021 Frequency ratio measurements at 18-digit accuracy using an optical clock network *Nature* **591** 564–9
[38] Marti G E, Hutson R B, Goban A, Campbell S L, Poli N and Ye J 2018 Imaging optical frequencies with 100 μHz precision and 1.1 μm resolution *Phys. Rev. Lett.* **120** 103201
[39] Rätzel D, Schneiter F, Braun D, Bravo T, Howl R, Lock M P E and Fuentes I 2018 Frequency spectrum of an optical resonator in a curved spacetime *New J. Phys.* **20** 053046
[40] Schücking E 1954 Das Schwarzschildsche linienelement und die expansion des Weltalls *Z. Phys.* **137** 595–603
[41] Nolan B C 1998 A point mass in an isotropic universe: existence, uniqueness, and basic properties *Phys. Rev.* D **58** 064006
[42] Nolan B C 1999 A point mass in an isotropic universe: II. Global properties *Class. Quantum Grav.* **16** 1227
[43] Nolan B C 1999 A point mass in an isotropic universe: III. The region R2m *Class. Quantum Grav.* **16** 3183
[44] Nolan B C 2014 Particle and photon orbits in McVittie spacetimes *Class. Quantum Grav.* **31** 235008
[45] Carrera M and Giulini D 2010 Generalization of McVittie's model for an inhomogeneity in a cosmological spacetime *Phys. Rev.* D **81** 043521
[46] Kottler F 1918 Über die physikalischen grundlagen der Einsteinschen gravitationstheorie *Ann. Phys.* **361** 401–62
[47] Islam J N 1983 The cosmological constant and classical tests of general relativity *Phys. Lett.* A **97** 239–41
[48] Stuchlík Z and Slanỳ P 2004 Equatorial circular orbits in the Kerr–de Sitter spacetimes *Phys. Rev.* D **69** 064001
[49] Kraniotis G V 2004 Precise relativistic orbits in Kerr and Kerr–(anti) de Sitter spacetimes *Class. Quantum Grav.* **21** 4743
[50] Hackmann E, Lämmerzahl C, Kagramanova V and Kunz J 2010 Analytical solution of the geodesic equation in Kerr-(anti-) de Sitter space-times *Phys. Rev.* D **81** 044020
[51] Ni W-T and Zimmermann M 1978 Inertial and gravitational effects in the proper reference frame of an accelerated, rotating observer *Phys. Rev.* D **17** 1473–6
[52] Misner C W, Thorne K S, Wheeler J A and Chandrasekhar S 1974 Gravitation *Phys. Today* **27** 47
[53] Carrera M 2010 Geometrical methods for kinematics and dynamics in relativistic theories of gravity with applications to cosmology and space physics *PhD Thesis*
[54] Hackmann E and Lämmerzahl C 2008 Geodesic equation in Schwarzschild-(anti-)de Sitter spacetimes: analytical solutions and applications *Phys. Rev.* D **78** 024035
[55] Carter B 1968 Hamilton–Jacobi and Schrodinger separable solutions of Einstein's equations *Commun. Math. Phys.* **10** 280–310
[56] Demianski M 1973 Some new solutions of the Einstein equations of astrophysical interest *Acta Astron.* **23** 197
[57] Gibbons G W, Lü H, Page D N and Pope C N 2005 The general Kerr–de Sitter metrics in all dimensions *J. Geom. Phys.* **53** 49–73
[58] Wald R M 2010 *General Relativity* (Chicago, IL: University of Chicago Press)
[59] Nandra R, Lasenby A N and Hobson M P 2012 The effect of a massive object on an expanding universe *Mon. Not. R. Astron. Soc.* **422** 2931–44
[60] Carroll S M 1997 Lecture notes on general relativity (arXiv:gr-qc/9712019)

[61] Maluf J W and Faria F F 2008 On the construction of Fermi–Walker transported frames *Ann. Phys.* **17** 326–35
[62] Klein D and Collas P 2008 General transformation formulas for Fermi–Walker coordinates *Class. Quantum Grav.* **25** 145019
[63] Brito J P B, Bernar R P and Crispino L C B 2020 Synchrotron geodesic radiation in Schwarzschild–de Sitter spacetime *Phys. Rev.* D **101** 124019

Paper [C].
Manuscript: Optical solitons in curved spacetime

Felix Spengler, Alessio Belenchia, Dennis Rätzel, and Daniel Braun
ArXiv Submission (2023)
DOI: 10.48550/arXiv.2301.04986 URL: arxiv.org/abs/2301.04986

Optical solitons in curved spacetime

Felix Spengler,[1] Alessio Belenchia,[1,2] Dennis Rätzel,[3,4] and Daniel Braun[1]

[1]*Institut für Theoretische Physik, Eberhard-Karls-Universität Tübingen, 72076 Tübingen, Germany*
[2]*Centre for Theoretical Atomic, Molecular, and Optical Physics, School of Mathematics and Physics, Queens University, Belfast BT7 1NN, United Kingdom*
[3]*ZARM, University of Bremen, Am Fallturm 2, 28359 Bremen, Germany*
[4]*Humboldt Universität zu Berlin, Institut für Physik, Newtonstraße 15, 12489 Berlin, Germany*

(Dated: January 13, 2023)

Light propagation in curved spacetime is at the basis of some of the most stringent tests of Einstein's general relativity. At the same time, light propagation in media is at the basis of several communication systems. Given the ubiquity of the gravitational field, and the exquisite level of sensitivity of optical measurements, the time is ripe for investigations combining these two aspects and studying light propagation in media located in curved spacetime. In this work, we focus on the effect of a weak gravitational field on the propagation of optical solitons in non-linear optical media. We derive a non-linear Schrödinger equation describing the propagation of an optical pulse in an effective, gradient-index medium in flat spacetime, encoding both the material properties and curved spacetime effects. In analyzing the special case of propagation in a 1D optical fiber, we also include the effect of mechanical deformations and show it to be the dominant effect for a fiber oriented in the radial direction in Schwarzschild spacetime.

INTRODUCTION

The properties of light propagating in optical media is a subject as old as optics itself. In recent years, the possibility to engineer novel metamaterials has opened the door to the so-called transformation optics [1], a field promising to enhance existing devices and create novel ones. At the basis of this revolution is the fact that, in the geometric optics limit – and neglecting dispersion –, light rays propagate in media following the geodesics of an effective Lorentzian metric, the so-called optical metric [2]. This has also led to the investigation of light in optical media as an analogue gravity model, i.e., a model in which field perturbations propagate *as if* in a curved spacetime background, particularly useful in the investigation of kinematic effects of quantum field theory in curved spacetime, like the Hawking radiation and cosmological particle production [3–5]. When also the effect of dispersion is considered, the metric description can be cast aside for a more powerful Hamiltonian formalism, giving rise to the so-called ray-optical structures [6, 7].

This analogy between optical media and curved spacetimes can be pushed even further by showing that Maxwell equations in vacuum, curved spacetime are equivalent to flat-spacetime Maxwell equations in the presence of a bi-anisotropic moving medium whose dielectric permittivity and magnetic permeability are determined entirely by the spacetime metric [8]. Spacetime itself can then be described as an optical medium at the level of full electromagnetism. It is then natural to wonder what would happen if light were to propagate in an optical medium placed in a curved spacetime. Far from being a far-fetched situation, this is exactly the case for light propagating in media on Earth due to the non-vanishing, albeit weak, gravitational field of our planet. In this work, we are interested in exactly this situation. In particular, while at the geometric optics level the formalism of ray-optical structures can be used, we aim here at a description, analogous to the one in [8], at the level of full Maxwell equations. Indeed, such a description allows for the modelling of the propagation of intense pulses in situations of physical interest, like soliton propagation in optical fibers, taking into account the effect of a weak gravitational field.

We show that light propagation in a medium in curved spacetime is equivalent to propagation in an effective medium in flat spacetime. We then use this formalism to investigate the propagation of intense light pulses in non-linear media, giving rise to optical solitons. Solitons, and more in general propagating pulses, in optical fibers are at the basis of several communication protocols. Given that fibers on Earth are *de facto* in a curved spacetime due to our planet's gravitational field, it is relevant to analyze how gravity influences light-pulses propagation. Our result allows us to set up a framework for the analysis of the effect of acceleration and curvature on the propagation of pulses in optical fibers in curved spacetimes. We numerically investigate some of these effects for the simple case of 1D propagation in the weak-field limit.

AN EFFECTIVE "SPACETIME MEDIUM"

While light in media can propagate as in a curved spacetime, curved spacetime can also be seen as an effective medium with non-trivial permeability and permittivity [8, 9]. It is not difficult to generalize the derivations in [8, 9] to the case in which light propagates in an optical medium placed in curved spacetime. Also in this case it can be shown that Maxwell's equations are equivalent to Maxwell's equations in flat spacetime for an effective medium whose properties encode both the ones of the physical medium and of curved spacetime.

Indeed, consider a dielectric and permeable medium in curved spacetime characterized by a Lorentzian metric $g_{\mu\nu}$ with mostly plus signature. We follow here the notation of [7],

also reported in the Supplemental Material [10]. Maxwell's equations in the absence of free charges and currents are given by

$$\nabla_k F^{*\,ik} = 0 \tag{1}$$

$$\nabla_k G^{ik} = 0, \tag{2}$$

where F^* is the Hodge dual of the electromagnetic tensor F, and G and F are related by the constitutive equations of the material. Choosing an observer field u^i, the electric and magnetic field strengths can be defined with respect to it as

$$B_a = -\frac{1}{2}\eta_{abcd}u^b F^{cd};\ E_i = F_{ij}u^j \tag{3}$$

$$H_a = -\frac{1}{2}\eta_{abcd}u^b G^{cd};\ D_i = G_{ij}u^j \tag{4}$$

$$F_{ab} = -\eta^{cd}_{ab}u_d B_c + 2u_{[a}E_{b]} \tag{5}$$

$$G_{ab} = -\eta^{cd}_{ab}u_d H_c + 2u_{[a}D_{b]}, \tag{6}$$

in the reference frame of the observer in which the medium is assumed to be at rest. Here $\eta_{ijkl} = \sqrt{-g}\delta_{ijkl}$ is the Levi-Civita tensor and $T_{[abc\ldots]}$ denotes the antisymmetrization of the tensor with respect to the indices in square brackets.

As discussed in [10], choosing $u^i = \delta^i_0/\sqrt{-g_{00}}$, the projection of Maxwell's equations in 3-dimensional form leads to

$$\delta^{\alpha\beta\gamma}\partial_\beta\mathcal{H}_\gamma - \partial_0\mathcal{D}^\alpha = 0;\ \partial_l\mathcal{D}^l = 0 \tag{7}$$

$$\delta^{\alpha\beta\gamma}\partial_\beta\mathcal{E}_\gamma + \partial_0\mathcal{B}^\alpha = 0;\ \partial_l\mathcal{B}^l = 0, \tag{8}$$

where $\mathcal{E}_\alpha = \sqrt{-g_{00}}E_\alpha$, $\mathcal{H}_\alpha = \sqrt{-g_{00}}H_\alpha$, and

$$\mathcal{D}^\alpha = -\sqrt{-g}\frac{g^{\alpha\beta}}{g_{00}}\mathfrak{D}_\beta - \delta^{\alpha\beta\gamma}\frac{g_{0\gamma}}{g_{00}}\mathcal{H}_\beta \tag{9}$$

$$\mathcal{B}^\alpha = -\sqrt{-g}\frac{g^{\alpha\beta}}{g_{00}}\mathfrak{B}_\beta + \delta^{\alpha\beta\gamma}\frac{g_{0\gamma}}{g_{00}}\mathcal{E}_\beta, \tag{10}$$

with $\mathfrak{B}_\alpha = \sqrt{-g_{00}}B_\alpha$, and $\mathfrak{D}_\alpha = \sqrt{-g_{00}}D_\alpha$. These expressions are equivalent to Maxwell's equations in flat spacetime in the presence of an optical medium. In particular, for a non-dispersive medium characterized by constitutive relations $D_a = \varepsilon^b_a E_b$, and $B_a = \mu^b_a H_b$, the effective medium will be characterized by a dielectric and magnetic permeability given by the product of the material ones and the ones characterizing the curved spacetime [8, 9]. Indeed, expressing $\mathcal{D}^\alpha = \tilde{\varepsilon}^{\alpha\beta}\mathcal{E}_\beta + \tilde{\gamma}^\beta_\alpha\mathcal{H}_\beta$ and correspondingly $\mathcal{B}^\alpha = \tilde{\mu}^{\alpha\beta}\mathcal{H}_\beta - \tilde{\gamma}^\beta_\alpha\mathcal{E}_\beta$, where $\tilde{\gamma}^\beta_\alpha$ encode magnetoelectric effects, we see that

$$\tilde{\mu}^{\alpha\beta} = -\sqrt{-g}\frac{g^{\alpha\gamma}}{g_{00}}\mu^\beta_\gamma \tag{11}$$

$$\tilde{\varepsilon}^{\alpha\beta} = -\sqrt{-g}\frac{g^{\alpha\gamma}}{g_{00}}\varepsilon^\beta_\gamma, \tag{12}$$

and $\tilde{\gamma}^{\alpha\beta} = -\delta^{\alpha\beta\gamma}g_{0\gamma}/g_{00}$[1]. As a direct consequence, whenever the refractive index of the *effective medium* can be defined, it will also be the product of the material refractive index times the vacuum spacetime effective one. The same result can be easily obtained at the level of geometric optics.

Finally, we make two observations relevant for the study of the propagation of light pulses. Firstly, a non-magnetic material in curved spacetime corresponds to a magnetic effective medium in Minkowski due to the "magnetic permeability" of the background spacetime. Secondly, when considering a non-linear material, we see that the non-linearity will also be affected by the curvature of spacetime as well as the linear polarizability.

PULSE PROPAGATION: NON-LINEAR SCHRÖDINGER EQUATION

We next consider the propagation of light pulses in a Kerr non-linear, non-magnetic material in curved spacetime. In particular, we focus on the case in which the material is in a stationary orbit of Schwarzschild spacetime and use isotropic coordinates. This situation well-captures the cases of interest for optical communication and laboratory experiments like, e.g., optical fibers hanging still above Earth's surface.

In flat spacetime, the non-linear Schrödinger equation (NLSE) is often used when considering the propagation of light pulses whose amplitude is well-described by a scalar envelope slowly varying with respect to the light period and wavelength [11, 12]. In the case of a medium stationary in Schwarzschild' spacetime, by employing the correspondence with an *effective medium* in flat spacetime as described in the previous section, the usual derivation of the NLSE can be carried out. However, the effective medium will be inhomogeneous due to the curved spacetime contribution to the polarizability and permeability of the material medium. This gives rise to extra terms in the NLSE which are of purely gravitational origin. Furthermore, another source of inhomogeneity in the medium can be included when considering the effect of tidal forces on the material that, through photoelasticity, render the refractive index position-dependent.

Neglecting for the moment photoelasticity, i.e., considering a rigid dielectric, we can write Maxwell's equation in flat spacetime for the effective medium in the familiar notation, using the fields and field strengths that we indicate with plain capital letters from now on,

$$\nabla\cdot B = 0,\ \nabla\cdot D = 0 \tag{13}$$

$$\nabla\times E = -\partial_t B,\ \nabla\times H = \partial_t D, \tag{14}$$

where $D = \tilde{\varepsilon}E$ and $H = B/\tilde{\mu}$. Here $\tilde{\mu} = \tilde{\mu}(r)$ and $\tilde{\varepsilon} = \tilde{\varepsilon}(E, r, \omega)$ in frequency space, allowing us to account for the effect of material dispersion, are the permeability and permittivity of the effective medium. Expressing the Schwarzschild' spacetime metric in isotropic coordinates as $ds^2 = -(B(t,r)/A(t,r))^2\,dt^2 + A^4(t,r)\delta_{\alpha\beta}dx^\alpha dx^\beta$, with $A(r) = 1 + r_S/4r$ and $B(r) = 1 - r_S/4r$, with r_S the Schwarzschild

[1] Note that, in the case the material itself possesses magnetoelectric terms in the constitutive equations, i.e., $D_a = \varepsilon^b_a E_b + \gamma^b_a H_b$, and $B_a = \mu^b_a H_b - \gamma^b_a E_b$ then $\tilde{\gamma}^{\alpha\beta} = -\delta^{\alpha\beta\gamma}\frac{g_{0\gamma}}{g_{00}} - \sqrt{-g}\frac{g^{\alpha\delta}}{g_{00}}\gamma^\beta_\delta$

radius, we have

$$\tilde{\varepsilon}(E,r,\omega) = \varepsilon_0\varepsilon_{\rm sp}\varepsilon = \varepsilon_0\frac{A(r)^3}{B(r)}\left(1+\chi^{(1)}(\omega)+3\chi^{(3)}\frac{|E|^2}{\Omega}\right), \tag{15}$$

$$\tilde{\mu} = \tilde{\mu}(r) = \mu_0\mu_{\rm sp} = \mu_0 A(r)^3 B(r)^{-1}, \tag{16}$$

with $\Omega = A(r)^{-4}$ the conformal factor relating the spacial part of the metric with the flat, Euclidean one[2]. The explicit radial dependence in the linear part of these effective quantities comes from the curved spacetime optical properties encoded in the diagonal terms $\sqrt{-g}g^{\alpha\alpha}/g_{00}$ (cf. eq.(11)) that we define as $\varepsilon_{\rm sp} = \mu_{\rm sp} = A(r)^3B(r)^{-1}$. The field dependency of $\tilde{\varepsilon}$ takes into account the non-linearity of the physical medium. Note also that dispersion implies that the dielectric permeability is a function of the physical frequency ω defined with respect to our stationary observer u^μ.

From eq. (13), and writing $D = \tilde{\varepsilon}_\ell E + P_{\rm NL}$, where $\tilde{\varepsilon}_\ell = \varepsilon_0\varepsilon_{\rm sp}(1+\chi^{(1)}(\omega))$ is the linear part of the dielectric permeability in eq. (15) and $P_{\rm NL}$ is the non-linear polarization, we can then obtain the wave equation, in frequency space,

$$\nabla^2 E - \nabla(\nabla\cdot E) + \tilde{\mu}\tilde{\varepsilon}_\ell\nu^2 E = -\tilde{\mu}\nu^2 P_{\rm NL} - (\nabla\log(\mu_{\rm sp}))\times(\nabla\times E)\,. \tag{17}$$

Here we indicate with ν the conjugate variable to the coordinate time t in the flat spacetime of the effective medium. Note that the homogeneous Maxwell equations imply that

$$\nabla\cdot E = -(\nabla\log\tilde{\varepsilon}_\ell)\cdot E - \frac{1}{\tilde{\varepsilon}_\ell}\nabla\cdot P_{\rm NL}, \tag{18}$$

and thus

$$\begin{aligned}-\nabla(\nabla\cdot E) = {} & (E\cdot\nabla)\nabla\log\tilde{\varepsilon}_\ell + ((\nabla\log\tilde{\varepsilon}_\ell)\cdot\nabla)\,E \\ & + (\nabla\log\tilde{\varepsilon}_\ell)\times(\nabla\times E) + \nabla\left(\frac{1}{\tilde{\varepsilon}_\ell}(\nabla\cdot P_{\rm NL})\right).\end{aligned} \tag{19}$$

Eq. (18) makes evident that $\nabla\cdot E$ is of the same order as the non-linearities and inhomogeneities in the electric permittivity, which is also why it is usually safely neglected in derivations of the NLSE.

The wave equation in eq. (17) is equivalent to Maxwell equations and, as such, presents the same level of complexity if analytical or numerical solutions are attempted. The NLSE is a scalar propagation equation for the electric field's slowly varying amplitude that allows one to numerically simulate the pulse propagation. We thus want to write the electric field as the product of a slowly varying amplitude times a phase propagating along the propagation direction, that we will identify with the z direction in the following. In this context, notice that the dispersion relation of the physical medium, in its rest frame, is given simply by $n(\omega) = c\kappa/\omega$, with κ the modulus of the spatial projection of the wave 4-vector. For the effective medium, this relation reads $\tilde{n} = c\tilde{\kappa}/\nu$, where $\tilde{n} = \sqrt{\varepsilon_{\rm sp}\mu_{\rm sp}}n$ is the product of the material refractive index and the "spacetime refractive index" $n_{\rm sp} = \sqrt{\varepsilon_{\rm sp}\mu_{\rm sp}}$. Moreover, since ν is the frequency defined with respect to Minkowski coordinate time, i.e., the conjugate Fourier variable to t, it is related to the physical frequency, i.e., the one measured by a physical observer in curved spacetime, by the gravitational redshift $\nu = \omega\sqrt{-g_{00}}$. From the equivalence of the dispersion relations, we see that $\tilde{\kappa}(r) = \kappa n_{\rm sp}(r)\sqrt{-g_{00}(r)}$. We will thus write $E(\mathbf{r},t) \propto \mathcal{E}(\mathbf{r})e^{i(\tilde{\kappa}_0 z-\nu_0 t)} + cc.$, with $\tilde{\kappa}_0 = \tilde{\kappa}(r,\nu_0)$ evaluated at a central frequency ν_0.

In order to proceed with the derivation of the NLSE, and to further simplify our equations, we consider two separate situations of physical interest: (i) pulse propagation at approximately constant radius; (ii) pulse propagating radially.

Horizontal motion at (almost) constant radius

We assume the propagation direction of the light pulse to be the z axis taken to be perpendicular to the radial direction for horizontal motion, and consider linearly polarized light propagating in a medium stationary on Earth for concreteness. Then, for propagation distances much smaller than Earth's radius ($r_\oplus$), i.e., $z \ll r_\oplus$, the horizontal motion can be considered as happening at constant radius. With these approximations, the spacetime permeability and permittivity are constant functions of $r_\oplus$, $\mu_{sp} = \varepsilon_{\rm sp} = A(r_\oplus)^3B(r_\oplus)^{-1}$ and also the physical frequency is not changing with z. Thus, we see that in eq. (17) the last term on the right-hand side vanishes.

We follow the derivation in [4] where the pulse propagation in a single-mode optical fiber was considered. Indeed, for $\mu_{sp}\,\varepsilon_{\rm sp}$ constant, eq. (17) is formally equivalent to eq. (S1) of [4] in frequency space. We thus end up with an effective one dimensional problem for the slowly varying envelope, and the derivation of the NLSE is the textbook one [10, 12]. In particular, recall that the slowly varying envelope approximation(s) (SVEA) consists in neglecting terms $\partial_z^2\mathcal{E} \ll \tilde{\kappa}_0\partial_z\mathcal{E}$ and $(\tilde{\kappa}_1/\tilde{\kappa}_0)\partial_t \ll 1$ on the basis that the envelope will contain many wavelengths and optical cycles. If we apply now the SVEA we end up with, in the time domain,

$$i(\partial_z + \tilde{\kappa}_1\partial_t)\mathcal{E} - \frac{\tilde{\kappa}_2}{2}\partial_t^2\mathcal{E} = -n_2\nu_0 n_{\rm sp}(r_\oplus)\varepsilon_0\frac{|\mathcal{E}|^2}{\Omega}\mathcal{E}, \tag{20}$$

where $\tilde{\kappa}_i(\nu_0)$ are the coefficients of the power series expansion $\tilde{\kappa}(\nu) = \sum_n \tilde{\kappa}_n(\nu_0)/n!\,(\nu-\nu_0)^n$ in $\nu-\nu_0$ and we are considering Kerr non-linear media for which the nonlinear index is $n_2 = 3\chi^{(3)}/(2n(\omega_0)c\varepsilon_0)$.

Considering an anomalous dispersive material, i.e., $\kappa_2(\nu_0) < 0$, an analytical solution of the NLSE can be found (see, e.g., [4]) and reads

$$\mathcal{E}(t,z) = \sqrt{\frac{\Omega|\tilde{\kappa}_2|}{\nu_0 n_2 n_{\rm sp}\varepsilon_0 T_0^2}}\cosh\left(\frac{t-\tilde{\kappa}_1 z}{T_0}\right)^{-1}\exp\left(\frac{iz|\tilde{\kappa}_2|}{2T_0^2}\right), \tag{21}$$

[2] This conformal factor arises due to the fact that E^aE_a in curved spacetime corresponds to $|E|^2/\Omega$ with $|E|^2 = E^aE^b\delta_{ab}$ the flat spacetime norm squared of the electric strength field.

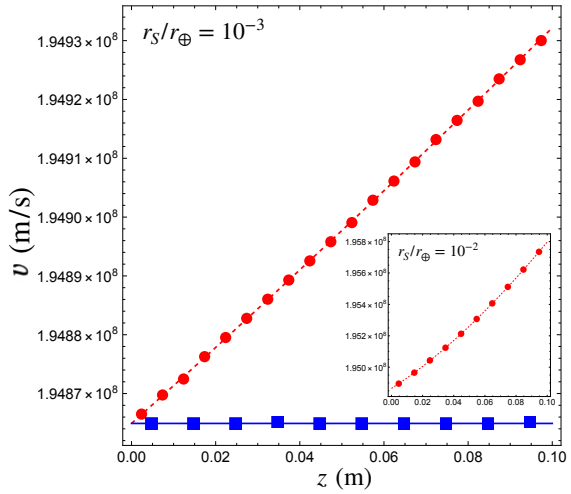

FIG. 1: Velocity of the soliton along the fiber, with respect to an observer comoving with the segment of the dielectric material where the (peak of the) soliton is located, for $L = 0.1$ m, $r_s = 10^{-3} r_\oplus$, and including photoelasticity. The red, dashed and blue, solid curves represent the analytical expression in eq. (25) including or in the absence, respectively, of photoelasticity. The red points and blue squares are obtained by numerical simulations and agrees perfectly with the analytical formula of eq. (25). The inset shows the case with photoelasticity in which $r_s = 10^{-2} r_\oplus$. This shows a deviation from a purely linear relation between the velocity and the propagation distance.

where T_0 is the pulse length, and $1/\tilde{\kappa}_1$ is its speed of propagation. This reduces to the result from Philbin et al.[4] – eq.(S74) of the supplementary material in [4] – in the limit of $r_S \to 0$. From this expression, combined with the fact that $\tilde{\kappa}_1(\nu_0) = n_{\rm sp}\kappa_1(\omega_0)$, we can conclude that the velocity of the horizontally propagating soliton in curved spacetime with respect to an observer comoving with the segment of the dielectric material[3] is given simply by $\kappa_1(\omega_0)^{-1}$.

Radial motion

Let us now consider the case in which the light pulse propagates radially along the z direction. Care is in order here, since now all the quantities appearing in the wave equation will change along the propagation direction, including the physical frequency that will be subject to gravitational redshift. Motivated by the symmetry of the problem, and in order to obtain a scalar, one-dimensional equation whose solution can be simulated, we assume that all the quantities entering the wave equation depend solely on z. This is tantamount to identifying the radial direction with the z-axis and work close to $x = y = 0$ so that $r = r_\oplus + z$, which is a reasonable assumption since we are considering the vertical propagation of a well localized pulse. With this approximation, the wave equations (17) reduce to a system of three decoupled equations [13]

$$\partial_z^2 E_{x(y)} + \tilde{\mu}\tilde{\varepsilon}_\ell \nu^2 E_{x(y)} = -\tilde{\mu}\nu^2 P_{{\rm NL},x(y)} + (\partial_z(\ln\tilde{\mu}))\,\partial_z E_{x(y)} \tag{22}$$

$$\partial_z^2 E_z + \tilde{\mu}\tilde{\varepsilon}_\ell \nu^2 E_z = -\tilde{\mu}\nu^2 P_{{\rm NL},z} - \partial_z\left(\frac{1}{\tilde{\varepsilon}_\ell}\partial_z P_{{\rm NL},z}\right) - 2(\partial_z \ln\tilde{\varepsilon}_\ell)\partial_z E_z - E_z\partial_z^2 \ln\tilde{\varepsilon}_\ell \tag{23}$$

It is immediate to realize that $E_z = 0$ is a solution of the corresponding equation so that we can consider the propagation of linearly polarized light (in a direction orthogonal to z) and we end up with a single equation of the form of eq. (22).

Proceeding as before with substituting the ansatz $E(z,t) \propto \mathcal{E}(z,t)e^{i(\tilde{\kappa}_0(z)z-\nu_0 t)} + cc.$, expanding $\tilde{\kappa}(z,\nu)$ around ν_0, and using the SVEA approximation(s) we obtain the NLSE given by

$$i(\partial_z + \tilde{\kappa}_1\partial_t)\mathcal{E} - \frac{\tilde{\kappa}_2}{2}\partial_t^2\mathcal{E} + 2i\frac{\partial_z\tilde{\kappa}_0}{2\tilde{\kappa}_0}\mathcal{E} + 2iz\frac{\partial_z\tilde{\kappa}_0}{2\tilde{\kappa}_0}\partial_z\mathcal{E} + iz\frac{\partial_z^2\tilde{\kappa}_0}{2\tilde{\kappa}_0}\mathcal{E} - z\partial_z\tilde{\kappa}_0\mathcal{E} - z^2\frac{(\partial_z\tilde{\kappa}_0)^2}{2\tilde{\kappa}_0}\mathcal{E} = -n_2\nu_0 n_{\rm sp}(r)\varepsilon_0|\mathcal{E}|^2\mathcal{E}/\Omega + \frac{\partial_z \ln n_{\rm sp}}{2\tilde{\kappa}_0}(i\tilde{\kappa}_0\mathcal{E} + \partial_z\mathcal{E} + iz(\partial_z\tilde{\kappa}_0)\mathcal{E})\,. \tag{24}$$

Eq. (24) contains several additional terms with respect to the equation for the horizontal propagation due to the fact that now the wavevector $\tilde{\kappa}_0$ depends explicitly on the coordinate along the propagation direction and so does the refractive index, i.e., we are propagating in a gradient-index medium (GRIN)[4]. All geometrical quantities appearing in the equation are evaluated at $r_\oplus + z$. Finally, consistently with the horizontal propagation case, upon setting $\tilde{\kappa}_0$ constant, we return to eq. (20).

INCLUDING PHOTOELASTICITY

Up until now, we have considered rigid dielectrics, i.e., dielectric media in which the speed of sound is infinite. For

[3] Indeed note that proper length and proper time for an observer comoving with the segment of the dielectric material and in connection with coordinate quantities are given by $\ell = A^2 z$ and $\tau = t\,B/A$ so that $v \equiv \ell/\tau = A^3 B^{-1} z/t = n_{\rm sp}\tilde{v}$.

[4] See also [14–16] for early studies of soliton propagation in inhomogeneous media.

realistic materials, this is of course never the case and the dielectric gets deformed by the action of forces, including the tidal ones in our set-up. Let us consider an optical fiber as a paradigmatic example. In this case, the deformation due to the action of gravity will be relevant only for the case of vertical propagation.

Deformations of a dielectric lead to a change in the relative permeability of the material, and thus of the refractive index, a phenomenon known as photoelasticity [17]. The contributions to this effect coming from the curvature of spacetime and the inertial acceleration of the fiber can be separately accounted for following the discussion in [18]. Consider a fiber of length L hanging from at support located at $r_\oplus + L$. As far as the strain is within the elastic limit of the material, we can relate it with the stresses through a linear relation, i.e., Hooke's law. Thus, we write the strain tensor as $\mathcal{S}_{kl} = \frac{1}{Y}\sigma_{kl}$, where Y is the Young's modulus of the material and $\sigma_{kl} = \frac{F_k}{A_l}$ is the stress tensor given by the ratio between the force F_k in direction $\hat{e}_k$ and the cross-sectional area A_l normal to $\hat{e}_l$ upon which the force acts. The photoelastic (or acousto-optic) effect consists in the change of the relative electric permeability by $\Delta(\varepsilon_r)^{-1}_{kl} = \mathcal{P}_{klmn}\mathcal{S}_{mn}$, where $\mathcal{P}$ is the photoelastic tensor. In the following, we limit ourselves to the case of isotropic materials and a diagonal stress tensor (see [10] for the details of the computation). It should be noted that photoelasticity is far from negligible in the case under investigation and becomes the dominant effect in the vertical propagation scenario, overwhelming the effect related to the optical properties of the background spacetime.

While photoelasticity introduces a further radial dependence in the optical properties of the effective medium, this does not affect the form of eq. (24), which remains valid. The only difference is in the expressions for the quantities $\tilde{\kappa}_i$ and their derivatives, due to the fact that now the refractive index of the medium is given by $n(\omega) = \sqrt{1 + \chi_1(\omega) + \Delta\varepsilon_r(\omega)}$ [10].

NUMERICAL RESULTS

While the wave equation in eq. (17) gives us the full Maxwell equations, including possibly interesting effects related to the vectorial nature of the electric field, and thus to the interplay between gravity and the light polarization, its numerical investigation is beyond the scope of the current work, and it is left for future investigations. Here, we focus on the propagation of light pulses as described by the simplified eq.(24), motivated by light propagation in optical fibers [4]. Note that in the case of eq. (20) an analytical solution was presented in eq. (21).

Equation (24) for the vertical propagation is solved numerically – being a non-linear PDE with coordinate dependent coefficients – using the split-step Fourier (SSF) method [11] and taking into account also the effect of the fiber deformation. For this purpose, we utilize the same fiber parameters as in [4] (see also table I in [10]) and initialize the temporal profile at

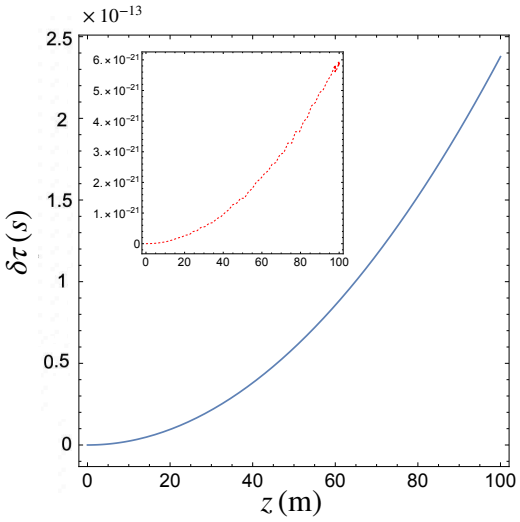

FIG. 2: Time of arrival of the soliton for the case of propagation in the gravitational field of Earth for which we assume $r_S = 9 \times 10^{-3}$ m. The main figure shows the difference in time of arrival, with respect to an observer comoving with the segment of the dielectric material where the soliton is located, between vertically and horizontally propagating solitons over the propagation coordinate length z. The inset shows the same in the case photoelasticity is neglected.

$z = 0$ as the one of the input pulse in the same reference.

The intuition based on the SSF method– where the propagation equation (24) is rewritten in the form $\partial_z\mathcal{E} = \left(\hat{D} + \hat{N}\right)\mathcal{E}$ with the diffusive dynamics enclosed in the operator $\hat{D} = \hat{D}(z, \partial_t)$ [10] – allows us to formulate the educated guess that the propagation speed of the soliton, in the effective flat spacetime, is given by

$$\tilde{v} = \frac{1 + z\,\tilde{\kappa}_0'(z)/\tilde{\kappa}_0(z)}{\tilde{\kappa}_1(z)}. \tag{25}$$

Indeed, this appears as (the real part of) the inverse of the coefficient of the time derivative in $\hat{D}(z, \partial_t)$. Then, in order to translate this result into the speed measured by an observer comoving with the segment of the dielectric material where the soliton peak is located, we need to just multiply eq. (25) by the spacetime refractive index. That this intuition is indeed correct is verified by the numerical simulations reported in Fig. 1. We see that the z-dependence of the propagation velocity is strongly enhanced by the effects of mechanical deformation of the fiber with respect to the case in which photoelasticity is ignored. The z-dependence of the vertical propagation velocity without photoelasticity is weak, and the velocity is close to the one of the horizontal case. To quantify the latter statement, in Fig. 2 we show the difference in the (proper) time of arrival of the soliton for the case of propagation in the gravitational field of Earth, corresponding to a Schwarzschild radius that

we take as $r_S = 9 \times 10^{-3}$ m. The main figure shows

$$\delta\tau = |z(\sqrt{-g_{00}(r_\oplus + z)}\tilde{v}_\uparrow^{-1}) - \sqrt{-g_{00}(r_\oplus)}\tilde{v}_\rightarrow^{-1})|, \qquad (26)$$

with $\tilde{v}_\uparrow$ and $\tilde{v}_\rightarrow$ the propagation velocities, in the effective flat spacetime, for vertical and horizontal propagation. The inset shows instead the case in which for the vertical propagation the photoelasticity is neglected, showing a much weaker dependence.

Finally, in Fig. 3 we show the deviation of the average velocity along the vertical direction $v_{av}(r_S)$ with respect to the constant velocity at $r_S = 0$ as a function of the dimensionless ratio $r_S/r_\oplus$. The average velocity is obtained numerically from the simulations as the ratio of the total length L and the propagation time of the soliton and transformed into the frame of the observer comoving with the fiber at its upper end-point – i.e., multiplied by $n_{sp}(r_\oplus + L)$. Analytically, we use $v_{av} = (\int_0^L v\,dz)/L$ with $v = n_{sp}\tilde{v}$ and $\tilde{v}$ given in eq. (25). Fig. 3 shows once again the agreement between the simulated data and our analytical ansatz and it also shows that the photoelasticity is the main effect that allows one to have a sizable difference between the flat and curved spacetime propagation.

Another quantity characterizing the propagating pulse is its temporal width. In the horizontal propagation case, the duration of the pulse is constant. The same is not, in general, true when considering the vertical propagation. In the Supplemental Material [10], we report the evolution of the temporal width along the fiber. In particular, our simulations show a focusing of the pulse which is however sizable only in the presence of photoelasticity.

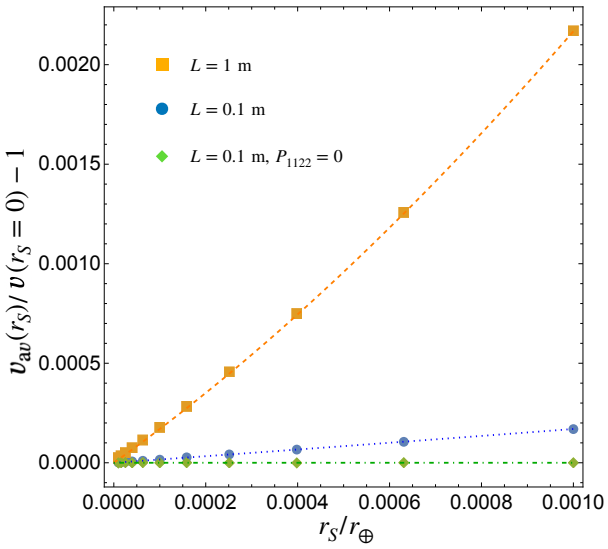

FIG. 3: Change in average velocity (v_{av}) of the soliton in the fiber – with respect to the observer comoving with the dielectric – compared to the case with $r_S = 0$. Orange, square points corresponds to the case of a $L = 1$ m propagation with photoelasticity. Blue, round points correspond to the case of a $L = 0.1$ m propagation with photoelasticity. Green, diamonds correspond to the case of a $L = 0.1$ m propagation without photoelasticity. The lines correspond to the analytical result that fits perfectly the different sets of data.

CONCLUSIONS

We have considered the propagation of light pulses in nonlinear, non-magnetic media stationary in curved spacetime. Taking some intuition from the seminal work of Plebanski [8], we showed that light propagation in such media can be equivalently described as the propagation in an effective medium in flat spacetime whose electric and magnetic properties acquire a multiplicative factor encoding the spacetime structure. Having done that, eq. (17) describes the propagation of light in the effective medium. It is interesting to note, even though we did not investigate it in this work, that the vectorial nature of this equation encodes the interplay between the light polarization and the gravitational field. Such interplay should be expected on the basis of the fact that the effective medium is an inhomogeneous, gradient-index medium for which it is well known that the propagation of light is influenced by its own polarization [19–21]. Furthermore, the effect of polarization on the propagation of light in curved, vacuum spacetime has been extensively considered in the literature and shown to take place also for static spacetimes [22, 23].

Neglecting the aforementioned effects, which would be undoubtedly small, by virtue of approximations we have been able to derive a scalar NLSE describing the propagation of a light pulse. It is important to notice that, when solving the NLSE employing the SSF method, we are implicitly considering a unidirectional equation and ignoring any possible back-propagating field in the boundary conditions imposed, for all times, at $z = 0$. This means that backscattered light from the pulse is assumed negligible relative to the pulse itself, a condition common to all unidirectional envelope propagation equations [24]. While this is not a problem for the horizontal propagation, in which case only the weak non-linearity could give rise to back-reflection, in the case of the vertical propagation light is effectively propagating in a gradient-index medium with the refracting index slowly varying in the propagation direction. This by itself can give rise to back-propagating fields, and effectively limits the validity of our treatment to regimes in which the photoelasticity allows to employ a unidirectional equation. Luckily, the regime of validity of the equation – which depends on the parameter chosen for the physical medium – can be readily estimated by following the discussion in [25] as we detail in [10].

Given these caveats, the NLSE that we have derived shows that an optical pulse propagating radially in a Kerr non-liner medium stationary in Schwarzschild spacetime experiences a change in its propagation velocity captured by eq. (25). This effect is mostly due to photoelasticity which overwhelms the purely spatiotemporal effects encoded in n_{sp}. The difference in propagation velocity between the vertically and horizon-

tally propagating pulses results, in turn, in a difference of the time of arrival of two pulses of the order of hundreds of femtoseconds in Earth gravitational field, a fact that puts this difference in the reach of current technologies (see [26–28] and references therein).

ACKNOWLEDGEMENTS

The authors thank Francesco Marino for interesting discussions. A. Belenchia and D. Braun acknowledge support from the Deutsche Forschungsgemeinschaft (DFG, German Research Foundation) project number BR 5221/4-1. D. Rätzel acknowledges funding by the Federal Ministry of Education and Research of Germany in the project "Open6GHub" (grant number: 16KISK016) and support through the Deutsche Forschungsgemeinschaft (DFG, German Research Foundation) under Germany's Excellence Strategy – EXC-2123 QuantumFrontiers – 390837967, the Research Training Group 1620 "Models of Gravity" and the TerraQ initiative from the Deutsche Forschungsgemeinschaft (DFG, German Research Foundation) – Project-ID 434617780 – SFB 1464.

[1] U. Leonhardt and T. G. Philbin, Transformation optics and the geometry of light, in *Progress in optics*, Vol. 53 (Elsevier, 2009) pp. 69–152.
[2] W. Gordon, Zur lichtfortpflanzung nach der relativitätstheorie, Annalen der Physik **377**, 421 (1923).
[3] C. Barceló, S. Liberati, and M. Visser, Analogue gravity, Living reviews in relativity **14**, 1 (2011).
[4] T. G. Philbin, C. Kuklewicz, S. Robertson, S. Hill, F. Konig, and U. Leonhardt, Fiber-optical analog of the event horizon, Science **319**, 1367 (2008).
[5] E. Rubino, F. Belgiorno, S. Cacciatori, M. Clerici, V. Gorini, G. Ortenzi, L. Rizzi, V. Sala, M. Kolesik, and D. Faccio, Experimental evidence of analogue hawking radiation from ultrashort laser pulse filaments, New Journal of Physics **13**, 085005 (2011).
[6] J. Bicak and P. Hadrava, General-relativistic radiative transfer theory in refractive and dispersive media., AAP **44**, 389 (1975).
[7] V. Perlick, *Ray optics, Fermat's principle, and applications to general relativity*, Vol. 61 (Springer Science & Business Media, 2000).
[8] J. Plebanski, Electromagnetic waves in gravitational fields, Physical Review **118**, 1396 (1960).
[9] F. de Felice, On the gravitational field acting as an optical medium, General Relativity and Gravitation **2**, 347 (1971).
[10] Supplementary Material available from [URL will be inserted by publisher].
[11] G. P. Agrawal, Nonlinear fiber optics, in *Nonlinear Science at the Dawn of the 21st Century* (Springer, 2000) pp. 195–211.
[12] R. W. Boyd, *Nonlinear optics* (Academic press, 2020).
[13] S. Habib Mazharimousavi, A. Roozbeh, and M. Halilsoy, Electromagnetic wave propagation through inhomogeneous material layers, Journal of Electromagnetic Waves and Applications **27**, 2065 (2013).
[14] H.-H. Chen and C.-S. Liu, Solitons in nonuniform media, Phys. Rev. Lett. **37**, 693 (1976).
[15] H. Chen and C.-S. Liu, Nonlinear wave and soliton propagation in media with arbitrary inhomogeneities, The Physics of Fluids **21**, 377 (1978).
[16] J. Herrera, Envelope solitons in inhomogeneous media, Journal of Physics A: Mathematical and General **17**, 95 (1984).
[17] C.-L. Chen, *Foundations for guided-wave optics* (John Wiley & Sons, 2006).
[18] D. Rätzel, F. Schneiter, D. Braun, T. Bravo, R. Howl, M. P. Lock, and I. Fuentes, Frequency spectrum of an optical resonator in a curved spacetime, New Journal of Physics **20**, 053046 (2018).
[19] K. Y. Bliokh, Geometrodynamics of polarized light: Berry phase and spin hall effect in a gradient-index medium, Journal of Optics A: Pure and Applied Optics **11**, 094009 (2009).
[20] V. Liberman and B. Y. Zel'dovich, Spin-orbit interaction of a photon in an inhomogeneous medium, Physical Review A **46**, 5199 (1992).
[21] K. Y. Bliokh, F. J. Rodríguez-Fortuño, F. Nori, and A. V. Zayats, Spin–orbit interactions of light, Nature Photonics **9**, 796 (2015).
[22] P. Gosselin, A. Bérard, and H. Mohrbach, Spin hall effect of photons in a static gravitational field, Physical Review D **75**, 084035 (2007).
[23] M. A. Oancea, J. Joudioux, I. Dodin, D. Ruiz, C. F. Paganini, and L. Andersson, Gravitational spin hall effect of light, Physical Review D **102**, 024075 (2020).
[24] M. Kolesik, J. V. Moloney, and M. Mlejnek, Unidirectional optical pulse propagation equation, Phys. Rev. Lett. **89**, 283902 (2002).
[25] P. Kinsler, Optical pulse propagation with minimal approximations, Phys. Rev. A **81**, 013819 (2010).
[26] J. Lee, Y.-J. Kim, K. Lee, S. Lee, and S.-W. Kim, Time-of-flight measurement with femtosecond light pulses, Nature photonics **4**, 716 (2010).
[27] T. Fortier and E. Baumann, 20 years of developments in optical frequency comb technology and applications, Communications Physics **2**, 1 (2019).
[28] E. D. Caldwell, L. C. Sinclair, N. R. Newbury, and J.-D. Deschenes, The time-programmable frequency comb and its use in quantum-limited ranging, Nature **610**, 667 (2022).
[29] P. Kabaciński, T. M. Kardaś, Y. Stepanenko, and C. Radzewicz, Nonlinear refractive index measurement by SPM-induced phase regression, Optics express **27**, 11018 (2019).
[30] D. K. Biegelsen, Photoelastic tensor of silicon and the volume dependence of the average gap, Physical Review Letters **32**, 1196 (1974).
[31] W. Primak and D. Post, Photoelastic constants of vitreous silica and its elastic coefficient of refractive index, Journal of Applied Physics **30**, 779 (1959).
[32] Heraeus Holding, Properties of fused silica (2022).
[33] F. Spengler, A. Belenchia, D. Rätzel, and D. Braun, Influence of cosmological expansion in local experiments, Classical and Quantum Gravity **39**, 055005 (2022).
[34] C. W. Misner, K. Thorne, J. Wheeler, and S. Chandrasekhar, Gravitation, Physics Today **27**, 47 (1974).
[35] E. Williams, Listening to the seafloor with optical fibers, Physics Today **75**, 70 (2022).
[36] R. Kitamura, L. Pilon, and M. Jonasz, Optical constants of silica glass from extreme ultraviolet to far infrared at near room temperature, Applied optics **46**, 8118 (2007).

Supplemental Material: Optical solitons in curved spacetime

Felix Spengler[1], Alessio Belenchia[1,2], Dennis Rätzel[3], Daniel Braun[1]

[1]*Institut für Theoretische Physik, Eberhard-Karls-Universität Tübingen, 72076 Tübingen, Germany*
[2]*Centre for Theoretical Atomic, Molecular, and Optical Physics, School of Mathematics and Physics, Queen's University, Belfast BT7 1NN, United Kingdom*
[3]*Humboldt Universität zu Berlin, Institut für Physik, Newtonstraße 15, 12489 Berlin, Germany*

In this supplemental material, we collect the detailed derivations of the results in the main text.

VACUUM SPACETIME AS AN OPTICAL MEDIUM & THE *EFFECTIVE MEDIUM* DESCRIPTION

Thanks to the seminal work of Plebanski in the '60s [8], it is well known that electromagnetism in curved spacetime is equivalent to propagation in an optical medium. Following the derivation presented in [9], Maxwell vacuum equations in curved spacetime are written as

$$\nabla_k F^{*ik} = 0 \tag{S1}$$
$$\nabla_k F^{ik} = 0, \tag{S2}$$

where F^* is the Hodge dual of the e.m. tensor, Latin indices run from 0 to 3, and the metric g_{ij} has mostly plus signature. As in the main text, we consider the case with no currents.

Choosing an observer field u^i, the electric and magnetic field strength can be defined with respect to it as

$$H^i = F^{*ij}u_j, \;\; E_i = F_{ij}u^j \tag{S3}$$
$$F_{ij} = \eta_{ijkl}u^l H^k + 2u_{[i}E_{j]}, \tag{S4}$$

where here $\eta_{ijkl} = \sqrt{-g}\delta_{ijkl}$ is the Levi-Civita tensor (with δ_{ijkl} the Levi-Civita alternating symbol in four dimensions) and $T_{[abc\dots]}$ denotes the antisymmetrization of the tensor with respect to the indices in square brackets. The Maxwell equations can then be projected in the u^i direction or orthogonal to it using the projection operator into the rest frame of u^i, $h_{ij} = g_{ij} + u_i u_j$. The end result is, in the case the observer field is chosen as $u^i = \delta^i_0/\sqrt{-g_{00}}$

$$\delta^{\alpha\beta\gamma}\partial_\beta \mathcal{H}_\gamma - \partial_0 \mathcal{D}^\alpha = 0; \;\; \partial_l \mathcal{D}^l = 0 \tag{S5}$$
$$\delta^{\alpha\beta\gamma}\partial_\beta \mathcal{E}_\gamma + \partial_0 \mathcal{B}^\alpha = 0; \;\; \partial_l \mathcal{B}^l = 0, \tag{S6}$$

where the first two equations come from Maxwell equations (S2) (with $\delta^{\alpha\beta\gamma}$ the Levi-Civita alternating symbol in three dimensions) while the second two from eq. (S1). Here, $\mathcal{H}_\alpha = \sqrt{-g_{00}}H_\alpha$, $\mathcal{E}_\alpha = \sqrt{-g_{00}}E_\alpha$, Greeks indices run from 1 to 3, and

$$\mathcal{D}^\alpha = -\sqrt{-g}\frac{g^{\alpha\beta}}{g_{00}}\mathcal{E}_\beta - \delta^{\alpha\beta\gamma}\frac{g_{0\gamma}}{g_{00}}\mathcal{H}_\beta \tag{S7}$$
$$\mathcal{B}^\alpha = -\sqrt{-g}\frac{g^{\alpha\beta}}{g_{00}}\mathcal{H}_\beta + \delta^{\alpha\beta\gamma}\frac{g_{0\gamma}}{g_{00}}\mathcal{E}_\beta. \tag{S8}$$

From here one can see that these equations are actually equivalent to Maxwell equations in flat spacetime in the presence of an optical medium whose constitutive relations are characterized by a dielectric ($\varepsilon^{\alpha\beta}_{\rm sp}$) and magnetic permeability ($\mu^{\alpha\beta}_{\rm sp}$) given by

$$\mu^{\alpha\beta}_{\rm sp} = \varepsilon^{\alpha\beta}_{\rm sp} = -\sqrt{-g}\frac{g^{\alpha\beta}}{g_{00}}. \tag{S9}$$

As shown in the main text, when a physical optical medium whose rest frame is characterized by u^i is added, we can follow the same derivation starting from Maxwell's equations in curved spacetime and with a material medium

$$\nabla_k F^{*ij} = 0 \tag{S10}$$
$$\nabla^k G_{ik} = 0, \tag{S11}$$

where now G and F are related by the material constitutive equations. Then we have

$$B_a = -\frac{1}{2}\eta_{abcd}u^b F^{cd};\ E_i = F_{ij}u^j \tag{S12}$$

$$H_a = -\frac{1}{2}\eta_{abcd}u^b G^{cd};\ D_i = G_{ij}u^j \tag{S13}$$

$$F_{ab} = -\eta^{cd}_{ab}u_d B_c + 2u_{[a}E_{b]} \tag{S14}$$

$$G_{ab} = -\eta^{cd}_{ab}u_d H_c + 2u_{[a}D_{b]}, \tag{S15}$$

where we have introduced the electric and magnetic excitation, D_a and H_a respectively, on top of the electric and magnetic strength E_a and B_a.

Note that the definitions of E, B, F are equivalent to the vacuum case, since the homogeneous Maxwell equations are the same. The inhomogeneous equations have also the same form as in the vacuum case, but with the substitution of E, B, F with D, H, G, where the definition of G with respect to H, D is the same as F with respect to E, B. From this simple observation we can immediately deduce that the projection of Maxwell equations in 3-dimensional form will, in the case the observer field is chosen as $u^i = \delta^i_0/\sqrt{-g_{00}}$, lead to

$$\delta^{\alpha\beta\gamma}\partial_\beta \mathcal{H}_\gamma - \partial_0 \mathcal{D}^\alpha = 0;\ \partial_l \mathcal{D}^l = 0 \tag{S16}$$

$$\delta^{\alpha\beta\gamma}\partial_\beta \mathcal{E}_\gamma + \partial_0 \mathcal{B}^\alpha = 0;\ \partial_l \mathcal{B}^l = 0, \tag{S17}$$

where $\mathcal{E}_\alpha = \sqrt{-g_{00}}E_\alpha$, $\mathcal{H}_\alpha = \sqrt{-g_{00}}H_\alpha$, and

$$\mathcal{D}^\alpha = -\sqrt{-g}\frac{g^{\alpha\beta}}{g_{00}}\mathfrak{D}_\beta - \delta^{\alpha\beta\gamma}\frac{g_{0\gamma}}{g_{00}}\mathcal{H}_\beta \tag{S18}$$

$$\mathcal{B}^\alpha = -\sqrt{-g}\frac{g^{\alpha\beta}}{g_{00}}\mathfrak{B}_\beta + \delta^{\alpha\beta\gamma}\frac{g_{0\gamma}}{g_{00}}\mathcal{E}_\beta, \tag{S19}$$

with $\mathfrak{B}_\alpha = \sqrt{-g_{00}}B_\alpha$, and $\mathfrak{D}_\alpha = \sqrt{-g_{00}}D_\alpha$. Once again, these equations are equivalent to Maxwell's equations in flat spacetime in the presence of an effective optical medium.

Consider the case of a linear, dispersionless medium. We can then write $G^{ij} = \frac{1}{2}\chi^{ijkl}F_{kl}$, with the material's constitutive tensor χ^{ijkl}, containing all material properties, which is symmetric under the exchange of the first and second pair of indices and antisymmetric with respect to the swap within an index pair. In particular, we can also write $D_a = \varepsilon^b_a E_b$, and $B_a = \mu^b_a H_b$, which are the constitutive relations in the reference frame of the observer in which the medium is at rest, neglecting magneto-electric effects. For an isotropic medium, we also have that the dielectric and permeability tensor assume the simplified form $\varepsilon^b_a = \varepsilon(\delta^b_a + U^b U_a)$ and $\mu^b_a = \mu(\delta^b_a + U^b U_a)$ for some scalar, positive functions ε and μ. The effective optical medium is such that its constitutive relations are then characterized by a dielectric and inverse magnetic permeability given by

$$\tilde{\varepsilon}^{\alpha\beta} = -\sqrt{-g}\frac{g^{\alpha\gamma}}{g_{00}}\varepsilon^\beta_\gamma, \tag{S20}$$

$$\tilde{\mu}^{\alpha\beta} = -\sqrt{-g}\frac{g^{\alpha\gamma}}{g_{00}}\mu^\beta_\gamma, \tag{S21}$$

while the antisymmetric parts of the constitutive tensor are completely characterized by the vacuum spacetime properties[5].

Non-linear media, with a Kerr-type non-linearity, can be treated analogously by promoting the dielectric and permeability tensors to explicitly depend on the field strengths. If also dispersion needs to be included in the game, we need to consider, as usual, the dispersion relation in frequency space in order to write it in a local form. Note that we can always write $D = \varepsilon_0 E + P$ (and analogously for the magnetic field and excitation), moving all non-linearity and dispersion in the polarization (magnetization) vector. Thus, from eq. (9) we can conclude that the effective medium will give rise to an effective electric excitation

$$D_{eff} = \varepsilon_{\rm sp}(\varepsilon_0 E + P), \tag{S22}$$

which can then be written, for the dispersive case of interest, locally in frequency space for the effective medium "living" in flat, Minkowski spacetime.

---

[5] More in general, one could also include in this description materials for which the magnetoelectric entries of the constitutive tensor are not negligible. In such a case, $D_a = \varepsilon^b_a E_b + \gamma^b_a H_b$, and $B_a = \mu^b_a H_b - \gamma^b_a E_b$ with γ_{ab} the antisymmetric part of the constitutive tensor. In this case, the same derivation still stands, with the only difference that the antisymmetric parts of the constitutive tensor for the effective medium are given by

$$\tilde{\gamma}^{\alpha\beta} = -\delta^{\alpha\beta\gamma}\frac{g_{0\gamma}}{g_{00}} - \sqrt{-g}\frac{g^{\alpha\delta}}{g_{00}}\gamma^\beta_\delta.$$

DERIVATION OF THE NLSE: TECHNICAL DETAILS

Let us consider now Maxwell's equations for the effective medium, thus in flat spacetime, written in the usual notation

$$\nabla \cdot B = 0,\ \nabla \cdot D = 0 \tag{S23}$$

$$\nabla \times E = -\partial_t B,\ \nabla \times H = \partial_t D, \tag{S24}$$

with $D = \tilde{\varepsilon} E$ and $H = B/\tilde{\mu}$. Here, we consider the case of a spherically symmetric spacetime in isotropic coordinates. The metric can then be written, in full generality, as

$$ds^2 = -\left(\frac{B(t,r)}{A(t,r)}\right)^2 dt^2 + a^2(t) A^4(t,r) \delta_{\alpha\beta} dx^\alpha dx^\beta, \tag{S25}$$

with $r = \sqrt{\delta_{\alpha\beta} x^\alpha x^\beta}$, $A(t,r), B(t,r)$ real functions, and $a(t)$ a scale factor analogous to the one appearing in FRLW spacetime. Note that this metric can be rewritten as

$$ds^2 = \Omega^{-1} \left(-\frac{B^2(t,r)}{a^2(t) A^6(t,r)} dt^2 + \delta_{\alpha\beta} dx^\alpha dx^\beta \right), \tag{S26}$$

where the "conformal factor" $\Omega = a(t)^{-2} A(t,r)^{-4}$.

In particular, we specialize to the case for which $a(t) = 1$, $A = A(r)$, $B = B(r)$ and such that, in frequency space, $\tilde{\varepsilon}(E, r, \omega) = \varepsilon_0 A(r)^3 B(r)^{-1} \left(1 + \chi^{(1)}(\omega) + 3\chi^{(3)} |E|^2/\Omega\right)$ and $\tilde{\mu} = \tilde{\mu}(r) = \mu_0 \mu_{\rm sp} = \mu_0 A(r)^3 B(r)^{-1}$, i.e., we are considering a non-magnetic material, where all the magnetic properties are induced by the curved background, with a Kerr non-linearity. As we previously discussed, ω is the physical frequency defined with respect to the stationary observer u^μ that we assume to be the rest frame of the physical medium. The conformal factor Ω appearing in the non-linear term in $\tilde{\varepsilon}$ arises due to the fact that $E^a E_a$ in curved spacetime corresponds to $|E|^2/\Omega$, with $|E|^2 = E^a E^b \delta_{ab}$ the flat spacetime norm squared of the electric strength, in the flat spacetime of the effective medium, as can be easily seen directly from eq. (S26).

For the sake of notation clarity, let us emphasized that, in the following, tilded quantities refer to quantities pertaining to the effective medium in flat spacetime while the untilded ones represent the optical properties of the physical medium that is stationary in (physical) curved spacetime.

In the following, we focus on Schwarzschild's spacetime, for which

$$A(r) = 1 + \frac{r_S}{4r} \tag{S27}$$

$$B(r) = 1 - \frac{r_S}{4r}, \tag{S28}$$

where r_S is the Schwarzschild's radius.

From Maxwell's equations, taking the curl of the third one, we obtain

$$\nabla^2 E - \nabla (\nabla \cdot E) = \partial_t \left(\tilde{\mu} \partial_t D - B \times \frac{\nabla \tilde{\mu}}{\tilde{\mu}} \right). \tag{S29}$$

and thus

$$\nabla^2 E - \nabla(\nabla \cdot E) - \tilde{\mu} \partial_t^2 D = -(\nabla \log(\mu_{\rm sp})) \times (\nabla \times E). \tag{S30}$$

Note that this last expression is valid for $\partial_t \tilde{\mu} = 0$, which includes the case of Schwarzschild spacetime. For a generic spherically symmetric metric, as in eq. (S26), additional terms would be present due to the explicit time dependence of $\tilde{\mu}$. Moving now to frequency space, where we indicate with ν the conjugate variable to the coordinate time t in the flat spacetime of the effective medium, and writing $D = \tilde{\varepsilon}_\ell E + P_{\rm NL}$, where $\tilde{\varepsilon}_\ell$ is the linear part of the dielectric permeability and $P_{\rm NL}$ contains the nonlinear components of the polarization, we obtain

$$\nabla^2 E - \nabla(\nabla \cdot E) + \tilde{\mu} \tilde{\varepsilon}_\ell \nu^2 E = -\tilde{\mu} \nu^2 P_{\rm NL} - (\nabla \log(\mu_{\rm sp})) \times (\nabla \times E). \tag{S31}$$

This is our starting point for the derivation of the scalar NLSE. Note that, apart from the last term, the equation resembles the textbook wave equation modulo the inhomogeneity of the medium encoded in the coordinate dependence of $\tilde{\varepsilon}, \tilde{\mu}$ [12].

Before starting the derivation of the NLSE, an observation is in order. In curved spacetime, the linear dispersion relation of the medium assumes the simple form, in the rest frame of the medium,

$$n(\omega) = c \sqrt{\mu_0 \varepsilon_0 \varepsilon_r(\omega)} = c \frac{\kappa}{\omega}, \tag{S32}$$

with κ the modulus of the spatial projection of the wave 4-vector , $\varepsilon_r = 1 + \chi^{(1)}(\omega)$, and ω the physical frequency[6], i.e., the frequency measured by an observer in curved spacetime. Thus, we write the dispersion relation for our effective medium as

$$\tilde{n} = c\frac{\tilde{\kappa}}{\nu}, \tag{S33}$$

where $\tilde{n} = n_{\rm sp} n$ with $n_{\rm sp}^2 = (\Omega|g_{00}|)^{-1}$. Eq. (S33) is the expression that we will use in deriving the NLSE. Note once again that here $\nu = \omega\sqrt{-g_{00}}$ where ν is the conjugate Fourier variable to the coordinate time t in flat spacetime. Since for consistency we want the two dispersion relations to be equivalent, we see that $\tilde{\kappa} = \kappa n_{\rm sp}\sqrt{-g_{00}}$. Once again, in the dispersive case, we will need to consider $\tilde{n} = \tilde{n}(\omega)$ since otherwise the two dispersion relations would not remain equivalent.

Derivation of the standard NLSE

Before delving into the derivation of the NLSE for our effective, inhomogeneous medium, we summarize here the derivation of the NLSE in the standard case, following [12].

In the standard case of a homogeneous, non-magnetic material in flat spacetime, writing the displacement electric field D as the sum of a linear part and the non-linear polarization, we have the wave equation in frequency space

$$\nabla^2 E - \nabla(\nabla\cdot E) + \mu_0\varepsilon_\ell \nu^2 E = -\mu_0\nu^2 P_{\rm NL}. \tag{S34}$$

Note that in this section we always work with untilded quantities that refer to the optical properties of the physical medium that is considered in flat spacetime. Indeed, in this case the effective medium coincides with the physical one since the optical properties of flat spacetime are trivial. Note however that, as previously specified, from the next section we will go back to consider the case of curved spacetime. Thus, we will need to distinguish once again between physical and effective medium, with the latter represented by tilded quantities in flat spacetime.

We recall that $\mu_0 = 1/(\varepsilon_0 c^2)$. We then neglect the vectorial operator $-\nabla(\nabla\cdot E)$ due to the fact that the homogeneous Maxwell equation for D implies this term to be in general negligible – and get

$$\nabla^2 E(\nu) + \varepsilon_r(\nu)\frac{\nu^2}{c^2}E(\nu) = -\frac{\nu^2}{\varepsilon_0 c^2}P_{\rm NL}(\nu), \tag{S35}$$

with $\varepsilon_r(\nu) = \varepsilon_\ell/\varepsilon_0$ the linear, relative polarizability.

For a linearly polarized field, this equation becomes a scalar one. We can then write the electric field as a slowly varying, complex amplitude $\mathcal{E}(\mathbf{r},t)$ times a plane wave propagating in the z direction with central frequency ν_0

$$E(\mathbf{r},t) = \mathcal{E}(\mathbf{r},t)e^{i(\kappa_0 z - \nu_0 t)} + cc., \text{ where } \kappa_0 = \frac{n(\nu_0)\nu_0}{c}. \tag{S36}$$

Using the Fourier transform w.r.t. t for E and the one for the amplitude[7] $\mathcal{E}$, eq. (S36) can be rewritten in frequency space as a sum of terms dependent on $\nu \pm \nu_0$. We can then discard the fast rotating, high frequency $(\nu + \nu_0)$ components. Indeed, the slowly varying in time envelope $\mathcal{E}(\mathbf{r},t)$ in which we are interested does not possess high-frequency Fourier components [12]. We thus obtain

$$E(\mathbf{r},\nu) \approx \mathcal{E}(\mathbf{r},\nu-\nu_0)e^{i\kappa_0 z}. \tag{S37}$$

The scalar wave equation for the amplitude then becomes

$$\nabla_\perp^2\mathcal{E} + \partial_z^2\mathcal{E} + 2i\kappa_0\partial_z\mathcal{E} + [\kappa^2(\nu) - \kappa_0^2]\mathcal{E} = -\frac{\nu^2}{\varepsilon_0 c^2}P_{\rm NL}e^{-i\kappa_0 z}, \tag{S38}$$

---

[6] This is connected to the frequency in flat spacetime via $\omega = (\sqrt{-g_{00}})^{-1}\nu$.

[7] We follow [12] in defining,

$$\begin{aligned} E(\mathbf{r},t) &= \int_{-\infty}^{\infty}\frac{d\nu}{2\pi}E(\mathbf{r},\nu)e^{-i\nu t} = \mathcal{E}(\mathbf{r},t)e^{i(\kappa_0 z-\nu_0 t)} + \mathcal{E}^*(\mathbf{r},t)e^{-i(\kappa_0 z-\nu_0 t)} \\ &= \int_{-\infty}^{\infty}\frac{d\nu}{2\pi}\mathcal{E}(\mathbf{r},\nu)e^{-i(\nu+\nu_0)t}e^{i\kappa_0 z} + \int_{-\infty}^{\infty}\frac{d\nu}{2\pi}\mathcal{E}^*(\mathbf{r},\nu)e^{-i(\nu-\nu_0)t}e^{-i\kappa_0 z} \\ &= \int_{-\infty}^{\infty}\frac{d\nu}{2\pi}\mathcal{E}(\mathbf{r},\nu-\nu_0)e^{-i\nu t}e^{i\kappa_0 z} + \int_{-\infty}^{\infty}\frac{d\nu}{2\pi}\mathcal{E}^*(\mathbf{r},\nu+\nu_0)e^{-i\nu t}e^{-i\kappa_0 z}. \end{aligned}$$

From these expressions we then obtain

$$E(\mathbf{r},\nu) = \mathcal{E}(\mathbf{r},\nu-\nu_0)e^{i\kappa_0 z} + \mathcal{E}^*(\mathbf{r},\nu+\nu_0)e^{-i\kappa_0 z}$$

with $\kappa(\nu) = n(\nu)\nu/c$. At this point, we approximate $\kappa(\nu)$ as a power series in $\nu - \nu_0$

$$\kappa(\nu) = \kappa_0 + \kappa_1(\nu - \nu_0) + \bar{\mathscr{D}}, \tag{S39}$$

with $\bar{\mathscr{D}} = \kappa_2(\nu - \nu_0)^2/2 + O\left((\nu - \nu_0)^3\right)$, such that

$$\kappa(\nu)^2 = \kappa_0^2 + 2\kappa_0\kappa_1(\nu - \nu_0) + 2\kappa_0\bar{\mathscr{D}} + 2\kappa_1\bar{\mathscr{D}}(\nu - \nu_0) + \kappa_1^2(\nu - \nu_0)^2 + \bar{\mathscr{D}}^2. \tag{S40}$$

Here κ_1 is the inverse of the group velocity v_g. We will neglect $\bar{\mathscr{D}}^2$ terms and convert back to the time domain[8] to obtain

$$\left(\nabla_\perp^2 + \partial_z^2 + 2i\kappa_0(\partial_z + \kappa_1\partial_t) + 2i\kappa_1\bar{\mathscr{D}}\partial_t + 2\kappa_0\bar{\mathscr{D}} - \kappa_1^2\partial_t^2\right)\mathcal{E}(\mathbf{r},t) = \frac{1}{\varepsilon_0 c^2}\partial_t^2\left(P_{\rm NL}(\mathbf{r},t)\right)e^{-i(\kappa_0 z - \nu_0 t)}. \tag{S41}$$

Note that now $\bar{\mathscr{D}}$ is a differential operator with $\bar{\mathscr{D}} = -(\kappa_2/2)\partial_t^2 + ...$ Finally, by writing also the polarization $P_{\rm NL}(\mathbf{r},t) = p(\mathbf{r},t)e^{i\kappa_0 z - \nu_0 t} + c.c.$, i.e., as a slowly-varying amplitude $p(\mathbf{r},t)$ times a plane wave $e^{i\kappa_0 z - \nu_0 t}$ propagating in the z direction, one can see that the right-hand side (RHS) becomes[9]

$$\frac{1}{\varepsilon_0 c^2}\partial_t^2 P_{\rm NL}(\mathbf{r},t)e^{-i(\kappa_0 z - \nu_0 t)} = -\frac{\nu_0^2}{\varepsilon_0 c^2}\left(1 + \frac{i}{\nu_0}\partial_t\right)^2 p(\mathbf{r},t) + c.c.. \tag{S42}$$

This is the starting point for implementing the slowly varying envelope approximation (SVEA). It usually involves moving to the frame moving with the pulse group velocity κ_1^{-1}, and then neglecting terms with second derivatives in the propagation direction. Let us sketch the procedure here:

- The retarded frame is defined as $z' = z$ and $\tau = t - z/v_g = t - \kappa_1 z$.
- Thus, $\partial_z = \partial_{z'} - \kappa_1\partial_\tau$, and $\partial_t = \partial_\tau \implies \partial_z^2 = \partial_{z'}^2 - 2\kappa_1\partial_{z'}\partial_\tau + \kappa_1^2\partial_\tau^2$.
- The wave equation thus becomes

$$\left(\nabla_\perp^2 + \partial_{z'}^2\mathcal{E} - 2\kappa_1\partial_{z'}\partial_\tau + 2i\kappa_0\partial_{z'} + 2i\kappa_1\bar{\mathscr{D}}\partial_\tau + 2\kappa_0\bar{\mathscr{D}}\right)\mathcal{E} = -\frac{\nu_0^2}{\varepsilon_0 c^2}\left(1 + \frac{i}{\nu_0}\partial_\tau\right)^2 p. \tag{S43}$$

- Now the SVEA in space is valid when the pulse is longer than just a few wavelengths so that $\partial_{z'}^2\mathcal{E} \ll \kappa_0\partial_{z'}\mathcal{E}$. With this approximation

$$\left(\nabla_\perp^2 - 2\kappa_1\partial_{z'}\partial_\tau + 2i\kappa_0\partial_{z'} + 2i\kappa_1\bar{\mathscr{D}}\partial_\tau + 2\kappa_0\bar{\mathscr{D}}\right)\mathcal{E} = -\frac{\nu_0^2}{\varepsilon_0 c^2}\left(1 + \frac{i}{\nu_0}\partial_\tau\right)^2 p. \tag{S44}$$

- Moreover, one can also implement a SVEA in time since[10] $\kappa_1/\kappa_0 = (v_{\rm ph}/v_g)\nu_0^{-1} \approx \nu_0^{-1}$ where $v_{\rm ph}$ and v_g are the phase and group velocities respectively. When the pulse length $T_{\rm pulse}$ is long enough to contain more than just a few optical cycles, with $T_{\rm optical} = 2\pi/\nu_0$, within the envelope, then $(\kappa_1/\kappa_0)\partial_\tau \approx T_{\rm optical}/T_{\rm pulse} \ll 1$ so that

$$\left(\nabla_\perp^2 + 2i\kappa_0\partial_{z'} + 2\kappa_0\bar{\mathscr{D}}\right)\mathcal{E}(\mathbf{r},t) = -\frac{\nu_0^2}{\varepsilon_0 c^2}p(\mathbf{r},t), \tag{S45}$$

where the time derivative of the slowly varying polarization envelope has been ignored, compared to the constant term, on the same basis that $T_{\rm optical}/T_{\rm pulse} \ll 1$. This approximation of the polarization term on the right hand side of eq. (S44) is equivalent to neglecting the self-steepening effect [11].

---

[8] This is achieved by multiplying the equation by $e^{-i(\nu-\nu_0)t}$ and integrating over all values of $\nu - \nu_0$. Recall that $P_{\rm NL}(\mathbf{r},t) = \int P_{\rm NL}(\mathbf{r},\nu)e^{-i\nu t}d\nu/2\pi$.

[9] Here we can write

$$\begin{aligned}\partial_t^2 P(\mathbf{r},t)e^{-i(\kappa_0 z - \nu_0 t)} &= \partial_t^2\left(p(\mathbf{r},t)e^{i(\kappa_0 z - \nu_0 t)}\right)e^{-i(\kappa_0 z - \nu_0 t)} \\ &= \left(-\nu_0^2 - 2i\nu_0\partial_t + \partial_t^2\right)p(\mathbf{r},t)\end{aligned}$$

[10] This is not true, for example, in slow light materials.

Setting up some important relations

In the case of the inhomogeneous effective medium, we need to investigate some relation between the effective medium quantities and the one of the physical material before delving into the derivation of the NLSE. We have seen that the dielectric permeability and the magnetic one can be written in frequency space as

$$\tilde{\varepsilon}(E, r, \omega) = \varepsilon_0 \varepsilon_{\rm sp}(r)\left(1 + \chi^{(1)}(\omega) + 3\chi^{(3)}|E|^2/\Omega\right) \tag{S46}$$

$$\tilde{\mu}(r, \omega) = \mu_{\rm sp}(r)\mu_0 \tag{S47}$$

where $\chi^{(1)}(\omega)$ is the material linear dielectric permeability, including the effect of dispersion. Note also that $\varepsilon_{\rm sp}(r) = \mu_{\rm sp}(r)$ in isotropic coordinates (that we are working with), so that $n_{\rm sp}(r) \equiv \sqrt{\varepsilon_{\rm sp}\mu_{\rm sp}} = \varepsilon_{\rm sp}(r)$. Thus, we have

$$\tilde{n}(\omega, r) = n_{\rm sp}(r)n(\omega) = c\varepsilon_{\rm sp}(r)\sqrt{\mu_0\varepsilon_0(1 + \chi^{(1)}(\omega))}. \tag{S48}$$

In the wave equation eq. (S31), we have the term $-\tilde{\mu}\tilde{\varepsilon}_\ell \nu^2 E$ with $\tilde{\varepsilon}_\ell = \varepsilon_0\varepsilon_{\rm sp}(1 + \chi_1(\omega))$. In light of the previous considerations, this term can be written as

$$-\tilde{\mu}\tilde{\varepsilon}_\ell \nu^2 E = -(\tilde{n}^2/c^2)\nu^2 E. \tag{S49}$$

When we move to the frequency space for the effective medium, we use the conjugate variable (ν) to Minkowski time. As we already noticed, this is related to the frequency measured by an observer at rest with respect to the medium in curved spacetime by $\nu = \omega\sqrt{-g_{00}}$. The effective dispersion relation is thus

$$\tilde{n}^2\nu^2 = c^2\tilde{\kappa}^2, \tag{S50}$$

as previously discussed (see eq. (S33)). In expanding in power series $\tilde{\kappa}$ around ν_0 we will then have

$$\tilde{\kappa} = \tilde{\kappa}_0 + \tilde{\kappa}_1(\nu - \nu_0) + \tilde{\mathscr{D}}. \tag{S51}$$

By comparing the dispersion relation in curved spacetime and the one of the effective medium it is easy to see that

$$\tilde{\kappa}_0 = \sqrt{-g_{00}}n_{\rm sp}\kappa_0 \tag{S52}$$

$$\tilde{\kappa}_1 = n_{\rm sp}\kappa_1 \tag{S53}$$

$$\tilde{\kappa}_2 = (n_{\rm sp}/\sqrt{-g_{00}})\kappa_2 \qquad \tilde{\mathscr{D}} = \frac{1}{2}\tilde{\kappa}_2(\nu - \nu_0)^2 + \ldots = n_{\rm sp}\sqrt{-g_{00}}\mathscr{D}, \tag{S54}$$

where the $\kappa_i(\omega_0)$ appearing in these expressions are the analogues of their tilded versions, i.e.,

$$\kappa_0 = \kappa|_{\omega_0} \tag{S55}$$

$$\kappa_1 = \partial_\omega\kappa|_{\omega_0} \tag{S56}$$

$$\kappa_2 = \partial^2_\omega\kappa|_{\omega_0}, \tag{S57}$$

and refer to the tabulated optical properties of the physical medium we are considering.

The expression in eq. (S53) implies that the group velocity in the effective medium is related to the physical one in curved spacetime by

$$\tilde{v}_{\rm g} = v_{\rm g}/n_{\rm sp}. \tag{S58}$$

Note that this is consistent with the way the phase-velocity in the effective medium is related to the one in curved spacetime via $\tilde{v}_{\rm ph} \equiv 1/\tilde{n} = 1/(n_{\rm sp}n) = v_{\rm ph}/n_{\rm sp}$. More in general, this is consistent with the relation between the coordinate velocity $\tilde{v} = dx/dt$, characterizing the propagation in the effective medium in flat spacetime, and the velocity with respect to an observer comoving with the dielectric $v = d\chi/d\tau$ where $\tau = \sqrt{-g_{00}}t$ is the proper time with respect to the stationary observer and $\chi_i = x_i/\sqrt{\Omega}$ represents the proper length. Indeed, we see immediately that $v = d\chi/d\tau = \tilde{v}n_{\rm sp}$.

Derivation of the NLSE for the effective medium

First let us notice that, in order for the effective medium description to be equivalent to the physical one in curved spacetime, we need to require that:

1. the dielectric permeability and magnetization are dependent on the radial coordinate with the expressions given in the previous section
2. dispersion enters via the physical frequency $\omega = \nu/\sqrt{-g_{00}}$ which corresponds to a position dependent correction to the Fourier variable ν.

Note that the rest of the relations in the previous section are not necessary in the derivation of the NLSE, but they are nonetheless important for connecting the effective medium properties with the ones of the physical medium in curved spacetime.

In order to derive the NLSE in this case, we go back to the wave equation in eq. (S31) that we report here for convenience

$$\nabla^2 E - \nabla(\nabla\cdot E) + \tilde{\mu}\tilde{\varepsilon}_\ell \nu^2 E = -\tilde{\mu}\nu^2 P_{\rm NL} - (\nabla \log(\mu_{\rm sp}))\times(\nabla\times E). \tag{S59}$$

To proceed further, as discussed in the main text, we can make use of the homogeneous Maxwell equation for D in order to write

$$\nabla\cdot D = 0 \implies \nabla\cdot E = -(\nabla\log\tilde{\varepsilon}_l)\cdot E - \frac{1}{\tilde{\varepsilon}_l}\nabla\cdot P_{\rm NL}$$
$$-\nabla(\nabla\cdot E) = (E\cdot\nabla)\nabla\log\tilde{\varepsilon}_l + ((\nabla\log\tilde{\varepsilon}_l)\cdot\nabla)\,E + (\nabla\log\tilde{\varepsilon}_l)\times(\nabla\times E) + \nabla\left(\frac{1}{\tilde{\varepsilon}_l}(\nabla\cdot P_{\rm NL})\right),$$

where we have used that $E\times(\nabla\times\nabla\log\tilde{\varepsilon}_l) = 0$ since the curl of the gradient vanishes. We obtain

$$\nabla^2 E + \tilde{\mu}\tilde{\varepsilon}_\ell\nu^2 E = -\tilde{\mu}\nu^2 P_{\rm NL} - \nabla\left(\frac{1}{\tilde{\varepsilon}_l}(\nabla\cdot P_{\rm NL})\right) - (E\cdot\nabla)\nabla\log\varepsilon_{\rm sp} - \Big((\nabla\log\varepsilon_{\rm sp})\cdot\nabla\Big)E - \Big(\nabla\log\mu_{\rm sp} + \nabla\log\varepsilon_{\rm sp}\Big)\times(\nabla\times E). \tag{S60}$$

As discussed in the main text, eq. (S60) does not allow, in general, to write down a scalar propagation equation since even by starting from a linearly polarized electric field we end up having coupled equations between all the components of the electric field. This is in general also true whenever one does not ignore the vectorial term $\nabla(\nabla\cdot E)$.

In order to bypass these problems, we resort to considering two cases of interest, which are the ones analyzed in the main text. See also Fig. S1. Before doing so, let us emphasize that we will be interested in the specific case of a Kerr non-linear medium. Thus, we write the (slow envelope of the) non-linear polarization of the effective medium as

$$p(\mathbf{r},t) = 3\varepsilon_0 n_{\rm sp}(r)\chi^{(3)}|\mathcal{E}|^2\mathcal{E}/\Omega, \tag{S61}$$

which includes the non-linearity of the material and the contribution coming from the curved spacetime. Using the expression for $\tilde{\kappa}_0$ in eq. (S52), the term containing the polarization can be written as

$$-\frac{n_{\rm sp}(r)\nu_0^2}{2\tilde{\kappa}_0\varepsilon_0 c^2}\,p(\mathbf{r},t) = -n_2\nu_0 n_{\rm sp}(r)\varepsilon_0|\mathcal{E}|^2\mathcal{E}/\Omega, \tag{S62}$$

where $n_2 = 3\chi^{(3)}/2n(\omega_0)c\varepsilon_0$ is the nonlinear index of the Kerr material. As before, we are also going to neglect the self-steepening effect [11]. Furthermore, in our simulations we use the parameters of a single-mode, fused silica optical fiber employed in [4] that we summarize here in Tab. I.

Horizontal propagation

As we have seen in the main text, considering linearly polarized light propagating – in a medium stationary on Earth – for distances much smaller than Earth's radius, the horizontal motion can be considered as happening at constant radius $r \geq r_\oplus$. We can then follow the derivation in [4] where the pulse propagation in a single-mode optical fiber was considered.

In a nutshell, whenever the coefficients in eq.(S59) are constant, so that the very last term vanishes since $\nabla\log(\mu_{\rm sp}) = 0$, we find an equation

$$\nabla^2 E - \nabla(\nabla\cdot E) + \tilde{\mu}\tilde{\varepsilon}_\ell\nu^2 E = -\tilde{\mu}\nu^2 P_{\rm NL}, \tag{S63}$$

Symbol	Name	Value
Soliton pulse properties from [4]:		
T_0	Duration (this corresponds to 70 fs total pulse length)	40 fs
E_s	Generating pulse energy (not used, only for reference)	5 pJ
$\lambda_0 = 2\pi c/\nu_0$	central soliton wavelength	803 nm
Fiber properties:		
$\kappa_0(\nu_0)$	$n(\nu_0)\nu_0/c$, assuming $n(\nu_0) = 1.5$	$1.17 \cdot 10^7$ /m
$\kappa_1(\nu_0)$	$1/v_g(\nu_0)$, assuming $v_g(\nu_0) = 0.65c$	$5.13176 \cdot 10^{-9}$ s/m
$\kappa_2(\nu_0)$	Group velocity dispersion from [4]	$-9.5 \cdot 10^{-27}$ s^2/m
n_2	Kerr non-linearity of silica from [29]	$2.19 \cdot 10^{-20}$ m^2/W
A_{eff}	Effective transverse mode area	$\pi\,(1.6\,\mu\text{m}/2)^2$
Properties of fused silica:		
$\mathcal{P}_{11\,22}$	Component for transverse stress of the photoelastic tensor from [30, 31]	0.271
c_s	Speed of sound tabulated in [32]	5720 m/s
Miscellaneous:		
$r_\oplus$	Earth equatorial radius	6378137 m
r_S (Earth)	Schwarzschild radius of Earth	$9 \cdot 10^{-3}$ m

TABLE I: Specifics of all the parameters entering the numerical simulations of the NLSE(s). The material parameters are extrapolated from Philbin et al. [4], $\kappa_0/\nu_0 = 1.5/c$ and $\kappa_1^{-1} \approx 0.65c$. Consistently, we use the properties of the Crystal Fibre NL-PM 750 from NKT photonics [4].

which is equivalent to eq. (S1) of [4] in frequency space.

Following [4], and considering the propagation of light pulses in an optical fiber, this equation can be solved by separation of variables between an amplitude that depends on the propagation direction and a vectorial part depending on the transverse directions, i.e., $E(\nu, \mathbf{r}) = E(\nu, z)U(\nu, x, y)$ in frequency space and with $U(\nu, x, y)$ a 3-dimensional vector. By solving the eigenvalue problem for the transverse part, we then remain with a one-dimensional problem given by

$$\partial_z^2 E(z) + \frac{\tilde{n}^2}{c^2}\nu^2 E(z) = -\tilde{\mu}\nu^2 P_{\text{NL}}(z) \tag{S64}$$

where the refractive index is set by the eigenvalue of the transverse fiber mode and accounts for the property of the fiber's core and of the transverse profile. In our case, we can then assume to start directly from this equation, where the property of the effective medium accounts also for the non-trivial spacetime background via n_{sp}.

At this point, the derivation of the NLSE proceeds as in the standard case discussed above. We introduce the field scalar amplitude via $E(z, \nu) \approx \mathcal{E}(z, \nu - \nu_0)e^{i\tilde{\kappa}_0 z}$ in our equation to obtain

$$\partial_z^2\mathcal{E} + 2i\tilde{\kappa}_0\partial_z\mathcal{E} + [\tilde{\kappa}^2(\nu) - \tilde{\kappa}_0^2]\mathcal{E} = -\nu^2\tilde{\mu}P_{\text{NL}}e^{-i\tilde{\kappa}_0 z}. \tag{S65}$$

We then proceed as before by expanding

$$\tilde{\kappa} = \tilde{\kappa}_0 + \tilde{\kappa}_1(\nu - \nu_0) + \tilde{\mathscr{D}} \tag{S66}$$

to get, neglecting $\tilde{\mathscr{D}}^2$ terms and converting back to the time domain,

$$\left(\partial_z^2 + 2i\tilde{\kappa}_0(\partial_z + \tilde{\kappa}_1\partial_t) + 2i\tilde{\kappa}_1\tilde{\tilde{\mathscr{D}}}\partial_t + 2\tilde{\kappa}_0\tilde{\tilde{\mathscr{D}}} - \tilde{\kappa}_1^2\partial_t^2\right)\mathcal{E}(z,t) = \tilde{\mu}\partial_t^2\left(P_{\text{NL}}(z,t)\right)e^{-i(\tilde{\kappa}_0 z - \nu_0 t)}, \tag{S67}$$

where $\tilde{\tilde{\mathscr{D}}} = -(\tilde{\kappa}_2/2)\partial_t^2 + \ldots$ in complete analogy with the standard derivation outlined above.

At this point, by neglecting the second derivatives in z as well as terms $(\tilde{\kappa}_1/\tilde{\kappa}_0)\partial_t$ and using eq. (S62) we arrive at eq. (20) of the main text, i.e.,

$$i(\partial_z + \tilde{\kappa}_1\partial_t)\mathcal{E} - \frac{\tilde{\kappa}_2}{2}\partial_t^2\mathcal{E} = -n_2\nu_0 n_{\text{sp}}(r_\oplus)\varepsilon_0\frac{|\mathcal{E}|^2}{\Omega}\mathcal{E}. \tag{S68}$$

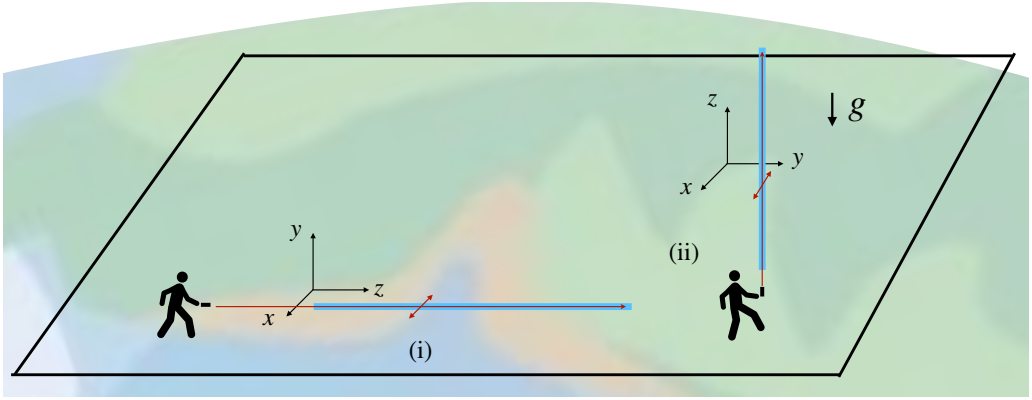

FIG. S1: Geometry of the problem. The two cases considered are labelled by (i) and (ii). In (i), the light pulse propagates in a horizontal fiber positioned at $r_\oplus = r \sim$ constant. In (ii), the light pulse propagates in a vertically positioned fiber.

Radial motion

As we already discussed, in the case of vertical motion, in which we identify the radial direction with the propagation direction along z with $r = r_\oplus + z$, the effective medium becomes a gradient-index medium with the refractive index changing along the propagation direction. We assume that all the quantities entering the wave equation depend solely on z. Upon considering linearly polarized light along a direction orthogonal to z, we end up with the system of three decoupled equations in eq. (22) of the main text that we report here for completeness

$$\partial_z^2 E_{x(y)} + \tilde{\mu}\tilde{\varepsilon}_\ell \nu^2 E_{x(y)} = -\tilde{\mu}\nu^2 P_{\mathrm{NL},x(y)} - (\partial_z \ln\tilde{\varepsilon}_\ell)\partial_z E_{x(y)} + (\partial_z(\ln\tilde{\varepsilon}_\ell + \ln\tilde{\mu}))\,\partial_z E_{x(y)} \tag{S69}$$

$$\partial_z^2 E_z + \tilde{\mu}\tilde{\varepsilon}_\ell \nu^2 E_z = -\tilde{\mu}\nu^2 P_{\mathrm{NL},z} - \partial_z\left(\frac{1}{\tilde{\varepsilon}_\ell}\partial_z P_{\mathrm{NL},z}\right) - 2(\partial_z \ln\tilde{\varepsilon}_\ell)\partial_z E_z - E_z\partial_z^2 \ln\tilde{\varepsilon}_\ell \tag{S70}$$

We can then: (1.) use the ansatz $E_x(z,t) \propto \mathcal{E}(z,t)e^{i(\tilde{\kappa}_0(z)z-\nu_0 t)} + cc.$; (2.) proceed as before in expanding the dispersion relation around the central frequency, i.e., expanding $\tilde{\kappa}(z,\nu)$ around ν_0; (3.) neglect $\tilde{\mathscr{D}}^2$ terms, to arrive at

$$\begin{aligned}&\frac{1}{2\tilde{\kappa}_0}\partial_z^2\mathcal{E} + i(\partial_z + \tilde{\kappa}_1\partial_t)\mathcal{E} - \frac{\tilde{\kappa}_2}{2}\partial_t^2\mathcal{E} - 2i\frac{\tilde{\kappa}_1\tilde{\kappa}_2}{4\tilde{\kappa}_0}\partial_t^3\mathcal{E} - \frac{\tilde{\kappa}_1^2}{2\tilde{\kappa}_0}\partial_t^2\mathcal{E} + 2i\frac{\partial_z\tilde{\kappa}_0}{2\tilde{\kappa}_0}\mathcal{E} + 2iz\frac{\partial_z\tilde{\kappa}_0}{2\tilde{\kappa}_0}\partial_z\mathcal{E} + iz\frac{\partial_z^2\tilde{\kappa}_0}{2\tilde{\kappa}_0}\mathcal{E} - z\partial_z\tilde{\kappa}_0\mathcal{E} - z^2\frac{(\partial_z\tilde{\kappa}_0)^2}{2\tilde{\kappa}_0}\mathcal{E} \\ &= -n_2\nu_0 n_{\mathrm{sp}}(r)\varepsilon_0|\mathcal{E}|^2\mathcal{E}/\Omega + \frac{\partial_z \ln n_{\mathrm{sp}}}{2\tilde{\kappa}_0}(i\tilde{\kappa}_0\mathcal{E} + \partial_z\mathcal{E} + iz(\partial_z\tilde{\kappa}_0)\,\mathcal{E}).\end{aligned} \tag{S71}$$

Upon using the SVEA approximation(s), that entail that $\partial_z^2\mathcal{E} \ll \kappa_0\partial_z\mathcal{E}$ and $(\tilde{\kappa}_1/\tilde{\kappa}_0)\partial_t \ll 1$, we then obtain the NLSE given by eq. (24) in the main text. It should also be noted that, in the weak field approximation, the terms $-z^2\left((\partial_z\tilde{\kappa}_0)^2/(2\tilde{\kappa}_0)\right)\mathcal{E}$ and $(\partial_z \ln n_{\mathrm{sp}})/(2\tilde{\kappa}_0)iz(\partial_z\tilde{\kappa}_0)\mathcal{E}$ are negligible since at least quadratic in $r_S/r_\oplus$.

SOLUTION OF THE 1D EQUATIONS

As discussed in the main text, in the case of horizontal propagation and considering a material with anomalous dispersion, we can solve eq. (20) analytically. Borrowing the solution from eq.(S74) of the supplementary material in [4] the analytical solution is given by (see also Fig. S2)

$$\mathcal{E}(t,z) = \sqrt{\frac{\Omega|\tilde{\kappa}_2|}{\nu_0 n_2 n_{\mathrm{sp}}\varepsilon_0 T_0^2}}\cosh\left(\frac{t-\tilde{\kappa}_1 z}{T_0}\right)^{-1}\exp\left(\frac{iz|\tilde{\kappa}_2|}{2T_0^2}\right), \tag{S72}$$

where T_0 is the pulse length, and $1/\tilde{\kappa}_1$ is its speed of propagation. This solution reduces exactly to eq.(S4) of [4] in the limit of $r_S \to 0$. Note that the propagation speed of the soliton is $\tilde{v}_{\mathrm{g}}(\nu_0) = v_{\mathrm{g}}(\omega_0)/n_{\mathrm{sp}}$. This is exactly the proper velocity with respect to the observer's proper time and proper length in curved spacetime, as found above in eq. (S58).

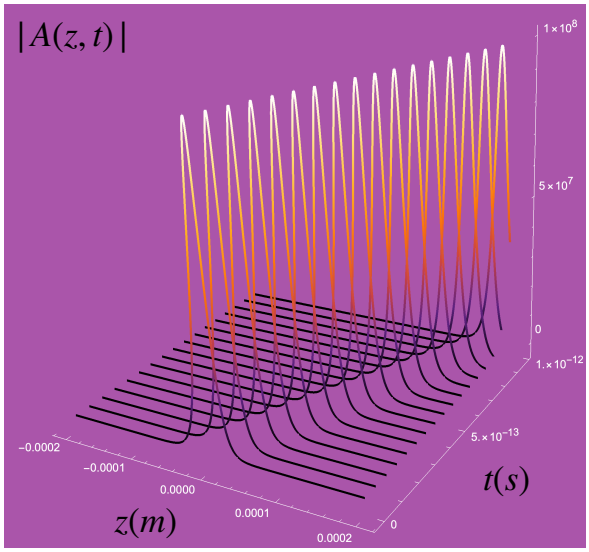

FIG. S2: Propagation of the 1D analytic soliton, eq. (20), for $r_S = 9 \times 10^{-3}$ m and $r_\oplus = 6 \times 10^6$ m.

In the case of the vertical propagation, we solve eq. (24) by way of the split-step Fourier method as showcased in [11]. In particular, we have adapted the Matlab code reported in [11] to our needs. In solving numerically the NLSE, we assign as initial temporal profile the soliton solution in flat spacetime of Philbin et al. [4], which coincides with the solution in the horizontal 1D propagation at $z = 0$ and for $r_S \to 0$.

Schematically, the split-step Fourier method consists in rewriting the NLSE as

$$\partial_z \mathcal{E} = \left(\hat{D} + \hat{N}\right)\mathcal{E}, \tag{S73}$$

where the non-linear operator $\hat{N} = \hat{N}(z, |\mathcal{E}|^2)$ accounts for the non-linearity and the diffusive dynamics is enclosed in the operator $\hat{D} = \hat{D}(z, \partial_t)$. We then need to separate the action of the non-linear term and the dissipative one by dividing the propagation distance in small steps such that

$$\mathcal{E}(z + h, t) \approx e^{\hat{N}h/2} e^{\hat{D}h} e^{\hat{N}h/2} \mathcal{E}(z, t). \tag{S74}$$

This can be easily accomplished by alternating the use of the fast-Fourier/inverse Fourier transform algorithm in order to apply $\hat{D}$ in frequency space as a multiplicative operator and going back to the time domain at each step. Furthermore, since our operator $\hat{D} = \hat{D}(z, \partial_t)$ depends on the z coordinate, a more precise implementation of the method would see to apply at each step $\exp\left(\int_z^{z+h} \hat{D}\right)$, which however is well approximated by $e^{\hat{D}h}$ in our simulations.

PHOTOELASTICITY – INCLUDING THE EFFECT OF MATERIAL DEFORMATION ON THE REFRACTIVE INDEX

As we have discussed so far, the optical medium in curved spacetime turns out to be equivalent to an effective one in flat spacetime, where the optical properties have a contribution coming from the curved spacetime background. However, whenever our physical medium is stationary in a curved spacetime, i.e., it follows the trajectories of the timelike Killing vector, it will also be subject to forces that can deform it. As discussed in the main text, deformations due to gravity of our physical medium lead to a change in the refractive index via the photoelastic effect [17].

Given our previous considerations, we will be interested in the effect of photoelasticity only for the vertical propagation equation. In order to include this effect and separate the contributions coming from the curvature of spacetime and the inertial acceleration of the fiber, we follow the discussion in [18] on the description of a deformable resonator. We choose to ignore the potential effects of photoelasticity on the nonlinear properties of the material, i.e., the nonlinear susceptibility $\chi^{(3)}$, as they would be mediated through different mechanisms compared to the effect on the linear refractive index.

Consider then the situation depicted in Fig. S3. A fiber of length L and constant mass density ρ_m is hanging from a support located at $r = r_0 \equiv r_\oplus + L$. In Schwarzschild spacetime, for an observer given by the stationary Killing vector $\partial_t / \|\partial_t\|$, the

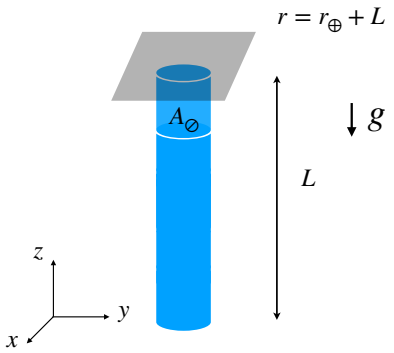

FIG. S3: Geometry of a fiber hanging in a weak gravitational field.

proper acceleration of the observer fixed at the support, i.e., an observer at constant radius in isotropic coordinates, and the local curvature projected into the proper detector frame of this observer are given by [33]

$$\mathbf{a}^J = \left(0, 0, \frac{\frac{r_S}{2r_0^2}c^2}{\left(1-\frac{r_S}{4r_0}\right)\left(1+\frac{r_S}{4r_0}\right)^3}\right) \tag{S75}$$

$$R_{0J0J} = \frac{r_S}{r_0^3\left(1+\frac{r_S}{4r_0}\right)^6}\left(\frac{1}{2}, \frac{1}{2}, -1\right), \tag{S76}$$

where we chose for the z direction to be aligned radially. Furthermore, consistently with the notation we have used so far, we want to consider the origin of our coordinate at $r = r_\oplus$. This entails shifting $z \to z - L$ to translate the origin from the support at r_0 to $r = r_\oplus$. Note that the proper detector frame is determined by an orthonormal tetrad Fermi-Walker transported along the timelike trajectory of the support of the fiber which, in our set-up, corresponds to a stationary observer [34].

We can now compute the acceleration of test particles in the proper detector frame by following the derivation in [18]. At linear order in $(z-L)/(r_\oplus + L)$, the acceleration is given by $a_p^z = -\left(\mathbf{a}^z + c^2 R_{0z0z}(z-L)\right)$. It should be noted that this expression is derived by neglecting acceleration squared terms in the proper detector frame metric as well as working at first order in the perturbations around flat spacetime (see discussion in [18]). This calls for care when wanting to extrapolate these expressions as generally valid. Each segment of the fiber is then stressed by the force $F_z(z)$ of the parts of the fiber hanging "below" it

$$F_z(z) = \int_0^z \mathrm{d}z' \rho_m A_\oslash a_p^z(z') = -\rho_m A_\oslash c^2 \frac{r_S}{2r_0^2}\left(\frac{z}{\left(1-\frac{r_S}{4r_0}\right)\left(1+\frac{r_S}{4r_0}\right)^3} - \frac{z^2-2Lz}{r_0\left(1+\frac{r_S}{4r_0}\right)^6}\right), \tag{S77}$$

where $A_\oslash$ is the cross-section of the fiber.

More generally, the fiber is subject to a stress $\sigma_{kl} = F_k/A_l$, where F_k is the force in direction $\hat{e}_k$ and A_l is the differential area normal to $\hat{e}_l$ upon which the force acts, caused by the inertial and tidal forces within the fiber. As long as we are considering strains within the elastic limit of the material, which is the case of interest here, we can employ Hooke's law and find that the strain in the fiber is $\mathcal{S}_{kl} = \sigma_{kl}/Y$, where Y is the Young modulus of the material. The relation to the electric permeability tensor ε_r is then given by $\Delta(\varepsilon_r)^{-1}_{kl} = \mathcal{P}_{kl\,mn}\mathcal{S}_{mn}$, where $\mathcal{P}$ is the photoelastic tensor [17]. The fact that the change in the inverse of ε_r is linear in the strain holds for small or moderate strain. Limiting ourselves to isotropic materials, and a diagonal stress tensor, the equations reduce in complexity to

$$\Delta(\varepsilon_r)^{-1}_{kk} = \mathcal{P}_{kk\,ll}\mathcal{S}_{ll} = \frac{\mathcal{P}_{kk\,ll}}{Y}\sigma_{ll} \tag{S78}$$

In our set-up, the stress and then the strain on the fiber are given explicitly by

$$\sigma_{zz}(z) = \frac{F(z)}{A_\oslash} = \rho_m c^2 \frac{r_S}{2r_0^2}\left(\frac{z}{\left(1-\frac{r_S}{4r_0}\right)\left(1+\frac{r_S}{4r_0}\right)^3} - \frac{z^2-2Lz}{r_0\left(1+\frac{r_S}{4r_0}\right)^6}\right) \tag{S79}$$

$$\mathcal{S}_{zz}(z) = \frac{c^2}{c_s^2}\frac{r_S}{2r_0^2}\left(\frac{z}{\left(1-\frac{r_S}{4r_0}\right)\left(1+\frac{r_S}{4r_0}\right)^3} - \frac{z^2-2Lz}{r_0\left(1+\frac{r_S}{4r_0}\right)^6}\right), \tag{S80}$$

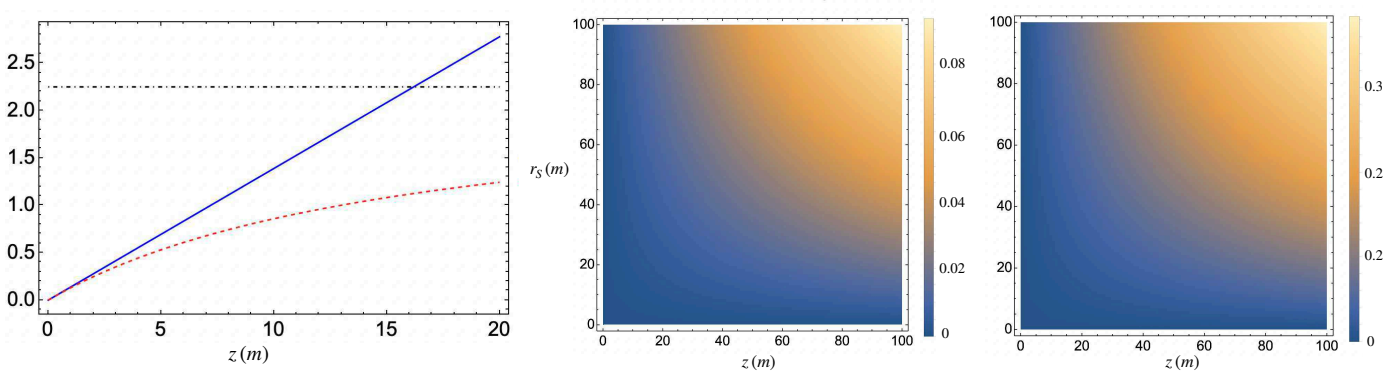

FIG. S4: Comparison between the full expression for $\Delta\varepsilon_r$ and the approximate one that are appearing in eq. (S81). **Left panel:** Here we have used the parameters tabulated in Tab. I and chosen a quite large $r_S = 3$ km. The solid, blue curve represents the approximate expression for $\Delta\varepsilon_r$, the dashed red curve the exact value of $\Delta\varepsilon_r$, while the dot-dashed black curve is the value of ε_r in the absence of photoelasticity. We see that (i) the full and approximate expressions start to deviate from propagation distances $O(1\text{m})$ onward and (ii) for relatively small propagation distances $\Delta\varepsilon_r$ is not anymore a small correction to the relative permeability ε_r but becomes equal or greater than ε_r. **Central panel:** Fractional difference between the full and approximated expressions for the photoelastic correction $\Delta\varepsilon_r$ i.e., $\left(|\Delta\varepsilon_r|_{\text{approx}} - |\Delta\varepsilon_r|_{\text{full}}\right)/\left(|\Delta\varepsilon_r|_{\text{full}} + |\Delta\varepsilon_r|_{\text{approx}}\right)$. Here r_S goes from zero to 10^4 times the Schwarzschild radius of Earth and the propagation distance reaches 100 m. We see that the difference between the two expressions remains below 10%. **Right panel:** $|\Delta\varepsilon_r|_{\text{full}}$. The value of $\Delta\varepsilon_r$, for r_S from zero to 10^4 times the Schwarzschild radius of Earth and propagation distance up to 100 m, is always well below the value of the relative permeability $\varepsilon_r \approx 2.25$.

where we used that the speed of sound in the fiber is $c_s = \sqrt{Y/\rho_m}$. Note that the strain and stress have a positive sign due to the force being directed in the negative z direction or, in other words, since we are considering an elongation of the fiber. Due to the axial symmetry of the problem, and the irrelevance of two directions orthogonal to the z-axis for the 1D case, the photoelastic tensor is a scalar.

The perturbation to the electric permeability, promoting $\varepsilon_r \to \varepsilon_r + \Delta\varepsilon_r$, is then also a scalar, and is given by

$$\Delta\varepsilon_r = -\frac{\varepsilon_r^2 \Delta(\varepsilon_r^{-1})}{1 + \varepsilon_r^0 \Delta(\varepsilon_r^{-1})} \approx -(\varepsilon_r^0)^2 \Delta(\varepsilon_r^{-1}), \tag{S81}$$

where ε_r indicates the electric permeability in the absence of photoelasticity and the last expression holds whenever the photoelastic effect is a small correction to the material properties giving[11]

$$\Delta\varepsilon_r \approx -(\varepsilon_r^0)^2 \mathcal{P}_{11\,22} \mathcal{S}_{zz}(z) = -(\varepsilon_r^0)^2 \mathcal{P}_{11\,22} \frac{c^2}{c_s^2} \frac{r_S}{2r_0^2} \left(\frac{z}{\left(1 - \frac{r_S}{4r_0}\right)\left(1 + \frac{r_S}{4r_0}\right)^3} - \frac{z^2 - 2Lz}{r_0 \left(1 + \frac{r_S}{4r_0}\right)^6} \right). \tag{S82}$$

Photoelasticity represents an additional correction to the electric permeability on top of the other effects accounting for the effective medium as described in the previous sections. For fused silica, the tabulated values in [30, 31] give $\mathcal{P}_{11\,22} = 0.271$ and $c_s = 5720$ m/s [32]. Then, from eq. (S81), for a 10 cm long fiber in the gravitational field of Earth, the contribution of the inertial acceleration (first term in eq. (S82)) at the end of the fiber to $\Delta\varepsilon_r$ is on the order 10^{-8} while the tidal acceleration (second term in eq. (S82)) contributes a term of order 10^{-16}. Note that, while the tidal contribution is clearly negligible, the correction to the relative permeability induced by the inertial acceleration is between one and two orders of magnitude greater than the correction due to the vacuum curved spacetime optical properties in our effective picture as quantified by $1 - \varepsilon_{\text{np}} \sim 10^{-9}$.

It is easy to check that, considering a $\mathcal{P}_{11\,22} \approx 0.271$, the approximate expression in eq. (S82) will start to fail around a propagation length of 2 m if we consider to be at one Earth's radius distance from an object whose mass corresponds to a

[11] Note that here we have $\Delta(\varepsilon_r^{-1}) = \mathcal{P}_{11\,22}\mathcal{S}_{zz}$. The indices are determined by the fact that we are considering an electric field linearly polarized in the x direction, we identify $\{x, y, z\} \leftrightarrow \{1, 2, 3\}$, and we consider an isotropic material. Thus, (1) the only component of the perturbation tensor of interest is $\Delta(\varepsilon_r^{-1})_{11}$, (2) the only component of the strain is S_{33}, and (3) we have $\mathcal{P}_{11\,33} = \mathcal{P}_{11\,22}$. See Appendix D of [17] where the notation and the example of isotropic materials are discussed in detailed.

Schwarzschild radius of 3 km. Indeed, Fig. S4 shows this failure as well as the fact that for such extreme values of r_S, $\Delta\varepsilon_r$ starts to be comparable or greater than ε_r at propagation distances less than 10 m. At the same time, the same figure shows that, for r_S up to 10^4 times the one of Earth, both the conditions for the validity of the approximate expression for $\Delta\varepsilon_r$ and the fact that the correction to ε_r is small are well satisfied.

CONDITIONS FOR VALIDITY OF THE UNIDIRECTIONAL APPROACH

As discussed in the main text, when considering the propagation of a light pulse in a gradient-index medium, we should account for the fact that the position-dependent refractive index will cause some light to be backscattered – this effect has also technological application in distributed acoustic sensing for seismology, see [35] and references therein. However, when solving the NLSE using the SSF method, the boundary condition completely ignores this fact – it would require already knowing the solution to include the backscattered light in the boundary condition. That this is a drawback of using the NLSE – which is a unidirectional equation for the validity of which, by definition, back-propagating fields must be negligible – in conjunction with the SSF method is well known [24, 25].

However, back-propagating fields cannot always be simply ignored. A formalism fully accounting for this issue would require to solve a system of coupled bidirectional equations, or just solve the full Maxwell equations. However, as argued in [25], we can define conditions that guarantee us that the backward reflected light is negligible. In our case, this sets a restriction on the parameter space that we can explore, where the description given by our solution to the NLSE can be trusted. Essentially, this regime corresponds to the one of weak-field and not large propagation distances. Indeed, physically, for vertical propagation, longer propagation distances and stronger gravitational accelerations would imply greater changes to the refractive index giving potentially rise to non-negligible back-propagating fields. To make this observation more quantitative, we follow here [25] where a more detailed discussion can be found.

We start from eq. (22) that we report here for convenience

$$\partial_z^2 E_x + \tilde{\mu}\tilde{\varepsilon}_\ell \nu^2 E_x = -\tilde{\mu}\nu^2 P_{\mathrm{NL},x} + (\partial_z \ln\tilde{\mu})\partial_z E_x. \tag{S83}$$

Following [25], we can rewrite this equation as

$$(\partial_z^2 + \beta^2)E_x(z) = -Q(z, E_x), \tag{S84}$$

where β is a reference momentum that can contain the dispersive character of the physical medium but no z dependence and that forms our underlying dynamics on top of which we have some perturbation encoded in Q, *the residual terms*. In our case, a sensible choice for β is

$$\beta^2 = \frac{n_0^2\nu^2}{c^2}, \tag{S85}$$

where $n_0 = \sqrt{\varepsilon_r(\bar{\omega}_0)}$ is the material refractive index without any additional effect from the spacetime (and ignoring the effect of redshift combined with the dispersion of the material) and not accounting for the photoelasticity. With this choice we have[12]

$$-Q(z, E_x) = -\tilde{\mu}\nu^2 P_{NL,x}(z) + (\partial_z \log\tilde{\mu})\partial_z E_x(z) + \beta^2[1 - n_{\mathrm{sp}}^2(1 + \Delta\varepsilon_r/\varepsilon_r)]E_x(z). \tag{S86}$$

Now, we can decompose the field in forward and backward directed (in time) fields $E_x = E_+ + E_-$ and find the equivalent system of two equations [25]

$$\partial_z E_\pm = \pm i\beta E_\pm \pm \frac{i}{2\beta}Q. \tag{S87}$$

The question is then when, starting with $E_- = 0$, E_- remains negligible. Indeed, if E_- remains negligible then we are left with a unidirectional equation and, more importantly, we know that the reflected light can be safely neglected even in comparison with the unperturbed propagation in flat spacetime in a linear medium.

---

[12] In a nutshell, from eq. (S83) we have

$$\partial_z^2 E_x + \mu_0\epsilon_0(\varepsilon_r + \Delta\varepsilon_r)\nu^2\mu_{sp}\varepsilon_{sp}E_x = -\mu_0\mu_{sp}\nu^2 P_{\mathrm{NL},x} + (\partial_z \ln\tilde{\mu})\partial_z E_x$$

Writing then $\mu_0\epsilon_0(\varepsilon_r + \Delta\varepsilon_r)\nu^2\mu_{sp}\varepsilon_{sp} = \mu_0\epsilon_0\nu^2\varepsilon_r(1 - (1 - n_{sp}^2)) + \mu_0\epsilon_0\nu^2 n_{sp}^2\Delta\varepsilon_r$ we arrive at

$$\partial_z^2 E_x + \beta^2 E_x = \beta^2\left[1 - n_{\mathrm{sp}}^2\left(1 + \frac{\Delta\varepsilon_r}{\varepsilon_r}\right)\right]E_x - \mu_0\mu_{\mathrm{sp}}\nu^2 P_{\mathrm{NL},x} + (\partial_z \ln\tilde{\mu})\partial_z E_x$$

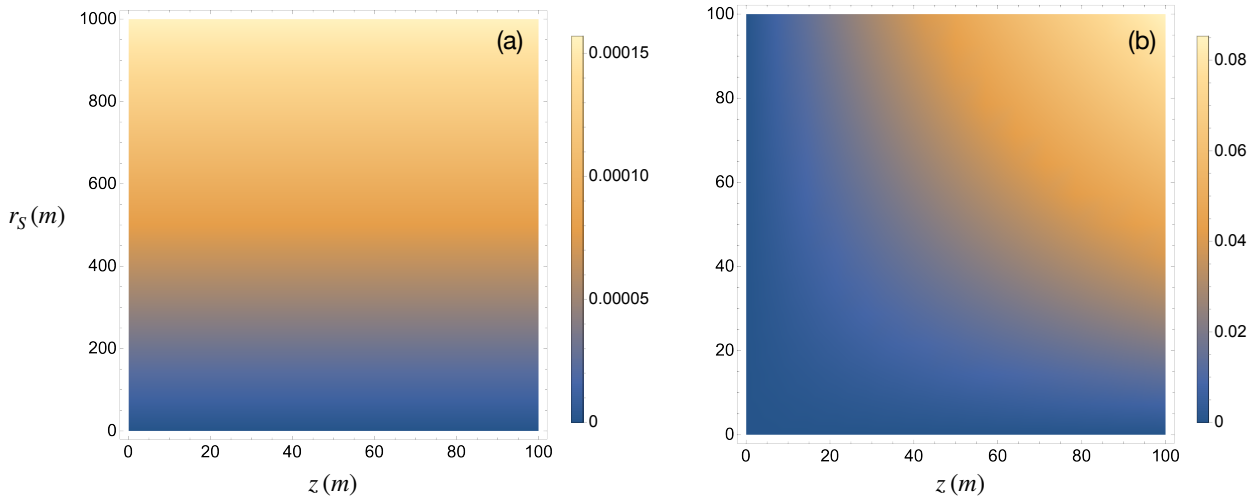

FIG. S5: **Panel (a)** shows the right-hand side of the slow-evolution condition of eq. (S88) in the case in which photoelasticity is not considered; **Panel (b)** shows the same when also photoelasticity in included. We see that without photoelasticity the condition is very well satisfied for a large set of parameters. When including photoelasticity, we see violations of the condition for values of r_S or the propagation length for which, from Fig. S4 and the corresponding discussion, we know that the $\Delta\varepsilon_r$ starts to be not anymore a small correction to the relative permeability.

Photoelasticity is the main culprit for the possible significance of the reflected light since, as we have argued before, it is the dominant effect giving rise to an effective gradient-index medium. It enters only in the term linear in the electric field. Thus, we focus solely on this term in the following. As discussed in [25], the first condition for the backward propagating light to be negligible is that the residual terms contained in the term $Q/2\beta$ in eq. (S87) are negligible with respect to βE_x. This translates to the condition

$$1 - n_{\rm sp}^2(1 + \Delta\varepsilon_r/\varepsilon_r) \ll 1. \tag{S88}$$

The second condition arises from considering the backward-evolving part of E_-(cf. the discussion in the appendix of [25])

$$\partial_z E_{-,\,\text{backwards}} \approx \frac{\partial_z \chi}{(k+\beta)^2}, \tag{S89}$$

where $Q = \chi E_x$ and $k^2(z) \equiv \beta^2 + \frac{Q(z)}{E_x(z)}$. For small Q and ignoring non-linearities, requiring that the change in the medium parameters does not cause significant back-propagation on the order of a wavelength leads to

$$\frac{\partial_z\left(n_{\rm sp}^2(1 + \Delta\varepsilon_r/\varepsilon_r)\right)}{(3/2 + n_{\rm sp}^2(1 + \Delta\varepsilon_r/\varepsilon_r))^2} \ll \beta. \tag{S90}$$

This *no-accumulation* condition requires that the derivative of the backpropagating fields is negligible and encodes the fact that there is no-accumulation of the reflected light giving in the end a non-negligible contribution.

From Fig. S5 and Fig. S6 we can see that, in the absence of photoelasticity, i.e., considering a rigid dielectric, these conditions are very well satisfied for the parameters in our simulations also when considering relatively large values of r_S and propagation lengths. When turning on photoelasticity, the situation changes, and we can arrive to regimes of large r_S and large propagation distances where the conditions are not satisfied anymore. In particular, from Fig. S5 and Fig. S6 we see that the main limiting factor is the slow-evolution condition. However, it should be noted that the slow-evolution condition starts to be violated in the same range of parameters in which $\Delta\varepsilon_r$ cannot anymore be considered a small correction and when it is arguable if the treatment of the photoelasticity as linear in the stresses is valid. To corroborate these observations, in the regime in which the slow-evolution condition is clearly violated we observe a non-negligible energy loss in the numerical solutions of the vertical propagation equation (see Fig. S7).

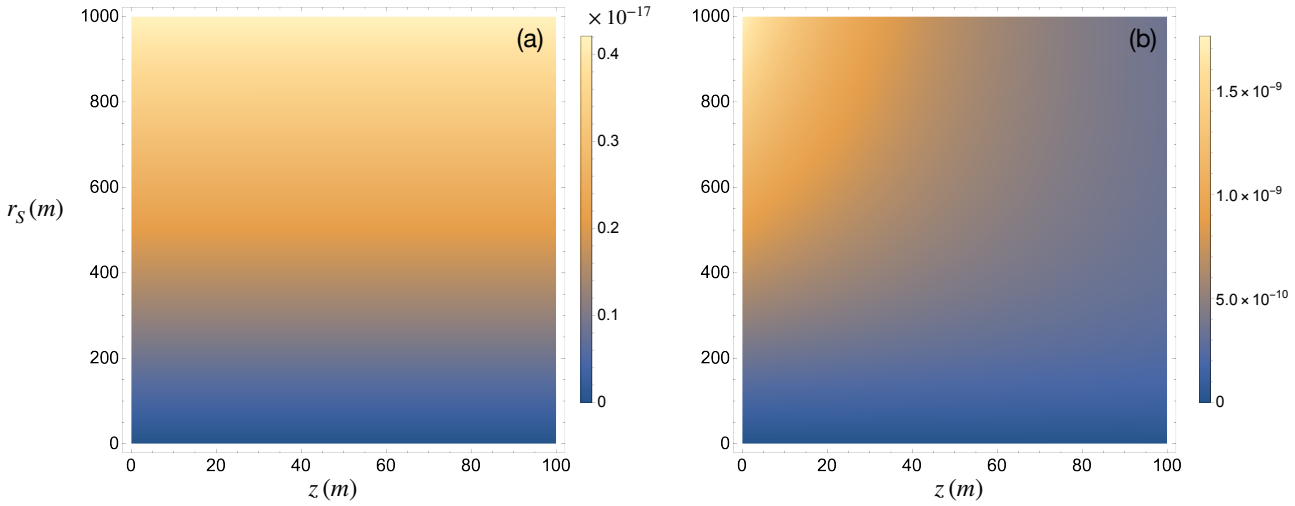

FIG. S6: **Panel (a)** shows the no-accumulation condition by depicting the ratio between the left and the right-hand sides of eq. (S90) in the case in which photoelasticity is not considered; **Panel (b)** shows the same when also photoelasticity in included. We see that this condition is actually well satisfied in both cases, while it remains that without photoelasticity the condition is much better satisfied. This analysis shows that the slow-evolution condition is the relevant one for the problem that we are considering.

COEFFICIENTS FOR THE NUMERICAL SIMULATIONS:

Finally, we report here the explicit expressions for the different coefficients entering the vertical propagation equation that we use in our simulations.

First, let us recall that, when including photoelasticity, we have

$$n(\omega) = \sqrt{\varepsilon_r(\omega) + \Delta\varepsilon_r(\omega)} = \sqrt{1 + \chi_1(\omega) + \Delta\varepsilon_r(\omega)} = \sqrt{n_0(\omega)^2 + \Delta\varepsilon_r(\omega)}, \tag{S91}$$

where $n_0(\omega)$ is the refractive index in the absence of photoelasticity. We can then proceed to compute all the κ_i coefficients of interest

$$\kappa_0 = \kappa|_{\omega_0} \tag{S92}$$
$$\kappa_1 = \partial_\omega \kappa|_{\omega_0} \tag{S93}$$
$$\kappa_2 = \partial^2_\omega \kappa|_{\omega_0}, \tag{S94}$$

where $\kappa = n\omega/c$. We start from κ_0, where we have

$$\kappa_0(\omega_0) = \frac{n(\omega_0)\omega_0}{c}. \tag{S95}$$

We now consider the case in which the pulse propagates from the bottom of the vertically oriented fiber, which is the case we simulate numerically. We thus refer the various quantities of interest to the initial physical frequency $\bar{\omega}_0$, i.e., the frequency measured by the stationary observer at the bottom of the fiber. We can then write

$$\kappa_0(\omega_0) = \frac{n\left(\bar{\omega}_0 \frac{\sqrt{-g_{00}(r_\oplus)}}{\sqrt{-g_{00}(r_\oplus+z)}}\right)\bar{\omega}_0 \frac{\sqrt{-g_{00}(r_\oplus)}}{\sqrt{-g_{00}(r_\oplus+z)}}}{c}. \tag{S96}$$

Note that, even for extreme values of r_S and z, like $r_S = 10^{-2} r_\oplus$ and $z = 100$ m we have that $1 - \sqrt{-g_{00}(r_\oplus)}/\sqrt{-g_{00}(r_\oplus + z)}$ is negligible when considering the dispersive properties of realistic materials at the optical frequencies of interest, i.e., the changes would be on scales way too fine-grained with respect to the tabulated values of the refractive index at the μm scale [36]. To account for this fact, calling $\zeta = 1 - \sqrt{-g_{00}(r_\oplus)}/\sqrt{-g_{00}(r_\oplus + z)}$ we perform an expansion of eq. (S96) at the first order in ζ.

In the following we report the expressions for all the coefficients necessary to simulate the vertical propagation of the pulse at first order in ζ. Note however that, for what concerns the simulations reported in the work, we can always safely neglect

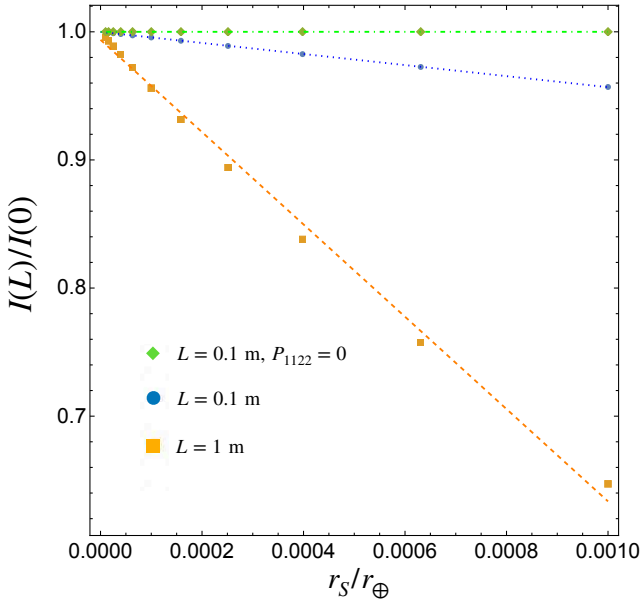

FIG. S7: Energy loss due to photoelasticity. We show the ratio between the final and initial energy $I(L)/I(0) \sim \varepsilon_r \int dt|E|^2\big|_{z=L} / \varepsilon_r \int dt|E|^2\big|_{z=0}$, in the proper detector frame. The orange, square points correspond to the case of a propagation length of 1 m while the blue, round points to a propagation length of 0.1 m. The lines represent the linear fit of the corresponding data. We obtain slopes of $-360.3 r_s/r_\oplus$ and $-43.2 r_s/r_\oplus$ respectively. The green, rhomboidal points correspond to the case without photoelasticity and are compatible with energy conservation up to a negligible energy loss accounted for by purely gravitational redshift.

also the corrections to the zeroth order terms for all the $\tilde{\kappa}_i$. The same holds true also for the terms $\partial_z\tilde{\kappa}_0$ and $\partial_z^2\tilde{\kappa}_0$ as far as photoelasticity is considered since the $z-$dependence is dominated by the photoelasticity. However, when considering the case with no photoelasticity, neglecting the $z-$dependence coming from the redshift factors in κ_0 amounts to a relative error of one part in 10^3. While still small, we have performed the simulations in which photoelasticity is not included considering also the ζ corrections in full to account for this small discrepancy.

The full expression including all the corrections at order ζ are reported in the following. Starting with κ_0 we have

$$\begin{aligned}\kappa_0(\omega_0) &\approx \kappa_0(\bar{\omega}_0) - \zeta\bar{\omega}_0\kappa_1(\bar{\omega}_0) \\ &= \kappa_0^{\rm b}\sqrt{1+\frac{\Delta\varepsilon_r}{\varepsilon_r}} - \zeta\left(\kappa_0^{\rm b}\sqrt{1+\frac{\Delta\varepsilon_r}{\varepsilon_r}} + \frac{\bar{\omega}_0^2}{c}\frac{\varepsilon_r'+\Delta\varepsilon_r'}{2n_0\sqrt{1+\frac{\Delta\varepsilon_r}{\varepsilon_r}}}\right),\end{aligned} \tag{S97}$$

where $\kappa_1(\bar{\omega}_0) = (n(\bar{\omega}_0) + \bar{\omega}_0\partial_\omega n|_{\bar{\omega}_0})/c$, while n_0 and $\kappa_0^{\rm b}$ are the tabulated refractive index and corresponding κ_0 of the material, without photoelasticity, i.e. $n_0 = \sqrt{\varepsilon_r(\bar{\omega}_0)}$ and $\kappa_0^{\rm b} = \bar{\omega}_0 n_0/c$, and a prime indicates the derivative with respect to the frequency.

Note that $\varepsilon_r' = \chi_1'$. We derive the expression for the latter, in terms of tabulated values, below. Before doing so, however, let us compute the derivatives of $\tilde{\kappa}_0$ at first order in ζ. Using the fact that $\tilde{\kappa}_0 = \sqrt{-g_{00}(r_\oplus+z)}n_{\rm sp}(z)\kappa_0(\omega_0)$, we find

$$\begin{aligned}\partial_z\tilde{\kappa}_0 \approx& \kappa_0^{\rm b}\sqrt{-g_{00}(r_\oplus)}\left(\partial_z n_{\rm sp}\sqrt{\frac{\Delta\varepsilon_r}{\varepsilon_r}+1} + \frac{n_{\rm sp}\partial_z\Delta\varepsilon_r}{2\varepsilon_r\sqrt{\frac{\Delta\varepsilon_r}{\varepsilon_r}+1}}\right) + \frac{\bar{\omega}_0^2}{4c(\Delta\varepsilon_r+\varepsilon_r(\bar{\omega}_0))^{3/2}}\Big[-2\zeta(\partial_z n_{\rm sp})\sqrt{-g_{00}\,(r_\oplus+z)}(\Delta\varepsilon_r+\varepsilon_r(\bar{\omega}_0))\,(\Delta\varepsilon_r'+\varepsilon_r') \\ &-2\zeta n_{\rm sp}(\partial_z\Delta\varepsilon_r')\sqrt{-g_{00}\,(r_\oplus+z)}(\Delta\varepsilon_r+\varepsilon_r) + \zeta n_{\rm sp}(\partial_z\Delta\varepsilon_r)\sqrt{-g_{00}\,(r_\oplus+z)}\,(\Delta\varepsilon_r'+\varepsilon_r') \\ &-2n_{\rm sp}(\partial_z\zeta)\sqrt{-g_{00}\,(r_\oplus+z)}(\Delta\varepsilon_r+\varepsilon_r)\,(\Delta\varepsilon_r'+\varepsilon_r') - 2\zeta n_{\rm sp}\partial_z\sqrt{-g_{00}(r_\oplus+z)}(\Delta\varepsilon_r+\varepsilon_r)\,(\Delta\varepsilon_r'+\varepsilon_r')\Big],\end{aligned} \tag{S98}$$

$$\partial_z^2\tilde{\kappa}_0 \approx \kappa_0^{\mathrm{b}}\sqrt{-g_{00}(r_\oplus)}\left(\partial_z^2 n_{\mathrm{sp}}\sqrt{\frac{\Delta\varepsilon_r}{\varepsilon_r}+1}+\frac{\partial_z n_{\mathrm{sp}}(\partial_z\Delta\varepsilon_r)}{\varepsilon_r\sqrt{\frac{\Delta\varepsilon_r}{\varepsilon_r}+1}}+n_{\mathrm{sp}}\left(\frac{\partial_z^2\Delta\varepsilon_r}{2\varepsilon_r\sqrt{\frac{\Delta\varepsilon_r}{\varepsilon_r}+1}}-\frac{(\partial_z\Delta\varepsilon_r)^2}{4\varepsilon_r^2\left(\frac{\Delta\varepsilon_r}{\varepsilon_r}+1\right)^{3/2}}\right)\right) \tag{S99}$$
$$-\frac{\bar{\omega}_0^2\sqrt{-g_{00}(r_\oplus+z)}\zeta(\partial_z^2 n_{\mathrm{sp}})\left(\Delta\varepsilon_r'+\varepsilon_r'\right)}{2c\sqrt{\Delta\varepsilon_r+\varepsilon_r}}-\frac{\bar{\omega}_0^2(\partial_z n_{\mathrm{sp}})\left(2\zeta(\partial_z\sqrt{-g_{00}(r_\oplus+z)})(\Delta\varepsilon_r+\varepsilon_r)\left(\Delta\varepsilon_r'+\varepsilon_r'\right)-\sqrt{-g_{00}(r_\oplus+z)}\zeta\partial_z\Delta\varepsilon_r\left(\Delta\varepsilon_r'+\varepsilon_r'\right)\right)}{2c(\Delta\varepsilon_r+\varepsilon_r)^{3/2}}$$
$$-\frac{\bar{\omega}_0^2(\partial_z n_{\mathrm{sp}})\left(2\sqrt{-g_{00}(r_\oplus+z)}\zeta(\partial_z\Delta\varepsilon_r')(\Delta\varepsilon_r+\varepsilon_r)+2\sqrt{-g_{00}(r_\oplus+z)}(\partial_z\zeta)(\Delta\varepsilon_r+\varepsilon_r)\left(\Delta\varepsilon_r'+\varepsilon_r'\right)\right)}{2c(\Delta\varepsilon_r+\varepsilon_r)^{3/2}}$$
$$-\frac{\bar{\omega}_0^2 n_{\mathrm{sp}}\left(4(\Delta\varepsilon_r+\varepsilon_r)\left(2(\partial_z\sqrt{-g_{00}(r_\oplus+z)})(\Delta\varepsilon_r+\varepsilon_r)-\sqrt{-g_{00}(r_\oplus+z)}\partial_z\Delta\varepsilon_r\right)\left(\zeta(\partial_z\Delta\varepsilon_r')+(\partial_z\zeta)\left(\Delta\varepsilon_r'+\varepsilon_r'\right)\right)\right)}{8c(\Delta\varepsilon_r+\varepsilon_r)^{5/2}}$$
$$-\frac{\bar{\omega}_0^2 n_{\mathrm{sp}}\left(-\zeta\left(\Delta\varepsilon_r'+\varepsilon_r'\right)\left(-4(\partial_z^2\sqrt{-g_{00}(r_\oplus+z)})(\Delta\varepsilon_r+\varepsilon_r)^2+4(\partial_z\sqrt{-g_{00}(r_\oplus+z)})\partial_z\Delta\varepsilon_r(\Delta\varepsilon_r+\varepsilon_r)+2\sqrt{-g_{00}(r_\oplus+z)}\partial_z^2\Delta\varepsilon_r(\Delta\varepsilon_r+\varepsilon_r)\right)\right)}{8c(\Delta\varepsilon_r+\varepsilon_r)^{5/2}}$$
$$-\frac{\bar{\omega}_0^2 n_{\mathrm{sp}}\left(-\zeta\left(\Delta\varepsilon_r'+\varepsilon_r'\right)\left(-3\sqrt{-g_{00}(r_\oplus+z)}(\partial_z\Delta\varepsilon_r)^2\right)\right)}{8c(\Delta\varepsilon_r+\varepsilon_r)^{5/2}}-\frac{\bar{\omega}_0^2 n_{\mathrm{sp}}\left(4\sqrt{-g_{00}(r_\oplus+z)}(\Delta\varepsilon_r+\varepsilon_r)^2\left(\zeta(\partial_z^2\Delta\varepsilon_r')+2(\partial_z\Delta\varepsilon_r')(\partial_z\zeta)+(\partial_z^2\zeta)\left(\Delta\varepsilon_r'+\varepsilon_r'\right)\right)\right)}{8c(\Delta\varepsilon_r+\varepsilon_r)^{5/2}}$$

Considering that

$$\Delta\varepsilon_r=-\frac{\varepsilon_r^2\Delta(\varepsilon_r^{-1})}{1+\varepsilon_r\Delta(\varepsilon_r^{-1})}, \tag{S100}$$

with

$$\Delta(\varepsilon_r^{-1})=\frac{c^2P_{1122}r_S\left(\frac{z}{\left(1-\frac{r_S}{4(L+r_\oplus)}\right)\left(\frac{r_S}{4(L+r_\oplus)}+1\right)^3}-\frac{(z-L)^2-L^2}{(L+r_\oplus)\left(\frac{r_S}{4(L+r_\oplus)}+1\right)^6}\right)}{2c_s^2(L+r_\oplus)^2} \tag{S101}$$

we also have

$$\partial_z\Delta\varepsilon_r=-\frac{\varepsilon_r^2\partial_z\Delta(\varepsilon_r^{-1})}{(\varepsilon_r\Delta(\varepsilon_r^{-1})+1)^2} \tag{S102}$$

$$\partial_z^2\Delta\varepsilon_r=\frac{\varepsilon_r^2\left(2\varepsilon_r(\partial_z\Delta(\varepsilon_r^{-1}))^2-(\varepsilon_r\Delta(\varepsilon_r^{-1})+1)\partial_z^2\Delta(\varepsilon_r^{-1})\right)}{(\varepsilon_r\Delta(\varepsilon_r^{-1})+1)^3}. \tag{S103}$$

Moving on, for κ_1 we need

$$\kappa_1(\omega_0)=(n(\omega_0)+\omega_0\partial_\nu n(\nu)|_{\omega_0})/c \tag{S104}$$

We proceed with the same approximation at first order in ζ as done above. We get

$$\kappa_1(\omega_0)\approx c^{-1}\left(\sqrt{\varepsilon_r+\Delta\varepsilon_r}+\bar{\omega}_0\frac{\epsilon_r'+\Delta\varepsilon_r'}{2\sqrt{\varepsilon_r+\Delta\varepsilon_r}}\frac{\sqrt{-g_{00}(r_\oplus)}}{\sqrt{-g_{00}(r_\oplus+z)}}\right) \tag{S105}$$
$$+c^{-1}\left[\zeta\left(\frac{1}{2}\bar{\omega}_0\left(\frac{-\bar{\omega}_0\Delta\varepsilon_r''-\bar{\omega}_0\varepsilon_r''}{\sqrt{\Delta\varepsilon_r+\varepsilon_r}}+\left(\frac{\bar{\omega}_0\Delta\varepsilon_r'+\bar{\omega}_0\varepsilon_r'}{2(\Delta\varepsilon_r+\varepsilon_r)^{3/2}}-\frac{1}{\sqrt{\Delta\varepsilon_r+\varepsilon_r}}\right)\left(\Delta\varepsilon_r'+\varepsilon_r'\right)\right)\right)\right],$$

where all quantities on the right-hand side are evaluated at $\bar{\omega}_0$.

Following the same notation as before, we indicate with κ_1^{b} the tabulated optical parameter for the material without photoelasticity. This tabulated quantity enters the previous expression through $\varepsilon_r'=\chi_1'(\bar{\omega}_0)$. Indeed, from $\kappa_1^{\mathrm{b}}=(n_0+\bar{\omega}_0\partial_\nu n_0(\nu)|_{\bar{\omega}_0})/c$, we have

$$\kappa_1^{\mathrm{b}}=c^{-1}(n_0+\bar{\omega}_0\partial_\nu n_0(\nu)|_{\bar{\omega}_0})=c^{-1}\left(n_0+\bar{\omega}_0\frac{\chi_1'}{2n_0}\right), \tag{S106}$$

from which we can read $\chi_1'=2c^2\left(-(\kappa_0^{\mathrm{b}})^2+\kappa_0^{\mathrm{b}}\kappa_1^{\mathrm{b}}\bar{\omega}_0\right)/\bar{\omega}_0^3$.

We thus remain with identifying $\Delta\varepsilon_r'$. Let us consider the full form of $\Delta\varepsilon_r$ in eq. (S100) and notice that $\Delta(\varepsilon_r^{-1})$ in there, as given in eq. (S101), does not depend on the frequency but only on the stresses and strains. Thus we get,

$$\Delta\varepsilon_r' = -\frac{\varepsilon_r'\varepsilon_r\Delta(\varepsilon_r^{-1})\left(2+\varepsilon_r\Delta(\varepsilon_r^{-1})\right)}{(1+\varepsilon_r\Delta(\varepsilon_r^{-1}))^2}, \tag{S107}$$

with

$$\varepsilon_r' = \chi_1', \tag{S108}$$

Finally, under the same assumption as before, we have

$$\kappa_2(\omega_0) = c^{-1}(2n(\nu)'|_{\omega_0} + \omega_0 n(\nu)''|_{\omega_0}). \tag{S109}$$

Thus we end up with

$$\begin{aligned}\kappa_2(\omega_0) \approx & c^{-1}\left(\frac{\Delta\varepsilon_r'+\varepsilon_r'}{\sqrt{\Delta\varepsilon_r+\varepsilon_r}} + \bar{\omega}_0\frac{2\left(\Delta\varepsilon_r+\varepsilon_r\right)\left(\Delta\varepsilon_r''+\varepsilon_r''\right)-\left(\Delta\varepsilon_r'+\varepsilon_r'\right)^2}{4\left(\Delta\varepsilon_r+\varepsilon_r\right)^{3/2}}\frac{\sqrt{-g_{00}(r_\oplus)}}{\sqrt{-g_{00}(r_\oplus+z)}}\right) \\ & + \frac{\zeta\bar{\omega}_0\left(-\left(-3\bar{\omega}_0\left(\Delta\varepsilon_r'+\varepsilon_r'\right)+4\Delta\varepsilon_r+4\varepsilon_r\right)\left(2(\Delta\varepsilon_r+\varepsilon_r)\left(\Delta\varepsilon_r''+\varepsilon_r''\right)-\left(\Delta\varepsilon_r'+\varepsilon_r'\right)^2\right)\right)}{8c(\Delta\varepsilon_r+\varepsilon_r)^{5/2}} \\ & - \frac{\zeta\bar{\omega}_0^2\left(\Delta\varepsilon_r'''+\varepsilon_r'''\right)}{2c(\Delta\varepsilon_r+\varepsilon_r)^{1/2}},\end{aligned} \tag{S110}$$

where all the quantities on the right-hand side are evaluated at $\bar{\omega}_0$.

As before, indicating the tabulated optical property of the material with κ_2^{b} and κ_3^{b} without photoelasticity, it is immediate to derive an expression for $\chi_1''(\bar{\omega}_0)$

$$\chi_1'' = \frac{2c^2}{\bar{\omega}_0^4}\left(3(\kappa_0^{\mathrm{b}})^2 - 4\kappa_0^{\mathrm{b}}\kappa_1^{\mathrm{b}}\bar{\omega}_0 + \left(\kappa_1^{\mathrm{b}}\bar{\omega}_0\right)^2 + \kappa_0^{\mathrm{b}}\kappa_2^{\mathrm{b}}\bar{\omega}_0^2\right), \tag{S111}$$

and

$$\chi_1''' = \frac{2c^2\left(-12(\kappa_0^{\mathrm{b}})^2 - 6\bar{\omega}_0^2\left(\kappa_0^{\mathrm{b}}\kappa_2^{\mathrm{b}} + (\kappa_1^{\mathrm{b}})^2\right) + \bar{\omega}_0^3(\kappa_0^{\mathrm{b}}\kappa_3^{\mathrm{b}} + 3\kappa_1^{\mathrm{b}}\kappa_2^{\mathrm{b}}) + 18\kappa_0^{\mathrm{b}}\kappa_1^{\mathrm{b}}\bar{\omega}_0\right)}{\bar{\omega}_0^5} \tag{S112}$$

while

$$\Delta\varepsilon_r'' = \frac{\Delta(\varepsilon_r^{-1})\left(-\varepsilon_r\left(\Delta(\varepsilon_r^{-1})\varepsilon_r+1\right)\left(\Delta(\varepsilon_r^{-1})\varepsilon_r+2\right)\varepsilon_r'' - 2\varepsilon_r'^2\right)}{\left(\Delta(\varepsilon_r^{-1})\varepsilon_r+1\right)^3}, \tag{S113}$$

and

$$\Delta\varepsilon_r''' = -\frac{\Delta(\varepsilon_r^{-1})\left(\varepsilon_r\varepsilon_r'''(\Delta(\varepsilon_r^{-1})\varepsilon_r+1)^2(\Delta(\varepsilon_r^{-1})\varepsilon_r+2) - 6\Delta(\varepsilon_r^{-1})\varepsilon_r'^3 + 6(\Delta(\varepsilon_r^{-1})\varepsilon_r+1)\varepsilon_r'\varepsilon_r''\right)}{(\Delta(\varepsilon_r^{-1})\varepsilon_r+1)^4}, \tag{S114}$$

with

$$\varepsilon_r'' = \chi_1'' \text{ and } \varepsilon_r''' = \chi_1'''. \tag{S115}$$

In Eq.(S112), we also neglect κ_3^{b} since this term is negligible.

WIDTH OF THE PULSE

While until now we have considered only the effect of a gravitational field on the propagation velocity of the optical pulse, we can also look at the width of the pulse while it propagates. In the horizontal case, the width remains constant, as can be seen from the analytical solution of eq. (20). In the vertical propagation case, however, this is no longer true. From Fig. S8, we see that spacetime effects, in conjunction with photoelasticity, reduce the width of the pulse. This is clearly negligible for realistic values of r_S, and it becomes relevant only at extreme values but shows, nonetheless, that gravity has a focusing effect on the propagating pulse.

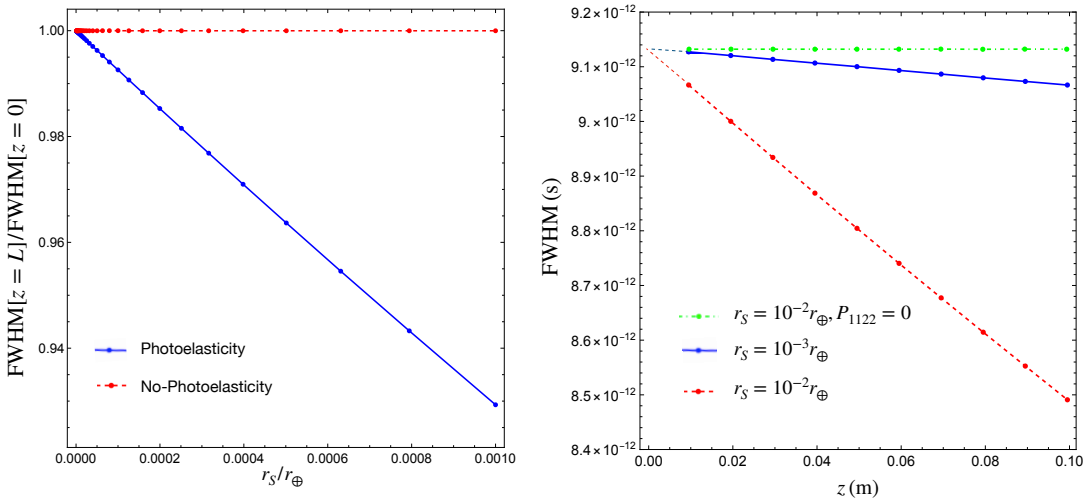

FIG. S8: **Left:** FWHM (full width at half maximum) of the pulse at $z = L$ normalized by the FWHM of the initial pulse at $z = 0$ as a function of $r_S/r_\oplus$ for an initial pulse with $T_0 = 40 \cdot 10^{-13}$ s propagating for 0.1 m. The blue solid line shows the case including the effect of photoelasticity, the red dotted line represents the case without photoelasticity. **Right:** pulse FWHM (in seconds) as a function of the propagation distance z for two different values of r_S, again using a pulse with $T_0 = 40 \cdot 10^{-13}$ s, longer than the one previously considered, for better numerical precision. The green dot-dashed line represents the case without photoelasticity.